Organo-Iridium Anticancer and Antibacterial Complexes

A Thesis Submitted for the Degree of

Doctor of Philosophy

By

Adam John Millett MChem, BSc.

University of Warwick

Department of Chemistry

July 2015

Dedicated to the memory of Ted Millett

Contents

Acknowledgements

Firstly, I would like to thank Prof. Peter Sadler for his supervision and guidance throughout this project. It has been a privilege to work within your research group and I am thankful for all of the opportunities you have given me throughout my time here.

Thank you to the ERC and the University of Warwick for the funding. I would also like thank my advisory panel, Prof. Tim Bugg and Prof. Peter Scott for their feedback. Thanks also to Prof. Martin Wills and Prof. Rob Deeth who have given me advice on various aspects of this work.

Thank you to Dr. Ivan Prokes for all of the NMR training and guidance, and Dr. Lijiang Song and Mr. Philip Aston for help with MS experiments. Also, thanks to Dr. Guy Clarkson for the X-ray crystallography.

Thank you to Dr. Isolda Romero-Canelón for all of the biological studies you have performed for me. Thanks also to Dr. Ruth McQuitty for the HPLC training. Thanks also goes to Dr. David Roper and Mr. Daniel McFeely (and Evyenia for training!) for allowing me to learn some microbiology techniques, it was both fun and frustrating! Thank you to Mr. Christopher Wootton for the UHR-MS work, you are truly an MS King among men and I know you will do brilliantly well in your PhD.

A special thank you must go to Mr. Nick Barker for giving me the opportunity to take part in the School Outreach programme, for all the hilarity, and most importantly for helping me see the bigger picture.

Now onto the crazy PJS group… It has certainly been a pleasure to work with you. In particular, I must thank the old C411 crew for all of the laughs (aloe vera), the support, and being truly awesome people to work alongside.

To my homies Evyenia and Khatija… what can I say? True friends are hard to come by, and I know we will remain homies for the years to come. It may not seem like it but you have helped keep me sane! Joan and Nichola; thanks for the fun, the chemistry knowledge, and for always providing crisp snacks, true legends! Carlos – I owe you a cider. Thanks for all the help, mein Freund. Jess, you are a ridiculous person. A big thank you for the most epic karaoke session anyone has ever had - truly memorable. Abraha, a massive thanks for all the help and for putting up with me through all of my worries and anxieties, you have been a real calming influence. I will miss our tea chats! Sassy PP (Prinessa, of course!), an amazing friend and such a massive help with the last stages of my PhD – thank you! Maria and Socorro, I really enjoyed getting to know both of you, thank you so much for all of your help and guidance. Thanks also to our friendly visitor Ziga for all the fun!

Friends out of the "Warwick Chemistry" bubble – I will soon be coming out of hibernation and will once again be able to socialise with you all!

My family, I have been a complete nightmare during the past four years, and I can only apologise for inflicting this upon you. Thank you, in particular, to my mother, my auntie Carole and siblings Louise and Chris for always being there.

Finally, Lauren… I really don't know how I would have coped without you. Thank you so much for being fiercely understanding and infinitely patient. I am truly grateful for everything you have done, and am looking forward to our lives post-PhD… Bring it on!

Declaration

I hereby declare that except where specific reference is made to other sources, the work contained in this thesis is the original work of the author. It has been composed by myself and has not been submitted, in whole or in part, for any other degree, diploma, or other qualification.

Some of the work presented in this thesis has been published:

1. Millett, A. J., Habtemariam, A., Romero-Canelón, I., Clarkson, G. J. and Sadler, P. J. Contrasting Anticancer Activity of Half-Sandwich Iridium(III) Complexes Bearing Functionally Diverse 2-Phenylpyridine Ligands. *Organometallics* **2015**, 34, 2683-2694.

Adam Millett

July 2015

Conferences Attended

1. Drug Discovery Oxford 2012 - "Drug discovery: a job too complex for academia or industry alone?" (January 2012, Oxford - UK, attendance)
2. Dalton Division Join Interests Group Meeting (University of Warwick, UK):

April 2012 (attendance)

April 2014 (poster presentation)

3. Postgraduate Chemistry Symposium (University of Warwick, UK):

June 2012 (attendance)

May 2013 (poster presentation)

May 2014 (oral presentation)

4. COST Action CM1105 Working Group # 4 meeting – "*Metallodrugs II: Design and mechanism of action*" (March 2013, University of Olomouc, Czech Republic, oral presentation)
5. International Symposium on Bioorganometallic Chemistry -ISBOMC14 (July 2014, University of Vienna, Austria, poster presentation)
6. Asian Biological Inorganic Chemistry Conference - AsBIC7 (December 2014, Gold Coast, Queensland, Australia, poster presentation)

Courses/Meetings Attended

1. Transferable skills in science
2. Avance Topspin Training Course
3. Weekly Chemical Biology cluster talks
4. RSC lectures
5. Research group meetings

Abstract

This thesis is concerned with the design of half-sandwich iridium(III) complexes of the type $[(\eta^5\text{-Cp*})\text{Ir}(2\text{-}(\text{R}'\text{-phenyl})\text{pyridine-R})\text{X}]^{0/+}$ (Cp* = pentamethylcyclopentadienyl), X = Cl^- or pyridine derivatives) as anticancer agents, with particular focus on the effects that functionality in the chelating and monodentate ligands has on their chemical and biological properties. A set of phenyliminopyridyl (ImPy) complexes of the type $[(\eta^5\text{-Cp}^{\text{x}})\text{Ir(ImPy)Cl}]\text{PF}_6$ (Cp^x = Cp*, tetramethyl(phenyl)-cyclopentadienyl (Cp^{xPh}) or tetramethyl(biphenyl)-cyclopentadienyl (Cp^{xBiPh}) was also synthesised and their solution chemistry and potential applications as antibacterial and anticancer agents investigated.

Electron donating (-CH_3, -OH, -CH_2OH and –OCH_3) or electron withdrawing (-F, -CF_3 -CHO and –NO_2) groups were introduced to various positions on the 2-PhPy ligand, giving rise to seventeen complexes $[(\eta^5\text{-Cp*})\text{Ir}(2\text{-}(\text{R}'\text{-phenyl})\text{pyridine-R})\text{Cl}]$. Three X-ray crystal structures were determined, showing the expected pseudo-octahedral configuration. The functional groups have a profound effect on the resulting anticancer activities against a range of cell lines. Some complexes showed activity against A2780 human ovarian cancer cells comparable to cisplatin, and similar activity to $[(\eta^5\text{-Cp}^{\text{xPh}})\text{Ir}(2\text{-phenyl})\text{pyridine})\text{Cl}]$. The complexes all show similar extents of hydrolysis. The complexes preferentially bind to the model nucleobase 9-EtG over 9-MeA, and show the ability to catalytically oxidise the coenzyme NADH to NAD^+. Contrasting anticancer activities were found for structural isomers. The hydrophobicity is related to substituent type and position on the ligand. The more hydrophobic complexes accumulated in A2780 cells to a greater extent. The extent of accumulation appeared to correlate with the potency of the complexes.

The most potent complex $[(\eta^5\text{-Cp*})\text{Ir}(2\text{-}(2'\text{-methylphenyl})\text{pyridine})\text{Cl}]$ **13** (IC_{50} = 1.18 μM against A2780 cells) was modified *via* replacement of the chlorido monodentate ligand with pyridine derivatives (**18** = pyridine (Py), **19** = 4-dimethylaminopyridine (Py-NMe_2), **20** = 4-trifluoromethylpyridine (Py-CF_3). The X-ray crystal structure was determined for **19**. These pyridine complexes show less monodentate ligand release in aqueous solution and less binding to 9-EtG than parent complex **13**. Complexes **13** and **19** show mild catalytic activity towards the oxidation of NADH to NAD^+. Reactivity towards glutathione (GSH) decreased only

in the case of **19** when compared with the parent complex **13**. The reaction products include [(η^5-Cp*)Ir(2-(2'-methylphenyl)pyridine)(S-O)G] (sulfenate) and [(η^5-Cp*)Ir(2-(2'-methylphenyl)pyridine)(S-O_2)G] (sulfinate) which are reliant on the presence of O_2. The antiproliferative activity against A2780 cells increased upon enhancement of stability at the monodentate site (**19** > **18** > **20** ~ **13**) when activity was measured with no cell recovery time, with **19** exhibiting nanomolar activity (IC_{50} = 650 nM). All of the complexes induced high levels of total reactive oxygen species (ROS). Apoptotic cell death after 24 h recovery time was only observed for the pyridyl complexes.

The ability to functionalise 2-PhPy complexes *via* Schiff base formation was examined using the aldehyde-containing complex [(η^5-Cp*)Ir(2-phenyl-5-pyridinecarboxaldehyde)Cl] **6**, and new conjugates were synthesised by conjugation to primary amines. Reactions with lysine-containing peptides were analysed by ultra-high resolution mass spectrometry (UHR-MS) techniques which showed formation of new iridium-peptide conjugates *via* Schiff base formation with the free amino group of lysine. The imine bond in a complex bearing the fluorescent dansyl moiety (for fluorescence microscopy) was reduced using the hydride source Et_3SiH, which appears to involve the metal centre through proposed formation of an Ir-H species.

Eighteen [(η^5-Cp^x)Ir(ImPy)Cl]PF_6 complexes with various ImPy ligands were synthesised and characterised, and six X-ray crystal structures were reported. They were found to exhibit more complex aqueous chemistry than the 2-PhPy complexes, but exhibit minimal hydrolysis at biologically-relevant concentrations of chloride, remaining predominantly as the chlorido species. The hydrophobicity of the complexes increased upon extension of the Cp^x capping ligand: Cp^{xBiPh} > Cp^{xPh} > Cp*. The complexes show minimal activity against Gram-negative *E. coli* but Cp^{xBiPh} complexes show good activity (MIC = 8 – 15 μM) against Gram-positive *S. aureus* bacteria. The antibacterial activity is generally dependent on the hydrophobicity and extension of the Cp^x capping ligand. Disruption of the bacterial cell membrane appears to be involved in the mechanism of action. The antiproliferative activity against A2780 cells follows the trend Cp^{xBiPh} > Cp^{xPh} > Cp*, where the complex [(η^5-Cp^{BiPh})Ir(ImPy-NMe_2)Cl]PF_6 **31** exhibits an IC_{50} value against A2780 cells of 640 nM.

Abbreviations

Å	Angstrom
bip	biphenyl
ca.	circa
CDDP	cisplatin
COSY	correlation spectroscopy
Cp*	1,2,3,4,5-pentamethylcyclopentadienyl
Cp^{xPh}	tetramethyl(phenyl)-cyclopentadienyl
Cp^{xBiPh}	tetramethyl(biphenyl)-cyclopentadienyl
δ	chemical shift
d	doublet
Da	Dalton
dd	doublet of doublets
DFT	density functional theory
DNA	deoxyribonucleic acid
EtBr	ethidium bromide
9-EtG	9-ethylguanine
equiv.	equivalents
ESI-MS	electrospray ionisation – mass spectrometry
GSH	L-glutathione
GSSG	oxidised L-glutathione
HPLC	high performance liquid chromatography
IC_{50}	50% growth inhibition concentration

ICP	inductively coupled plasma
ICP-OES	inductively coupled plasma – optical emission spectroscopy
ICP-MS	inductively coupled plasma – mass spectrometry
i.e.	*id est*
ImPy	phenyliminopyridyl
J	coupling constant
λ	wavelength
LC-MS	liquid chromatography – mass spectrometry
m	multiplet
9-MeA	9-methyladenine
mM	millimolar
μM	micromolar
mol equiv.	molar equivalents
MS	mass spectrometry
m/z	mass/charge
NAD^+	*ß*-nicotinamide adenine dinucleotide (oxidised)
NADH	*ß*-nicotinamide adenine dinucleotide (reduced)
ng	nanograms
nm	nanometers
nM	nanomolar
NMR	nuclear magnetic resonance
NOESY	nuclear overhauser effect spectroscopy
NP-HPLC	normal phase –high performance liquid chromatography
OD	optical density

2-PhPy	2-phenylpyridine
PI	propidium iodide
pp	polypyridyl
ppb	parts per billion
Py	pyridine
Py-CF_3	4-(trifluoromethyl)pyridine
Py-NMe_2	4-(dimethylamino)pyridine
ROS	reactive oxygen species
RP-HPLC	reverse phase –high performance liquid chromatography
s	singlet
SRB	sulfurhodamine B
t	triplet
TFA	trifluoroacetic acid
Trx-R	thioredoxin reductase 1
UV-Vis	ultraviolet-visible
VWD	variable wavelength detector

Chapter 1

Introduction

1.1 Metals in Medicine

The use of metals in medicine can be dated back to ancient civilisations, where for example, the Greeks and Egyptians used silver to treat wounds and copper to purify water for drinking. Historically, the development of the arsenic based arsphenamine (salvarsan) in the early 1900's for the treatment of syphilis is considered to be the foundations of chemotherapy.[1]

In modern medicine, metal complexes have found a wide variety of uses as diagnostic and therapeutic agents (Figure 1.1). Gadolinium(III) complexes $[Gd(DOTA)]^{-}C_7H_{18}NO_5^{+}$ (Dotarem) and $[Gd(DTPA)]^{2-}(C_7H_{18}NO_5)_2^{+}$ (Magnevist) are used extensively as MRI contrast agents,[2] which exploit the paramagnetic nature of the Gd(III) ion to increase the T_1 (longitudinal) relaxation rate of surrounding water protons.[3] The radiopharmaceutical agent $[^{99m}Tc(sestamibi)]^{+}$ (Cardiolite) is used for the evaluation of cardiac problems and as a diagnostic test for breast cancer utilising single photon emission computed tomography (SPECT). Gold(I) complexes such as auranofin are anti-inflammatory drugs for the treatment of rheumatoid arthritis,[4,5] while bismuth compounds such as bismuth subsalicylate (Pepto-Bismol) is used to treat minor digestive discomfort.[6] Metal-based compounds have also been explored as anticancer and antibacterial agents which are the focus of this thesis.[7]

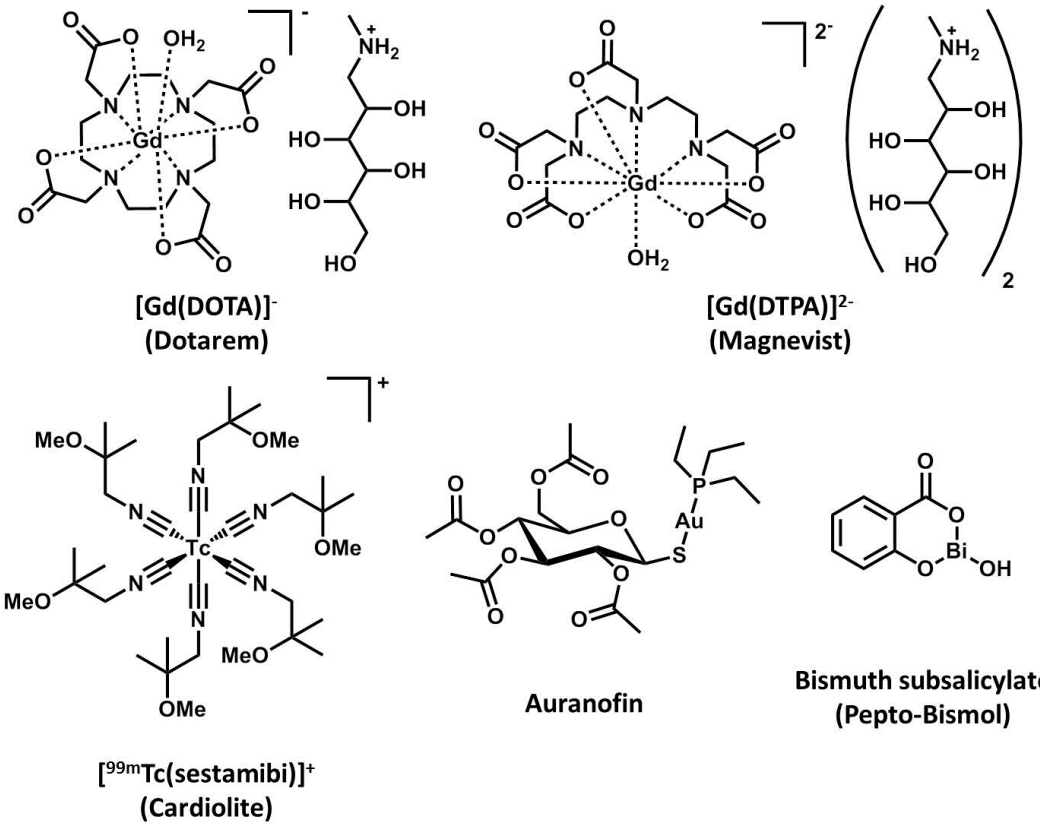

Figure 1.1. Some metal-based compounds currently used in medicine for diagnosis and therapy.

1.2 Cancer

Cancer is defined as the rapid division of abnormal cells which can infiltrate healthy cells and spread throughout the body, forming secondary tumours otherwise known as metastases. There are over 200 types of different cancers, and it is now estimated that 1 in 2 people in the UK will develop cancer in their lifetime.[8] Cancer is also one of the leading causes of death in both developed and developing countries.[9] This vast prevalence makes the effective treatment of cancer a research priority within medicine.

Cancer is commonly treated using either one or a combination of different methods. Surgery is used to remove a solid tumour mass when localised around a particular tissue, radiotherapy utilises ionising radiation to destroy cancerous tissue and

chemotherapy exploits the antiproliferative nature of particular chemical compounds to kill cancer cells. Platinum-based treatments account for around 50% of the total chemotherapeutic drugs used to treat patients, either alone or in combination therapy with other antiproliferative agents.[10]

1.3 Metal-based Anticancer Agents

1.3.1 Platinum and Ruthenium Coordination Complexes

The most successful metallodrug to date for the treatment of cancer is the square-planar Pt(II) complex *cis*-$[PtCl_2(NH_3)_2]$ cisplatin (Figure 1.2 a). Its antiproliferative properties against sarcoma 180 (Lewis lung model) and leukaemia L1210 in mice were first reported in 1969 by Rosenberg *et al.*[11] Since the discovery of its remarkable anticancer activity, it has been used either alone or in combination to treat bladder, cervical, lung, ovarian, head and neck, and testicular cancers, in which cisplatin has helped achieve a 95% cure rate against the latter.[12]

The mechanism of action (MoA) is widely accepted to involve the direct binding to nuclear deoxyribonucleic acid (DNA) *via* predominantly 1,2-intrastrand cross-links with guanine bases.[13,14] This occurs through hydrolysis of the chloride ligands which is favoured in the cell cytoplasm, due to a decrease in the chloride ion concentration from around 104 mM (blood plasma) to 23 mM, forming the "active" *cis*-$[Pt(H_2O)_2(NH_3)_2]^{2+}$ species (Figure 1.2 b). The binding causes a kink in the DNA duplex and recognition by high mobility group (HMG) proteins prevents DNA repair, eventually leading to apoptosis (programmed cell death).[15]

Cisplatin suffers from a lack of specificity, leading to associated side-effects including nephrotoxicity, neurotoxicity, ototoxicity and nausea and vomiting. This is due to its primary target being DNA which is also present in non-cancerous cells.

The second generation Pt(II) drugs [Pt(NH_3)$_2$(cyclobutane-1,1-dicarboxylate-*O*,*O*′)] carboplatin and [(1*R*,2*R*)-cyclohexane-1,2-diamine]Pt(ethanedioato-*O*,*O*′)] oxaliplatin (Figure 1.2 a) also exert their antiproliferative mechanism through DNA damage, however, they exhibit less side-effects due to their greater chemical stability.[16]

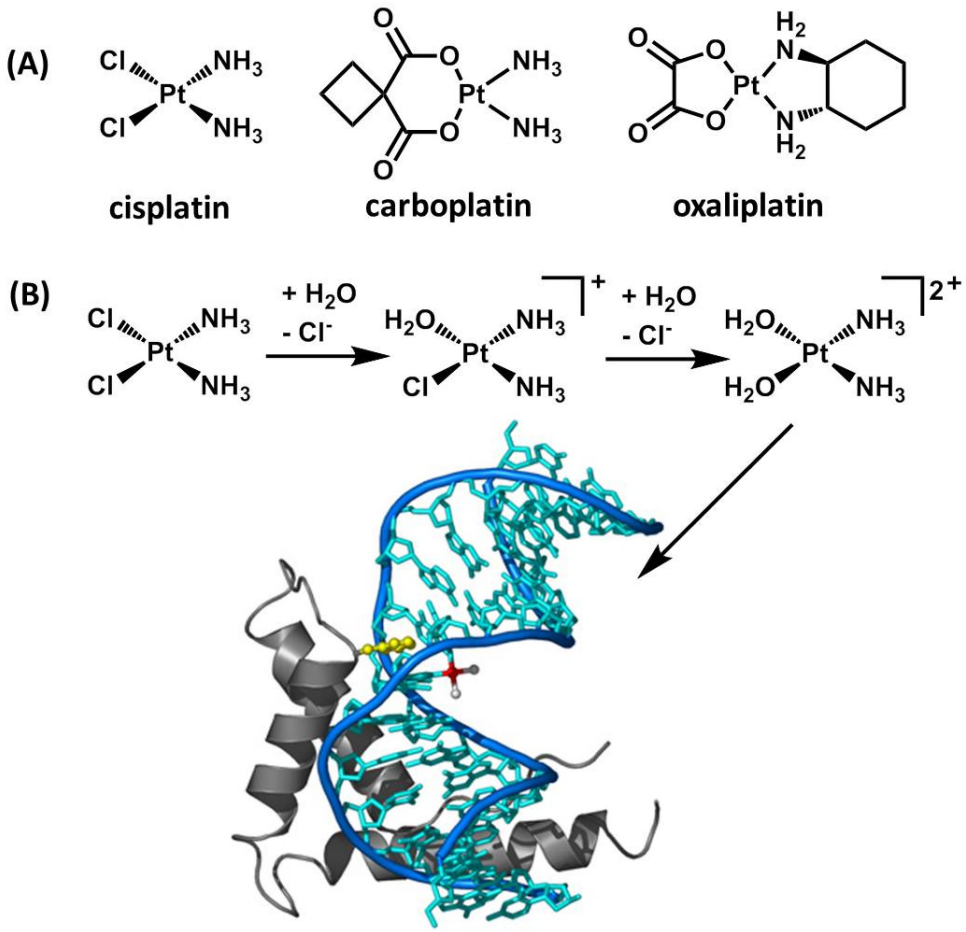

Figure 1.2. (a) Structures of clinically used Pt(II) drugs cisplatin, carboplatin and oxaliplatin. (b) Activation of cisplatin via hydrolysis, promoting binding to the DNA duplex (red = Pt). The kink is recognised by the HMG protein (grey) which inserts a phenylalanine group (yellow) in the groove formed. Picture taken from reference.[17]

Inert low-spin octahedral Pt(IV) complexes, which can be activated by intracellular reduction to Pt(II) species by reaction with ascorbic acid or glutathione (GSH), have shown some success as potential anticancer agents,[18,19] such as *cis,cis,trans*-

[$PtCl_2$(isopropylamine)$_2$($OH)_2$)] iproplatin (Figure 1.3).[20,21] Another promising approach studied by Sadler *et al.* have been Pt(IV) complexes that can be photoactivated by irradiation with UV or blue light as anticancer agents, the most notable example being *trans*,*trans*,*trans*-[$Pt(N_3)_2(OH)_2$(pyridine)$_2$] (FM190) (Figure 1.3).[22-24]

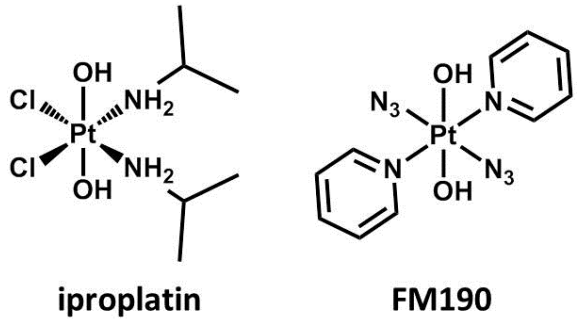

iproplatin **FM190**

Figure 1.3. Inert octahedral Pt(IV) complexes which exhibit anticancer activities upon reduction to Pt(II) by either reaction with intracellular reducing agents or irradiation with UV/blue light.

The successes and failings of Pt(II)-based treatments have led to the exploration of transition metal complexes as new antiproliferative agents. The octahedral Ru(III) complexes [*trans*-$RuCl_4$(dimethylsulfoxide)(imidazole)]imidazolium NAMI-A (Sava *et al.*) and [*trans*-$RuCl_4$(indazole)$_2$]indazolium KP1019 (Keppler *et al.*) (Figure 1.4) have shown promise for the treatment of metastases[25] and colorectal cancers,[26] respectively, and have both entered phase I clinical trials. It is believed that the intracellular reduction from Ru(III) to Ru(II) is responsible for their antiproliferative action, in which the Ru(II)-Cl bond is believed to be more kinetically labile than in Ru(III).[27] This intracellular reduction is more easily achieved in cancer cells than in healthy cells due to the more reducing environment, contributing to greater selectivity than the clinically used Pt(II) drugs.

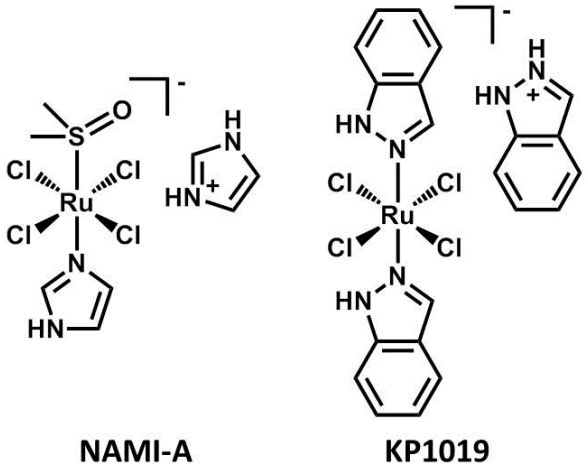

Figure 1.4. Anticancer Ru(III) coordination complexes NAMI-A and KP1019 which are currently in clinical trials

1.3.2 Organometallic Anticancer Complexes

The study of organometallic complexes (a metal compound which contains at least one metal-carbon bond) as anticancer agents is a rapidly expanding field of research, contributing to the now widely used term of bioorganometallic chemistry.[28,29] Along with coordination complexes, organometallic complexes can exhibit a wide range of coordination modes and numbers, oxidation states and can accommodate a variety of different ligands.

The first organometallic compound to show promise as a potential chemotherapeutic agent was the bent-metallocene titanocene dichloride [(η^5-Cp)$_2$TiCl$_2$] (Cp = cyclopentadienyl) (Figure 1.5 a),[30] which reached stage II clinical trials for treatment of renal-cell carcinoma[31] and metastatic breast cancer.[32] The mechanism of action was proposed to be similar to cisplatin, involving DNA cross-links, however, it is now believed that it binds more strongly to the DNA phosphate backbone.[33] Issues arising from complicated aqueous behaviour and drug formulation prevented further clinical investigations. Derivatives of titanocene dichloride have been studied by

McGowan *et al.* Functionalisiation of the Cp ring with ionic amine tethers led to increase in activity and better aqueous solubility.[34,35] Tacke *et al.* synthesised ansa-bridged derivatives which led to greater aqueous stability of the Cp rings and increased activity compared to titanocene dichloride.[36]

Another promising organometallic drug candidate is ferrocifen (Jaouen *et al.*), in which one Cp ring in ferrocene is conjugated to one of the active metabolites of the organic breast cancer drug tamoxifen (Figure 1.5 b), which showed good activity against both ER^+ and ER^- breast cancer cells.[37] Proposed mechanisms of action include binding to the ERα subtype, suppressing estradiol-mediated DNA transcription (similar mechanism to tamoxifen)[38] and the production of reactive oxygen species (ROS) which may be related to the redox activation by the ferrocene moiety.[39]

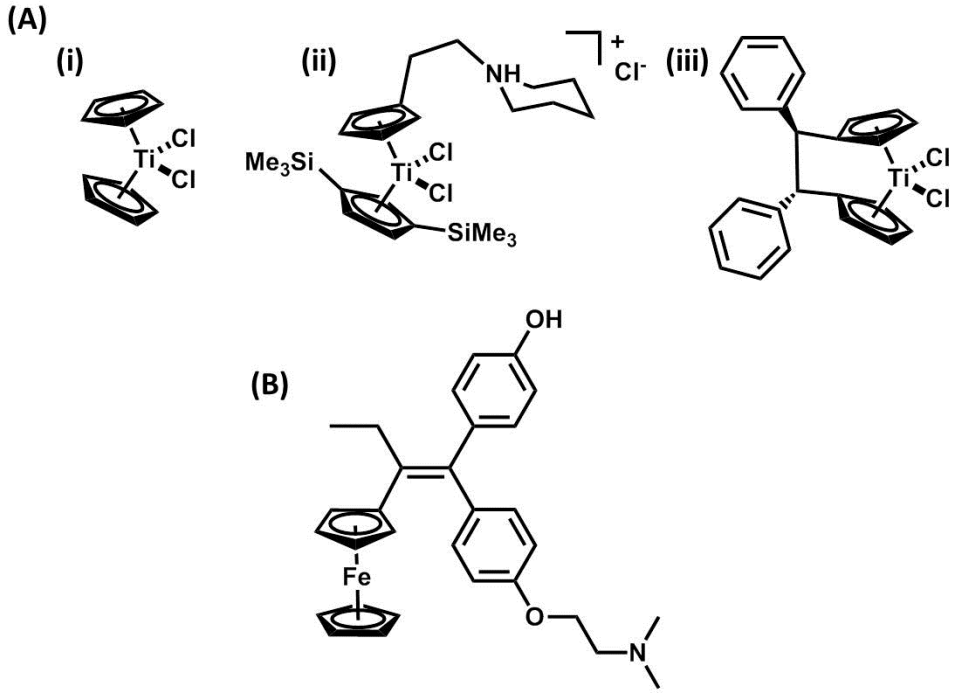

Figure 1.5. (A) Structures of the organometallic anticancer agents (i) titanocene dichloride, (ii) ionic tether derivative and (iii) ansa-bridged derivative. (B) The organometallic iron anticancer agent ferrocifen.

1.3.3 Half-sandwich Complexes

One of the most promising series of organometallic anticancer agents is half-sandwich complexes. The general structure of half-sandwich complexes can be described in relation to a piano-stool, where the seat is represented by the coordination of a neutral arene for Ru(II) and Os(II), or negatively charged Cp* (Cp* = pentamethylcyclopentadienyl) ring for Rh(III) and Ir(III) by binding of all 6 (η^6) or 5 (η^5) carbons present in the ring system, followed by the three legs of piano stool which correspond to mono- (X, Y and Z), bi (X-Y with Z monodentate) or tridentate (X-Y-Z) ligands (Figure 1.6). The surrounding ligands can provide control of the reactivity towards biomolecules and can also govern physicochemical properties such as hydrophobicity, a property which has been demonstrated to be of importance for the anticancer activity of many organometallic complexes.[40,41]

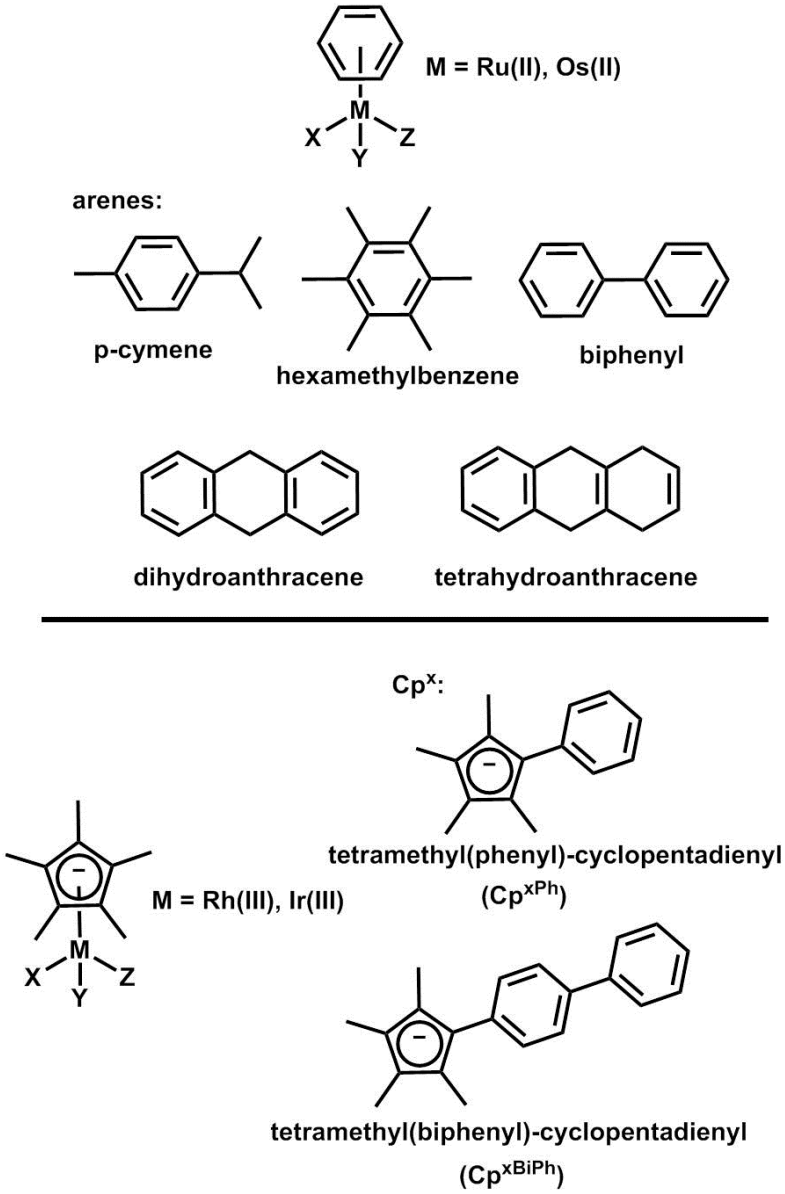

Figure 1.6. General structure of half-sandwich "piano-stool" complexes with typical arenes and Cp rings commonly used.

1.3.3.1 Ruthenium

Half-sandwich complexes of ruthenium have been shown to be encouraging anticancer agents,[42] and may be attractive alternatives to the platinum complexes currently used in the clinic. One of the most successful examples [(η^6-biphenyl)Ru(ethylenediamine)Cl]PF_6 (RM175) was reported by Sadler *et al.*, which showed excellent anti-tumour activity *in vitro* with an IC_{50} value

(concentration which inhibits 50% cell growth) against A2780 human ovarian cancer cells of 5 μM,[43] and demonstrated activity *in vivo* (Figure 1.7).[44]

The primary target of RM175 is believed to be DNA, where it can form monofunctional adducts *via* binding to guanine residues, leading to different metal-adducts compared with cisplatin. This occurs after aquation of the chloride monodentate ligand. The Ru(II)-guanine interaction is enhanced by the formation of strong hydrogen-bonds between the NH_2 protons on the ethylenediamine chelating ligand and the C6 carbonyl of guanine (Figure 1.7), resulting in a strong preference for binding to guanine residues over adenine.[45] It was found that the complex [(η^6-p-cymene)Ru(1,2-bis(dimethylamino)ethane)Cl]PF_6 which has no hydrogen bonding donors exhibits no cytotoxic activity against A2780 cells, suggesting that this interaction is integral to the mechanism of action.[46]

The *in vitro* anticancer activity of [(η^6-arene)Ru(ethylenediamine)Cl]$^+$ complexes is directly related to the type of arene capping ligand present. Increasing the size of the coordinated arene results in enhanced antiproliferative activity. The order of activity based on the presence of the capping ligand is benzene < p-cymene < biphenyl < dihydroanthracene < tetrahydroanthracene.[44] This can be attributed to increased hydrophobicity which can lead to enhanced cellular accumulation *via* passive diffusion into the cell. The presence of extended arene systems can also increase the ability to intercalate between DNA base pairs.[45]

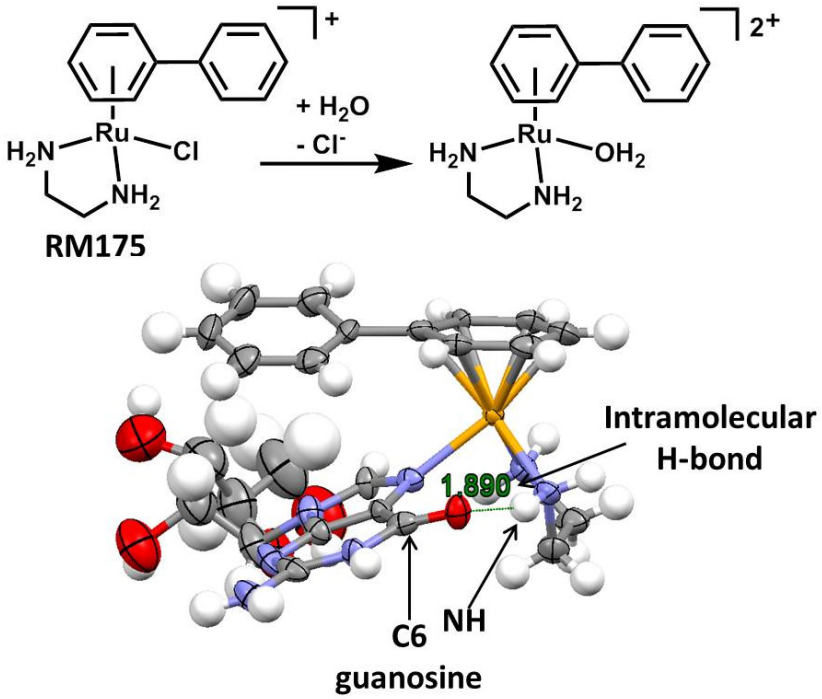

Figure 1.7. Activation *via* aquation of [(η^6-biphenyl)Ru(ethylenediamine)Cl]PF_6 (RM175) and subsequent binding to guanosine on DNA, as illustrated in the X-ray crystal structure [(η^6-biphenyl)Ru(ethylenediamine)guanosine]$(PF_6)_2$. The strong H-bond interactions (1.890 Å) between the C6 carbonyl and NH_2 protons on the chelating ligand stabilise the Ru-guanine interaction.

Work by Hartinger *et al.* has shown that the coordination of bioactive chelating ligands such as 3-hydroxyflavones and lapchol to half-sandwich Ru(II) complexes (Figure 1.8 i) can lead to highly active anticancer complexes, where mechanisms such as DNA binding and metal-centred ROS production may be involved.[47,48] Another interesting class of Ru piano-stool complexes are the RAPTA series (Figure 1.8 ii) developed by Dyson *et al.* which show excellent antitumor activities against metastases rather than primary tumours.[49] It is proposed that DNA binding *via* protonation may be responsible for the selective activity towards cancer cells over healthy cells due the slightly acidic microtumour environment exhibited by cancer cells.[50,51] It is also believed that interaction with proteins such as Cathepsin B may also be responsible for the antiproliferative activity.[52] Meggers *et al.* have also

developed a series of Ru(II) Cp kinase inhibitors bearing a pyridocarbazole chelating ligand which exhibit promising anticancer activity. It was demonstrated that blocking the inhibitory kinase action by methylation of the nitrogen in the ligand abolished the antiproliferative activity, showing that the active complex is acting as a structural scaffold for kinase inhibition.[53,54] These scaffolds are inert and do not interact with DNA *via* the monodentate site unlike RM175.

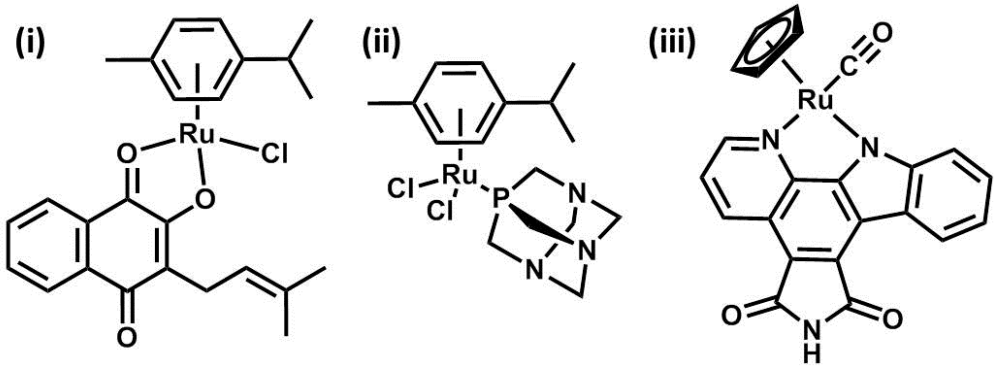

Figure 1.8. Half-sandwich Ru(II) complexes with promising anticancer activities, (i) lapchol derived complex, (ii) RAPTA-C and (iii) the substitutionally inert kinase inhibitor.

1.3.3.2 Osmium

Half-sandwich osmium(II) complexes have been less studied compared to ruthenium, presumably due to being considered less kinetically labile and the general consensus of being a toxic metal ion, a phobia which can be traced to the highly toxic OsO_4. Osmium compounds are now gaining increasing interest as potential anticancer agents.[55]

Studies by Sadler *et al.* on the osmium analogue of RM175 [(η^6-biphenyl)Os(ethylenediamine)Cl]BF_4 (Figure 1.9 i) showed an IC_{50} value against A2780 human ovarian cancer cells of 7 μM.[56] The rate of aquation was found to be 40 times slower than RM175, and the pK_a* of the aqua adduct was also lower than

RM175 (6.3 vs. 7.7), indicating that the hydroxide adduct is likely to be dominant at physiological pH. In contrast, studies on anionic *O,O*-chelated complexes like [(η^6-biphenyl)Os(acetyl-acetonate)Cl] (Figure 1.9 ii) showed no anticancer activity. They rapidly hydrolyse forming the biologically inactive hydroxo-bridged dimer,[57] indicating that the chelating ligand can have a dramatic effect on the chemical reactivity and the observed biological activity of half-sandwich metal complexes.

Another series of osmium half-sandwich complexes bearing *N,O*-chelated picolinic acid ligands showed encouraging *in vitro* anticancer activities in the low-micromolar range.[41,58] One of the most promising Os(II) arene complexes to date is [(η^6-p-cymene)Os(azpy-NMe_2)I]PF_6 (Figure 1.9 iii)) which exhibits nanomolar activity against a range of cancer cell lines including ovarian, lung and colon.[59] Interestingly, the iodido monodentate ligand exhibits minimal hydrolysis in aqueous media, yet is 10 times more potent than its chloride analogue,[60] suggesting that "activation *via* aquation" is not always required for anticancer activity within chelated half-sandwich complexes. It is believed that a redox-based MoA involving mitochondrial dysfunction may be responsible for its antiproliferative activity.

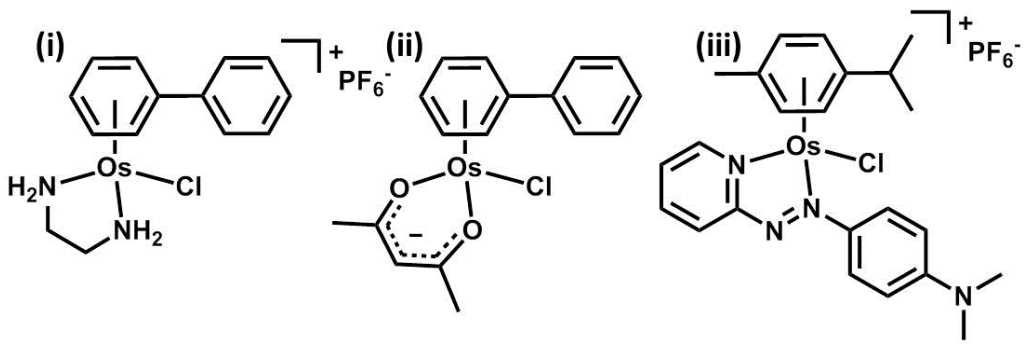

Figure 1.9. Os(II) arene complexes studied as anticancer agents.

1.4 Iridium

Iridium is a late-transition metal element and is one of the six platinum group metals. First discovered in 1803 as an impurity in platinum metal, it is named after the Greek Goddess Iris, the personification of the rainbow, due to the numerous different colours of its salts. A relatively rare metal, the global consumption of iridium was 5,540 kg in 2012.[61] The oxidation state of iridium complexes can range from -1 to +5, allowing for a range of adopted geometries including square planar (+1), tetrahedral (-1, 0), trigonal-bipyramidal (+1) octahedral (+3) and pseudo-octahedral (+3, +4). Iridium has only two naturally occurring isotopes, ^{191}Ir and ^{193}Ir where the latter is the most abundant. Upon formation of coordination/organometallic complexes, the presence of organic compounds and halogens such as Cl and Br create a distinctive isotopic pattern which aids the assignment of compounds by mass spectrometry (Figure 1.10).

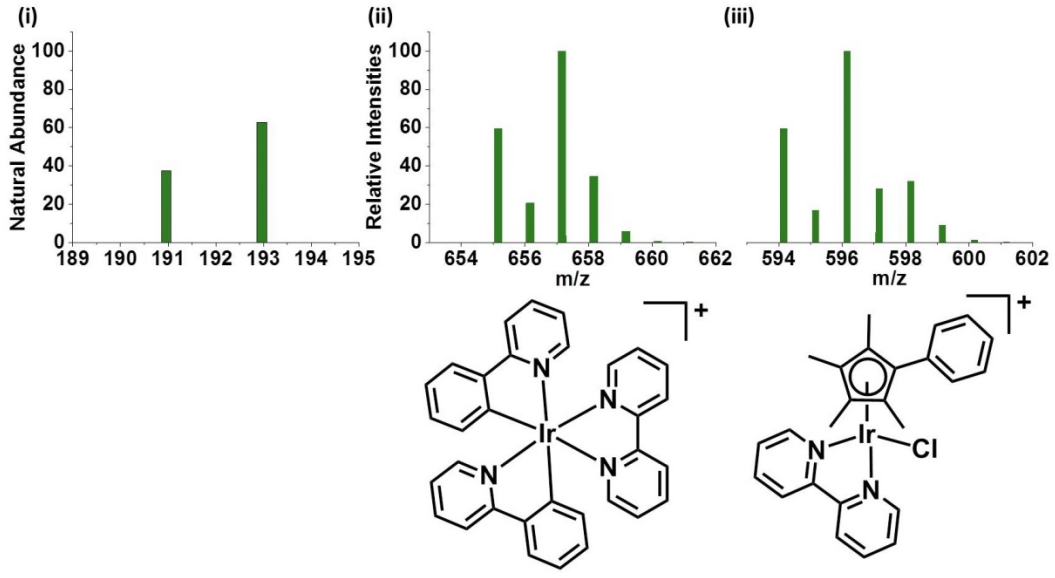

Figure 1.10. Calculated isotopic pattern of (i) iridium natural abundance, and the calculated mass spectra of the positive ions of representative organometallic complexes (ii) [Ir(2-phenylpyridine)$_2$(2,2'-bipyridine)]$^+$ and (iii) [(η^5-Cp^{xPh})Ir(2,2'-bipyridine)Cl]$^+$.

Iridium complexes can exhibit interesting catalytic and photochemical properties, for example, the highly active Crabtree's catalyst is a square-planar Ir(I) complex for homogeneous hydrogenation of highly-substituted olefins.[62,63] Cyclometalated octahedral Ir(III) complexes exhibit favourable luminescence properties which have been shown to be potentially useful as biological probes.[64,65] Half-sandwich Ir(III) complexes are also excellent catalysts for a range of organic transformations, including hydrogenation reactions of ketones[66] and imines,[67] and have also recently been reported as efficient water oxidation catalysts in the presence of a chemical oxidant.[68,69]

To date, iridium is only currently used in the clinic as a brachytherapy agent, a type of internal radiotherapy, where sealed radioactive iridium-192 (ß$^-$, half life – 73.83 d) is placed inside the body next to or in the tumour site. It is most commonly used for cervical, womb, vaginal and prostate cancers.[70,71] Research into iridium cancer chemotherapeutic agents is still in its infancy, compared with the years of research on platinum and ruthenium complexes.

1.4.1 Iridium(I) Anticancer Complexes

Following the success of square-planar Pt(II) anticancer complexes, early research was focussed on $5d^8$ square-planar Ir(I) complexes of the type $[IrCl(cyclooctadiene)]_2$[72] and [Ir(acetyl-acetonate)(cyclooctadiene)][73] (Figure 1.11 i-ii) which exhibited antimetastatic activity against the Lewis lung model and inhibition of primary Lewis lung carcinoma in mice, respectively. At the time of discovery their mechanisms of action were not investigated. The rhodium analogues showed no interaction with DNA, in which the authors claim a potentially different mechanism of action than cisplatin.

More recently, some Ir(I)-NHC (NHC = N-heterocyclic carbene) complexes with anticancer activity have been reported.[74] One of the more promising candidates was reported by Metzle-Nolte *et al.* The complex [IrCl(NHC)(cyclooctadiene)] (Figure 1.11 iii) showed good activity against the human breast MCF-7 and colon HT-29 cancer cell lines (IC_{50} = 14.6 and 19.3 μM, respectively).[75] Preliminary mechanistic studies have shown that the complex can bind to proteins such as cytochrome c via loss of the chloride and cyclooctadiene ligands, followed by oxidation of Ir(I) allowing formation of kinetically inert Ir(III) octahedral protein adducts.

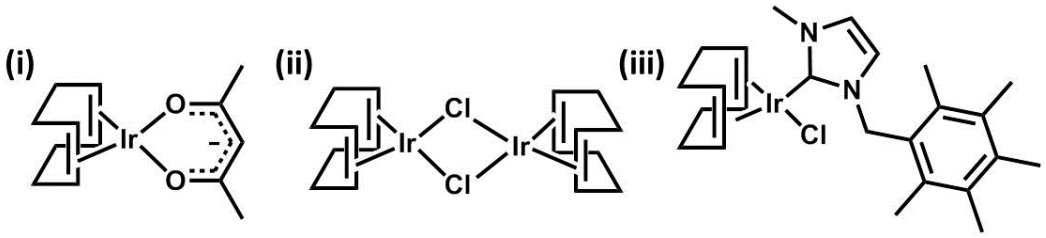

Figure 1.11. Squre-planar Ir(I) complexes studied for anticancer activity.

1.4.2 Octahedral Iridium(III) Anticancer Complexes

Due to the success of Ru(III) octahedral complexes NAMI-A and KP1019, Ir(III) analogues have been studied for their anticancer properties (Figure 5.13). Interestingly, no anticancer activity was observed for either [*trans*-$IrCl_4$(dimethylsulfoxide)(imidazole)]imidazolium[76] or [*trans*-$IrCl_4$(imidazole)$_2$]imidazolium,[77] suggesting that the greater kinetic stability of the octahedral Ir(III) ion results in poor activity.

Octahedral complexes of Ir(III) exhibit interesting luminescence properties. Emission tends to occur *via* triplet metal-to-ligand charge-transfer (^{3}MLCT). They have been widely studied as biological probes. Interaction with the analyte of interest (e.g. DNA, proteins) generally results in an increase in luminescence. Lo *et al.* have

reported a series of cyclometallated polypyridyl Ir(III) complexes that have been extensively studied for this purpose.[65,78] Interestingly, some of these complexes also exhibit antiproliferative activity against cancerous cells, such as [Ir(2-phenylquinoline)$_2$(*N,N*)]PF_6 (where *N,N* = indole-functionalised 2,2'-bypyridine) (Figure 1.12 i) with IC_{50} values of down to 1.1 μM against the HeLa cell line. Hydrophobicity appears to be an important characteristic for good activity.[79]

Ruiz *et al.* have reported cyclometallated Ir(III) complexes bearing thiosemicarbazone ligands (Figure 1.12 ii) that show potent activity against A2780 human ovarian cancer cells with no cross-resistance against A2780*cis*R (cisplatin resistant human ovarian cancer cell line) observed.[80] The complexes are capable of inhibiting Cathepsin B as well as binding to the minor groove of DNA. No direct binding to the model nucleobase 9-ethylguanine (9-EtG) was observed by ^{1}H NMR spectroscopy.

Octahedral Ir(III) complexes can also be designed as structural scaffolds for the inhibition of kinases, as demonstrated by Meggers *et al.*[81,82] An interesting example is the complex *trans,trans*-[(CH_3)SeCNIr(pyridocarbazole)-(dibenzo[a,e]cyclooctatetraene)] (Figure 1.12 iii) which shows dual anticancer activity through both antiangiogenic activity *via* inhibition of vascular endothelial growth factor receptor kinases (VEGFR) and photoinduced antiproliferation *via* irradiation with visible light, resulting in loss of the selanocyanide ligand, allowing binding to biological targets.[83] Recently, Ma *et al* reported the first metallo-inhibitor of the tumour necrosis factor-α converting enzyme (TACE) based on an octahedral Ir(III) complex (Figure 1.12 iv) which shows promise in the development of treatment of inflammatory diseases and cancer.[84]

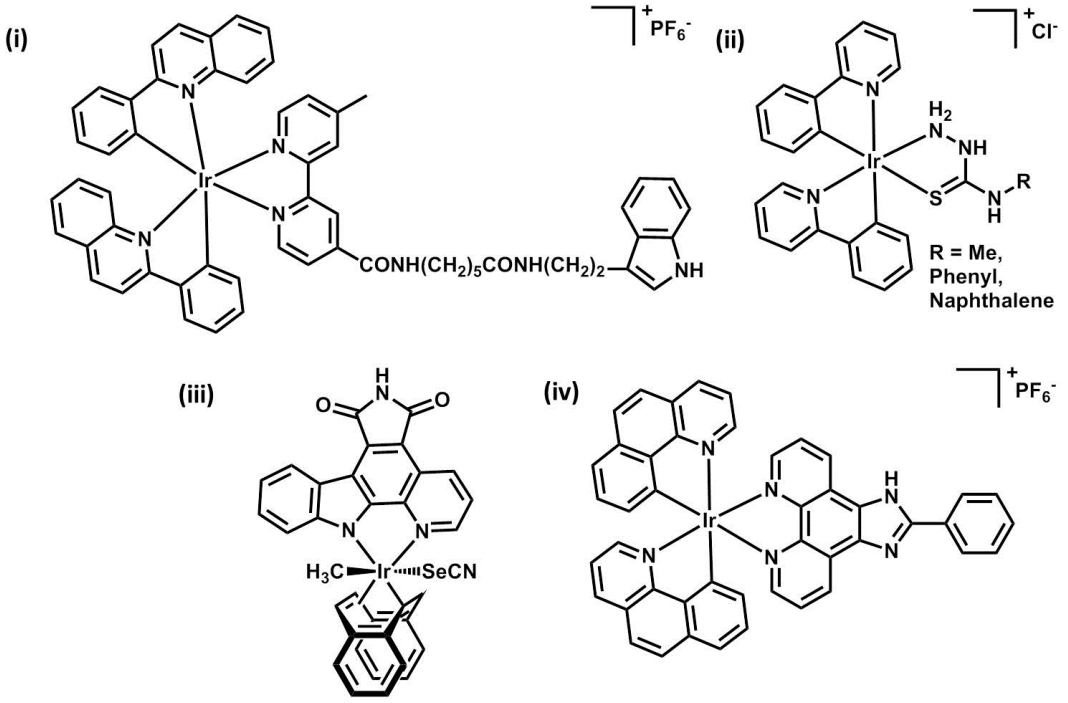

Figure 1.12 Octahedral iridium(III) complexes that show promise as potential anticancer agents.

1.4.3 Half-sandwich Iridium(III) Anticancer Complexes

There is an increasing interest in the use of half-sandwich iridium(III) complexes for biological use.[85,86] The first examples were reported by Sheldrick *et al.* They initially studied DNA intercalators using complexes of the general structure $[(\eta^5\text{-Cp*})\text{Ir}(N,N)\text{X}]^{+/2+}$ (N,N = polypyridyl (pp) chelating ligand, X = chloride/L-methionine) (Figure 1.13 a). Enhanced interactions with DNA were observed upon an increase in the surface area of the pp ligand. DNA intercalation was detected using 2D NOESY for the complex $[(\eta^5\text{-Cp*})\text{Ir(dppz)(L-methionineH)}]^{3+}$ (dppz = dipyridophenazine) with the hexanucleotide d(GTCGAC)_2.[87] Studies on the antiproliferative activity showed that the ability to intercalate between DNA bases could be responsible for their biological activity. Complexes containing ethylenediamine or 1,10-phenanthroline were poor intercalators and showed no antiproliferative activity.[88] The complexes were also shown to bind to DNA

nucleobases directly at the metal centre, showing a dual-mode of DNA interaction. The increase in size of the polypyridyl ligand also results in an increase in hydrophobicity, which can increase cellular accumulation of compounds *via* passive diffusion through the lipophilic cell membrane.

McGowan *et al.* have recently reported cytotoxic neutral half-sandwich Ir(III) complexes bearing anionic picolinamide and *ß*-ketoiminate chelating ligands (Figure 1.13) which show promising activity against a variety of different cancer cell lines.[89,90] The picolinamide complexes were shown to be potent inhibitors of thioredoxin reductase 1 (Trx-R) which may contribute towards their mechanism of action. The *ß*-ketoiminate complex [(η^5-Cp*)Ir(3′-fluorophenyl-3(phenylamino)-2-buten-1-one)Cl] also showed Trx-R inhibition and was able to retain modest antiproliferative activity under hypoxic conditions against the HT-29 colon cancer cell line, demonstrating that it can act as normoxic and hypoxic antitumor agent.[91]

Within the Sadler laboratory, a series of Ir(III) complexes bearing phenyl- or biphenyl-substituted cyclopentadienyl capping ligands have been developed using neutral *N,N*-chelating ligands (2,2'-bipyridine, 1,10-phenathroline and ethylenediamine), Figure 1.14. An increase in activity against A2780 human ovarian cancer cells was observed following the order Cp^{xBiPh} > Cp^{xPh} > Cp*.[92] Determination of the log *P* values indicated that an increase in extension of the Cp^x ligand resulted in greater hydrophobicity, which correlates with the extent of Ir accumulation in A2780 cells.

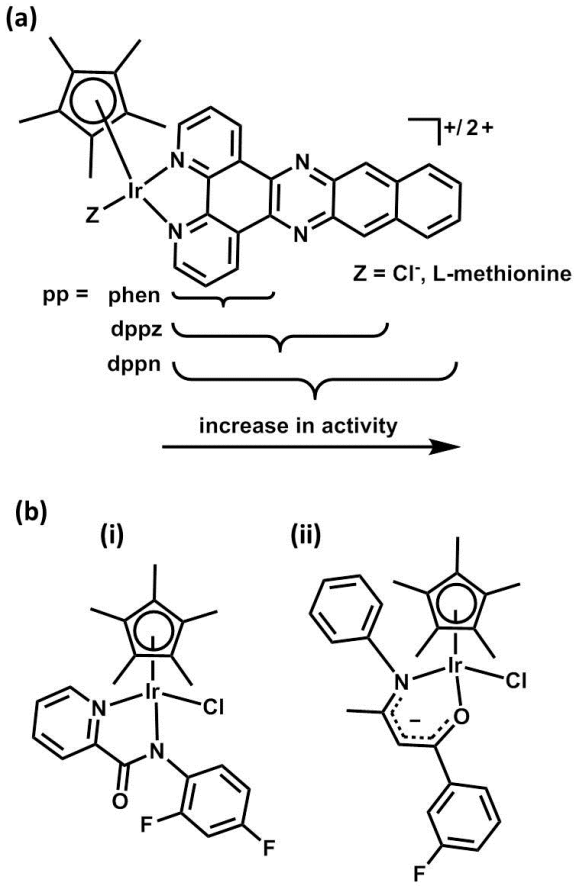

Figure 1.13. Half-sandwich Ir(III) complexes studied for anticancer activity (a) use of extended pp chelating ligands results in enhanced activity and (b) neutral anticancer complexes that show Trx-R inhibition.

This study was extended further by replacing the neutral *N,N*-chelating ligands with isoelectronic anionic *C,N*-chelating ligands (2-phenylpyridine, 7,8-benzoquinoline, Figure 1.14).[93] An increase in activity was observed which was attributed to an increase in hydrophobicity of the resulting neutral complex ([(η^5-Cp*)Ir(2,2'-bipyridine)Cl]PF_6 log *P* = -0.95 vs. ([(η^5-Cp*)Ir(2-phenylpyridine)Cl] log *P* = 1.57).[94] The same trend was also observed upon introduction of the extended Cp^x ligands as determined for the *N,N*-chelated compounds, resulting in highly potent complexes. Furthermore, the replacement of the chloride monodentate ligand with pyridine (Py) in ([(η^5-Cp^{xBiPh})Ir(2-phenylpyridine)Py]PF_6 resulted in enhanced

anticancer activity against A2780 cells (Ir-Cl IC_{50} = 0.7 μM vs. Ir-Py IC_{50} = 0.12 μM) and selectivity over healthy cells comparable to cisplatin.[95]

Despite Ir(III) being normally an inert low spin d^6 metal ion, the monodentate ligand in organo-Ir(III) chelated half-sandwich complexes can be kinetically labile.[96] Hydrolysis studies show that equilibrium between Ir-Cl and Ir-OH_2/OH in $[(\eta^5\text{-Cp}^x)\text{Ir(X-Y)Cl}]^{0/+}$ (X-Y = neutral *N,N*- or anionic *C,N*- chelating ligands) complexes is reached within under 5 mins at 310 K. The extent of hydrolysis is greatest for the neutral complexes over charged complexes (as monitored by ^{1}H NMR spectroscopy), which can be attributed to the anionic *C,N*-chelating ligand facilitating chloride loss by increasing the electron density on the metal centre. This also leads to the aqua adducts having higher pK_a values in *C,N*-chelated complexes over *N,N*-chelated systems ($[(\eta^5\text{-Cp*})\text{Ir}(2,2'\text{-bipyridine})\text{OH}_2]^{2+}$ pK_a = 6.86 vs. $[(\eta^5\text{-Cp*})\text{Ir}(2\text{-phenylpyridine})\text{OH}_2]^{+}$ pK_a = 8.75).[94] Interestingly, the use of pyridine as a monodentate ligand dramatically decreases the rate of hydrolysis, where the half-life ($t_{1/2}$) of hydrolysis for $([(\eta^5\text{-Cp}^{xBiPh})\text{Ir}(2\text{-phenylpyridine})\text{Py}]\text{PF}_6$ is 77.8 min.[95] This complex also shows 18% conversion to the chloride complex under 104 mM NaCl (chloride concentration in blood plasma) after 1 h incubation.

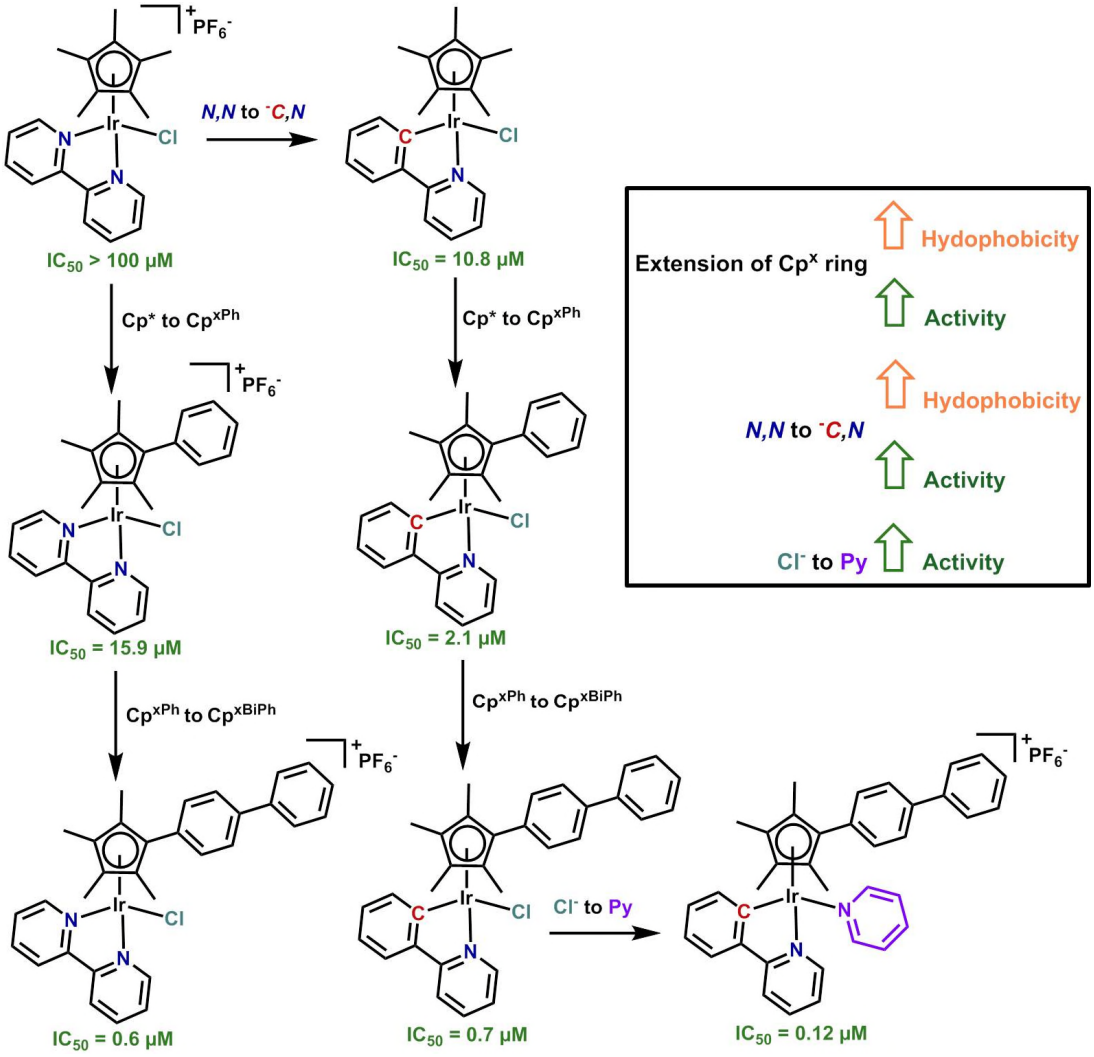

Figure 1.14. Half-sandwich Ir(III) anticancer complexes investigated within the Sadler laboratory with IC_{50} values against A2780 human ovarian cancer cells.

Studies into potential mechanisms of action have been focussed initially on interactions with DNA, which have been shown to be of importance for many metallo-anticancer complexes.[97,98] Both *N,N*- and *C,N*-chelated complexes can bind to 9-EtG, but only the *C,N*-chelated complexes show any affinity towards 9-methyladenine (9-MeA), although binding to 9-EtG appears to be preferred in competition experiments.[94] DNA replication mapping also showed that guanine was the preferred binding site for complexes $[(\eta^5\text{-Cp}^x)\text{Ir(1,10-phenanthroline)Cl}]\text{PF}_6$. ($\text{Cp}^x$ = Cp*, Cp^{xPh}, Cp^{xBiPh}).[92] The ability to intercalate between DNA base pairs as

determined by ethidium bromide (EtBr) displacement is strongly dependent on the type of capping ligand used, in which the more extended ligands result in enhanced EtBr displacement, suggesting that intercalation as well as direct nucleobase binding may be important for antiproliferative activity. This has also been observed for Ru(II) and Os(II) half-sandwich complexes that bear extended arene ligands.[99,100]

More recently, Ir(III) half-sandwich complexes bearing *N,N*- and *C,N* chelating ligands have been shown to induce high levels of ROS causing mitochondrial dysfunction.[101,102] Incubation with *L*-buthionine sulfoximine (*L*-BSO), which reduces the cellular levels of the ROS scavenger GSH,[103] results in a two-fold increase in antiproliferative activity for ([(η^5-Cp^{xBiPh})Ir(2-phenylpyridine)Py]PF_6, confirming the role of ROS in the MoA of these complexes. Therefore, it is likely that these complexes not only bind to DNA, but also cause mitochondrial damage.

Interestingly, it has been demonstrated that half-sandwich Ir(III) complexes can catalytically oxidise reduced *ß*-nicotinamide adenine dinucleotide (NADH) to NAD^+.[104,105] The disruption of the NAD^+/NADH redox couple could have implications for cellular energy processes, including the citric acid cycle and the oxidative phosphorylation of adenosine diphosphate (ADP) to adenosine triphosphate (ATP).[106] It has also been reported that the levels of NADH in cancer cells can be twice as high as in healthy cells, which may make NADH a good biological target for cancer therapy.[107]

The oxidation of NADH by complexes [(η^5-Cp^x)Ir(1,10-phenanthroline)OH_2]$^{2+}$ (Cp^x – Cp*, Cp^{xPh}) has been proposed to proceed by interaction of the amide unit with the Ir centre (displacing H_2O), along with ring slippage of the Cp^x from $\eta^5$to η^3 allowing formation of the Ir-H species (detected by ^{1}H NMR spectroscopy).[104] The hydride species can then become protonated to form H_2 gas or can reduce biological

substrates such as the quinone vitamin K_3 to the semiquinone derivative, where coordination of another water molecule completes the catalytic cycle (Figure 1.15).[108]

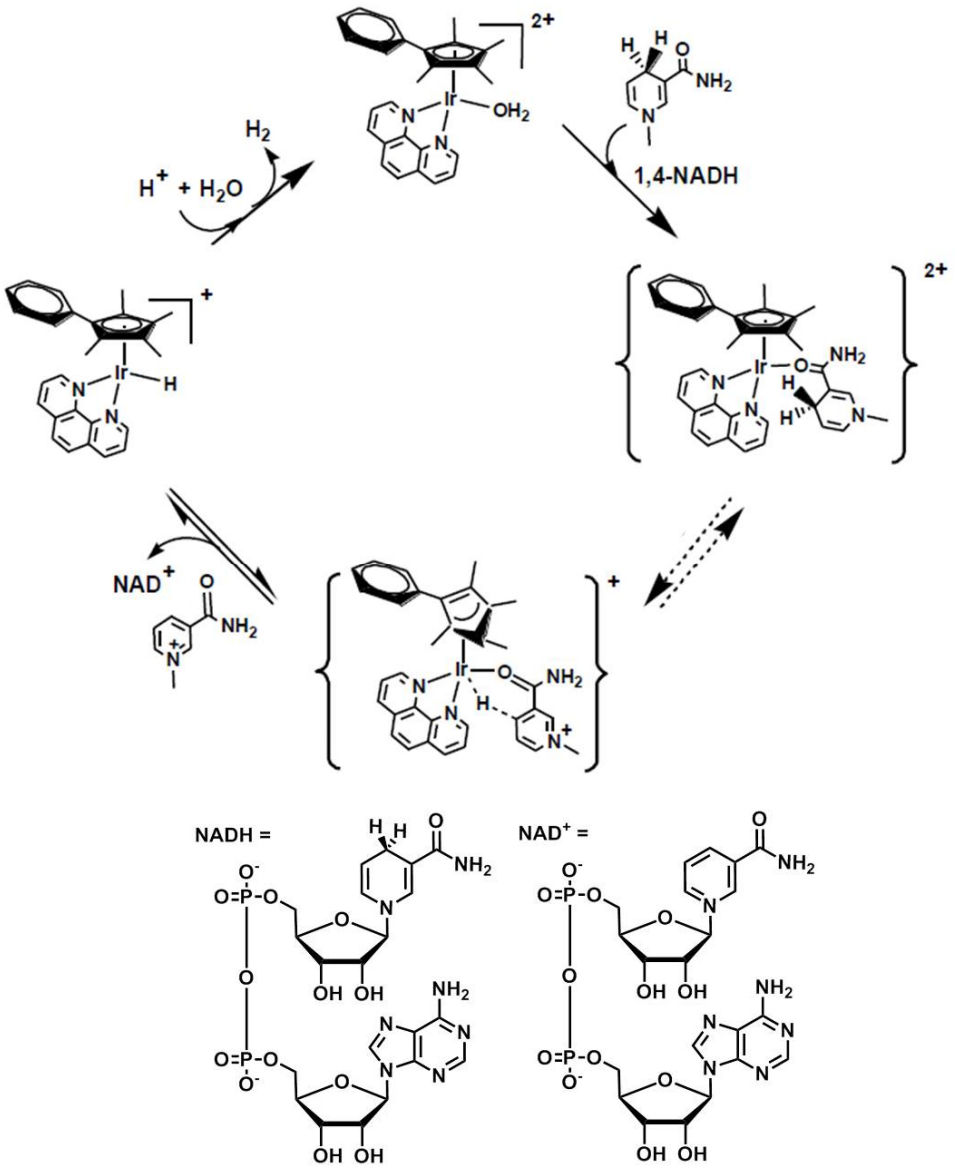

Figure 1.15. Proposed catalytic cycle for the oxidation of NADH to NAD^+ by the half-sandwich Ir(III) anticancer complex $[(\eta^5\text{-}Cp^{xPh})Ir(1,10\text{-phenanthroline})OH_2]^{2+}$ (taken from reference).[104]

The complex $[(\eta^5\text{-}Cp^{xBiPh})Ir(2\text{-phenylpyridine})Py]PF_6$ is also able to oxidise NADH to NAD^+ forming H_2O_2 *via* hydride transfer to molecular oxygen and protonation.[95]

This may contribute to the elevated levels of ROS observed in A2780 cells for this complex. The rate of reaction with NADH is slower than its chloride analogue. However, it has been hypothesised that the more stable pyridine ligand protects the complex from deactivation from biomolecules such as GSH (present in mammalian cells at a concentration of between 0.5-10 mM),[109] which may inhibit the desired reaction, ultimately leading to a more active complex (Figure 1.16).

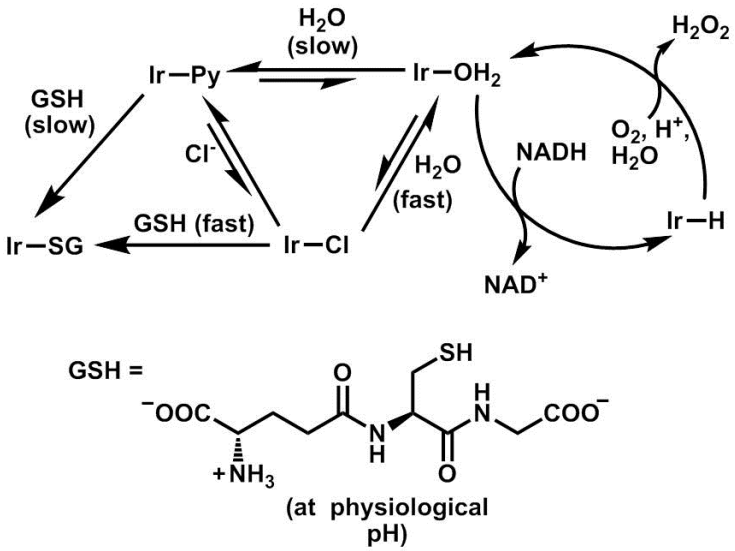

Figure 1.16. Proposed reaction pathway of [(η^5-Cp^{xBiPh})Ir(2-phenylpyridine)Py]PF_6 with NADH forming H_2O_2, and the protection from deactivation with GSH.[95]

It was demonstrated that these complexes can increase the ratio of NAD^+/NADH in A2780 cells, presumably as a consequence of their ability to oxidise NADH to NAD^+, potentially a novel mechanism of action.[104] Recently, arene Ru(II) sulfonamido ethyleneamine complexes were shown to perform the reverse function. Addition of non-toxic amounts of formate (hydride source) leads to catalytic reduction of NAD^+ to NADH in A2780 cells.[110] Indeed, performing catalysis in cells by synthetic metal complexes is an expanding field of research, which includes carbon-carbon bond formation and the removal of protection groups by organometallic compounds of palladium, ruthenium, iron and iridium.[111,112]

1.5 Bacterial Resistance

The rise of antibacterial resistance is becoming an increasing issue. Simple medical procedures may soon become dangerous due to the risk of infection,[113] with strains of bacteria such as methicillin resistant *Staphylococcus aureus* (MRSA) becoming more prominent in hospitals. Therefore, new antibacterial agents are required that can overcome this resistance. The resistance to traditional antibiotics has been partially blamed on overuse and misuse. Bacteria can build resistance through various mechanisms, including modification of the particular protein target site, the up- or down-regulation of specific membrane pumps which facilitate transport of the antimicrobial agent in/out of the cell, and the production of enzymes that can break down the active agent.[114]

1.5.1 Metal-based Antibacterial Agents

Metal-based antibacterial agents may provide hope for the treatment of bacterial infections that are becoming resistant to many organic drugs. To date, silver nitrate and silver sulfadiazine (Figure 1.17 a i) are used to prevent infections developing in burn wounds.[115] The Ag(I) ion is believed to exhibit the antibacterial activity (as well the organic fragment in silver sulfadiazene), in which silver ions may react with thiol groups in enzymes and also cause disruption of bacterial cell membranes.[116] There appears to be no intrinsic toxicity of Ag(I) ions to the human body at low concentrations, however, over-exposure to silver salts can lead to the condition of argyria in which the skin turns a silver-grey colour.[117] Silver-NHC complexes have started to receive attention as alternatives to the traditionally used silver salts as antibacterial agents (Figure 1.16 a ii).[118,119]

Although not an antibacterial, it is worth highlighting the success of the organometallic antimalarial agent ferroquine, which contains the organic antimalarial chloroquine combined with ferrocene (Figure 1.16 b) and has reached phase II clinical trials.[120] Ferroquine shows a similar mechanism of action as chloroquine against chloroquine-sensitive *P. falciparum*, centred on the inhibition of hemozoin formation. However, it is also highly active against chloroquine-resistant strains, in which it has been proposed that the change in the physicochemical, geometrical and electronic properties result in its activity.[121] It has also been hypothesised that the ability to induce ROS and interference with lipids may contribute to the enhanced antimalarial activity of ferroquine over chloroquine.[122]

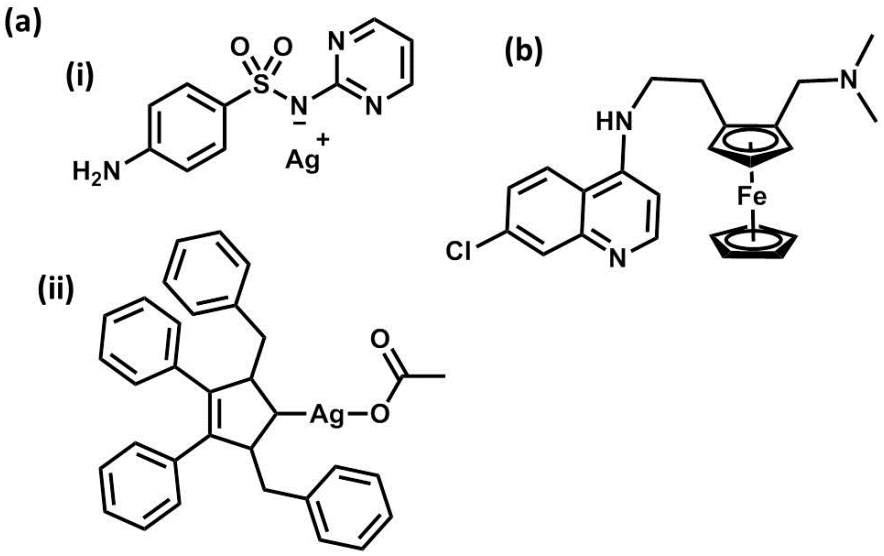

Figure 1.16 (A) Silver antibacterial agents and (B) the antimalarial agent ferroquine.

Other transition metal ions have also been investigated for antibacterial activity,[123] including Cu(II), Zn(II), Co(II), Ni(II) and Mn(II) bearing Schiff base chelating ligands, and have shown promising activities against Gram-negative *E. coli*.[124] Recently, research by Metzle-Nolte *et al.* have shown the promise of tri-metallic complexes containing a rhenium carbonyl moiety as a new class of antibacterial

agent. They show high activity against Gram-positive bacteria such as *S. aureus* and MRSA,[125] where a recent study highlighted that the Re-$(CO)_3$ unit is essential for activity.[126]

Research on the platinum-group metals as antibacterial agents has centred predominantly on Ru(II) complexes.[127] Early studies on Ru(II) coordination complexes by Dwyer *et al.* in the 1960's were focussed on inert pp scaffolds which showed good activity against Gram-positive bacteria.[128] However, further development was not performed, which may be as a consequence of the large number of antibacterial agents being investigated at that time. Due to the increasing concern over antibacterial resistance, new interest has arisen. Aldrich-Wright *et al.* have reported a series of antibacterial Ru(II) complexes that are DNA intercalators (Figure 1.17 i).[129] It appears that lipophilicity and charge are of importance for high activity against Gram-positive bacteria.[130] However, these properties can also make them toxic to healthy cells, especially when DNA is a biological target.

Organometallic Ru(II) complexes have also shown promise,[131-133] for example, a ruthenocene complex conjugated to 6-aminopenicillic acid (6-APA), incorporating an organometallic fragment with a novel ß-lactam unit (Figure 1.17 ii) shows high activity against MRSA strains.[134] The complex exhibits enhanced activity over the ferrocene derivative and 6-APA on its own, showing that the metal fragment plays a role in activity as well as the ß-lactam unit.

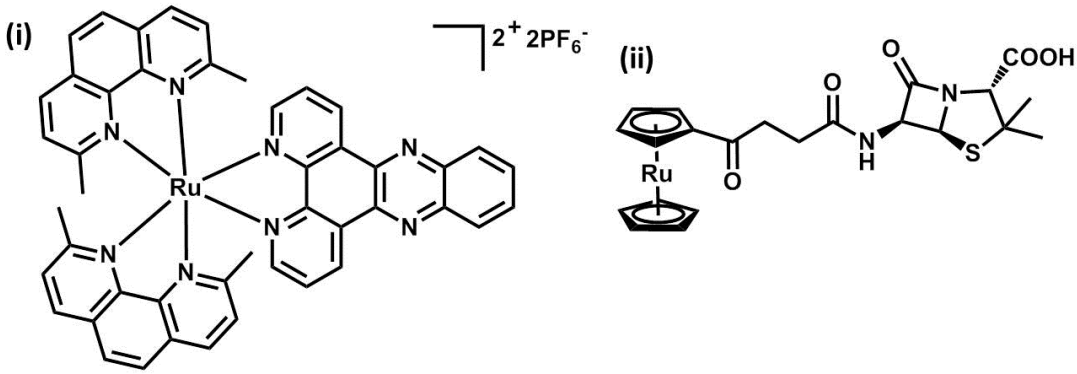

Figure 1.17 Ru(II) complexes which show promising antibacterial activity.

There are very few previous studies on the antibacterial activity of iridium complexes, with most reports being over the past 5 years. Inert polypyridyl Ir(III) octahedral complexes analogous to the Ru(II) complexes previously discussed have been studied, but showed no antibacterial activity.[135] This was attributed to switching from an overall Ru 2+ to Ir 3+ charge resulting in decreased cellular accumulation. Despite this initial result, it was then demonstrated that dinuclear octahedral Ir(III) complexes with one labile coordination site show high activity against *S. aureus* and MRSA, Figure 1.18 (i).[136] However, the complexes were shown to be bacteriostatic rather than bactericidal.

Studies into antibacterial half-sandwich Ir(III) complexes are limited, but it has been demonstrated that [(η^5-Cp*)Ir(quinolin-8-olato)Cl] showed mild activity against Gram-positive bacteria but no activity against Gram-negative bacteria (Figure 1.18 ii).[137] The complex also exhibits antiproliferative activity against the SK-MEL human melanoma cell line. Further to this, a recent report on Ru(II), Rh(III) and Ir(III) piano-stool complexes bearing a hydrazone Schiff base chelating ligand showed good antibacterial activity for Ru(II) analogue against *S. aureus* and *E. coli*, while the Rh(III) and Ir(III) derivatives showed no activity.[131] More promising are aminoacidato complexes of the type [(η^5-Cp*)Ir(aminoacidato)Cl] (Figure 1.18 iii)

which show good activity against Mycobacterium strains. Intriguningly, the L-amino acid complexes exhibit better activity than D-amino acids. Hydrophobicity appears to be important, where coordinated amino acids such as phenylalanine exhibit enhanced activity compared to glycine.

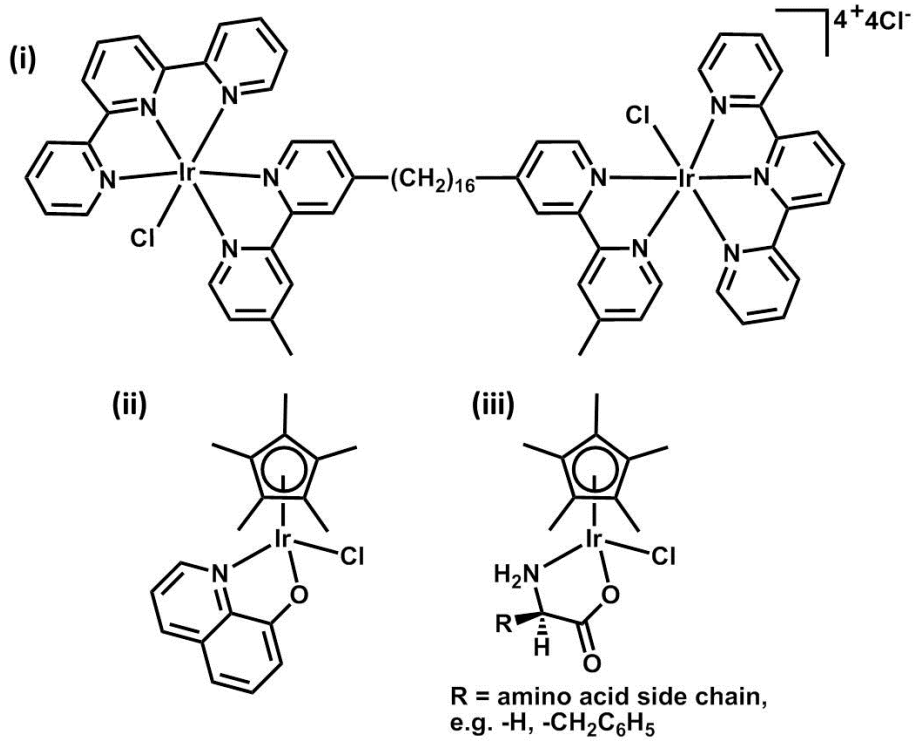

Figure 1.18 Ir(III) complexes which exhibit antibacterial activity.

1.6 Functionalising Metal Complexes

One of the major advantages of the use of metal complexes in medicinal chemistry is their ability to affect a wide range of chemical and biological properties by modification of the coordinated ligands.[29,138] Traditionally, these properties are tuned *via* the binding of different ligands to the metal complexes. For example, the use of a pyridine monodentate ligand in *N,N*-chelated Ru(II) arene complexes blocks the reactivity of the monodentate site towards hydrolysis and nucleobase binding, but the complex can be photoactivated to release the pyridine ligand.[139,140] This allows

for controlled DNA binding and hence a greater control over the cytotoxic properties of the complex.

The ability to add organic fragments that exert a particular function in the resulting complex, such as aiding selectivity towards uptake in cancerous cells over healthy cells, or delivery to a particular organelle, is an expanding area of research.[141] Pt(II) anticancer complexes cisplatin, carboplatin and oxaliplatin have been functionalised for active drug transport and delivery *via* conjugation to organic/bioorganic moieties such as estrogens, carbohydrates and peptides.[142] Metal complexes can also be modified to attach them to nanoparticles, carbon-nanotubes and polymers.[143-145] This can be advantageous for exploiting the enhanced permeability and retention (EPR) effect, where molecules of high molecular weight (such as polymers) accumulate in tumour tissue to a greater extent than in healthy cells. Polymer systems can also be decorated with molecules to enhance receptor-mediated targeting, further increasing their drug delivery and selectivity.[146]

Post-modifications to metal complexes allow for a diverse range of new complexes to be prepared from one "parent" complex, without the need to make individual ligands for coordination to the metal. In order to post-functionalise metal complexes, a functional group is generally required on one of the ligands (unless the complex is functionalised *via* addition of a ligand) that confers a particular reactivity towards another functional group. Metzler Nolte *et al.* have pioneered the bioconjugation of peptides and PNA oligomers to ferrocenyl and octahedral metal complexes using click chemistry[147] and Sonogashira coupling[148] which require the presence of an azide/alkyne or alkyne/iodide group, respectively (Figure 1.19).

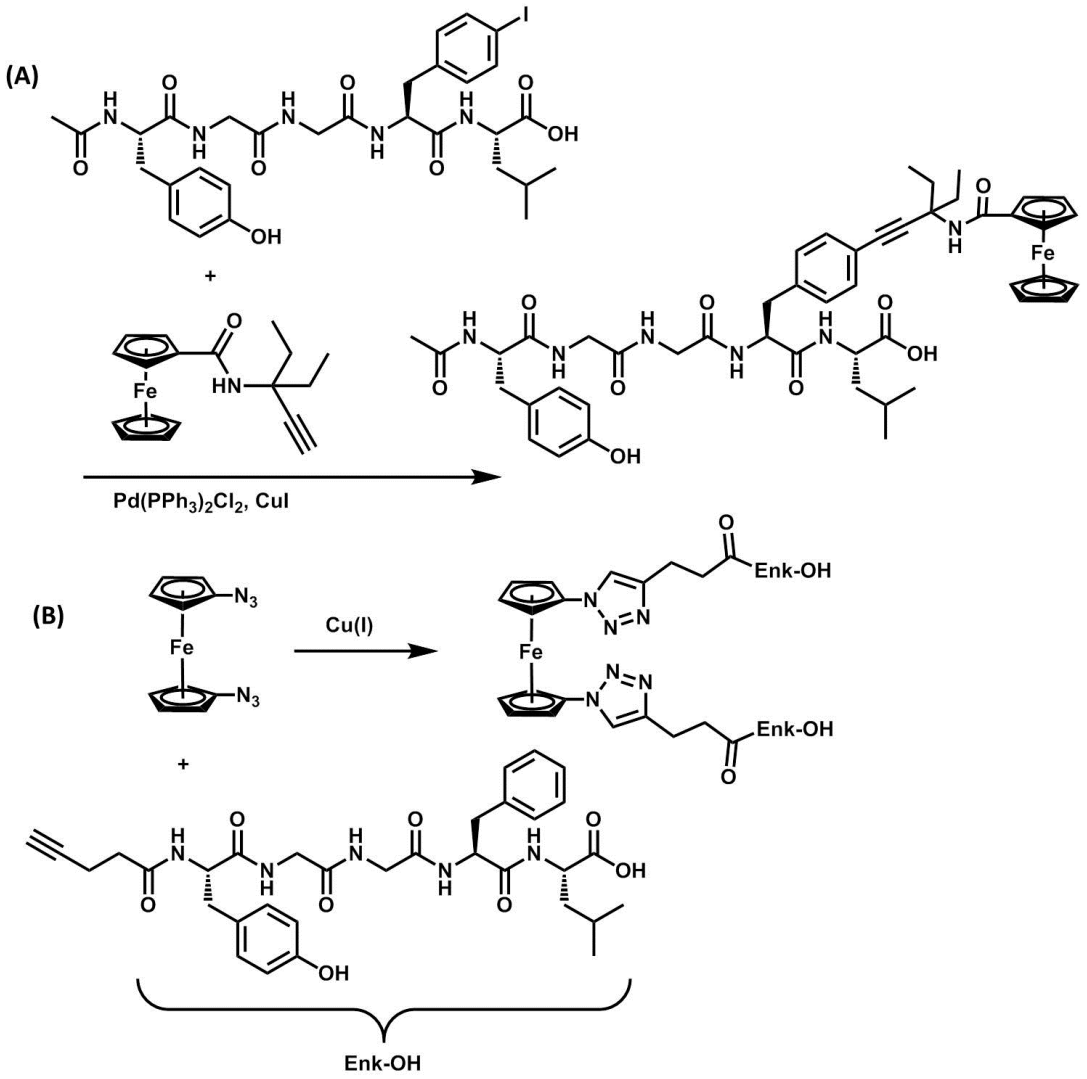

Figure 1.19 Bio-conjugation of ferrocenyl and octahedral metal complexes to the peptide enkephalin using (A) Sonogashira coupling and (B) "click-chemistry".

The use of aldehyde groups on ligands to functionalise metal complexes has recently gained some attention. The advantage of using this system is the high reactivity that aldehydes have towards nucleophilic attack by amines, which allows both organic and bioorganic amines such as peptides and proteins (which contain a free amino group) to be conjugated without using highly forcing conditions. The condensation reaction produces the imine functional group (Figure 1.20), also known as a Schiff base, which is susceptible to hydrolysis and is enhanced at acidic pH. In polymer research, this has led to the development of polymers that contain pH-sensitive imine

bonds as drug delivery vehicles for cancer drugs, where upon hydrolysis in the more acidic microtumour environment the drugs are preferentially released in cancer cells.[149,150]

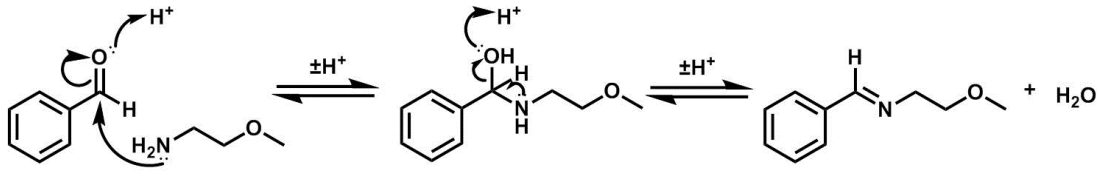

Figure 1.20 Reaction of benzaldehyde with 2-methoxylethylamine to form the corresponding imine conjugate.

The exploitation of the reactivity of aldehyde groups on a Pt(II)-NHC complex was recently demonstrated by Bellemin-Laponnaz *et al.*, who showed that either primary amines or hydroxylamines can form imines or oximes, respectively.[151] C-protected amino acids can be easily conjugated to the complex to form Schiff bases, and it was even demonstrated that the reduction of the imine to the secondary amine can be performed using the weak reducing agent $NaHB(OAc)_3$. Lo *et al*. have also demonstrated how an octahedral Ir(III) complex bearing aldehyde substituents can react with bovine serum albumin (BSA) *via* surface lysine residues, followed by reduction using $NaCNBH_3$ to form stable Ir(III)-bioconjugates with luminescent properties.[152]

1.7 Aims

Due to promising results reported for the use of *C,N*-chelated iridium(III) half-sandwich complexes as anticancer agents, a major part of this thesis is concerned with the further study of this series, with particular focus on tuning the properties

and activities of Cp* compounds *via* functionalisation of chelating and monodentate ligands. Iminopyridine *N,N*-chelated iridium(III) complexes were also investigated, examining the effects that functionality on the Cp^x ring and chelating ligand have on the chemical, antibacterial and anticancer activity. More specific aims were as follows.

1. Synthesis, characterisation and evaluation of the chemical, physicochemical and anticancer properties that arise from functionalising 2-phenylpyridine ligands in complexes of the type [(η^5-Cp*)Ir(2-phenylpyridine)Cl] with electron-donating and electron-withdrawing groups.
2. Studying the effects on the chemical and anticancer properties of chlorido and pyridyl monodentate ligands on the complex [(η^5-Cp*)Ir(2-(2'-methylphenyl)pyridine)X]$^{0/+}$.
3. Exploring the functionalisation of the anticancer complex [(η^5-Cp*)Ir(2-phenyl-5-pyridinecarboxaldehyde)Cl] by reactions with amines and peptides to form new Schiff base conjugates, including the addition of a fluorescent dansyl moiety. Reduction of the dansyl conjugate to the secondary amine was investigated to enable investigations into tracking the complex *via* confocal microscopy.
4. The synthesis, characterisation and evaluation of the solution chemistry of complexes of the type [(η^5-Cp^x)Ir(phenyliminopyridyl)Cl]PF_6 with investigations into their antibacterial and anticancer activity.

1.8 References

(1) Williams, K. J. *J. R. Soc. Med.* **2009**, *102*, 343.

(2) Zhou, Z.; Lu, Z.-R. *Wiley Interdiscip. Rev. Nanomed. Nanobiotechnol.* **2013**, *5*, 1.

(3) Caravan, P.; Ellison, J. J.; McMurry, T. J.; Lauffer, R. B. *Chem. Rev.* **1999**, *99*, 2293.

(4) Crooke, S. T.; Mirabelli, C. K. *Am. J. Med.* **1983**, *75*, 109.

(5) Vane, J.; Botting, R. *The FASEB Journal* **1987**, *1*, 89.

(6) Bierer, D. W. *Rev. Infect. Dis.* **1990**, *12*, S3.

(7) Medici, S.; Peana, M.; Nurchi, V. M.; Lachowicz, J. I.; Crisponi, G.; Zoroddu, M. A. *Coord. Chem. Rev.* **2015**, *284*, 329.

(8) Maddams, J.; Utley, M.; Moller, H. *Br. J. Cancer* **2012**, *107*, 1195.

(9) Jemal, A.; Bray, F.; Center, M. M.; Ferlay, J.; Ward, E.; Forman, D. *CA Cancer J. Clin.* **2011**, *61*, 69.

(10) Harper, B. W.; Krause-Heuer, A. M.; Grant, M. P.; Manohar, M.; Garbutcheon-Singh, K. B.; Aldrich-Wright, J. R. *Chem. Eur. J.* **2010**, *16*, 7064.

(11) Rosenberg, B.; Vancamp, L.; Trosko, J. E.; Mansour, V. H. *Nature* **1969**, *222*, 385.

(12) Hanna, N.; Einhorn, L. H. *J. Clin. Oncol.* **2014**, *32*, 3085.

(13) Lippert, B. *Cisplatin - Chemistry and Biochemistry of a Leading Anticancer Drug*; Helvetica Chimica Acta: Würzburg, 1999.

(14) Takahara, P. M.; Rosenzweig, A. C.; Frederick, C. A.; Lippard, S. J. *Nature* **1995**, *377*, 649.

(15) Ohndorf, U.-M.; Rould, M. A.; He, Q.; Pabo, C. O.; Lippard, S. J. *Nature* **1999**, *399*, 708.

(16) van der Vijgh, W. F. *Clin. Pharmacokinet.* **1991**, *21*, 242.

(17) Figure taken from http://web.mit.edu/lippardlab/gallery.html (last accessed 05/06/15).

(18) Hall, M. D.; Mellor, H. R.; Callaghan, R.; Hambley, T. W. *J. Med. Chem.* **2007**, *50*, 3403.

(19) Shi, Y.; Liu, S.-A.; Kerwood, D. J.; Goodisman, J.; Dabrowiak, J. C. *J. Inorg. Biochem.* **2012**, *107*, 6.

(20) Pendyala, L.; Cowens, J. W.; Chheda, G. B.; Dutta, S. P.; Creaven, P. J. *Cancer Res.* **1988**, *48*, 3533.

(21) Sessa, C.; Vermorken, J.; Renard, J.; Kaye, S.; Smith, D.; ten Bokkel Huinink, W.; Cavalli, F.; Pinedo, H. *J. Clin. Oncol.* **1988**, *6*, 98.

(22) Gandioso, A.; Shaili, E.; Massaguer, A.; Artigas, G.; Gonzalez-Canto, A.; Woods, J. A.; Sadler, P. J.; Marchan, V. *Chem. Commun.* **2015**, *51*, 9169.

(23) Farrer, N. J.; Woods, J. A.; Munk, V. P.; Mackay, F. S.; Sadler, P. J. *Chem. Res. Toxicol.* **2009**, *23*, 413.

(24) Farrer, N. J.; Woods, J. A.; Salassa, L.; Zhao, Y.; Robinson, K. S.; Clarkson, G.; Mackay, F. S.; Sadler, P. J. *Angew. Chem. Int. Ed.* **2010**, *49*, 8905.

(25) Sava, G.; Pacor, S.; Mestroni, G.; Alessio, E. *Clin. Exp. Metastasis* **1992**, *10*, 273.

(26) Berger, M. R.; Garzon, F. T.; Keppler, B. K.; Schmähl, D. *Anticancer Res.* **1989**, *9*, 761.

(27) Clarke, M. J.; Zhu, F.; Frasca, D. R. *Chem. Rev.* **1999**, *99*, 2511.

(28) Jaouen, G.; Beck, W.; McGlinchey, M. J. *Bioorganometallics: Biomolecules, Labeling, Medicine* **2006**, 1.

(29) Hartinger, C. G.; Dyson, P. J. *Chem. Soc. Rev.* **2009**, *38*, 391.

(30) Köpf, H.; Köpf-Maier, P. *Angew. Chem. Int. Ed. Engl.* **1979**, *18*, 477.

(31) Lümmen, G.; Sperling, H.; Luboldt, H.; Otto, T.; Rübben, H. *Cancer Chemother. Pharmacol.* **1998**, *42*, 415.

(32) Kröger, N.; Kleeberg, U. R.; Mross, K.; Edler, L.; Hossfeld, D. K. *Onkologie* **2000**, *23*, 60.

(33) Guo, M.; Guo, Z.; Sadler, P. *J. Biol. Inorg. Chem.* **2001**, *6*, 698.

(34) Allen, O. R.; Croll, L.; Gott, A. L.; Knox, R. J.; McGowan, P. C. *Organometallics* **2004**, *23*, 288.

(35) Allen, O. R.; Gott, A. L.; Hartley, J. A.; Hartley, J. M.; Knox, R. J.; McGowan, P. C. *Dalton Trans.* **2007**, 5082.

(36) Strohfeldt, K.; Tacke, M. *Chem. Soc. Rev.* **2008**, *37*, 1174.

(37) Jaouen, G.; Top, S.; Vessieres, A.; Leclercq, G.; McGlinchey, M. J. *Curr. Med. Chem.* **2004**, *11*, 2505.

(38) Gasser, G.; Ott, I.; Metzler-Nolte, N. *J. Med. Chem.* **2010**, *54*, 3.

(39) Hillard, E.; Vessières, A.; Thouin, L.; Jaouen, G.; Amatore, C. *Angew. Chem. Int. Ed.* **2006**, *45*, 285.

(40) Ganeshpandian, M.; Loganathan, R.; Suresh, E.; Riyasdeen, A.; Akbarsha, M. A.; Palaniandavar, M. *Dalton Trans.* **2014**, *43*, 1203.

(41) van Rijt, S. H.; Mukherjee, A.; Pizarro, A. M.; Sadler, P. J. *J. Med. Chem.* **2009**, *53*, 840.

(42) Nazarov, A. A.; Hartinger, C. G.; Dyson, P. J. *J. Organomet. Chem.* **2014**, *751*, 251.

(43) Morris, R. E.; Aird, R. E.; del Socorro Murdoch, P.; Chen, H.; Cummings, J.; Hughes, N. D.; Parsons, S.; Parkin, A.; Boyd, G.; Jodrell, D. I.; Sadler, P. J. *J. Med. Chem.* **2001**, *44*, 3616.

(44) Aird, R. E.; Cummings, J.; Ritchie, A. A.; Muir, M.; Morris, R. E.; Chen, H.; Sadler, P. J.; Jodrell, D. I. *Br. J. Cancer* **2002**, *86*, 1652.

(45) Chen, H.; Parkinson, J. A.; Parsons, S.; Coxall, R. A.; Gould, R. O.; Sadler, P. J. *J. Am. Chem. Soc.* **2002**, *124*, 3064.

(46) Habtemariam, A.; Melchart, M.; Fernández, R.; Parsons, S.; Oswald, I. D. H.; Parkin, A.; Fabbiani, F. P. A.; Davidson, J. E.; Dawson, A.; Aird, R. E.; Jodrell, D. I.; Sadler, P. J. *J. Med. Chem.* **2006**, *49*, 6858.

(47) Kandioller, W.; Balsano, E.; Meier, S. M.; Jungwirth, U.; Goschl, S.; Roller, A.; Jakupec, M. A.; Berger, W.; Keppler, B. K.; Hartinger, C. G. *Chem. Commun.* **2013**, *49*, 3348.

(48) Kurzwernhart, A.; Kandioller, W.; Enyedy, E. A.; Novak, M.; Jakupec, M. A.; Keppler, B. K.; Hartinger, C. G. *Dalton Trans.* **2013**, *42*, 6193.

(49) Dyson, P. J.; Sava, G. *Dalton Trans.* **2006**, 1929.

(50) Fukamachi, T.; Chiba, Y.; Wang, X.; Saito, H.; Tagawa, M.; Kobayashi, H. *Cancer Lett.* **2010**, *297*, 182.

(51) Allardyce, C. S.; Dyson, P. J.; Ellis, D. J.; Heath, S. L. *Chem. Commun.* **2001**, 1396.

(52) Casini, A.; Gabbiani, C.; Sorrentino, F.; Rigobello, M. P.; Bindoli, A.; Geldbach, T. J.; Marrone, A.; Re, N.; Hartinger, C. G.; Dyson, P. J.; Messori, L. *J. Med. Chem.* **2008**, *51*, 6773.

(53) Meggers, E.; Atilla-Gokcumen, G. E.; Grundler, K.; Frias, C.; Prokop, A. *Dalton Trans.* **2009**, 10882.

(54) Martin, E. K.; Pagano, N.; Sherlock, M. E.; Harms, K.; Meggers, E. *Inorg. Chim. Acta* **2014**, *423, Part A*, 530.

(55) Hanif, M.; Babak, M. V.; Hartinger, C. G. *Drug Discov. Today* **2014**, *19*, 1640.

(56) Peacock, A. F. A.; Habtemariam, A.; Moggach, S. A.; Prescimone, A.; Parsons, S.; Sadler, P. J. *Inorg. Chem.* **2007**, *46*, 4049.

(57) Peacock, A. F. A.; Habtemariam, A.; Fernández, R.; Walland, V.; Fabbiani, F. P. A.; Parsons, S.; Aird, R. E.; Jodrell, D. I.; Sadler, P. J. *J. Am. Chem. Soc.* **2006**, *128*, 1739.

(58) Peacock, A. F. A.; Parsons, S.; Sadler, P. J. *J. Am. Chem. Soc.* **2007**, *129*, 3348.

(59) Fu, Y.; Habtemariam, A.; Pizarro, A. M.; van Rijt, S. H.; Healey, D. J.; Cooper, P. A.; Shnyder, S. D.; Clarkson, G. J.; Sadler, P. J. *J. Med. Chem.* **2010**, *53*, 8192.

(60) Fu, Y.; Habtemariam, A.; Basri, A. M. B. H.; Braddick, D.; Clarkson, G. J.; Sadler, P. J. *Dalton Trans.* **2011**, *40*, 10553.

(61) *U.S. Geological Survey Mineral Commodity Summaries: Platinum Group Metals*, 2013, http://minerals.usgs.gov/minerals/pubs/commodity/platinum/myb1-2012-plati.pdf.

(62) Crabtree, R. H.; Felkin, H.; Morris, G. E. *J. Organomet. Chem.* **1977**, *141*, 205.

(63) Xu, Y.; Mingos, D. M. P.; Brown, J. M. *Chem. Commun.* **2008**, 199.

(64) You, Y.; Cho, S.; Nam, W. *Inorg. Chem.* **2014**, *53*, 1804.

(65) Lo, K. K.-W.; Li, S. P.-Y.; Zhang, K. Y. *New J. Chem.* **2011**, *35*, 265.

(66) Prakash, O.; Singh, P.; Mukherjee, G.; Singh, A. K. *Organometallics* **2012**, *31*, 3379.

(67) Hopmann, K. H.; Bayer, A. *Coord. Chem. Rev.* **2014**, *268*, 59.

(68) Savini, A.; Bucci, A.; Bellachioma, G.; Giancola, S.; Palomba, F.; Rocchigiani, L.; Rossi, A.; Suriani, M.; Zuccaccia, C.; Macchioni, A. *J. Organomet. Chem.* **2014**, *771*, 24.

(69) Blakemore, J. D.; Schley, N. D.; Balcells, D.; Hull, J. F.; Olack, G. W.; Incarvito, C. D.; Eisenstein, O.; Brudvig, G. W.; Crabtree, R. H. *J. Am. Chem. Soc.* **2010**, *132*, 16017.

(70) Borghede, G.; Hedelin, H.; Holmäng, S.; Johansson, K. A.; Aldenborg, F.; Pettersson, S.; Sernbo, G.; Wallgren, A.; Mercke, C. *Radiother. Oncol.* **1997**, *44*, 237.

(71) Mazeron, J.-J.; Langlois, D.; Glaubiger, D.; Huart, J.; Martin, M.; Raynal, M.; Calitchi, E.; Ganem, G.; Faraldi, M.; Feuilhade, F.; Brun, B.; Marin, L.; Le Bourgeois, J.-P.; Baillet, F.; Pierquin, B. *Int. J. Radiat. Oncol. Biol. Phys.* **1987**, *13*, 957.

(72) Sava, G.; Zorzet, S.; Perissin, L.; Mestroni, G.; Zassinovich, G.; Bontempi, A. *Inorg. Chim. Acta* **1987**, *137*, 69.

(73) Giraldi, T.; Sava, G.; Mestroni, G.; Zassinovich, G.; Stolfa, D. *Chem. Biol. Interact.* **1978**, *22*, 231.

(74) Simpson, P. V.; Schmidt, C.; Ott, I.; Bruhn, H.; Schatzschneider, U. *Eur. J. Inorg. Chem.* **2013**, *2013*, 5547.

(75) Gothe, Y.; Marzo, T.; Messori, L.; Metzler-Nolte, N. *Chem. Commun.* **2015**, *51*, 3151.

(76) Messori, L.; Marcon, G.; Orioli, P.; Fontani, M.; Zanello, P.; Bergamo, A.; Sava, G.; Mura, P. *J. Inorg. Biochem.* **2003**, *95*, 37.

(77) Marcon, G.; Casini, A.; Mura, P.; Messori, L.; Bergamo, A.; Orioli, P. *Met.-Based Drugs* **2000**, *7*, 195.

(78) Lo, K. K.-W.; Zhang, K. Y.; Leung, S.-K.; Tang, M.-C. *Angew. Chem.* **2008**, *120*, 2245.

(79) Lau, J. S.-Y.; Lee, P.-K.; Tsang, K. H.-K.; Ng, C. H.-C.; Lam, Y.-W.; Cheng, S.-H.; Lo, K. K.-W. *Inorg. Chem.* **2009**, *48*, 708.

(80) Ruiz, J.; Vicente, C.; de Haro, C.; Bautista, D. *Inorg. Chem.* **2013**, *52*, 974.

(81) Feng, L.; Geisselbrecht, Y.; Blanck, S.; Wilbuer, A.; Atilla-Gokcumen, G. E.; Filippakopoulos, P.; Kräling, K.; Celik, M. A.; Harms, K.; Maksimoska, J.; Marmorstein, R.; Frenking, G.; Knapp, S.; Essen, L.-O.; Meggers, E. *J. Am. Chem. Soc.* **2011**, *133*, 5976.

(82) Dörr, M.; Meggers, E. *Curr. Opin. Chem. Biol.* **2014**, *19*, 76.

(83) Kastl, A.; Wilbuer, A.; Merkel, A. L.; Feng, L.; Di Fazio, P.; Ocker, M.; Meggers, E. *Chem. Commun.* **2012**, *48*, 1863.

(84) Leung, C.-H.; Liu, L.-J.; Lu, L.; He, B.; Kwong, D. W. J.; Wong, C.-Y.; Ma, D.-L. *Chem. Commun.* **2015**, *51*, 3973.

(85) Liu, Z.; Sadler, P. J. *Acc. Chem. Res.* **2014**, *47*, 1174.

(86) Omae, I. *Coord. Chem. Rev.* **2014**, *280*, 84.

(87) Schäfer, S.; Sheldrick, W. S. *J. Organomet. Chem.* **2007**, *692*, 1300.

(88) Schäfer, S.; Ott, I.; Gust, R.; Sheldrick, W. S. *Eur. J. Inorg. Chem.* **2007**, *2007*, 3034.

(89) Almodares, Z.; Lucas, S. J.; Crossley, B. D.; Basri, A. M.; Pask, C. M.; Hebden, A. J.; Phillips, R. M.; McGowan, P. C. *Inorg. Chem.* **2014**, *53*, 727.

(90) Lucas, S. J.; Lord, R. M.; Wilson, R. L.; Phillips, R. M.; Sridharan, V.; McGowan, P. C. *Dalton Trans.* **2012**, *41*, 13800.

(91) Lord, R. M.; Hebden, A. J.; Pask, C. M.; Henderson, I. R.; Allison, S.; Shepherd, S. L.; Phillips, R. M.; McGowan, P. C. *J. Med. Chem.* **2015**, *58*, 4940.

(92) Liu, Z.; Habtemariam, A.; Pizarro, A. M.; Fletcher, S. A.; Kisova, A.; Vrana, O.; Salassa, L.; Bruijnincx, P. C. A.; Clarkson, G. J.; Brabec, V.; Sadler, P. J. *J. Med. Chem.* **2011**, *54*, 3011.

(93) Liu, Z.; Habtemariam, A.; Pizarro, A. M.; Clarkson, G. J.; Sadler, P. J. *Organometallics* **2011**, *30*, 4702.

(94) Liu, Z.; Salassa, L.; Habtemariam, A.; Pizarro, A. M.; Clarkson, G. J.; Sadler, P. J. *Inorg. Chem.* **2011**, *50*, 5777.

(95) Liu, Z.; Romero-Canelón, I.; Qamar, B.; Hearn, J. M.; Habtemariam, A.; Barry, N. P. E.; Pizarro, A. M.; Clarkson, G. J.; Sadler, P. J. *Angew. Chem. Int. Ed.* **2014**, *53*, 3941.

(96) Poth, T.; Paulus, H.; Elias, H.; Dücker-Benfer, C.; van Eldik, R. *Eur. J. Inorg. Chem.* **2001**, *2001*, 1361.

(97) Boerner, L. J. K.; Zaleski, J. M. *Curr. Opin. Chem. Biol.* **2005**, *9*, 135.

(98) Pizarro, A. M.; Sadler, P. J. *Biochimie* **2009**, *91*, 1198.

(99) Liu, H.-K.; Berners-Price, S. J.; Wang, F.; Parkinson, J. A.; Xu, J.; Bella, J.; Sadler, P. J. *Angew. Chem.* **2006**, *118*, 8333.

(100) Kostrhunova, H.; Florian, J.; Novakova, O.; Peacock, A. F. A.; Sadler, P. J.; Brabec, V. *J. Med. Chem.* **2008**, *51*, 3635.

(101) Novohradsky, V.; Zerzankova, L.; Stepankova, J.; Kisova, A.; Kostrhunova, H.; Liu, Z.; Sadler, P. J.; Kasparkova, J.; Brabec, V. *Metallomics* **2014**, *6*, 1491.

(102) Hearn, J. M.; Romero-Canelón, I.; Qamar, B.; Liu, Z.; Hands-Portman, I.; Sadler, P. J. *ACS Chem. Biol.* **2013**, *8*, 1335.

(103) Goto, S.; Iida, T.; Cho, S.; Oka, M.; Kohno, S.; Kondo, T. *Free Radical Res.* **1999**, *31*, 549.

(104) Betanzos-Lara, S.; Liu, Z.; Habtemariam, A.; Pizarro, A. M.; Qamar, B.; Sadler, P. J. *Angew. Chem. Int. Ed.* **2012**, *51*, 3897.

(105) Maenaka, Y.; Suenobu, T.; Fukuzumi, S. *J. Am. Chem. Soc.* **2011**, *134*, 367.

(106) Ying, W. *Antioxid. Redox Signaling* **2007**, *10*, 179.

(107) Yu, Q.; Heikal, A. A. *J. Photochem. Photobiol. B: Biol.* **2009**, *95*, 46.

(108) Liu, Z.; Deeth, R. J.; Butler, J. S.; Habtemariam, A.; Newton, M. E.; Sadler, P. J. *Angew. Chem. Int. Ed.* **2013**, *52*, 4194.

(109) Hwang, C.; Sinskey, A.; Lodish, H. *Science* **1992**, *257*, 1496.

(110) Soldevila-Barreda, J. J.; Romero-Canelón, I.; Habtemariam, A.; Sadler, P. J. *Nat. Commun.* **2015**, *6*.

(111) Völker, T.; Meggers, E. *Curr. Opin. Chem. Biol.* **2015**, *25*, 48.

(112) Soldevila-Barreda, J. J.; Sadler, P. J. *Curr. Opin. Chem. Biol.* **2015**, *25*, 172.

(113) Davies, J.; Davies, D. *Microbiol. Mol. Biol. Rev.* **2010**, *74*, 417.

(114) Tenover, F. C. *Am. J. Infect. Control.* **2006**, *34*, S3.

(115) Dai, T.; Huang, Y.-Y.; Sharma, S. K.; Hashmi, J. T.; Kurup, D. B.; Hamblin, M. R. *Recent. Pat. Antiinfect. Drug. Discov.* **2010**, *5*, 124.

(116) Jung, W. K.; Koo, H. C.; Kim, K. W.; Shin, S.; Kim, S. H.; Park, Y. H. *Appl. Environ. Microbiol.* **2008**, *74*, 2171.

(117) Fisher, N. M.; Marsh, E.; Lazova, R. *J. Am. Acad. Dermatol.* **2003**, *49*, 730.

(118) Tacke, M. *J. Organomet. Chem.* **2015**, *782*, 17.

(119) Asekunowo, P. O.; Haque, R. A.; Razali, M. R.; Budagumpi, S. *Appl. Organomet. Chem.* **2015**, *29*, 126.

(120) Dive, D.; Biot, C. *ChemMedChem* **2008**, *3*, 383.

(121) Biot, C.; Taramelli, D.; Forfar-Bares, I.; Maciejewski, L. A.; Boyce, M.; Nowogrocki, G.; Brocard, J. S.; Basilico, N.; Olliaro, P.; Egan, T. J. *Mol. Pharm.* **2005**, *2*, 185.

(122) Dubar, F.; Khalife, J.; Brocard, J.; Dive, D.; Biot, C. *Molecules* **2008**, *13*, 2900.

(123) Ng, N. S.; Leverett, P.; Hibbs, D. E.; Yang, Q.; Bulanadi, J. C.; Jie Wu, M.; Aldrich-Wright, J. R. *Dalton Trans.* **2013**, *42*, 3196.

(124) Neelakantan, M. A.; Esakkiammal, M.; Mariappan, S. S.; Dharmaraja, J.; Jeyakumar, T. *Indian. J. Pharm. Sci.* **2010**, *72*, 216.

(125) Wenzel, M.; Patra, M.; Senges, C. H. R.; Ott, I.; Stepanek, J. J.; Pinto, A.; Prochnow, P.; Vuong, C.; Langklotz, S.; Metzler-Nolte, N.; Bandow, J. E. *ACS Chem. Biol.* **2013**.

(126) Patra, M.; Wenzel, M.; Prochnow, P.; Pierroz, V.; Gasser, G.; Bandow, J. E.; Metzler-Nolte, N. *Chem. Sci.* **2015**, *6*, 214.

(127) Li, F.; Collins, J. G.; Keene, F. R. *Chem. Soc. Rev.* **2015**.

(128) Dwyer, F. P.; Gyarfas, E. C.; Rogers, W. P.; Koch, J. H. *Nature* **1952**, *170*, 190.

(129) Bolhuis, A.; Hand, L.; Marshall, J. E.; Richards, A. D.; Rodger, A.; Aldrich-Wright, J. *Eur. J. Pharm. Sci.* **2011**, *42*, 313.

(130) Dwyer, F. P.; Reid, I. K.; Shulman, A.; Laycock, G. M.; Dixson, S. *Aust. J. Exp. Biol. Med.* **1969**, *47*, 203.

(131) Palepu, N.; Nongbri, S. L.; Premkumar, J. R.; Verma, A.; Bhattacharjee, K.; Joshi, S. R.; Forbes, S.; Mozharivskyj, Y.; Thounaojam, R.; Aguan, K.; Kollipara, M. *J. Biol. Inorg. Chem.* **2015**, *20*, 619.

(132) Allardyce, C. S.; Dyson, P. J.; Ellis, D. J.; Salter, P. A.; Scopelliti, R. *J. Organomet. Chem.* **2003**, *668*, 35.

(133) Tripathy, S. K.; Taviti, A. C.; Dehury, N.; Sahoo, A.; Pal, S.; Beuria, T. K.; Patra, S. *Dalton Trans.* **2015**, *44*, 5114.

(134) Lewandowski, E. M.; Skiba, J.; Torelli, N. J.; Rajnisz, A.; Solecka, J.; Kowalski, K.; Chen, Y. *Chem. Commun.* **2015**, *51*, 6186.

(135) Pandrala, M.; Li, F.; Wallace, L.; Steel, P. J.; Moore II, B.; Autschbach, J.; Collins, J. G.; Keene, F. R. *Aust. J. Chem.* **2013**, *66*, 1065.

(136) Pandrala, M.; Li, F.; Feterl, M.; Mulyana, Y.; Warner, J. M.; Wallace, L.; Keene, F. R.; Collins, J. G. *Dalton Trans.* **2013**, *42*, 4686.

(137) Śliwińska, U.; Pruchnik, F. P.; Ułaszewski, S.; Latocha, M.; Nawrocka-Musiał, D. *Polyhedron* **2010**, *29*, 1653.

(138) Noffke, A. L.; Habtemariam, A.; Pizarro, A. M.; Sadler, P. J. *Chem. Commun.* **2012**, *48*, 5219.

(139) Betanzos-Lara, S.; Salassa, L.; Habtemariam, A.; Novakova, O.; Pizarro, A. M.; Clarkson, G. J.; Liskova, B.; Brabec, V.; Sadler, P. J. *Organometallics* **2012**, *31*, 3466.

(140) Barragán, F.; López-Senín, P.; Salassa, L.; Betanzos-Lara, S.; Habtemariam, A.; Moreno, V.; Sadler, P. J.; Marchán, V. *J. Am. Chem. Soc.* **2011**, *133*, 14098.

(141) Noor, F.; Kinscherf, R.; Bonaterra, G. A.; Walczak, S.; Wölfl, S.; Metzler-Nolte, N. *ChemBioChem* **2009**, *10*, 493.

(142) Wang, X.; Guo, Z. *Chem. Soc. Rev.* **2013**, *42*, 202.

(143) Butler, J. S.; Sadler, P. J. *Curr. Opin. Chem. Biol.* **2013**, *17*, 175.

(144) Mi, P.; Cabral, H.; Kokuryo, D.; Rafi, M.; Terada, Y.; Aoki, I.; Saga, T.; Takehiko, I.; Nishiyama, N.; Kataoka, K. *Biomaterials* **2013**, *34*, 492.

(145) Huang, C.; Neoh, K. G.; Xu, L.; Kang, E. T.; Chiong, E. *Biomacromolecules* **2012**, *13*, 2513.

(146) Eliezar, J.; Scarano, W.; Boase, N. R. B.; Thurecht, K. J.; Stenzel, M. H. *Biomacromolecules* **2015**, *16*, 515.

(147) Gasser, G.; Pinto, A.; Neumann, S.; Sosniak, A. M.; Seitz, M.; Merz, K.; Heumann, R.; Metzler-Nolte, N. *Dalton Trans.* **2012**, *41*, 2304.

(148) Hoffmanns, U.; Metzler-Nolte, N. *Bioconjugate Chem.* **2006**, *17*, 204.

(149) Xu, X.; Flores, J. D.; McCormick, C. L. *Macromolecules* **2011**, *44*, 1327.

(150) Bae, Y.; Jang, W.-D.; Nishiyama, N.; Fukushima, S.; Kataoka, K. *Mol. Biosyst.* **2005**, *1*, 242.

(151) Dahm, G.; Borré, E.; Guichard, G.; Bellemin-Laponnaz, S. *Eur. J. Inorg. Chem.* **2015**, *2015*, 1665.

(152) Lee, P.-K.; Liu, H.-W.; Yiu, S.-M.; Louie, M.-W.; Lo, K. K.-W. *Dalton Trans.* **2011**, *40*, 2180.

Chapter 2

Methods and Instrumentation

This chapter describes the experimental techniques and instrumentation used throughout this thesis. The syntheses of the iridium dimers used to make the half-sandwich complexes are described. Detailed procedures for specific experiments are described in the appropriate chapters.

2.1 Synthesis of Iridium Dimers

2.1.1 Materials

$IrCl_3.3H_2O$ (99%) was purchased from Precious Metals Online (Australia). 1,2,3,4,5-Pentamethylcyclopentadiene (95%), 2,3,4,5-tetramethyl-2-cyclo-pentenone (95%), 4-bromobiphenyl (98%), n-butyllithium (1.6 M in hexanes) and phenyllithium (1.6 M in dibutylether) were purchased from Sigma-Aldrich (UK). All solvents used for synthesis were anhydrous and used without further drying/purification. The synthesis of 3-phenyl-1,2,4,5-tetramethyl-1,3-cyclopentandiene ($Cp^{xPh}H$)[1] and 3-biphenyl-1,2,4,5-tetramethyl-1,3-cyclopentandiene ($Cp^{xBiPh}H$)[2] was carried out as previously reported (Figure 2.1).

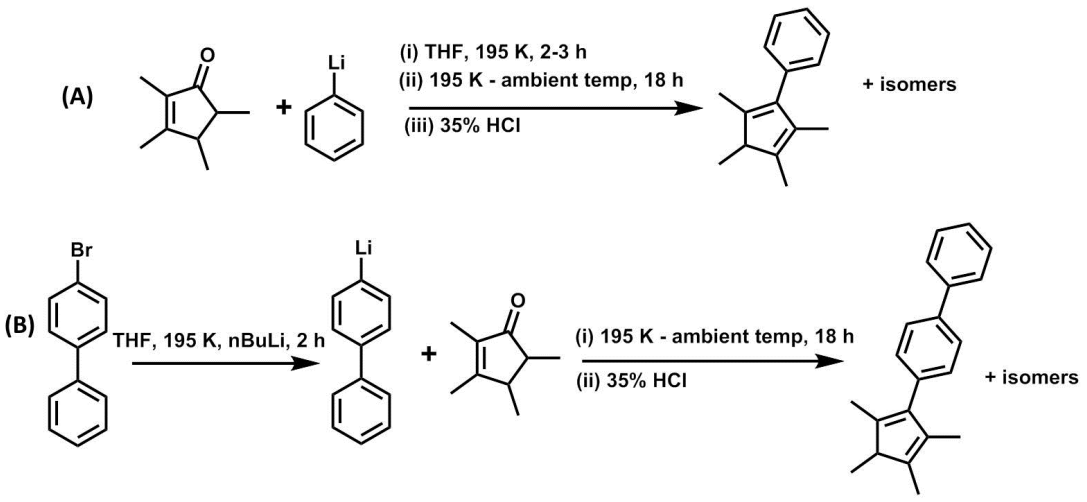

Figure 2.1. Synthetic route to (A) $Cp^{xPh}H$ and (B) $Cp^{xBiPh}H$.

2.1.2 Preparation of Iridium Dimers

The preparation of **$[(\eta^5\text{-Cp*})IrCl_2]_2$** was carried out using two different routes reported in literature.

Method A:[3] 1,2,3,4,5-pentamethylcyclopentadiene (7 g, 51.5 mmol) was dissolved in anhydrous MeOH (200 mL) under N_2 and was stirred at ambient temp for 5 min. $IrCl_3.3H_2O$ (2 g, 5.67 mmol) was added and the reaction mixture was heated under reflux for 48 h. The solution was cooled to ambient temperature and the precipitate was isolated *via* filtration under reduced pressure and washed with Et_2O without further purification (1.815 g, 80%). **^{1}H NMR** (400 MHz, $CDCl_3$) δ = 1.59 (s, 30 H).

Method B:[4] 1,2,3,4,5-pentamethylcyclopentadiene (1.16 g, 1.34 mL, 8.56 mmol) was placed in a microwave vial, MeOH (10 mL) was added and the solution stirred at ambient temp for 5 min. $IrCl_3.3H_2O$ (1 g, 2.84 mmol) was added and the vial was placed in a microwave reactor (413 K, 150 W, 250 psi, 5 min). The reaction was cooled to ambient temp, where the product was isolated *via* filtration under reduced pressure and washed with Et_2O without further purification (0.92 g, 81%). **^{1}H NMR** (400 MHz, $CDCl_3$) δ = 1.59 (s, 30H).

$[(\eta^5\text{-Cp}^{xPh})IrCl_2]_2$ [2] 3-phenyl-1,2,4,5-tetramethyl-1,3-cyclopentandiene (1.7 g, 8.5 mmol) was dissolved in anhydrous MeOH (60 mL) under N_2 and was stirred at ambient temp for 5 min. $IrCl_3.3H_2O$ (1.7 g, 4.82 mmol) was added and the reaction mixture was heated under reflux for 48 h. The solution was cooled to ambient temperature and the precipitate was isolated *via* filtration under reduced pressure and washed with Et_2O without further purification (1.01 g, 46%). **^{1}H NMR** (400 MHz, $CDCl_3$) δ = 7.57-7.56 (m, 4H), 7.36-7.35 (m, 6H), 1.72 (s, 12H), 1.63 (s, 12H).

The synthesis of **[(η^5-Cp^{xBiPh})IrCl$_2$]$_2$** has been previously reported[2] but not *via* microwave synthesis. The yield obtained using the microwave reactor (65%) is higher than that obtained using the previously reported route (22%).

[(η^5-Cp^{xBiPh})IrCl$_2$]$_2$ 3-biphenyl-1,2,4,5-tetramethyl-1,3-cyclopentandiene (1.5 g, 5.47 mmol) was placed in a microwave vial, MeOH (13 mL) added and the solution stirred at ambient temp for 5 min. $IrCl_3.3H_2O$ (0.814 g, 2.31 mmol) was added and the vial was placed in a microwave reactor (413 K, 150 W, 250 psi, 5 min). The reaction was cooled to ambient temp, where the product was isolated *via* filtration under reduced pressure and washed with Et_2O without further purification (0.802 g, 65%). **^{1}H NMR** (400 MHz, $CDCl_3$) δ =7.67-7.64 (m, 4H), 7.60-7.56 (m, 8H), 7.45-7.41 (m, 4H), 7.37-7.32 (m, 2H), 1.75 (s, 12H), 1.69 (s, 12H).

2.2 Methods and Instrumentation

2.2.1 Microwave Reactor

Some syntheses were performed using microwave-assisted chemistry, which utilises the ability to increase the temperatures at which reactions take place beyond traditional laboratory techniques, and increase solvent molecular vibrations, allowing reactions to proceed at a faster rate.[5] The CEM Discovery-SP microwave reactor was used with specific conditions given in the appropriate chapters.

2.2.2 Nuclear Magnetic Resonance (NMR) Spectroscopy

^{1}H NMR spectra were obtained in 5 mm NMR tubes at 298 K (unless stated otherwise) on either Bruker DPX-300, Bruker DPX-400, or AV III 600 NMR spectrometers. ^{1}H NMR chemical shifts were internally referenced to ($CHCD_2$)(CD_3)SO (2.50 ppm) for dmso-d_6, $CHCl_3$ (7.26 ppm) for chloroform-d_1,

($C\mathit{H}D_2$)(CD_3)CO (2.05 ppm) for acetone-d_6, ($C\mathit{H}D_2$)CD_2OD (1.11 ppm) for ethanol-d_6, and 1,4-dioxane (3.75 ppm) for aqueous solutions.

1D ^{1}H NMR spectra were recorded using standard pulse sequences. Data were typically acquired using 16-128 transients into 32 k data points over a spectral width of 14 ppm. For detection of Ir-H species, data was acquired using 128-256 transients into 32 k data points over a spectral width of 40 ppm, with the centre at 0 ppm relative to the signal for dioxane (3.75 ppm) and T_1 relaxation time of 2 s. 2D correlation spectroscopy (COSY) spectra were acquired using 8 transients into 1024 data points.

Experiments in aqueous solution were performed using the Shaka (Double Pulse Field Gradient Spin Echo - DPFGSE) water suppression technique to reduce the intensity of the *H*OD signal.[6]

2.2.3 Mass Spectrometry

2.2.3.1 Electro-Spray Ionisation Mass Spectrometry (ESI-MS)

Positive-ion ESI spectra were obtained on a Bruker Esquire 2000 ion trap spectrometer. Samples were prepared in either MeOH or CH_3CN. The mass spectra were recorded with a scan range of either m/z 50-500 or m/z 400-1000. Data were processed using Data Analysis 3.3 (Bruker Daltonics). Assignment of iridium species was aided by the Ir isotopic pattern as described in section 1.4.

2.2.3.2 High-Resolution Mass Spectrometry (HR-MS)

Positive-ion spectra were obtained on a Bruker MaXis UHR-TOF spectrometer by Dr. Lijang Song and Mr. Phillip Aston (Department of Chemistry, University of Warwick). Samples were prepared in either MeOH or CH_3CN and typically injected at 2 μL min^{-1}. Source conditions used were as follows: nebuliser gas (N_2) 0.4 bar;

dry gas (N_2) 4 L min^{-1} and dry temp 453 K; funnel RF 200V; multiple RF 200; quadrupole ion energy 4 eV; collision cell 5 eV; ion cooler RF settings, ramp from 50 to 250 V. Data were processed using Data Analysis 3.3 (Bruker Daltonics). Assignment of iridium species was aided by the Ir isotopic pattern as described in section 1.4.

2.2.4 Elemental Analysis

CHN elemental analyses were carried out on a CE-440 elemental analyser by Exeter Analytical (UK) Ltd.

2.2.5 High Performance Liquid Chromatography (HPLC)

HPLC was utilised to determine the purity of samples, the relative hydrophobicity of a series of complexes and to resolve enantiomeric mixtures chirally. Where reactions or stability have been analysed by HPLC, specific conditions are stated in the relevant chapter.

2.2.5.1 Purity Determination

Purity determinations by RP-HPLC were made using the Agilent 1200 system with a VWD and 100 μL loop. The column used was an Agilent Zorbax Eclipse Plus C18, 250 × 4.6 mm with a 5 μm pore size. The mobile phase was H_2O 0.1% TFA and CH_3CN 0.1% TFA, with a flow rate of 1 mL min^{-1}. The detection wavelength was set at 254 nm and the reference wavelength at either 360 nm or 510 nm. Sample injections were half the loop volume (50 μL) with needle washes of MeOH and H_2O between injections. It was assumed that all species in a sample have the same extinction coefficient at 254 nm. All peaks were manually integrated to gain the percentage area. The gradient used is shown in Figure 2.2.

Time (min)	%B
0	10
30	80
40	80
41	10
55	10

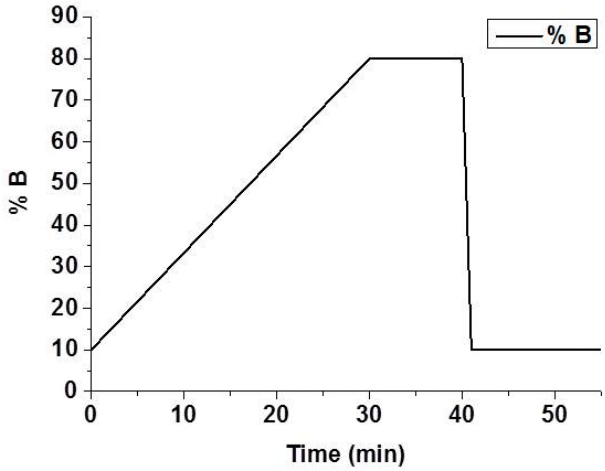

Figure 2.2. HPLC method used the solvent gradients for purity determinations using H_2O 0.1% TFA (solvent A) and CH_3CN 0.1% TFA (solvent B).

2.2.5.2 Relative Hydrophobicity Measurements

RP-HPLC relies on the relative interactions of the species of interest with the hydrophobic stationary phase and the hydrophilic mobile phase, in which a more hydrophobic compound will have a higher retention time (t_R) than a less hydrophobic compound under the same conditions. This allows the evaluation of the relative hydrophobicity of a series of structurally similar compounds.

Measurements were performed using the Agilent 1200 system with a VWD and 100 μL loop. The column was an Agilent Zorbax Eclipse Plus C18, 150 × 4.6 mm with a 5 μm pore size. The mobile phase was H_2O (50 mM NaCl)/H_2O/CH_3CN 1:1 (50 mM NaCl), with a flow rate of 1 mL min^{-1}. The detection wavelength was set at 254 nm with the reference wavelength at 360 nm. Sample injections were half the loop volume (50 μL) with needle washes of H_2O between injections. All compounds were dissolved in 10% MeOH/90% H_2O (v/v) in 50 mM NaCl to ensure that hydrolysis was prevented. The gradient used is shown in Figure 1.3.

Time (min)	%B
0	20
15	100
40	100
52	20
57	20

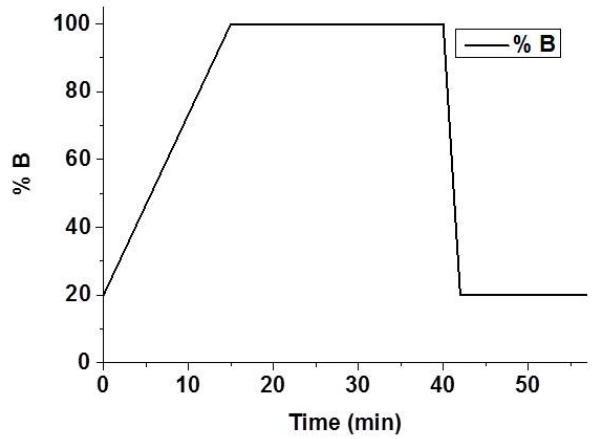

Figure 2.3. HPLC method used for relative hydrophobicity measurements using H_2O 50 mM NaCl (solvent A) and H_2O/CH_3CN 1:1 50 mM NaCl (solvent B).

2.2.5.3 Chiral Resolution

Enantiomeric separation of complexes was performed using chiral NP-HPLC with the assistance of Dr. Ruth McQuitty (Department of Chemistry, University of Warwick). The Agilent 1200 system with a VWD and 50 μL loop was used together with a CHIRALPAK® IA column (amylose tris(3,5-dimethylphenylcarbamate)) immobilised on 3 μm silica-gel, 250 × 4.6 mm. The mobile phase was heptane (70%) and ethanol (30%) with both solvents containing 0.5% TEA and 0.3% TFA. The detection wavelength was 260 nm, with a volume injection of half the loop volume (25 μL) at a concentration of 1 mg mL^{-1}.

2.2.6 Liquid Chromatography – Mass Spectrometry (LC-MS)

LC-MS analyses were carried out on amaZon X Agilent system coupled to a Bruker HCT-Ultra ETD II PTR PTM mass spectrometer. The mass spectrometer was operated in electrospray positive ion mode with a scan range of 50 – 2,000 m/z. Source conditions used were: end plate offset at – 500 V; capillary at -4500 V; nebuliser gas (N_2) 1.7 bar; dry gas (N_2) 8 L min^{-1} and dry temp 473 K; funnel RF 309 Vpp; multiple RF 309 Vpp; quadrupole ion energy 4 eV; collision cell 5 eV; ion

cooler RF settings, ramp from 50 to 250 V. Data were processed using Data Analysis 3.3 (Bruker Daltonics). Assignment of iridium species was aided by the Ir isotopic pattern as described in section 1.4.

2.2.7 Electronic Absorption (UV-Vis) Spectroscopy

UV-Vis absorption spectra were recorded on a Varian Cary 300 UV-Vis spectrophotometer in 1 cm path-length quartz cuvettes (600 μL) with a PTP1 Peltier temperature controller. Spectra were recorded at either 298 or 310 K (specific solvents are specified in relevant chapters) over a spectral width of 200-800 nm, bandwith of 1.0 nm and a scan rate of 600 nm min^{-1}. The spectra were processed using UV-Winlab software for Windows.

2.2.8 X-ray Crystallography

X-ray diffraction data were collected and processed by Dr. Guy Clarkson (Department of Chemistry, University of Warwick). Diffraction data were obtained on an Oxford Diffraction Gemini four-circle system with a Ruby CCD area detector using Mo Kα radiation. Absorption corrections were applied using ASPACK.[7] The crystals were mounted in oil and held at either 100 or 150 K with the Oxford Cryosystem Cobra. The structures were solved by direct methods using SHELXS (TREF)[8] with additional light atoms found by Fourier methods. Complexes were refined against F^2 using SHELXL.[9]

Mercury 3.3 was used to analyse the data and to generate the structural images.

To assess whether bond distances were statistically different (bond difference > 3σ), σ was defined as:

$$\sigma = \sqrt{(\sigma_1^2 + \sigma_2^2)}$$

where σ_1 and σ_2 are the bond length standard deviations of the two bond lengths being compared.

2.2.9 Density Functional Theory (DFT) Calculations

This work was carried out under the guidance of Prof. Rob Deeth (Department of Chemistry, University of Warwick). All calculations were performed using the Gaussian 03 package.[10] Geometry optimisation calculations were performed in the gas phase with the hybrid functional PBE1PBE.[11] The LanL2DZ basis set and effective core potential[12] were used for the Ir atom, and the 6-31+G** basis set was used for all other atoms.[13] The nature of all stationary points was confirmed by performing a normal-mode analysis. The calculations performed were used to generate electrostatic potential surfaces (EPS) of the complexes. Positive and negative regions are represented by a colour scale of blue and red, respectively, and mapped on electron density (isovalue = 0.04) of the molecules.

2.2.10 Inductively Coupled Plasma – Optical Emission Spectroscopy (ICP-OES)

ICP-OES analyses were carried out on a PerkinElmer Optima 5300 DV series ICP-OES instrument. The water used for ICP-OES analysis was doubly deionise water (DDW) using a Millipore Milli-Q water purification system and a USF Elga UHQ water deionizer. The iridium Specupure plasma standard (Alfa Asar, 1000 ppm in 10% HCl) was diluted with 2.5% HNO_3 DDW to prepare calibrants freshly at the required concentration range (see appropriate sections for concentration of standards

used). The calibrants and blanks were all spiked with NaCl to match the salt content of the samples being analysed.

2.2.11 Inductively Coupled Plasma – Mass Spectrometry (ICP-MS)

ICP-MS analyses were carried out on an Agilent Technologies 75000 series ICP-MS instrument, using DDW from a Millipore Milli-Q water purification system and a USF Elga UHQ water deionizer. The iridium Specupure plasma standard (Alfa Asar, 1000 ppm in 10% HCl) was diluted with 2.5% HNO_3 DDW to prepare calibrants freshly at the required concentration range (see appropriate sections for concentration of standards used). The ICP-MS instrument was set to detect ^{193}Ir in no-gas mode.

2.2.12 pH and pH* Measurements

All pH and pH* (pH meter reading without correcting for the effect of deuterium on the glass electrode) values were recorded using a minilab IQ125 pH meter equipped with a ISFET silicon chip pH sensor referenced in KCl gel. The electrode was calibrated with Aldrich buffer solutions of pH 4, 7 and 10. The pH values of reaction mixtures and buffers were measured at 298 K with adjustment (when required) by addition of $HClO_4$ (aq) or KOH (aq). The pH* of aqueous NMR samples were also measured at 298 K and adjusted (when required) by addition of $DClO_4$ (aq) and KOD (aq).

2.2.13 pK_a* Determination

p*K*a* (pH* at which half of the aqua ligand in a compound is deprotonated, where * denotes the measurement was performed in D_2O) measurements were made on the acidity of the aqua ligand in complexes by following shifts in the ^1H NMR chemical

shifts for protons on the chelating ligands caused by a change in the pH* of the solution. pH* was measured and adjusted as described in section 2.2.12. ^{1}H NMR spectra were recorded at 298 K on a 600 MHz spectrometer and spectra were referenced to dioxane (3.75 ppm). The change in chemical shift as a function of pH* was plotted and fitted to the Henderson-Hasselbalch equation using Origin 9.1:

$$pH = pK_a + \log_{10}\left(\frac{[A^-]}{[HA]}\right)$$

2.2.14 Eukaryotic Cellular Biological Studies

This work was performed by Dr. Isolda Romero-Canelón (Department of Chemistry, University of Warwick). General cell maintenance and antiproliferative assays are outlined here, with more specific experiments described in the appropriate chapters.

2.2.14.1 Cell Maintenance[14]

The cell lines used in this work, A2780 human ovarian carcinoma, A549 human Caucasian lung carcinoma, HCT116 human colon carcinoma, MCF7 human Caucasian breast carcinoma and MRC5 human fetal lung fibroblasts were obtained from the European Collection of Cell Cultures (ECACC). A2780 ovarian and MRC5 cells were grown in Roswell Park Memorial Institute medium (RPMI-1640), A549 and MCF7 in Dulbecco's Modified Eagle medium (DMEM) and HCT116 in McCoy′s Modified 5A medium. All media were supplemented with 10% v/v of fetal calf serum, 1% v/v of 2 mM glutamine and 1% v/v penicillin/streptomycin.

All cells were grown in 75 cm^2 culture flasks as adherent monolayers, and they were split two to three times a week when around 80-90% confluence was reached, using 0.25% v/v trypsin for A2780 or 0.25% v/v trypsin/EDTA for all other cell lines.

2.2.14.2 *In Vitro* Growth Inhibition Assays

96-well plates were used to seed 5000 cells per well; they were left to pre-incubate in drug-free media at 310 K for 48 h before adding various concentrations of the compounds to be tested. Stock solutions of the Ir complexes were firstly prepared in 5% v/v dmso and a mixture of 0.9% w/v saline and medium (1:1) followed by serial dilutions in the corresponding cell culture medium. A drug exposure period of 24 h was allowed. After this, the supernatant was removed by suction and each well was washed with PBS. A further 72 h was allowed for the cells to recover in drug-free medium at 310 K. The sulforhodamine B (SRB) assay was used to determine cell viability. This assay, first developed by Skehan *et al.* in 1990, is based on the ability of the sulforhodamine B to bind electrostatically to basic amino acid residues of proteins from fixed cells.[15] Absorbance measurements of solubilised dye allowed the determination of the amount of viable treated cells against an untreated control. These measurements were carried out using a BioRad iMark microplate reader with a 470 nm filter. IC_{50} values (concentrations which cause 50% of inhibition of cell growth) were determined as duplicates of triplicates in two independent sets of experiments, and their standard deviations calculated.

2.2.15 Prokaryotic Cellular Biological Studies

This work was performed with the help of Dr. Evyenia Shaili (Department of Chemistry, University of Warwick) with guidance from Mr. Daniel McFeely (School of Life Science, University of Warwick).

2.2.15.1 Cell Maintenance

The bacterial cell lines used in this work, *Staphylococcus aureus* (strain R34) and *Escherichia coli* (strain Top10), were all obtained from cultures in the School of Life

Sciences, University of Warwick. Bacterial stocks were made by plating cells on Lysogeny Broth (LB) agar plates and allowing growth at 310 K overnight. Colonies were then collected and dissolved in glycerol (which had been previously autoclaved) to an optical density at 600 nm (OD_{600}) of 0.01, then placed in Eppendorf tubes and stored at 193 K until required.

2.2.15.2 *In Vitro* Growth Inhibition Assays

Bacteria stocks for growth inhibition assays were made by dissolving concentrated stocks of OD_{600} = 0.01 by dilution with LB to OD_{600} = 0.002. Stock solutions of Ir complexes were prepared by dissolving compounds in dmso (5 mM) and then diluting to desired concentrations by addition of LB medium. The bacterial solutions were then plated onto 96-well plates (100 μL), and then solutions of Ir complexes were added (100 μL) to give a final OD_{600} = 0.001. The 96-well plate was covered with a clear gas permeable seal and placed in an iEMs plate reader with the following settings; incubation temperature = 310 K, shaking for 10 s every 5 min at a speed of 360 RPM; measurement under stepping mode every 30 min; filter = 600 nm; time = 22 h. Data were processed using Ascent software version 2.6. The experiments were performed as duplicates of duplicates and were undertaken on separate days.

The minimal inhibitory concentration (MIC) is defined as the minimum concentration of compound that inhibits visible growth of a microorganism over a given incubation period (22 h). This is the value that is reported as a measure of a compound's antibacterial activity.

The minimum bactericidal concentration (MBC) is defined as the minimum concentration of compound that will kill a particular bacterium. This was evaluated

by plating an LB agar plate with bacterial solutions (10 μL) which showed no growth over the initial 22 h incubation period. The agar plate was then incubated at 310 K overnight. The MBC was determined as the concentration of iridium complex that prevented colony growth overnight.

2.2.15.3 Cell Membrane Viability Assay

The membrane integrity of *S. aureus* after exposure to complexes was performed using the BacLight™ DEAD/ALIVE bacterial viability kit (Invitrogen) according to the supplier's instructions.[16] The kit works on the premise that the dye SYTO 9 can penetrate through both intact and compromised cell membranes and fluoresce green when bound to nuclear DNA. The dye propidium iodide (PI) only enters membrane compromised cells and fluoresces red when bound to nuclear DNA.[17] The ratio of green/red fluorescence indicates the degree of membrane-damage when compared to prepared standards.

Briefly, 96 well plates were plated with cells (90 μL) at OD_{600} = 0.310 dissolved with 0.85% w/v NaCl solution, followed by addition of iridium complexes (10 μL) to give final a concentration of compound at 4 × MIC value. The well plate was incubated at 310 K for 25 min. SYTO 9 and PI (1:1 mix) were added (100 μL) and incubated at ambient temperature in the dark for 15 min before taking fluorescence readings (530 and 630 nm) on a Variascan Flash Multimode microplate reader by excitation at 470 nm at 298 K. Confocal microscopy images were also taken using an IX71 Olympus microscope with a 100× objective by Mr Ian Hands-Portman (School of Life Sciences, University of Warwick).

2.3 References

(1) Björgvinsson, M.; Halldorsson, S.; Arnason, I.; Magull, J.; Fenske, D. *J. Organomet. Chem.* **1997**, *544*, 207.

(2) Liu, Z.; Habtemariam, A.; Pizarro, A. M.; Fletcher, S. A.; Kisova, A.; Vrana, O.; Salassa, L.; Bruijnincx, P. C. A.; Clarkson, G. J.; Brabec, V.; Sadler, P. J. *J. Med. Chem.* **2011**, *54*, 3011.

(3) Churchill, M. R.; Julis, S. A. *Inorg. Chem.* **1977**, *16*, 1488.

(4) Tönnemann, J.; Risse, J.; Grote, Z.; Scopelliti, R.; Severin, K. *Eur. J. Inorg. Chem.* **2013**, *2013*, 4558.

(5) Lidström, P.; Tierney, J.; Wathey, B.; Westman, J. *Tetrahedron* **2001**, *57*, 9225.

(6) Hwang, T. L.; Shaka, A. J. *J. Magn. Reson.* **1995**, *112*, 275.

(7) *CrysAlis PRO*, Oxford Diffraction Ltd.: Abington.

(8) Sheldrick, G. *Acta Crystallogr., Sect. A: Found. Crystallogr.* **1990**, *46*, 467.

(9) Sheldrick, G. *SHELXL-97*, Univeristy of Göttingen: Göttingen.

(10) M. J. Frisch, G. W. T., H. B. Schlegel, G. E. Scuseria, ; M. A. Robb, J. R. C., J. A. Montgomery, Jr., T. Vreven, ; K. N. Kudin, J. C. B., J. M. Millam, S. S. Iyengar, J. Tomasi, ; V. Barone, B. M., M. Cossi, G. Scalmani, N. Rega, ; G. A. Petersson, H. N., M. Hada, M. Ehara, K. Toyota, ; R. Fukuda, J. H., M. Ishida, T. Nakajima, Y. Honda, O. Kitao, ; H. Nakai, M. K., X. Li, J. E. Knox, H. P. Hratchian, J. B. Cross, ; V. Bakken, C. A., J. Jaramillo, R. Gomperts, R. E. Stratmann, ; O. Yazyev, A. J. A., R. Cammi, C. Pomelli, J. W. Ochterski, ; P. Y. Ayala, K. M., G. A. Voth, P. Salvador, J. J. Dannenberg, ; V. G. Zakrzewski, S. D., A. D. Daniels, M. C. Strain, ; O. Farkas, D. K. M., A. D. Rabuck, K. Raghavachari, ; J. B. Foresman, J. V. O., Q. Cui, A. G. Baboul, S. Clifford, ; J. Cioslowski, B. B. S., G. Liu, A. Liashenko, P. Piskorz, ; I. Komaromi, R. L. M., D. J. Fox, T. Keith, M. A. Al-Laham, ; C. Y. Peng, A. N., M. Challacombe, P. M. W. Gill, ; B. Johnson, W. C., M. W. Wong, C. Gonzalez, and J. A. Pople *Gaussian 03, Revision D.02* **2004**, *Gaussian, Inc., Wallingford CT*.

(11) Adamo, C.; Barone, V. *J. Chem. Phys.* **1999**, *110*, 6158.

(12) Hay, P. J.; Wadt, W. R. *J. Chem. Phys.* **1985**, *82*, 270.

(13) McLean, A. D.; Chandler, G. S. *J. Chem. Phys.* **1980**, *72*, 5639.

(14) Maramorosch, K. *Practical Tissue Culture Applications*; Elsevier Science: New York, 2012.

(15) Skehan, P.; Storeng, R.; Scudiero, D.; Monks, A.; McMahon, J.; Vistica, D.; Warren, J. T.; Bokesch, H.; Kenney, S.; Boyd, M. R. *J. Natl. Cancer Inst.* **1990**, *82*, 1107.

(16) Boulos, L.; Prévost, M.; Barbeau, B.; Coallier, J.; Desjardins, R. *J. Microbiol. Methods* **1999**, *37*, 77.

(17) Stocks, S. M. *Cytometry A* **2004**, *61A*, 189.

Chapter 3

Iridium(III) Half-Sandwich Anticancer Complexes Bearing Functionally Diverse 2-Phenylpyridine Ligands

3.1 Introduction

There is an increasing interest in the design of organometallic anticancer complexes,[1-5] especially complexes which are active against cisplatin resistant cancers.[6-8] One of the most successful anticancer organometallic complexes to date include titanocene dichloride[9] which reached stage II clinical trials for advanced renal-cell carcinoma[10] and metastatic breast cancer.[11] A major focus has been on the development of organometallic complexes of the platinum group metals, with the majority of research being performed on half-sandwich ruthenium(II) complexes. [5,12-16]

Increasing interest in the chemical reactivity and unique structural scaffolds organometallic complexes can offer compared with organic-based pharmacores has led to other metal ions being studied for their anticancer activities, where organo-iridium(III) complexes are showing promise in this regard.[17-25]

The biological activity of half-sandwich pentamethylcyclopentadienyl (Cp*) iridium(III) complexes can be increased by the incorporation of phenyl substituents as in Cp^{xPh} and Cp^{xBiPh} ligands.[26,27] This increase in activity may be due in part to an increase in hydrophobicity resulting in enhanced cellular uptake and accumulation. Extended cyclopentadienyl systems have also been shown to strengthen interactions with DNA via intercalation between DNA base pairs.[26]

The introduction of the negatively-charged *C,N*-chelated ligands in place of neutral *N,N* ligands has also been shown to improve antiproliferative activity.[28] Again, the increase in activity may be attributed to an increase in hydrophobicity of the resulting neutral complex. The incorporation of anionic ligands in place of neutral ligands in other iridium systems have also been explored.[22,29]

Chelated half-sandwich pseudo-octahedral iridium(III) complexes have been shown to bind to DNA nucleobases *via* the monodentate site, and can inhibit the synthesis of DNA by DNA polymerases.[26] It has also been shown that they can bind to the minor-groove of CT-DNA.[30] Some of these complexes also inhibit thioredoxin reductase 1 (Trx-R).[19] Intriguingly they can also catalyse the oxidation of NADH to NAD^+ and modulation of the NAD^+/NADH ratio has been demonstrated in A2780 human ovarian cancer cells.[31,32] Disruption of this redox process may contribute to a multi-targeting mechanism of action.[33]

The effect of incorporating functionality on the chelating ligand in half-sandwich iridium(III) complexes has not been widely explored, although previous studies have indicated that the incorporation of simple functional groups on the chelating ligand, such as fluoro, nitro and methyl groups, enhances the activity.[19,30,34] This chapter evaluates the effect that functionality on the 2-phenylpyridine (2-PhPy) chelating ligand has on the chemical, physio-chemical and biological properties of complexes of the type [(η^5-Cp*)Ir(2-(R'-phenyl)-R-pyridine)Cl] where R/R' is an electron-withdrawing or electron-donating group. Investigations into the resulting electronic effects, aqueous chemistry (including nucleobase binding and catalytic NADH oxidation) and antiproliferative activity have been carried out. The rationalisation of anticancer activity has been investigated for pairs of structural isomers, including studies into hydrophobicity, cellular-iridium accumulation and distribution to determine structure activity relationships (SARs), with the overall goal of finding novel complexes that exhibit high potency without using extended cyclopentadienyl capping systems.

Chart 3.1. [(η^5-Cp*)Ir(2-(R'-phenyl)-R-pyridine)Cl] complexes studied in this work

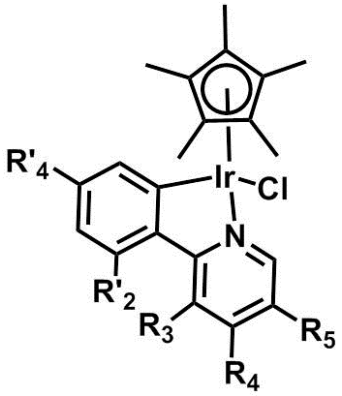

Complex	R'$_4$	R'$_2$	R_3	R_4	R_5
1	H	**F**	H	H	H
2	**F**	H	H	H	H
3	H	H	**F**	H	H
4	H	H	H	H	**F**
5	**CHO**	H	H	H	H
6	H	H	H	H	**CHO**
7	**NO_2**	H	H	H	H
8	H	H	H	**NO_2**	H
9	**CH_2OH**	H	H	H	H
10	H	H	H	**CH_2OH**	H
11	**OH**	H	H	H	H
12	H	H	H	H	**OH**
13	H	**CH_3**	H	H	H
14	H	H	H	**CH_3**	H
15	H	H	H	H	**CH_3**
16	**CF_3**	H	H	H	H
17	**OCH_3**	H	H	H	H

3.2 Experimental Section

3.2.1 Materials

$IrCl_3.3H_2O$ (99%) was purchased from Precious Metals Online (Australia). 1,2,3,4,5-pentamethylcyclopentadiene, NaCl (>99.999%), tetrakis(triphenylphosphine)-palladium (99%), phenylboronic acid, 6-bromo-3-pyridinecarboxaldehyde, 2-bromo-4-nitropyridine, 4-formylphenylboronic acid, 4-(hydroxymethyl)phenylboronic acid, 4-hydroxyphenylboronic acid, 2-bromo-4-hydroxymethylpyridine, 2-bromo-4-

methylpyridine, 2-bromo-5-fluoropyridine (97%), *p*-tolylboronic acid (97%), 4-nitrophenylboronic acid (95%), 9-ethylguanine (≥98%), 9-methyladenine (97%) and *β*-nicotinamide adenine dinucleotide - reduced dipotassium salt (NADH) (≥95%) were purchased from Sigma-Aldrich (UK). 2-Bromopyridine, 2-flurophenylboronic acid and 4-fluorophenylboronic were purchased from Fisher Scientific (UK), 2-bromo-5-hydroxypyridine and 2-bromo-5-methylpyridine from VWR International Ltd. (UK) and 2-bromo-3-fluoropyridine from Tokyo Chemical Industry Ltd. (UK). Solvents used for synthesis were of laboratory grade and used without further purification. Solvents for RP-HPLC (water and acetonitrile) were of HPLC grade with added trifluoroacetic acid (purchased from Sigma-Aldrich (UK)) for purity measurements. $[(\eta^5\text{-Cp*})IrCl_2]_2$ was synthesised as described in Chapter 2.

3.2.2 Syntheses

3.2.2.1 Synthesis of 2-(R'-phenyl)-R-pyridine Ligands.

The synthesis of ligands **L1-17** was performed using the following adapted literature procedure.[35] Phenylboronic acid/derivatives (1.4 mol eq) and 2-bromopyridine/derivatives (1 mol equiv) were dissolved in 1:1:1 (v/v) of tetrahydrofuran:water:1 M aqueous sodium carbonate solution and stirred at ambient temperature under nitrogen for 1 h. Tetrakis(triphenylphosphine)palladium (2% cat) was added in one portion and the reaction mixture was heated under reflux at 373 K for 24 h. The reaction mixture was cooled to ambient temperature, and extracted with dichloromethane. The organic layer was washed with saturated sodium hydrogencarbonate solution and brine, then dried with magnesium sulphate and concentrated to dryness, yielding the crude material. Purification by silica flash chromatography was performed using chloroform/ethyl acetate as the eluent mixture.

2-(2'-Fluorophenyl)pyridine (**L1**) As described in the above method using 2-fluorophenylboronic acid (400 mg, 2.86 mmol), 2-bromopyridine (195 μL, 2.04 mmol), a 1:1:1 mixture of tetrahydrofuran:water:1 M aqueous sodium carbonate (24 mL) and tetrakis(triphenylphosphine)palladium (47 mg, 0.041 mmol). Purification by silica flash chromatography was performed using 3:1 chloroform:ethyl acetate (R_f = 0.75) yielding a yellow oil (156 mg, 44%). **^{1}H NMR** (300 MHz, $CDCl_3$) δ = 8.65 (d, 1H, J = 5.0 Hz), 7.89 (td, 1H, J = 7.8, 1.8 Hz), 7.72-7.60 (m, 2H), 7.30-7.26 (m, 1H), 7.20-7.15 (m, 2H), 7.10-7.05 (m, 1H). **ESI-MS** (MeOH) m/z = 174.1 $[M+H]^+$.

2-(4'-Fluorophenyl)pyridine (**L2**) As described in the above method using 4-fluorophenylboronic acid (400 mg, 2.86 mmol), 2-bromopyridine (195 μL, 2.04 mmol), 1:1:1 mixture of tetrahydrofuran:water:1 M aqueous sodium carbonate (24 mL) and tetrakis(triphenylphosphine)palladium (47 mg, 0.041 mmol). Purification by silica flash chromatography was performed using 3:1 chloroform:ethyl acetate (R_f = 0.73) yielding a yellow oil (254 mg, 72%). **^{1}H NMR** (400 MHz, acetone-d_6) δ = 8.66 (dq, 1H, J = 4.8, 1.0 Hz), 8.20-8.15 (m, 2H), 7.92 (dt, 1H, J = 8.0, 1.0 Hz), 7.86 (td, 1H, J = 8.0, 1.8 Hz), 7.31 (ddd, 1H, J = 7.3, 4.8, 1.2 Hz), 7.27-7.21 (m, 2H). **ESI-MS** (MeOH) m/z = 174.1 $[M+H]^+$.

2-Phenyl-3-fluoropyridine (**L3**) As described in the above method using phenylboronic acid (243 mg, 1.99 mmol), 2-bromo-3-fluoropyridine (144 μL, 1.42 mmol), 1:1:1 mixture of tetrahydrofuran:water:1 M aqueous sodium carbonate (15 mL) and tetrakis(triphenylphosphine)palladium (33 mg, 0.028 mmol). Purification by silica flash chromatography was performed using 1:1 chloroform:ethyl acetate (Rf = 0.837) yielding a yellow oil (130 mg, 53%). **^{1}H NMR** (400 MHz, dmso-d_6) δ = 8.56-8.54 (m, 1H), 7.91 (d, 2H, J = 8.3 Hz), 7.83 (m, 1H), 7.54-7.46 (m, 4H). **ESI-MS** (MeOH) m/z = 174.1 $[M+H]^+$.

2-Phenyl-5-fluoropyridine (**L4**) As described in the above method using phenylboronic acid (243 mg, 1.99 mmol), 2-bromo-5-fluoropyridine (250 mg, 1.42 mmol), 1:1:1 mixture of tetrahydrofuran:water:1 M aqueous sodium carbonate (15 mL) and tetrakis(triphenylphosphine)palladium (33 mg, 0.028 mmol). Purification by silica flash chromatography was performed using 1:1 chloroform:ethyl acetate (Rf = 0.897) yielding a yellow oil (165 mg, 67%). **^{1}H NMR** (400 MHz, acetone-d_6) δ = 8.57 (d, 1H, J = 2.7 Hz), 8.07 (d, 2H, J = 7.3 Hz), 7.99 (dd, 1H, J = 8.8, 4.2 Hz), 7.69 (td, 1H, J = 8.6, 2.9 Hz), 7.50-7.40 (m, 3H). **ESI-MS** (MeOH) m/z = 174.1 $[M+H]^+$.

2-(4'-formylphenyl)pyridine (**L5**) As described in the above method using 4-formylphenylboronic acid (250 mg, 1.67 mmol), 2-bromopyridine (114 μL, 1.19 mmol), 1:1:1 mixture of tetrahydrofuran:water:1 M aqueous sodium carbonate (15 mL) and tetrakis(triphenylphosphine)palladium (27 mg, 0.024 mmol). Purification by silica flash chromatography was performed using 1:1 chloroform:ethyl acetate (R_f = 0.780) yielding a yellow oil (164 mg, 75%). **^{1}H NMR** (400 MHz, acetone-d_6) δ = 10.12 (s, 1H), 8.74 (dq, 1H, J = 4.7, 0.9 Hz), 8.35 (d, 2H, J = 8.3 Hz), 8.08-8.02 (m, 3H), 7.93 (td, 1H, J = 7.6, 1.8 Hz), 7.41 (ddd, 1H, J = 7.5, 4.8, 1.1 Hz). **ESI-MS** (MeOH) m/z = 183.8 $[M+H]^+$.

2-Phenyl-5-pyridinecarboxaldehyde (**L6**) As described in the above method using phenylboronic acid (300 mg, 2.46 mmol), 6-bromo-3-pyridinecarboxaldehyde (327 mg, 1.76 mmol), 1:1:1 mixture of tetrahydrofuran:water:1 M aqueous sodium carbonate (15 mL) and tetrakis(triphenylphosphine)palladium (40 mg, 0.034 mmol). Purification by silica flash chromatography was performed using 1:1 chloroform:ethyl acetate (Rf = 0.800) yielding a dark yellow oil that solidified upon standing (152 mg, 47%). **^{1}H NMR** (400 MHz, acetone-d_6) δ = 10.18 (s, 1H), 9.15 (d,

1H, J = 2.0 Hz), 8.30-8.28 (m, 1H), 8.24-8.18 (m, 2H), 8.12 (d, 1H, J = 8.2 Hz), 7.56-7.50 (m, 3H). **ESI-MS** (MeOH) m/z = 184.1 $[M+H]^+$.

2-(4'-nitrophenyl)pyridine (**L7**) As described in the above method using 4-nitrophenylboronic acid (250 mg, 1.50 mmol), 2-bromopyridine (102 μL, 1.07 mmol), 1:1:1 mixture of tetrahydrofuran:water:1 M aqueous sodium carbonate (15 mL) and tetrakis(triphenylphosphine)palladium (25 mg, 0.021 mmol). Purification by silica flash chromatography was performed using 1:1 chloroform:ethyl acetate (R_f = 0.708) yielding an off white solid (150 mg, 70%). **^{1}H NMR** (400 MHz, $CDCl_3$) δ = 8.75 (d, 1H, J = 5.0 Hz), 8.63 (d, 2H, J = 8.6 Hz), 8.19 (d, 2H, J = 8.6 Hz), 7.87-7.81 (m, 2H), 7.37-7.34 (m, 1H). **ESI-MS** (MeOH) m/z = 201.0 $[M+H]^+$.

2-Phenyl-4-nitropyridine (**L8**) As described in the above method using phenylboronic acid (210 mg, 1.72 mmol), 2-bromo-4-nitropyridine (250 mg, 1.23 mmol), 1:1:1 mixture of tetrahydrofuran:water:1 M aqueous sodium carbonate (15 mL) and tetrakis(triphenylphosphine)palladium (28 mg, 0.025 mmol). Purification by silica flash chromatography was performed using 3:1 chloroform:ethyl acetate (Rf = 0.915) yielding a yellow solid (175 mg, 71%). **^{1}H NMR** (400 MHz, dmso-d_6) δ = 9.03 (d, 1H, J = 5.4 Hz), 8.58 (d, 1H, J = 1.7 Hz), 8.20 (d, 2H, J = 8.0 Hz), 8.08 (dd, 1H, J = 5.3, 2.0 Hz), 7.58-7.52 (m, 3H). **ESI-MS** (MeOH) m/z = 201.0 $[M+H]^+$.

2-(4'-hydroxymethylphenyl)pyridine (**L9**) As described in the above method using 4-hydroxymethlphenylboronic acid (250 mg, 1.64 mmol), 2-bromopyridine (112 μL, 1.17 mmol), 1:1:1 mixture of tetrahydrofuran:water:1 M aqueous sodium carbonate (15 mL) and tetrakis(triphenylphosphine)palladium (27 mg, 0.024 mmol). Purification by silica flash chromatography was performed using 1:1 chloroform:ethyl acetate (R_f = 0.260) yielding a yellow oil (125 mg, 57%). **^{1}H NMR** (400 MHz, acetone-d_6) δ = 8.65 (d, 1H, J = 5.1 Hz), 8.08 (d, 2H, J = 8.2 Hz), 7.90

(dt, 1H, J = 8.1, 1.1 Hz), 7.83 (td, 1H, J = 7.4, 1.9 Hz), 7.48 (d, 2H, J = 8.4 Hz), 7.29 (ddd, 1H, J = 7.3, 4.8, 1.2 Hz), 4.70 (d, 2H, J = 5.3 Hz), 4.34 (t, 1H, J = 5.6 Hz). **ESI-MS** (MeOH) m/z = 186.1 $[M+H]^+$.

2-Phenyl-4-hydroxymethylpyridine (**L10**) As described in the above method using phenylboronic acid (227 mg, 1.86 mmol), 2-bromo-4-hydroxymethylpyridine (250 mg, 1.33 mmol), 1:1:1 mixture of tetrahydrofuran:water:1 M aqueous sodium carbonate (15 mL) and tetrakis(triphenylphosphine)palladium (31 mg, 0.027 mmol). Purification by silica flash chromatography was performed using 1:1 chloroform:ethyl acetate (Rf = 0.360) yielding a dark yellow oil that solidified upon standing (176 mg, 71%). **^{1}H NMR** (400 MHz, acetone-d_6) δ = 8.59 (d, 1H, J = 5.2 Hz), 8.13-8.10 (m, 2H), 7.90 (s, 1H), 7.50-7.45 (m, 2H), 7.42 (td, 1H, J = 7.3, 1.5 Hz), 7.31 (dd, 1H, J = 5.1, 1.0 Hz), 4.76 (s, 2H). **ESI-MS** (MeOH) m/z = 186.1 $[M+H]^+$.

2-(4'-hydroxyphenyl)pyridine (**L11**) As described in the above method using 4-hydroxyphenylboronic acid (250 mg, 1.81 mmol), 2-bromopyridine (124 μL, 1.29 mmol), 1:1:1 mixture of tetrahydrofuran:water:1 M aqueous sodium carbonate (15 mL) and tetrakis(triphenylphosphine)palladium (30 mg, 0.026 mmol). Purification by silica flash chromatography was performed using 1:1 chloroform:ethyl acetate (R_f = 0.800) yielding an off-white solid (50 mg, 23%). **^{1}H NMR** (400 MHz, dmso-d_6) δ = 9.72 (s 1H), 8.58 (d, 1H, J = 4.6 Hz), 7.93 (d, 2H, J = 8.5 Hz), 7.83-7.76 (m, 2H), 7.23 (ddd, 1H, J = 6.4, 4.8, 1.5 Hz), 6.86 (d, 2H, J = 8.6 Hz). **ESI-MS** (MeOH) m/z = 172.0 $[M+H]^+$.

2-Phenyl-5-hydroxypyridine (**L12**) As described in the above method using phenylboronic acid (245 mg, 2.01 mmol), 2-bromo-5-hydroxypyridine (250 mg, 1.44 mmol), 1:1:1 mixture of tetrahydrofuran:water:1 M aqueous sodium carbonate (15

mL) and tetrakis(triphenylphosphine)palladium (33 mg, 0.029 mmol). Purification by silica flash chromatography was performed using 1:1 chloroform:ethyl acetate (Rf = 0.556) yielding an off-white solid (80 mg, 33%). **^{1}H NMR** (400 MHz, dmso-d_6) δ = 10.01 (s, 1H), 8.21 (d, 1H, J = 2.9 Hz), 7.95 (d, 2H, J = 7.6 Hz), 7.78 (d, 1H, J = 8.7 Hz), 7.44-7.40 (m, 2H), 7.33 (tt, 1H, J = 7.3, 1.4 Hz), 7.24 (dd, 1H, J = 8.7, 2.9 Hz). **ESI-MS** (MeOH) m/z = 172.1 $[M+H]^+$.

2-(2'-methylphenyl)pyridine (**L13**) As described in the above method using o-tolylphenylboronic acid (250 mg, 1.84 mmol), 2-bromopyridine (125 μL, 1.31 mmol), 1:1:1 mixture of tetrahydrofuran:water:1 M aqueous sodium carbonate (15 mL) and tetrakis(triphenylphosphine)palladium (30 mg, 0.026 mmol). Purification by silica flash chromatography was performed using 1:1 chloroform:ethyl acetate (R_f = 0.725) yielding a yellow oil (140 mg, 63%). **^{1}H NMR** (400 MHz, dmso-d_6) δ = 8.66 (dq, 1H, J = 4.8, 0.8 Hz), 7.86 (td, 1H, J = 7.7, 1.8 Hz), 7.50 (d, 1H, J = 7.8 Hz), 7.38-7.34 (m, 2H) 7.32-7.26 (m, 3H), 2.31 (s, 3H). **ESI-MS** (MeOH) m/z = 170.1 $[M+H]^+$.

2-Phenyl-4-methylpyridine (**L14**) As described in the above method using phenylboronic acid (248 mg, 2.03 mmol), 2-bromo-4-methylpyridine (162 μL, 1.45 mmol), 1:1:1 mixture of tetrahydrofuran:water:1 M aqueous sodium carbonate (15 mL) and tetrakis(triphenylphosphine)palladium (34 mg, 0.029 mmol). Purification by silica flash chromatography was performed using 1:1 chloroform:ethyl acetate (R_f = 0.765) yielding a yellow oil (64 mg, 22%). **^{1}H NMR** (400 MHz, acetone-d_6) δ = 8.50 (d, 1H, J = 5.0 Hz), 8.12 (d, 2H, J = 8.1 Hz), 7.76-7.74 (m, 1H), 7.49-7.44 (m, 2H), 7.41 (tt, 1H, J = 7.2, 1.5 Hz), 7.14 (dd, 1H, J = 5.0, 0.8 Hz), 2.41 (s, 3H). **ESI-MS** (MeOH) m/z = 170.1 $[M+H]^+$.

2-Phenyl-5-methylpyridine (**L15**) As described in the above method using phenylboronic acid (248 mg, 2.03 mmol), 2-bromo-5-methylpyridine (250 mg, 1.45 mmol), 1:1:1 mixture of tetrahydrofuran:water:1 M aqueous sodium carbonate (15 mL) and tetrakis(triphenylphosphine)palladium (34 mg, 0.029 mmol). Purification by silica flash chromatography was performed using 1:1 chloroform:ethyl acetate (R_f = 0.869) yielding a yellow oil (153 mg, 62%). **^{1}H NMR** (400 MHz, $CDCl_3$) δ = 8.53 (s, 1H), 7.97 (d, 2H, J = 8.2 Hz), 7.63 (d, 1H, J = 8.4 Hz), 7.56 (dd, 1H, J = 8.1, 2.4 Hz), 7.48-7.45 (m, 2H), 7.39 (tt, 1H, J = 7.5, 1.5 Hz), 2.37 (s, 3H). **ESI-MS** (MeOH) m/z = 170.1 $[M+H]^+$.

2-(4'-Trifluoromethylphenyl)pyridine (L16) As described in the above method using 4-trifluoromethylphenylboronic acid (372 mg, 1.96 mmol), 2-bromopyridine (134 μL, 1.40 mmol), 1:1:1 mixture of tetrahydrofuran:water:1M aqueous sodium carbonate solution (15 mL) and tetrakis(triphenylphosphine)palladium (32 mg, 0.028 mmol). Purification by silica flash chromatography was performed using 3:1 chloroform:ethyl acetate (R_f = 0.844) yielding a pale yellow solid (162 mg, 52%). **^{1}H NMR** (400 MHz, dmso-d_6) δ = 8.72 (d, 1H, J = 4.3 Hz), 8.29 (d, 2H, J = 8.2 Hz), 8.05 (d, 1H, J = 8.0 Hz), 7.93 (td, 1H, J = 7.8, 1.8 Hz), 7.83 (d, 2H, J = 8.3 Hz), 7.43 (dd, 1H, J = 7.3, 4.7 Hz). **ESI-MS** (MeOH) m/z = 223.8 $[M+H]^+$.

2-(4'-methoxyphenyl)pyridine (L17) As described in the above method using 4-methoxyphenylboronic acid (250 mg, 1.645 mmol), 2-bromopyridine (112 μL, 1.175 mmol), 1:1:1 mixture of tetrahydrofuran:water:1M aqueous sodium carbonate solution (15 mL) and tetrakis(triphenylphosphine)palladium (27 mg, 0.024 mmol). Purification by silica flash chromatography was performed using 1:1 chloroform:ethyl acetate (R_f = 0.757) yielding a yellow solid (160 mg, 74%). **^{1}H NMR** (400 MHz, dmso-d_6) δ = 8.61 (dq, 1H, J = 5, 1 Hz), 8.04 (d, 2H, J = 9 Hz),

7.88 (dt, 1H, J = 8, 1 Hz), 7.82 (td, 1H, J = 7, 2 Hz), 7.29-7.26 (m, 1H) 7.04 (d, 2H, 9 Hz), 3.81 (s, 1H). **ESI-MS** (MeOH) m/z = 186.1 $[M+H]^+$.

3.2.2.2 Synthesis of [(η^5-Cp*)Ir(2-(R'-phenyl)-R-pyridine)Cl] complexes

The synthesis of complexes **1-17** was performed using an adapted literature procedure.[27] 2-(R'-phenyl)-R-pyridine (2 mol equiv) was dissolved in anhydrous dichloromethane, sodium acetate (4 mol equiv) was added in one portion and stirred at ambient temperature under nitrogen for 30 min. $[(\eta^5\text{-Cp*})IrCl_2]_2$ (1 mol equiv) was added in one portion and the reaction mixture stirred at ambient temperature for 18 h. The mixture was filtered through celite under suction and the filtrate was concentrated to dryness on a rotary evaporator. The crude product was recrystallized from chloroform/hexane at 273 K to yield purified complexes.

[(η^5-Cp*)Ir(2-(2'-fluorophenyl)pyridine)Cl] (1) As described in the above method using 2-(2'-fluorophenyl)pyridine (40 mg, 0.231 mmol), dichloromethane (20 mL), sodium acetate (38 mg, 0.462 mmol) and $[(\eta^5\text{-Cp*})IrCl_2]_2$ (92 mg, 0.115 mmol) The crude product was recrystallised from chloroform/hexane at 273 K to yield an orange crystalline solid (57 mg, 46%). **^{1}H NMR** (300 MHz, $CDCl_3$) δ = 8.75 (d, 1H, J = 5.8 Hz), 8.26 (d, 1H, J = 8.5 Hz), 7.72-7.65 (m, 1H), 7.58 (d, 1H, J = 7.5 Hz), 7.20-7.08 (m, 2H), 6.73-6.66 (m, 1H) 1.67 (s, 15H). **ESI-MS** (MeOH) m/z = 550.0 $[M\text{-}PF_6]^+$. **CHN analysis** calc. for $C_{21}H_{22}NClFIr.H_2O$ C – 45.60%, H – 4.37%, N – 2.53%. Found C – 45.44%, H – 3.97%, N – 2.29%. **HPLC Purity** 254 nm – 98.8 %. Crystals suitable for X-ray diffraction were obtained by slow evaporation of a chloroform/hexane solution at 278 K.

[(η^5-Cp*)Ir(2-(4'-fluorophenyl)pyridine)Cl] (2) As described in the above method using 2-(4'-fluorophenyl)pyridine (30 mg, 0.173 mmol), dichloromethane (18 mL), sodium acetate (28 mg, 0.340 mmol) and [(η^5-Cp*)$IrCl_2$]$_2$ (69 mg, 0.087 mmol). The crude product was recrystallised from chloroform/hexane at 273 K to yield an orange crystalline solid (48 mg, 52%). **^{1}H NMR** (400 MHz, acetone-d_6) δ = 8.77 (d, 1H, J = 5.7 Hz), 8.01-7.98 (m, 1H), 7.85-7.81 (m, 2H), 7.44 (dd, 1H, J = 8.7, 2.6 Hz), 7.28-7.24 (m, 1H), 6.74 (td, 1H, J = 8.8, 2.6 Hz), 1.68 (s, 15H) **ESI-MS** (MeOH) m/z = 500.1 $[M\text{-}Cl]^+$. **CHN analysis** calc. for $C_{21}H_{22}NClFIr$ C – 47.14%, H – 4.14%, N – 2.62%. Found C – 46.83%, H – 4.02%, N – 2.66%. **HPLC Purity** 254 nm – 99.4 %. Crystals suitable for X-ray diffraction were obtained by slow evaporation of a chloroform/hexane solution at 278 K.

[(η^5-Cp*)Ir(2-phenyl-3-fluoropyridine)Cl] (3) As described in the above method using 2-phenyl-3-fluoropyridine (38 mg, 0.218 mmol), dichloromethane (20 mL), sodium acetate (36 mg, 0.436 mmol) and [(η^5-Cp*)$IrCl_2$]$_2$ (87 mg, 0.109 mmol). The crude product was recrystallised from chloroform/hexane at 273 K to yield an orange crystalline solid (35 mg, 30%). **^{1}H NMR** (400 MHz, $CDCl_3$) δ = 8.59 (dd, 1H, J = 5.6, 1.1 Hz), 8.13 (dd, 1H, J = 8.0, 1.3 Hz), 7.83 (dd, 1H, J = 7.7, 1.2 Hz), 7.43-7.38 (m, 1H), 7.21 (td, 1H, J = 7.4, 1.4 Hz), 7.07-7.03 (m, 2H), 1.67 (s, 15H). **ESI-MS** (MeOH) m/z = 500.1 $[M\text{-}Cl]^+$. **CHN analysis** calc. for $C_{21}H_{22}NClFIr$ C – 47.14%, H – 4.14%, N – 2.62%. Found C – 46.85%, H – 3.90%, N – 2.58%. **HPLC Purity** 254 nm – 99.4 %.

[(η^5-Cp*)Ir(2-phenyl-5-fluoropyridine)Cl] (4) As described in the above method using 2-phenyl-5-fluoropyridine (38 mg, 0.218 mmol), dichloromethane (20 mL), sodium acetate (36 mg, 0.436 mmol) and [(η^5-Cp*)$IrCl_2$]$_2$ (87 mg, 0.109 mmol). The crude product was recrystallised from chloroform/hexane at 273 K to yield an orange

crystalline solid (56 mg, 48%). **^{1}H NMR** (400 MHz, dmso-d_6) δ = 8.60 (t, 1H, J = 2.6 Hz), 8.18 (dd, 1H, J = 9.3, 5.5 Hz), 7.95-7.90 (m, 1H), 7.79 (d, 1H, J = 7.8 Hz), 7.69 (d, 1H, J = 7.7 Hz), 7.12 (td, 1H, J = 7.3, 1.3 Hz), 6.99 (td, 1H, J = 7.8, 1.0 Hz), 1.61 (s, 15H). **ESI-MS** (MeOH) m/z = 500.1 $[M\text{-}Cl]^+$. **CHN analysis** calc. for $C_{21}H_{22}NClFIr.0.5H_2O$ C – 46.36%, H – 4.26%, N – 2.57%. Found C – 46.54%, H – 4.14%, N – 2.40%. **HPLC Purity** 254 nm – 98.2 %.

[(η^5-Cp*)Ir(2-(4'-formylphenyl)pyridine)Cl] (5) As described in the above method using 2-(4'-formylphenyl)pyridine (32 mg, 0.173 mmol), dichloromethane (18 mL), sodium acetate (28 mg, 0.346 mmol) and $[(\eta^5\text{-Cp*})IrCl_2]_2$ (69 mg, 0.087 mmol). The crude product was recrystallised from chloroform/hexane at 273 K to yield a red crystalline solid (70 mg, 74%). **^{1}H NMR** (300 MHz, dmso-d_6) δ = 10.08 (s, 1H), 8.79 (d, 1H, J = 5.4 Hz), 8.27-8.21 (m, 2H), 8.04 (d, 1H, J = 8.1 Hz), 7.95 (td, 1H, J = 7.8, 1.4 Hz), 7.51 (dd, 1H, J = 8.1, 1.6 Hz), 7.44-7.40 (m, 1H), 1.63 (s, 15H). **ESI-MS** (MeOH) m/z = 510.1 $[M\text{-}Cl]^+$. **CHN analysis** calc. for $C_{22}H_{23}NClIrO.0.5H_2O$ C – 47.69%, H – 4.37%, N – 2.53%. Found C – 47.55%, H – 4.16%, N – 2.31%. **HPLC Purity** 254 nm – 99.0 %.

[(η^5-Cp*)Ir(2-phenyl-5-pyridinecarboxaldehyde)Cl] (6) As described in the above method using 2-phenyl-5-pyridinecarboxaldehyde (40 mg, 0.218 mmol), dichloromethane (20 mL), sodium acetate (36 mg, 0.436 mmol) and $[(\eta^5\text{-Cp*})IrCl_2]_2$ (87 mg, 0.109 mmol). The crude product was recrystallised from chloroform/hexane at 273 K to yield a red crystalline solid (76 mg, 64%). **^{1}H NMR** (400 MHz, dmso-d_6) δ = 10.13 (s, 1H), 9.13 (d, 1H, J = 1.5 Hz), 8.29 (d, 1H, J = 8.5 Hz), 8.24 (dd, 1H, J = 8.4, 1.8 Hz), 7.95 (dd, 1H, J = 7.7, 1.0 Hz), 7.77 (dd, 1H, J = 7.6, 0.8 Hz), 7.16 (td, 1H, J = 7.4, 1.2 Hz), 7.04 (td, 1H, J = 7.0, 1.2 Hz), 1.64 (s, 15H). **ESI-MS** (MeOH) m/z = 510.1 [M-Cl]+. **CHN analysis** calc. for $C_{22}H_{23}NClIrO.0.5H_2O$ C – 47.69%, H

– 4.37%, N – 2.53%. Found C – 47.51%, H – 4.16%, N – 2.23%. **HPLC Purity** 254 nm – 99.1 %.

[(η^5-Cp*)Ir(2-(4'-nitrophenyl)pyridine)Cl] (7) As described in the above method using 2-(4'-nitrophenyl)pyridine (44 mg, 0.218 mmol), dichloromethane (20 mL), sodium acetate (36 mg, 0.436 mmol) and [(η^5-Cp*)$IrCl_2$]$_2$ (87 mg, 0.109 mmol). The crude product was recrystallised from chloroform/hexane at 273 K to yield a red crystalline solid (95 mg, 78%). **^{1}H NMR** (400 MHz, dmso-d_6) δ = 8.81 (d, 1H, J = 5.9 Hz), 8.44 (d, 1H, J = 2.4 Hz), 8.31 (d, 1H, J = 8.0 Hz), 8.12 (d, 1H, J = 8.6 Hz), 8.00 (td, 1H, J = 7.7, 1.5 Hz), 7.84 (dd, 1H, J = 8.5, 2.4 Hz), 7.47 (ddd, 1H, J = 6.6, 5.6, 1.2 Hz), 1.63 (s, 15H). **ESI-MS** (MeOH) m/z = 527.1 $[M\text{-}Cl]^+$. **CHN analysis** calc. for $C_{21}H_{22}N_2ClIrO_2$ C – 44.87%, H – 3.95%, N – 4.98%. Found C – 44.51%, H – 3.77%, N – 4.88%. **HPLC Purity** 254 nm – 98.3 %.

[(η^5-Cp*)Ir(2-phenyl-4-nitropyridine)Cl] (8) As described in the above method using 2-phenyl-4-nitropyridine (34 mg, 0.17 mmol), dichloromethane (18 mL), sodium acetate (28 mg, 0.341 mmol) and [(η^5-Cp*)$IrCl_2$]$_2$ (69 mg, 0.086 mmol). The crude product was recrystallised from chloroform/hexane at 273 K to yield a dark brown solid (76 mg, 64%). **^{1}H NMR** (400 MHz, dmso-d_6) δ = 9.00 (d, 1H, J = 6.4 Hz), 8.73 (d, 1H, J = 2.5 Hz), 8.08 (d, 1H, J = 7.8 Hz), 7.93 (dd, 1H, J = 6.4, 2.5 Hz), 7.76 (d, 1H, J = 7.7 Hz), 7.21 (td, 1H, J = 7.5, 1.2 Hz), 7.07-7.04 (m, 1H), 1.63 (s, 15H). **ESI-MS** (MeOH) m/z = 527.1 $[M\text{-}Cl]^+$. **CHN analysis** calc. for $C_{21}H_{22}N_2ClIrO_2.0.5H_2O$. C – 44.17%, H – 4.06%, N – 4.91%. Found C – 44.51%, H – 3.93%, N – 4.66%. **HPLC Purity** 254 nm – 99.5 %.

[(η^5-Cp*)Ir(2-(4'-hydroxymethylphenyl)pyridine)Cl] (9) As described in the above method using 2-(4'-hydroxymethylphenyl)pyridine (40 mg, 0.218 mmol), dichloromethane (20 mL), sodium acetate (36 mg, 0.436 mmol) and [(η^5-Cp*)$IrCl_2$]$_2$

(87 mg, 0.109 mmol). The crude product was recrystallised from chloroform/hexane at 273 K to yield a yellow crystalline solid (26 mg, 22%). **^{1}H NMR** (300 MHz, dmso-d_6) δ = 8.68 (d, 1H, J = 6.6 Hz), 8.04 (d, 1H, J = 8.6 Hz), 7.83 (t, 1H, J = 7.6 Hz), 7.75 (d, 1H, J = 8.1 Hz), 7.66 (s, 1H), 7.26 (t, 1H, J = 6.8 Hz), 6.94 (d, 1H, J = 8.4 Hz), 5.18 (t, 1H, J = 5.6 Hz), 4.55 (d, 2H, J = 5.8 Hz), 1.60 (s, 15H). **ESI-MS** (MeOH) m/z = 512.2 $[M\text{-}Cl]^+$. **CHN analysis** calc. for $C_{22}H_{25}NClIrO.0.5H_2O$ C – 47.52%, H – 4.71%, N – 2.52%. Found C – 47.44%, H – 4.39%, N – 2.41%. **HPLC Purity** 254 nm – 97.1 %.

[(η^5-Cp*)Ir(2-phenyl-4-hydroxymethylpyridine)Cl] (10) As described in the above method using 2-phenyl-4-hydroxymethylpyridine (40 mg, 0.218 mmol), dichloromethane (20 mL), sodium acetate (36 mg, 0.436 mmol) and $[(\eta^5\text{-Cp*})IrCl_2]_2$ (87 mg, 0.109 mmol). The crude product was recrystallised from chloroform/hexane to yield a yellow solid (95 mg, 80%). **^{1}H NMR** (400 MHz, dmso-d_6) δ = 8.62 (d, 1H, J = 5.9 Hz), 7.95 (s, 1H), 7.75 (dd, 1H, J = 7.7, 1.1 Hz), 7.70 (dd, 1H, J = 7.6, 0.8 Hz), 7.25 (dd, 1H, J = 6.1, 1.3 Hz), 7.11 (td, 1H, J = 7.4, 1.3 Hz), 6.98 (td, 1H, J = 7.7, 1.1 Hz), 5.59 (t, 1H, J = 5.9 Hz), 4.73 (d, 2H, J = 5.9 Hz), 1.60 (s, 15H). **ESI-MS** (MeOH) m/z = 512.2 $[M\text{-}Cl]^+$. **CHN analysis** calc. for $C_{22}H_{25}NClIrO.H_2O$ C – 46.76%, H – 4.82%, N – 2.48%. Found C – 46.58%, H – 4.35%, N – 2.34%. **HPLC Purity** 254 nm – 99.2 %.

[(η^5-Cp*)Ir(2-(4′-hydroxyphenyl)pyridine)Cl] (11) As described in the above method using 2-(4′-hydroxyphenyl)pyridine (37 mg, 0.218 mmol), dichloromethane (20 mL), sodium acetate (36 mg, 0.436 mmol) and $[(\eta^5\text{-Cp*})IrCl_2]_2$ (87 mg, 0.109 mmol). Yellow precipitate formed after 24 h which was isolated via vacuum filtration and washed with hexane (80 mg, 69%). **^{1}H NMR** (400 MHz, dmso-d_6) δ = 9.32 (s, 1H), 8.58 (d, 1H, J = 5.7 Hz), 7.85 (d, 1H, J = 8.0 Hz), 7.74 (t, 1H, J = 7.4

Hz), 7.62 (d, 1H, J = 8.5 Hz), 7.16-7.11 (m, 2H), 6.41 (dd, 1H, J = 8.3, 2.2 Hz), 1.59 (s, 15H). **ESI-MS** (MeOH) m/z = 498.0 $[M\text{-}Cl]^+$. **CHN analysis** calc. for $C_{21}H_{23}NClIrO.H_2O$ C – 45.77%, H – 4.57%, N – 2.54%. Found C – 45.64%, H – 4.00%, N – 2.47%. **HPLC Purity** 254 nm – 99.4 %.

[(η^5-Cp*)Ir(2-phenyl-5-hydroxypyridine)Cl] (12) As described in the above method using 2-phenyl-5-hydroxypyridine (37 mg, 0.218 mmol), dichloromethane (20 mL), sodium acetate (36 mg, 0.436 mmol) and $[(\eta^5\text{-Cp*})IrCl_2]_2$ (87 mg, 0.109 mmol). The crude product was recrystallised from hot chloroform to yield a yellow powder (19 mg, 16%). **^{1}H NMR** (400 MHz, dmso-d_6) δ = 10.44 (bs, 1H), 8.31 (d, 1H, J = 2.7 Hz), 7.88 (d, 1H, J = 8.9 Hz), 7.65-7.60 (m, 2H), 7.32 (dd, 1H, J = 8.7, 2.5 Hz), 7.03 (td, 1H, J = 7.3, 1.2 Hz), 6.92 (td, 1H, J = 7.4, 1.1 Hz), 1.59 (s, 15H). **ESI-MS** (MeOH) m/z = 498.0 $[M\text{-}Cl]^+$. **CHN analysis** calc. for $C_{21}H_{23}NClIrO.0.5H_2O$ C – 46.53%, H – 4.46%, N – 2.58%. Found C – 46.71%, H – 4.19%, N – 2.50%. **HPLC Purity** 254 nm – 99.5 %.

[(η^5-Cp*)Ir(2-(2′-methylphenyl)pyridine)Cl] (13) As described in the above method using 2-(2′-methylphenyl)pyridine (37 mg, 0.218 mmol), dichloromethane (20 mL), sodium acetate (36 mg, 0.436 mmol) and $[(\eta^5\text{-Cp*})IrCl_2]_2$ (87 mg, 0.109 mmol). The crude product was recrystallised from chloroform/hexane at 273 K to yield a yellow crystalline solid (81 mg, 70%). **^{1}H NMR** (400 MHz, dmso-d_6) δ = 8.81 (dd, 1H, J = 5.6, 1.5 Hz), 8.12 (d, 1H, J = 8.5 Hz), 7.89-7.84 (m, 1H), 7.59 (d, 1H, J = 7.8 Hz), 7.31-7.27 (ddd, 1H, J = 7.0, 5.6, 1.2 Hz), 6.97 (t, 1H, J = 7.5 Hz), 6.78 (d, 1H, J = 7.5 Hz), 2.64 (s, 3H), 1.59 (s, 15H). **ESI-MS** (MeOH) m/z = 496.1 $[M\text{-}Cl]^+$. **CHN analysis** calc. for $C_{22}H_{25}NClIr$ C – 49.75%, H – 4.74%, N – 2.64%. Found C – 49.65%, H – 4.71%, N – 2.61%. **HPLC Purity** 254 nm – 98.8 %.

[(η^5-Cp*)Ir(2-phenyl-4-methylpyridine)Cl] (14) As described in the above method using 2-phenyl-4-methylpyridine (37 mg, 0.218 mmol), dichloromethane (20 mL), sodium acetate (36 mg, 0.436 mmol) and [(η^5-Cp*)$IrCl_2$]$_2$ (87 mg, 0.109 mmol). The crude product was recrystallised from chloroform/hexane at 273 K to yield a yellow crystalline solid (58 mg, 50%). **^{1}H NMR** (400 MHz, acetone-d_6) δ = 8.60 (d, 1H, J = 6.0 Hz), 7.83 (s, 1H), 7.77-7.73 (m, 2H), 7.11-7.07 (m, 2H), 6.95 (td, 1H, J = 7.7, 1.2 Hz), 2.54 (s, 3H), 1.66 (s, 15H). **ESI-MS** (MeOH) m/z = 496.0 $[M\text{-}Cl]^+$. **CHN analysis** calc. for $C_{22}H_{25}NClIr$ C – 49.75%, H – 4.74%, N – 2.64%. Found C – 49.48%, H – 4.66%, N – 2.58%. **HPLC Purity** 254 nm – 98.2 %.

[(η^5-Cp*)Ir(2-phenyl-5-methylpyridine)Cl] (15) As described in the above method using 2-phenyl-5-methylpyridine (41 mg, 0.242 mmol), dichloromethane (20 mL), sodium acetate (40 mg, 0.484 mmol) and [(η^5-Cp*)$IrCl_2$]$_2$ (96 mg, 0.121 mmol). The crude product was recrystallised from chloroform/hexane at 273 K to yield an orange crystalline solid (60 mg, 47%). **^{1}H NMR** (400 MHz, dmso-d_6) δ = 8.48 (s, 1H), 7.98 (d, 1H, J = 8.3 Hz), 7.76-7.66 (m, 3H), 7.09 (td, 1H, J = 7.3, 1.2 Hz), 6.96 (td, 1H, J = 7.4, 0.9 Hz), 2.39 (s, 3H), 1.60 (s, 15H). **ESI-MS** (MeOH) m/z = 496.0 $[M\text{-}Cl]^+$. **CHN analysis** calc. for $C_{22}H_{25}NClIr$ C – 49.75%, H – 4.74%, N – 2.64%. Found C – 49.36%, H – 4.61%, N – 2.51%. **HPLC Purity** 254 nm – 98.6 %.

[(η^5-Cp*)Ir(2-(4′-trifluoromethylphenyl)pyridine)Cl] (16) As described in the above method using 2-(4′-trifluoromethylphenyl)pyridine (39 mg, 0.173 mmol), dichloromethane (18 mL), sodium acetate (28 mg, 0.340 mmol) and [(η^5-Cp*)$IrCl_2$]$_2$ (69 mg, 0.087 mmol). The crude product was recrystallised from chloroform/hexane at 273 K to yield an orange crystalline solid (51 mg, 52%). **^{1}H NMR** (400 MHz, acetone-d_6) δ = 8.86 (d, 1H, J = 5.7 Hz), 8.18 (d, 1H, J = 8.2 Hz), 8.03 (d, 1H, J = 6.3 Hz), 7.98-7.91 (m, 2H), 7.41-7.37 (m, 1H), 7.29 (dd, 1H, J = 8.1, 1.5 Hz), 1.69 (s,

15H). **ESI-MS** (MeOH) m/z = 550.1 $[M\text{-}Cl]^+$. **CHN analysis** calc. for $C_{22}H_{22}NClF_3Ir$ C – 45.16%, H – 3.79%, N – 2.39%. Found C – 44.86%, H – 3.66%, N – 2.26%. **HPLC Purity** 254 nm – 99.1 %. Crystals suitable for X-ray diffraction were obtained by slow evaporation of a chloroform/hexane solution at 278 K.

[(η^5-Cp*)Ir(2-(4'-methoxyphenyl)pyridine)Cl][36] (17) As described in the above method using 2-(4'-methoxyphenyl)pyridine (40 mg, 0.218 mmol), dichloromethane (20 mL), sodium acetate (36 mg, 0.436 mmol) and $[(\eta^5\text{-Cp*})IrCl_2]_2$ (87 mg, 0.109 mmol). The crude product was recrystallised from chloroform/hexane at 273 K to yield a yellow crystalline solid (60 mg, 50%). **^{1}H NMR** (300 MHz, dmso-d_6) δ = 8.63 (d, 1H, J = 5.9 Hz), 7.95 (d, 1H, J = 7.8 Hz), 7.82-7.74 (m, 2H), 7.21-7.17 (m, 2H), 6.59 (dd, 1H, J = 8.4, 2.4 Hz), 3.83 (s, 3H), 1.60 (s, 15H). **ESI-MS** (MeOH) m/z = 512.2 $[M\text{-}Cl]^+$. **CHN analysis** calc. for $C_{22}H_{25}NClIrO$ C – 48.30%, H – 4.61%, N – 2.56%. Found C – 47.96%, H – 4.29%, N – 2.52%. **HPLC Purity** 254 nm – 98.5 %.

3.2.3 Methods

3.2.3.1 X-ray Crystallography

The X-ray crystal structures of complexes **1**, **2** and **16** were determined by Dr. Guy Clarkson (Department of Chemistry, University of Warwick) as described in Chapter 2 (section 2.2.8).

3.2.3.2 HPLC

3.2.3.2.1 Purity Measurements

RP-HPLC purity measurements of complexes **1-17** (ca. 100 μM, 2.7% dmso/97.3% H_2O v/v) were performed as described in Chapter 2 9 (section 2.2.5.1).

3.2.3.2.2 Separation of Enantiomers

The enantiomeric separation of complexes **1**, **2**, **6** and **16** was performed using chiral NP-HPLC as described in Chapter 2 (section 2.2.5.3) with the assistance of Dr. Ruth McQuitty (Department of Chemistry, University of Warwick).

The stability of the separated enantiomers of complex **6** was determined by multiple collections of each peak where the fractions were stored at 273 K for 3 days before being concentrated to dryness under vacuum with no heating, followed by re-dissolution and injection into the HPLC to analyse the stability of each enantiomer.

3.2.3.2.3 Relative Hydrophobicity Measurements

Relative hydrophobicity measurements of complexes **2**, **4**, **7**, **8** and **11-14** using RP-HPLC were performed as described in Chapter 2 (section 2.2.5.2). Samples were dissolved in 10% MeOH/90% H_2O (v/v) in 50 mM NaCl at ca 100 μM. Reported retention times (t_R) and standard deviations (SD) are from duplicate of triplicate measurements.

3.2.3.3 Computation

DFT calculations were performed as described in Chapter 2 (section 2.2.9). Electrostatic potential surfaces (EPS) for complexes **2**, **4**, **7**, **8** and **11-13** where the EPSs are shown both in space (with positive and negative regions in blue and red, respectively) and mapped on electron density (isovalue 0.04) of the molecules. The electrostatic potential is represented with a colour scale ranging from red (-0.040 au) to blue (+0.250 au).

3.2.3.4 Hydrolysis Studies

The aquation of complexes (ca. 500 μM) was monitored by 600 MHz ^{1}H NMR spectroscopy over 24 h in 26.7% MeOD/73.3% D_2O (v/v) at 310 K using a Bruker

AV III 600 NMR spectrometer. All spectra were internally referenced to 1,4-dioxane (3.75 ppm) and water suppression was performed using Shaka techniques.[37] NaCl was added to aid assignment of species to either the Ir-OD_2/OD or Ir-Cl adducts. Percentages of each adduct were based on ^{1}H NMR peak integrations.

3.2.3.5 Reactions with Model Nucleobases

The reactions of complexes **2**, **4**, **7**, **8** and **11-14** (*ca*. 500 μM) with 9-EtG and 9-MeA (ca. 500 μM) were monitored by ^{1}H NMR spectroscopy. Typically, one mol equiv of 9-EtG in D_2O was added to a solution of complex in MeOD-d_4/D_2O to give a final complex concentration of ca. 500 μM in 26.7% MeOD-d_4/73.3% D_2O (v/v). ^{1}H NMR spectra were recorded at various time intervals at 310 K and samples incubated at this temperature during the course of the reaction. Percentage binding was based on peak integrations.

3.2.3.6 Catalytic Oxidation of NADH to NAD^+

Complexes **2**, **4**, **11** and **12** were evaluated for the catalytic oxidation of NADH to NAD^+ by UV-visible spectroscopy over a 24 h period in 0.5% MeOH/99.5% H_2O.(v/v) at 310 K in 5 mM Na_2HPO_4/NaH_2PO_4 buffer, pH 7.5. The complex concentration remained fixed at 2.5 μM with NADH concentrations of 69, 103, 127 and 146 μM. The conversion of NADH to NAD^+ was followed by absorption at 339 nm (ε_{NADH} = 6220 cm^{-1} M^{-1}) to allow evaluation of kinetic data.

The reaction between complex **2** (250 μM) and NADH (750 μM) in 50% MeOD/50% H_2O (v/v) at 310 K, pH* 7.4 was monitored by ^{1}H NMR spectroscopy.

Detection of the production of H_2O_2 was attempted during the reaction between complex **2** (250 μM) and NADH (750 μM) in 1:1 MeOH:H_2O at 310 K using quantofix peroxide test sticks.

Detection of the production of H_2 was investigated for the reaction between complex **2** (250 μM) and NADH (750 μM) in 50% MeOD/ 50% H_2O (v/v) at 310 K after 24 h reaction time by gas chromatography by taking aliquots (100 μL) of the headspace. The instrument used was an Agilent GC 7890A equipped with a thermal conductivity detector; a 5-Å molecular sieve column, using N_2 as the carrier gas. Under these conditions, H_2 has a retention time of 0.39 min.

3.2.3.7 Antiproliferative Activity

Antiproliferative activity assays were performed by Dr. Isolda Romero-Canelón (Department of Chemistry, University of Warwick) as described in Chapter 2 (section 2.2.14.2). Complexes **1-17** were evaluated for activity in the A2780 human ovarian cancer cell line and complexes **1**, **2**, **5**, **6**, **8**, **10**, **11** and **14** in HCT-116 (colon), MCF-7 (breast) and A549 (lung) cancer cell lines. Concentrations of stock solutions were determined by ICP-OES measurements.

3.2.3.8 Metal Accumulation in A2780 Cancer Cells

Metal accumulation studies for complexes **2**, **4**, **7**, **8** and **11-14** were conducted on the A2780 ovarian carcinoma cell line by Dr. Isolda Romero-Canelón (Department of Chemistry, University of Warwick). Briefly, 1.5 x 10^6 cells were seeded on a 6 well plate, after 24 h of pre-incubation time in drug-free medium, at 310K in a 5% CO_2 humidified atmosphere; the test complexes were added to give final concentrations equal to IC_{50} and then allowed a further 24 h of drug exposure under similar conditions. These experiments did not include any cell recovery time in drug-free media. After this time, cells were treated with trypsin, counted, and cell pellets were collected. Each pellet was digested overnight in concentrated nitric acid (73%) at 353 K; the resulting solutions were diluted to 5% v/v HNO_3 using doubly

deionized water, and the amount of iridium taken up by the cells was determined by ICP-MS. They were all carried out in triplicate in two set of independent experiments and the standard deviations were calculated.

3.2.3.9 Metal Distribution in A2780 Cancer Cells

Metal distribution studies for complexes **2** and **4** were conducted on the A2780 ovarian carcinoma cell line by Dr. Isolda Romero-Canelón (Department of Chemistry, University of Warwick). Cell pellets were obtained as described above (section 3.2.3.8), and were fractionated using the FractionPREP kit from BioVision according to the supplier's instructions. Each sample was digested overnight in concentrated nitric acid (73%) and the amount of Ir taken up by the cells was determined by ICP-MS. The experiments were all carried out in triplicate and the standard deviations were calculated. Statistical significance between results was established from the Student's T test where ** = ($p < 0.01$).

3.2.3.10 ICP-OES Analysis

ICP-OES analyses were carried out as described in Chapter 2 (section 2.2.10). Calibrants were freshly prepared at concentrations of 1000, 800, 600, 400, 200 and 100 ppb which and were spiked with NaCl to match the salt content of the samples being analysed.

3.2.3.11 ICP-MS Analysis

ICP-MS analyses were carried out as described in Chapter 2 (section 2.2.11). Calibrants were freshly prepared at concentrations of 100, 80, 60, 40, 20, 5, 1, 0.8 and 0.5 ppb.

3.3 Results

3.3.1 Synthesis and Characterisation

Seventeen iridium(III) half-sandwich complexes bearing functionally diverse 2-PhPy ligands (Chart 3.1) were synthesised and characterised by ^{1}H NMR spectroscopy, ESI-MS, CHN analysis and RP-HPLC. Functionalised 2-PhPy ligands bearing either electron-withdrawing or electron-donating substituents were synthesised using Suzuki-Miyaura palladium cross-coupling chemistry following an adapted literature protocol.[35] They were purified using flash silica gel chromatography with mixtures of chloroform/ethyl acetate yielding 2-(R'-phenyl)-R-pyridine ligands **L1-17**. The synthesis of the corresponding complexes [(η^5-Cp*)Ir(2-(R'-phenyl)-R-pyridine)Cl] (**1-17**) was carried out using an adapted literature procedure,[27] involving stirring of 2 mol equiv of 2-(R'-phenyl)-R-pyridine ligand in DCM with 4 mol equiv of sodium acetate followed by addition of 1 mol equiv of [η^5-Cp*)$IrCl_2]_2$ at ambient temperature for 18 h. After filtering the reaction mixture through celite, the mixture was concentrated to dryness then recrystallised in chloroform/hexane at 278 K. The synthetic routes for the complexes are shown in Scheme 3.1. The introduction of electron-withdrawing nitro (-NO_2) and aldehydic (-CHO) groups and the electron-donating hydroxymethyl group (-CH_2OH) in complexes **5-10** are the first to be reported in complexes of the type [(η^5-Cp*)Ir(2-PhPy)X]$^{0/+}$. Complex [(η^5-Cp*)Ir(2-(4'-methoxyphenyl)pyridine)Cl] **17** has been previously reported[36] but investigations into its biological activity have not been performed.

Scheme 3.1. Synthetic route for 2-(R'-phenyl)-R-pyridine ligands **L1-17** (**A**) and [(η^5-Cp*)Ir(2-(R'-phenyl)-R-pyridine)Cl] complexes **1-17** (**B**).

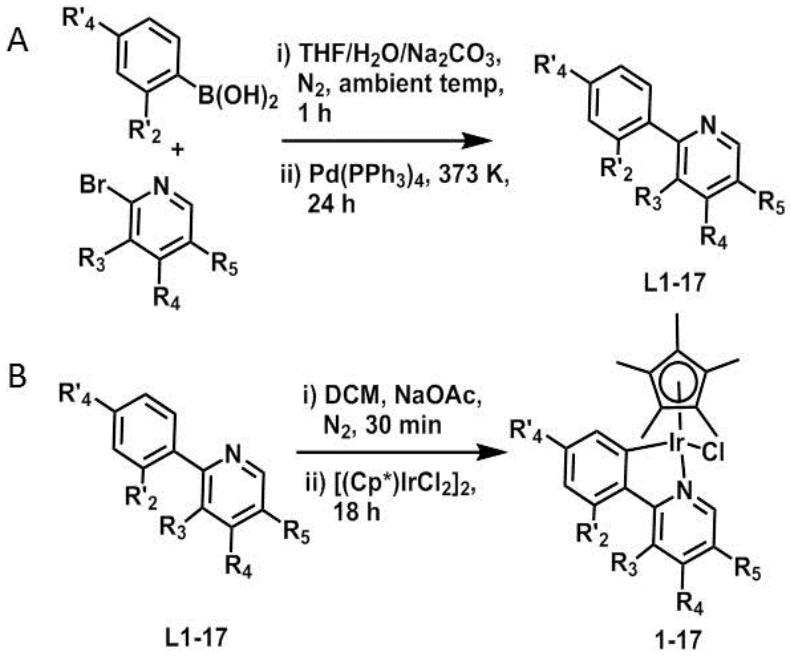

The X-ray crystal structures of complexes [(η^5-Cp*)Ir(2-(2'-fluorophenyl)pyridine)Cl] **1**, [(η^5-Cp*)Ir(2-(4'-fluorophenyl)pyridine)Cl] **2** and [(η^5-Cp*)Ir(2-(4'-trifluoromethylphenyl)pyridine)Cl] **16** were determined and are shown in Figure 3.1, with X-ray crystallographic data listed in Table 3.1 and selected bond lengths and angles in Table 3.2. The complexes exhibit the expected pseudo-octahedral half-sandwich structure, with the Cp* ring occupying three coordination sites. The 2-PhPy chelating ligand occupies two sites and the monodentate chlorido ligand occupies the sixth coordination position. The Ir-centroid distances range from 1.828-1.837 Å, Ir-C distances from 2.0346-2.0482 Å, Ir-N distances from 2.0797-2.093 Å and Ir-Cl distances from 2.4026-2.4159 Å. The bond angle between the chelating ligand and iridium centre (C-Ir-N) is the smallest in all cases, ranging from 77.84-78.13°.

Complex **1** was modelled as disordered over two positions related by swapping the position of the pyridine and the 2-fluorophenyl rings. The disorder was simply modelled by interchanging the carbon (C12) and the associated carbon and fluorine atoms on that ring with the nitrogen (N1) bound to the metal. This was refined to an occupancy of 80:20. Therefore, in any particular position the site is occupied 80% by one enantiomer and 20% by the other enantiomer. As there is an inversion centre in the space group (P2(1)/n), there is another position occupied by 80% of the time by the other enantiomer and 20% of the time by the other. This results in an overall 50:50 racemate.

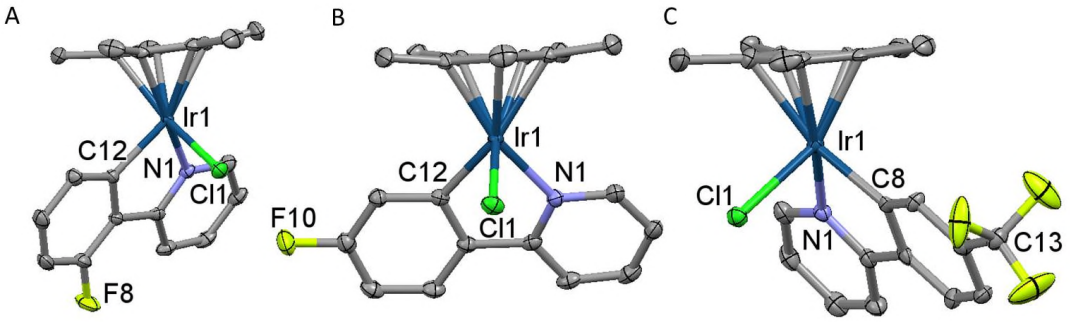

Figure 3.1. X-ray crystal structures of [(η^5-Cp*)Ir(2-(2'-fluorophenyl)pyridine)Cl] **1**, [(η^5-Cp*)Ir(2-(4'-fluorophenyl)pyridine)Cl] **2** and [(η^5-Cp*)Ir(2-(4'-trifluoromethylphenyl)pyridine)Cl] **16**. Hydrogen atoms have been omitted for clarity and thermal ellipsoids are shown at 50% probability. Disorder found in complex **1** is omitted for clarity.

Table 3.1. Summary of the X-ray crystallographic data for complexes [(η^5-Cp*)Ir(2-(2'-fluorophenyl)pyridine)Cl] **1**, [(η^5-Cp*)Ir(2-(4'-fluorophenyl)pyridine)Cl] **2** and [(η^5-Cp*)Ir(2-(4'-trifluoromethylphenyl)pyridine)Cl] **16**

	1	**2**	**16**
Formula	$C_{21}H_{22}ClFIrN$	$C_{21}H_{22}ClFIrN$	$C_{22}H_{22}ClF_3IrN$
MW	535.05	535.05	585.06
Crystal Colour	Yellow	Yellow	Yellow
Cryst size (mm)	0.30 x 0.20 x 0.12	0.40 x 0.18 x 0.10	0.20 × 0.20 × 0.08
λ (Å)	0.71073	0.71073	1.54184
Temp (K)	150	150	100
Cryst system	Monoclinic	Monoclinic	Monoclinic
Space group	P2(1)/n	P2(1)/n	P2(1)/c
a (Å)	8.37197(9)	8.27453(11)	15.4953(4)
b (Å)	15.71819(18)	15.70747(16)	7.76677(19)
c (Å)	13.73371(17)	13.83772(14)	16.4333(3)
α (°)	90	90	90
β (°)	92.8873(11)	93.1162(11)	92.690(2)
γ (°)	90	90	90
Vol (Å^3)	1804.95(4)	1795.86(3)	1975.54(8)
Z	4	4	4
$R(Fo^2)$	0.0172	0.0199	0.0363
$Rw(Fo^2)$	0.0381	0.0490	0.0997
GOF	1.092	1.095	1.050

Table 3.2. Selected bond lengths (Å) and bond angles (deg) for complexes [(η^5-Cp*)Ir(2-(2'-fluorophenyl)pyridine)Cl] **1**, [(η^5-Cp*)Ir(2-(4'-fluorophenyl)-pyridine)Cl] **2** and [(η^5-Cp*)Ir(2-(4'-trifluoromethylphenyl)pyridine)Cl] **16**

Bond/angle	**1**	**2**	**16**
Ir-C (Cp* ring)	2.163(2)	2.160(2)	2.157(4)
	2.1675(19)	2.1609(19)	2.169(5)
	2.177(2)	2.172(2)	2.170(4)
	2.239(2)	2.2522(19)	2.265(5)
	2.247(2)	2.272(2)	2.284(4)
Ir-C (centroid)	1.828	1.833	1.837
Ir-C	2.0482(18)	2.0346(19)	2.045(5)
Ir-N	2.0797(17)	2.0931(16)	2.093(4)
Ir-Cl	2.4056(5)	2.4026(5)	2.4159(11)
C-Ir-N	77.84(7)	78.13(7)	77.95(18)
C-Ir-Cl	85.96(5)	85.68(5)	88.40(13)
N-Ir-Cl	87.60(5)	87.30(5)	85.94(11)

Weak off-set intermolecular π-π stacking between the 2-PhPy ligands is observed in the X-ray crystal structures of complexes **1** and **2** with a centroid-centroid distance of 4.140 Å and 4.059 Å, respectively (Figure 3.2).

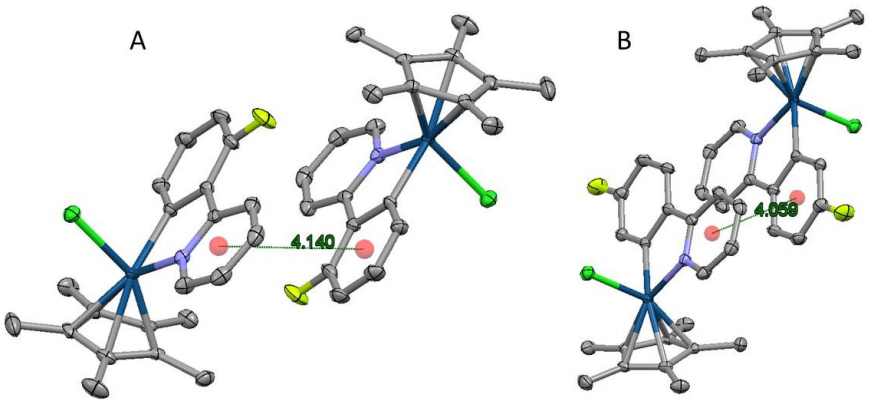

Figure 3.2. Diagram showing the π-π stacking interaction in the X-ray crystal structures of complexes [(η^5-Cp*)Ir(2-(2'-fluorophenyl)pyridine)Cl] **1** (A) and [(η^5-Cp*)Ir(2-(4'-fluorophenyl)pyridine)Cl] **2** (B) where the centroid – centroid distance between pyridyl-phenyl rings of independent molecules is 4.140 and 4.059 Å for **1** and **2**, respectively. Thermal ellipsoids drawn at 50% with hydrogen atoms removed for clarity.

The electrostatic potential surfaces (EPS) of complexes [(η^5-Cp*)Ir(2-(4'-fluorophenyl)pyridine)Cl] **2**, [(η^5-Cp*)Ir(2-phenyl-5-fluoropyridine)Cl] **4**, [(η^5-Cp*)Ir(2-(4'-nitrophenyl)pyridine)Cl] **7**, [(η^5-Cp*)Ir(2-phenyl-4-nitropyridine)Cl] **8**, [(η^5-Cp*)Ir(2-(4'-hydroxyphenyl)pyridine)Cl] **11**, [(η^5-Cp*)Ir(2-phenyl-5-hydroxypyridine)Cl] **12** and [(η^5-Cp*)Ir(2-(2'-methylphenyl)pyridine)Cl] **13** were calculated using DFT methods at the PBE0/Lanl2DZ/6-31+G** level,[38-40] based on the crystal structure of complex **2**, with functional group modifications being made with GaussView 3.0.[41] for the rest of the complexes. The resulting EPS of each complex is shown in Figure 3.3. The phenyl ring in the chelating ligand exhibits a more negative electrostatic potential than the pyridyl ring due to the deprotonated

carbon bonded to the Ir centre. There are no major differences in the charge distribution at the iridium centre, Cp* ring or chlorido ligands among the complexes, indicating that the substituent on the chelating ligand causes only a localised effect. Complexes **7** and **8** contain the electron-withdrawing nitro group on the phenyl and pyridyl ring, respectively, causing a more positive surface. Complex **13** bears a methyl group on the phenyl ring which pushes electron density into the ring, causing a more negative EPS. The substituents themselves cause the outer EPS of each complex to alter significantly.

The calculated bond lengths at the metal centre are shown in Table 3.3, which shows minimal difference among the complexes, with the exception of **13** which exhibits a shorter Ir-N bond. Generally, the calculated bond lengths of complex **2** are in good agreement with those obtained by X-ray diffraction.

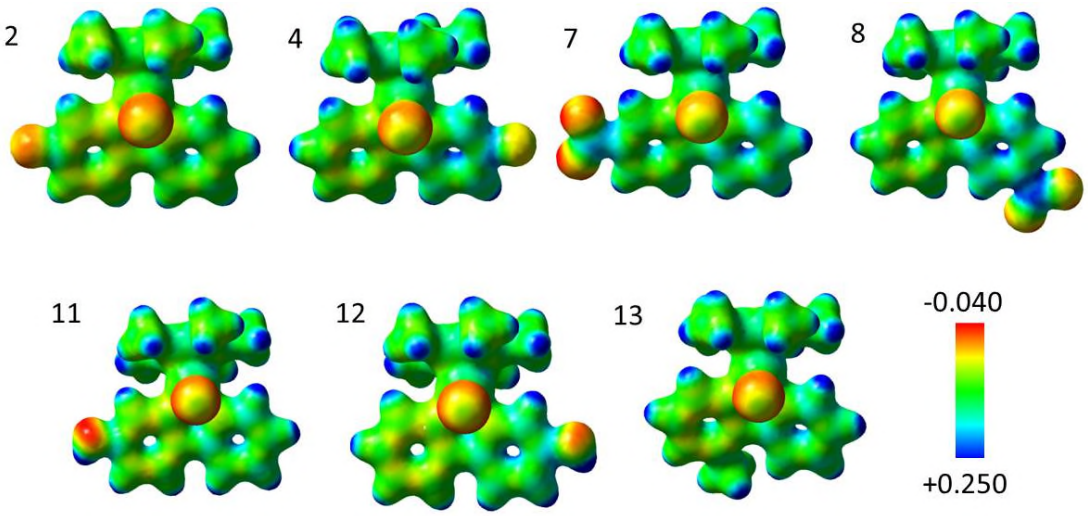

Figure 3.3. Electrostatic potential surfaces for complexes **2**, **4**, **7**, **8** and **11-13** (calculated at the PBE0/Lanl2DZ/6-31+G** level) where the EPS are shown both in space (with positive and negative regions in blue and red, respectively) and mapped on electron density (isovalue 0.04) of the molecules. The electrostatic potential is represented with a colour scale ranging from red (-0.040 au) to blue (+0.250 au).

Table 3.3. Calculated bond lengths for complexes **2**, **4**, **7**, **8** and **11-13** (calculated at the PBE0/Lanl2DZ/6-31+G** level).

	Calculated bond lengths (Å)			
Complex	Ir-Cp* (centroid)	Ir-C	Ir-N	Ir-Cl
2	1.862	2.008	2.078	2.410
4	1.862	2.011	2.076	2.411
7	1.861	2.006	2.078	2.412
8	1.864	2.009	2.069	2.408
11	1.862	2.009	2.078	2.411
12	1.862	2.012	2.077	2.412
13	1.868	2.004	2.058	2.414

3.3.2 Separation of Enantiomers

The complexes studied in this chapter exhibit chirality at the metal centre, resulting in the formation of a racemic solution of R and S enantiomers. The enantiomeric separation of complexes [(η^5-Cp*)Ir(2-(2'-fluorophenyl)pyridine)Cl] **1**, [(η^5-Cp*)Ir(2-(4'-fluorophenyl)pyridine)Cl] **2**, [(η^5-Cp*)Ir(2-phenyl-5-pyridine-carboxaldehyde)Cl] **6** and [(η^5-Cp*)Ir(2-(4'-trifluorophenyl)pyridine)Cl] **16** was attempted using chiral HPLC, where the stationary phase (CHIRALPAK® IA) is a chiral sugar (amylose tris(3,5-dimethylphenylcarbamate)) immobilized on 3 μm silica-gel. The resulting HPLC traces from the injection of the racemic solutions of each complex (EtOH, 1 mg mL^{-1}) are shown in Figure 3.4. Two peaks are present in each case, indicating the presence of two enantiomers in each solution. Integration of each peak shows that a racemic mixture is present for **1**, **6** and **16**, while **2** appears to have a slight excess of one enantiomer. Complexes **1**, **2** and **6** show good separations of enantiomers while the enantiomers of **16** exhibit similar retention times (6.94 and 7.50 min).

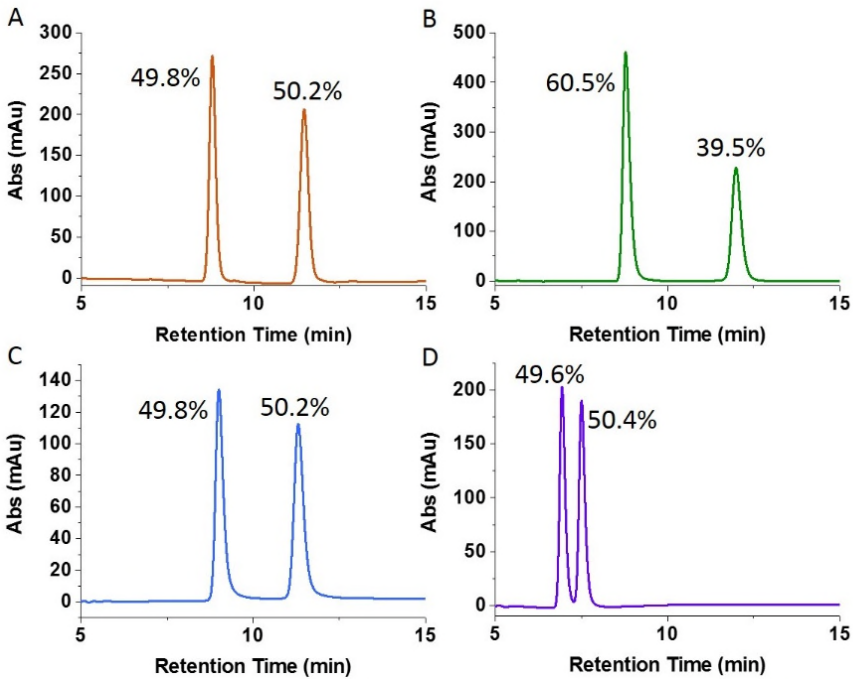

Figure 3.4. Chiral HPLC traces of complexes **1** (A), **2** (B), **6** (C) and **16** (D) (1 mg mL^{-1}, $\lambda = 260$ nm)

The stability of the separated enantiomers of complex **6** was assessed by collecting the two eluting peaks. The fractions were stored at 273 K for 3 days before being concentrated to dryness under vacuum with no heating, followed by re-dissolution and injection into the column. The resulting HPLC traces are shown in Figure 3.5, which show that each enantiomer epimerises to a racemic mixture of R and S under the conditions they were stored under.

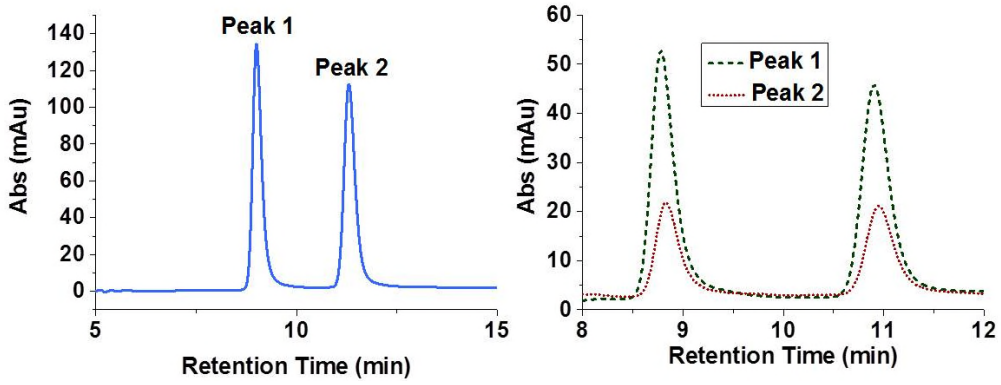

Figure 3.5 Chiral HPLC traces of complex **6** after re-injection of collected peaks. The appearance of two peaks in each fraction indicates epimerisation to a racemic mixture has occurred.

3.3.3 Hydrolysis Studies

The hydrolysis of complexes **1-17** (ca 500 μM) was studied by ^{1}H NMR spectroscopy in 26.7% MeOD-d_4/ 73.3% D_2O at 310 K. Methanol was required to ensure sufficient solubility of the complexes in aqueous solution. Hydrolysis equilibrium was reached before the time taken to acquire the first spectra (15 min), consistent with previous reports of Ir(III) *C,N*-chelated half-sandwich complexes.[27] Hydrolysis was confirmed by the sequential addition of NaCl, showing an increase in the peaks associated with the Ir-Cl species and a decrease in the peaks associated with the Ir-OD_2/OD species, as exemplified for complex **11** in Figure 3.6 a. Between 66-80% was found to be in the hydrolysed form, based on peak integrations (Figure 3.6 b). With 4 mM NaCl present, almost all of the Ir-OD_2/OD species had been converted to the Ir-Cl complexes. Above this concentration of NaCl, precipitation of the complexes was observed. The hydrolysed complexes exhibit a down-field shift of the aromatic protons of around 0.15 ppm compared to the parent chlorido complexes. Determination of the pK_a values of the complexes was attempted, but solubility issues prevented reliable analysis by ^{1}H NMR spectroscopy.

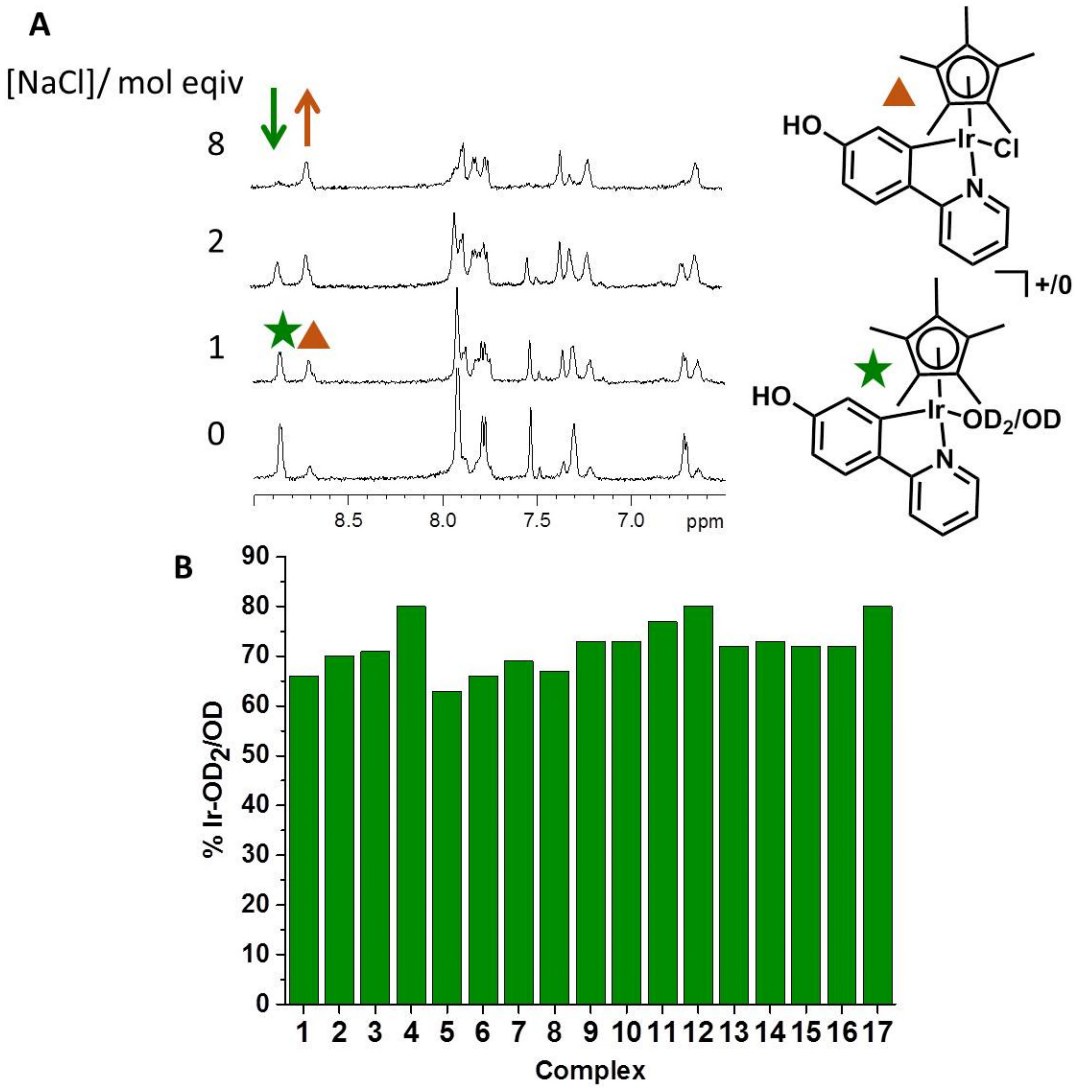

Figure 3.6. (A) ^{1}H NMR (600 MHz) spectra of complex **11** (c.a. 500 μM) in 26.7% MeOD-d_4/73.3% D_2O (v/v) at 310 K. Hydrolysis equilibrium was reached within the time taken to acquire the first spectrum. Sequential addition of NaCl resulted in conversion from the **11-OD$_2$/OD** (★) complex to the **11-Cl** (▲) complex. (B) Percentage of hydrolysis (Ir-OD_2/OD) for complexes **1-17** at equilibrium (15 min).

3.3.4 Binding to Nucleobases

As DNA is believed to be a major target for anticancer coordination complexes, compounds **2**, **4**, **7**, **8** and **11-14** (ca 500 μM) were evaluated for their ability to bind to model nucleobases 9-EtG and 9-MeA in ca. 1:1 mol ratios of complex:nucleobase by ^{1}H NMR spectroscopy in 26.7% MeOD-d_4/ 73.3% D_2O at 310 K, pH* 7.4 after

incubation for 15 min and 24 h (shown for complex **2** in Figure 3.7). All complexes showed 100% binding to 9-EtG and ca. 50-80% binding to 9-MeA after 15 min, which remained unchanged over a period of 24 h (Table 3.4). The binding of complex **2** to 9-EtG was confirmed by ESI-MS where the m/z peak 679.2 was observed which corresponds to the species $[(\eta^5\text{-Cp*})\text{Ir}(2\text{-}(4'\text{-fluorophenyl})\text{pyridine})9\text{-EtG}]^+$ (calculated m/z = 679.22). Binding of 9-EtG to **2** and **4** in the presence of 4 mM NaCl, where the complexes exist primarily as the Ir-Cl species, reached 100% after 24 h. Complex **11** shows markedly higher affinity towards 9-MeA binding at 82%, while the structural isomer **12** exhibits the next highest 9-MeA binding (64%). In most cases, only one set of peaks corresponding to 9-MeA binding was observed, with the exception of complex **12** where two peaks were present, perhaps indicating binding through both N1 and N7 atoms.

Competitive binding of 9-EtG and 9-MeA was also investigated under the same conditions. This resulted in mostly 9-EtG binding for all the complexes (Table 3.4). Complexes **2**, **4** and **14** show 5-10% binding to 9-MeA in the presence of 9-EtG.

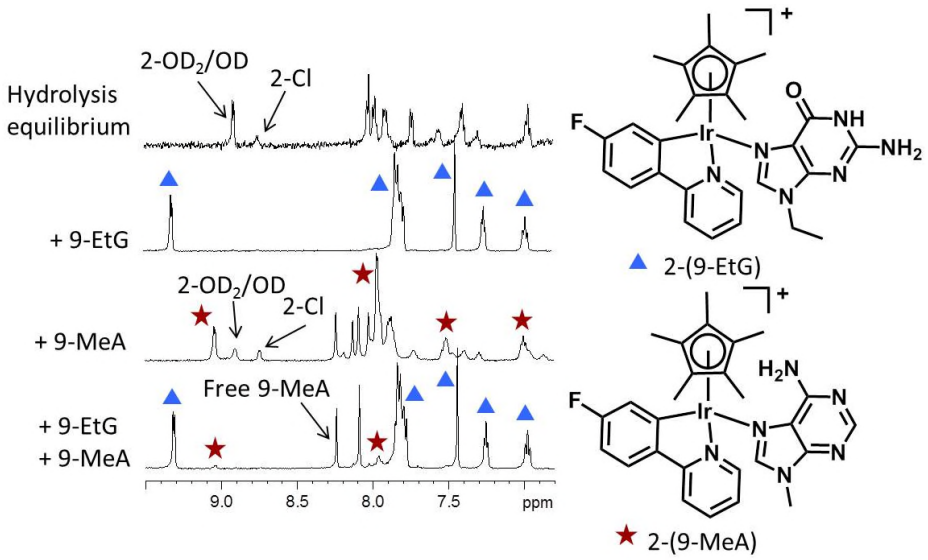

Figure 3.7. Interaction of complex **2** (ca. 500 μM) with equimolar amounts of 9-EtG, 9-MeA and competition binding by ^{1}H NMR spectroscopy (600 MHz, 26.7% MeOD-d_4/ 73.3% D_2O (v/v) at 310 K, pH* 7.4, 24 h). Complex **2** shows 100% binding to 9-EtG (▲) and around 50% binding to 9-MeA (★) and a preference for binding to 9-EtG upon co-incubation with 9-EtG and 9-MeA.

Table 3.4. Percentage binding of complexes **2**, **4**, **7**, **8** and **11-14** (ca 500 μM) with 9-EtG, 9-MeA and competition binding upon co-incubation at 1:1 mol ratios. Percentage binding was determined by ^{1}H NMR spectroscopy (600 MHz, 26.7% MeOD-d_4/ 73.3% D_2O at 310 K, pH* 7.4, 24 h) based on peak integrations.

Complex	Percentage binding (%)			
			Competitive binding	
	9-EtG	9-MeA[a]	9-EtG	9-MeA
2	100	56	90	10
4	100	54	90	10
7	100	54	100	0
8	100	58	100	0
11	100	82	100	0
12	100	64	100	0
13	100	58	100	0
14	100	50	95	5

[a]Overlapping peaks in the ^{1}H NMR spectra made accurate quantitative analysis difficult.

3.3.5 Catalysis of NADH oxidation

The ability to disrupt the redox balance of cells by the catalytic oxidation of NADH has been suggested to be of importance to the mechanism of action of iridium(III) half-sandwich complexes.[31,32,42] The reaction between NADH and complexes **2**, **4**, **11** and **12** was monitored by UV-Vis spectroscopy at varying concentrations of NADH (69, 103 and 146 μM) with a fixed concentration of complex (2.5 μM) over a period of 24 h at 310 K, pH 7.5 (Na_2HPO_4/NaH_2PO_4 buffer, 5 mM). The decrease in the band at 339 nm was monitored as it corresponds to conversion of NADH to NAD^+ (Figure 3.8 a). The data were also the basis for the calculation of the turnover number (TON) and turnover frequency (TOF, h^{-1}) for each complex at different concentrations (Table 3.5). After 24 h, the maximum TON was found for each complex at the highest concentration of NADH (146 μM), and ranged from 22-28. Maximum TOF was also reached at 146 μM NADH, ranging from 1.1-3.2 h^{-1}. The reaction proceeded via first order kinetics with respect to [NADH] (Figure 3.8 b), with an average rate constant *k* of 3.79×10^{-4} min^{-1} for **2** and 4.03×10^{-4} min^{-1} for **4.** However, complexes **11** and **12**, which bear the hydroxyl group, gave a non-first order reaction with respect to [NADH] during the first 3 h, followed by the expected first-order kinetics (exemplified for complex **11** in Figure 3.8 c). These results indicate that each of these complexes shows catalytic behaviour towards the oxidation of NADH.

Table 3.5. TONs and TOFs for complexes **2**, **4**, **11** and **12** for the catalytic oxidation of NADH to NAD^+ monitored *via* UV-visible spectroscopy at various concentrations of NADH (69, 103 and 146 μM) with a fixed complex concentration of 2.5 μM over a 24 h period in 0.5% MeOH/99.5% H_2O (v/v) at 310 K in 5 mM Na_2HPO_4/NaH_2PO_4 buffer, pH 7.5. The conversion of NADH to NAD^+ was followed from the absorption at 339 nm.

Complex	NADH (μM)	TON (24 h)	TOF (h^{-1})[a]
[(η^5-Cp*)Ir(2-(4'-fluorophenyl)pyridine)Cl] **2**	69	11	0.6
	103	19	1.1
	146	22	1.2
[(η^5-Cp*)Ir(2-phenyl-5-fluoropyridine)Cl] **4**	69	13	0.7
	103	20	1.2
	146	22	1.1
[(η^5-Cp*)Ir(2-(4'-hydroxyphenyl)pyridine)Cl] **11**	69	14	1.9
	103	21	2.6
	146	28	3.2
[(η^5-Cp*)Ir(2-phenyl-5-hydroxypyridine)Cl] **12**	69	13	1.4
	103	15	1.8
	146	22	2.6

[a]TOFs were calculated as the gradient of time vs. TON during the first 2 h of the reaction time.

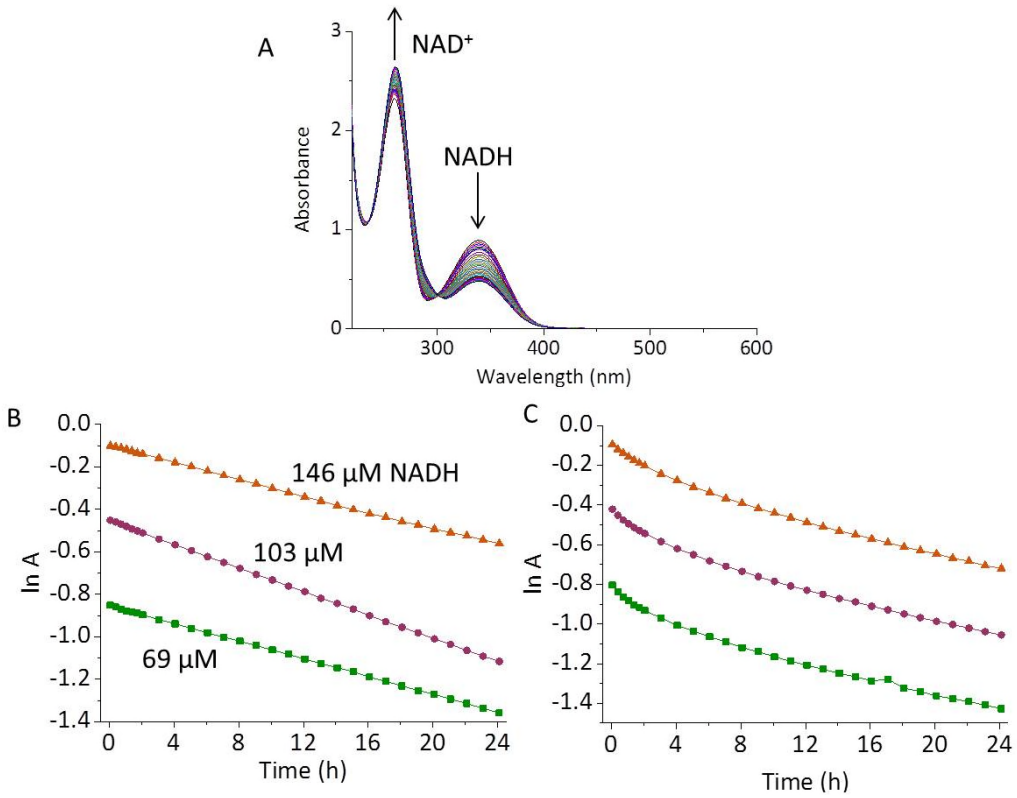

Figure 3.8. (a) UV-Visible spectra for the catalytic oxidation of NADH (146 µM) to NAD^+ in the presence of complex **2** (2.5 µM) over a 24 h period in 0.5% MeOH/99.5% H_2O at 310 K in 5 mM Na_2HPO_4/NaH_2PO_4 buffer, pH 7.5. (b) First order kinetic plot for complex **2** [NADH] = 69 µM (green), 103 µM (purple) and 146 µM (orange). (c) First order kinetic plot for complex **11** [NADH] = 69 µM (green), 103 µM (purple) and 146 µM (orange) showing unusual kinetics for first 3 h followed by first-order reaction kinetics.

In order to probe whether the oxidation proceeds *via* the formation of an iridium-hydride species, the reaction of complex **2** (250 µM) with NADH (750 µM) in 50% MeOD-d_4/ 50% D_2O (v/v) at 310 K was monitored by ^1H NMR spectroscopy over a 15 h period. After 15 min, a peak corresponding to an Ir-H species was observed at -14.84 ppm (Figure 3.9), which was no longer visible after 15 h. The conversion of NADH to NAD^+ was also confirmed by the appearance of a new set of peaks corresponding to the formation of NAD^+.

Complex **2** (250 μM) was studied for the production of hydrogen by gas chromatography after 24 h as a by-product of the reaction with NADH (750 μM) in 1:1 MeOH:H_2O at 310 K in 5 mM Na_2HPO_4/NaH_2PO_4 buffer, pH 7.5. Analysis of the head space revealed no detectable H_2 production. The production of H_2O_2 upon reaction of complex **2** (250 μM) with NADH (750 μM) in the presence of O_2 in 1:1 MeOH: H_2O at 310 K was measured by Quantofix peroxide sticks after periods of 8, 12 and 24 h reaction times, but no H_2O_2 was detected during the course of the reaction.

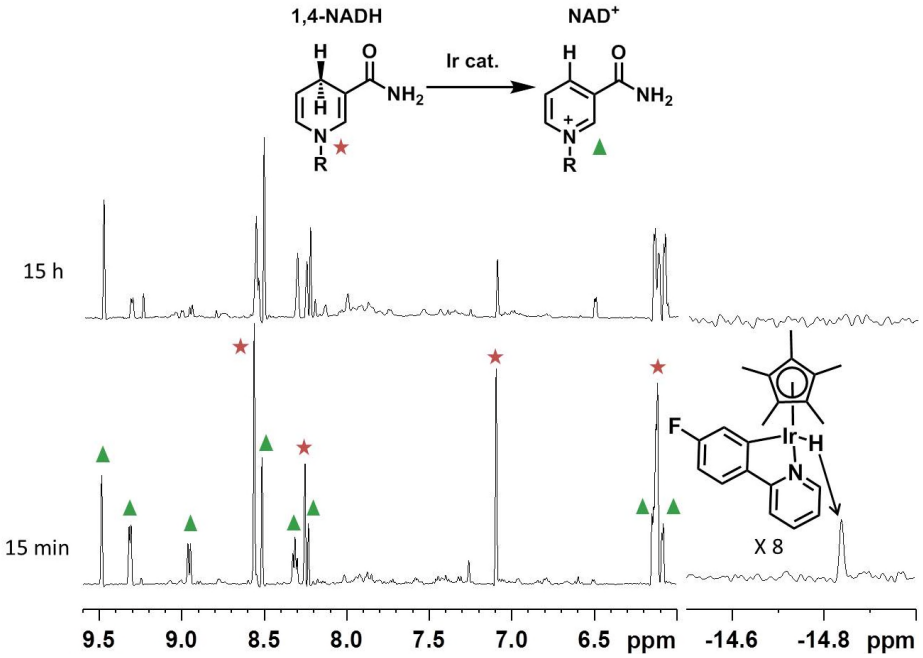

Figure 3.9. ^1H NMR (600 MHz, 50% MeOD-d_4/50% D_2O (v/v), 310 K) of the reaction between complex **2** (250 μM) and NADH (750 μM). The iridium-hydride species is observed after 15 min at -14.84 ppm, alongside the conversion of NADH (★) to NAD^+ (▲).

3.3.6 Antiproliferative Activity

The antiproliferative activity of complexes **1-17** in A2780 (ovarian) cancer cells and complexes **1**, **2**, **5**, **6**, **8**, **10**, **11**, **14** and **16** in HCT-116 (colon), MCF-7 (breast) and A549 (lung) cancer cells is shown in Table 3.6. The activity of previously reported[27] iridium complexes [(η^5-Cp*)Ir(2-PhPy)Cl] and [(η^5-Cp^{xPh})Ir(2-PhPy)Cl] with no substituents on the chelating ligand are also shown for comparison.

It is evident that the presence of substituents on the chelating ligand greatly affects the antiproliferative activity of the complexes with IC_{50} values ranging from 1 to 60 μM in the A2780 cell line. Complex [(η^5-Cp*)Ir(2-(2′-methylphenyl)pyridine)Cl] **13** is the most potent with an IC_{50} value of 1.18 μM in A2780 ovarian cancer cells making it more potent than the extended cyclopentadienyl complex [(η^5-Cp^{xPh})Ir(2-phenylpyridine)Cl] (IC_{50} = 2.14 μM). Complexes **2**, **8**, **13** and **15** also show similar potency to the clinical drug cisplatin (CDDP). Interestingly, structural isomers exhibit contrasting activities against A2780 cells; for example, complexes [(η^5-Cp*)Ir(2-(4′-fluorophenyl)pyridine)Cl] **2** (2.7 μM) and [(η^5-Cp*)Ir(2-phenyl-5-fluoropyridine)Cl] **4** (>60 μM), and complexes [(η^5-Cp*)Ir(2-(4′-hydroxyphenyl)pyridine)Cl] **11** (47.3 μM) and [(η^5-Cp*)Ir(2-phenyl-5-hydroxypyridine)Cl] **12** (13.29 μM). Contrasting activity for structural isomers also occurs for other cell lines, most notably against the A549 lung cancer cell line for complexes [(η^5-Cp*)Ir(2-(2′-fluorophenyl)pyridine)Cl] **1** (10.36 μM) and [(η^5-Cp*)Ir(2-(4′-fluorophenyl)pyridine)Cl] **2** (2.1 μM). There is also variation in activity of complexes in different cells lines, most notably complex [(η^5-Cp*)Ir(2-phenyl-4-nitropyridine)Cl] **8** with IC_{50} values of 2.7, 27.4, 11.4 and 20.1 μM in A2780, HCT-116, MCF-7 and A549 cell lines, respectively. In general, the most sensitive cell line to this set of complexes is the A2780 ovarian cancer cell line, followed by

MCF-7 breast cancer cells. The complexes are less effective against HCT-116 colon and A549 lung cancer cells.

Table 3.6. IC_{50} values for complexes **1-17** in A2780 cells and complexes **1**, **2**, **5**, **6**, **8**, **10**, **11**, **14** and **16** in HCT-116, MCF-7 and A549 cells. Drug exposure time was 24 h followed by a 72 h recovery time.

	IC_{50} values (μM)			
Complex	A2780	HCT-116	MCF-7	A549
1	4.5 ± 0.2	3.7 ± 0.3	9.6 ± 0.4	10.36 ± 0.07
2	2.7 ± 0.3	6.8 ± 0.1	4.8 ± 0.3	2.1 ± 0.3
3	>50	n.d.	n.d.	n.d.
4	>60	n.d.	n.d.	n.d.
5	6.9 ± 0.3	21.3 ± 0.7	11.6 ± 0.5	15.8 ± 0.4
6	4.4 ± 0.4	18.8 ± 0.5	6.5 ± 0.3	5.9 ± 0.1
7	24.73 ± 2.30	n.d.	n.d.	n.d.
8	2.7 ± 0.1	27.5 ± 0.9	11.4 ± 0.4	20.1 ± 0.3
9	>50	n.d.	n.d.	n.d.
10	47 ± 1	57.3 ± 0.9	47 ± 2	89 ± 1
11	47.3 ± 0.1	29.3 ± 0.8	28.6 ± 0.9	56.67 ± 0.04
12	13.29 ± 0.88	n.d.	n.d.	n.d.
13	1.18 ± 0.08	n.d.	n.d.	n.d.
14	3.9 ± 0.2	9.6 ± 0.6	3.7 ± 0.1	8.7 ± 0.3
15	1.26 ± 0.01	n.d.	n.d.	n.d.
16	4.4 ± 0.2	7.0 ± 0.2	8.9 ± 0.2	2.7 ± 0.1
17	6 ± 1	n.d.	n.d.	n.d.
[(η^5-Cp*)Ir(2-PhPy)Cl][a]	10.78 ± 1.72	n.d.	n.d.	n.d.
[(η^5-Cp^{xPh})Ir(2-PhPy)Cl][a]	2.14 ± 0.50	n.d.	n.d.	n.d.
cisplatin	1.2 ± 0.2	5.2 ± 0.3	7.0 ± 0.1	3.5 ± 0.2

[a] From ref 27.

3.3.7 Relative Hydrophobicity

Hydrophobicity can be an important design feature for metallodrugs and has been correlated with enhanced potency.[43-45] The relative hydrophobicities of complexes **2/4**, **7/8**, **11/12** and **13/14** (four pairs of structural isomers) were determined by RP-HPLC. The more hydrophobic complexes have longer retention times (t_R). To ensure solubility of the complexes, methanol was used (MeOH:H_2O 1:9 v:v) with NaCl (50

mM) present to suppress the hydrolysis of the complexes in both sample preparation and in the HPLC solvents. The resulting retention times are shown in Table 3.7. Complex **11** shows the shortest retention time (least hydrophobic) at 15.11 min while complex **14** shows the longest retention time (most hydrophobic) at 20.9 min.

Table 3.7. Retention times (t_R) by RP-HPLC of complexes **2**, **4**, **7**, **8** and **11-14.** Measurements were taken as an average of duplicate of triplicate experiments.

Complex	2-PhPy ligand	t_R (min)
2	2-(4'-fluorophenyl)pyridine	18.74 ± 0.05
4	2-phenyl-5-fluoropyridine	18.60 ± 0.02
7	2-(4'-nitrophenyl)pyridine	18.8 ± 0.2
8	2-phenyl-4-nitropyridine	18.0 ± 0.1
11	2-(4'-hydroxyphenyl)pyridine	15.11 ± 0.03
12	2-phenyl-5-hydroxypyridine	17.8 ± 0.2
13	2-(2'-methylphenyl)pyridine	20.4 ± 0.2
14	2-phenyl-5-methylpyridine	20.9 ± 0.9

3.3.8 Cellular-Iridium Accumulation

Accumulation of metal drugs in cancer cells can be related to the hydrophobicity of the complexes. Cellular-iridium accumulation in A2780 cells after 24 h exposure to complexes **2**, **4**, **7**, **8** and **11-14** at equipotent (IC_{50}) concentrations was determined by ICP-MS and is shown in Table 3.8. Complex **11** shows the lowest accumulation of 1.6 ng Ir/10^6 cells while complex **13** exhibits the highest extent of accumulation of 18 ng Ir/10^6 cells.

Table 3.8. Cellular-iridium accumulation in A2780 cells for complexes **2**, **4**, **7**, **8** and **11-14** determined at equipotent (IC_{50}) concentrations as duplicate of triplicate experiments.

Complex	2-PhPy ligand	Cellular-Ir (ng Ir/10^6 A2780 cells)
2	2-(4′-fluorophenyl)pyridine	13.5 ± 0.3
4	2-phenyl-5-fluoropyridine	11.1 ± 0.1
7	2-(4′-nitrophenyl)pyridine	8 ± 1
8	2-phenyl-4-nitropyridine	9.0 ± 0.2
11	2-(4′-hydroxyphenyl)pyridine	1.6 ± 0.1
12	2-phenyl-5-hydroxypyridine	10.2 ± 0.2
13	2-(2′-methylphenyl)pyridine	18 ± 1
14	2-phenyl-5-methylpyridine	16.0 ± 0.3

3.3.9 Cellular-Iridium Distribution

To examine if small structural changes on the chelating ligand affect intracellular-localisation of iridium complexes, structural isomers [(η^5-Cp*)Ir(2-(4′-fluorophenyl)pyridine)Cl] **2** and [(η^5-Cp*)Ir(2-phenyl-5-fluoropyridine)Cl] **4** (which show contrasting anticancer activities) were examined for their cellular-iridium distribution in A2780 human ovarian cancer cells at IC_{50} concentrations, Figure 3.10. The cytosol contains the highest amount of iridium (51.4% for **2** and 69.2% for **4**), followed by the cell membrane and particulate fractions (28.4% for **2** and 17.9% for **4)**. Complex **4** localises in the cytosol to a greater extent than complex **2** ($p < 0.01$), which in turn localises in the cell membrane to a greater extent than **4** ($p < 0.01$). The nuclear fraction contains different amounts of iridium, with 10.4% and 6.7% ($p < 0.01$) for complexes **2** and **4**, respectively, while the cytoskeletal fraction contains similar levels of iridium with 9.8% and 6.1% ($p > 0.05$) for **2** and **4**, respectively.

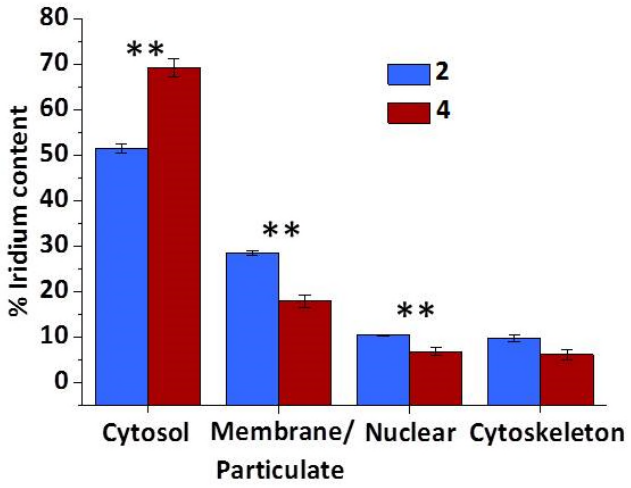

Figure 3.10. Cellular-iridium distribution of structural isomers **2** and **4** in A2780 human ovarian cancer cells. Complex **4** localises in the cytosol to a greater extent than **2**, while complex **2** localises in the membrane and particulate fractions to a greater extent than **4**. Student's t-test at $p < 0.01$ level indicated by **.

3.4 Discussion

3.4.1 Characterisation

The X-ray crystal structures of complexes [(η^5-Cp*)Ir(2-(2'-fluorophenyl)pyridine)Cl] **1**, [(η^5-Cp*)Ir(2-(4'-fluorophenyl)pyridine)Cl] **2** and [(η^5-Cp*)Ir(2-(4'-trifluoromethylphenyl)pyridine)Cl] **16** show the "piano-stool" structure expected for half-sandwich metal complexes with bond lengths/angles comparable to similar previously-reported structures.[27,46,47] The position of the fluorine on the phenyl ring does not appear to influence exhibited bond lengths. Complexes **1** and **2** exhibit weak off-set π-π stacking between the 2-PhPy ligand (Figure 3.2), with a centroid-centroid distance of 4.140 Å for **1** and 4.059 Å for **2**.

DFT calculations on complexes **2**, **4**, **7**, **8** and **11-13** indicate that the presence of substituents does not affect the electronic density on the iridium centre, Cp* ring or chlorido ligands (Figure 3.3), which implies that the reactivity at the metal centre

may remain relatively the same for all complexes. The EPS also show that the phenyl ring in the chelating ligand has a more negative electrostatic potential than the pyridyl ring, due to the negative charge associated with the deprotonation of the bound carbon. The electron-withdrawing/electron-donating nature of the substituents affects the EPS of the chelating ligand by either diminishing or enhancing the electronic charge density on the ring system to which the substituent is bound. The electron-withdrawing $–NO_2$ and -F groups provide a more positive EPS within the ring while the electron-donating –OH and $–CH_3$ groups generate a more negative EPS within the ring. The presence of the substituents significantly changes the EPS of the chelating ligand, with areas of higher electronic charge density for complexes **2**, **4**, **7**, **8**, **11** and **12** due to the presence of heteroatoms with differing electronegativities. As weak electrostatic forces are often important for binding and recognition interactions with biomolecules such as peptides, proteins and enzymes,[48] the nature and position of substituent may play a significant role in the interaction of the complexes studied here with target sites.

3.4.2 Separation of Enantiomers

The detrimental effects caused by the antimetic drug thalidomide,[49] which occurs as two enantiomers due to the presence of a chiral carbon centre, where the (-)(S)-thalidomide enantiomer is responsible for the teratogenic effects, has led to the increasing importance of the separation of enantiomers of any racemic drug candidate. The separation of the enantiomers of complexes [(η^5-Cp*)Ir(2-(2'-fluorophenyl)pyridine)Cl] **1**, [(η^5-Cp*)Ir(2-(4'-fluorophenyl)pyridine)Cl] **2**, [(η^5-Cp*)Ir(2-phenyl-5-pyridinecarboxaldehyde)Cl] **6** and [(η^5-Cp*)Ir(2-(4'-trifluoromethylphenyl)pyridine)Cl] **16** was performed using chiral HPLC, where the

presence of two peaks in the HPLC trace is indicative of the R and S enantiomers (Figure 3.4). The stability of the enantiomer of complex **6** was assessed by the collection of each peak which contains either the R or S enantiomer and storage of the solution at 273 K for 3 days. The solutions were then concentrated to dryness at ambient temperature, re-dissolved and re-injected into the column. The appearance of two sets of peaks from each collected peak shows that the enantiomers epimerise in solution to a racemic mixture (Figure 3.5). It has been previously observed that half-sandwich Ir(III) complexes can exhibit fast exchange between Ir_R and Ir_S configurations for complexes bearing a disasterotopic centre in the chelating ligand.[50] Under the conditions used, the assessment of the biological properties of each enantiomer is unlikely to be feasible. Time studies would be useful to see if the epimerisation occurs on a scale that would make the isolation, characterisation and assessment of biological activity of the R and S enantiomers possible.

3.4.3 Hydrolysis

Hydrolysis studies by ^{1}H NMR showed that all complexes are converted to an equilibrium mixture of Ir-Cl and Ir-OD_2/OD at 310 K within the time taken to complete the first spectrum (15 min) with 67-80% existing as the aqua/hydroxido adduct (Figure 3.6). This is consistent with previous findings that iridium(III) half-sandwich complexes can exhibit fast rates of ligand exchange[26,51] in comparison to their non-"piano stool" octahedral counterparts.[52] The rate of aquation in iridium(III) half-sandwich complexes has been shown to be dependent on the charge associated with the chelating ligand, where anionic ligands like 2-PhPy show faster rates of hydrolysis than neutral ligands such as 2,2'-bipyridine.[26,27] The type of substituent on the 2-PhPy chelating ligand does not appear to greatly affect the rate or extent of

hydrolysis. The hydrolysis can be readily reversed by addition of NaCl, and a concentration of 4 mM NaCl almost completely suppresses hydrolysis. This would imply that at biologically relevant chloride concentrations (i.e. in the nucleus) the complexes would exist as the Ir-Cl rather than aqua species.

Analysis of the pK_a of aqua adducts of these complexes proved difficult due to the concentrations of complex in solution, however, previous reports on *C,N*-chelated half-sandwich iridium(III) complexes showed that the pK_a values are in the range of 8.3-8.9.[27] Therefore the complexes studied here are likely to exist as the aqua rather than the hydroxido adduct at physiological pH.

3.4.4 Interactions with Nucleobases

DNA is a major target for many transition-metal anticancer compounds.[53-55] The interaction of complexes **2**, **4**, **7**, **8** and **11-14** with model nucleobases 9-EtG and 9-MeA indicated a strong preference for 9-EtG, with 100% binding after 15 min (Figure 3.7 and Table 3.4). Complexes **2** and **4** also exhibited 100% binding to 9-EtG after 15 min even in the presence of 4 mM NaCl where the complex exists as the Ir-Cl species. All complexes were able to bind to 9-MeA, but to a lesser extent than with 9-EtG. Intriguingly, hydroxyl complex **11** binds to 9-MeA to a far greater extent than the other complexes studied. Its structural isomer **12** exhibits the second greatest extent of binding. This may indicate that a secondary interaction such as hydrogen-bonding between the 9-MeA and the hydroxyl group may be stabilising the interaction, although this was not further investigated.

In competitive binding experiments between 9-EtG and 9-MeA, only complexes **2**, **4** and **14** formed 9-MeA adducts (5-10%), highlighting that binding to 9-MeA was less strong than to 9-EtG. Complex **11** formed no 9-MeA adducts in competitive binding

studies despite exhibiting the highest extent of binding to 9-MeA (82%) when no 9-EtG was present. The weaker binding of 9-MeA may be attributed to the steric hindrance caused by the $-NH_2$ group at the 4 position. Guanine is also known to be a stronger electron-donor than adenine, which may also contribute to the selectivity in 9-EtG binding.[56] Guanine is therefore a potential binding site on DNA, as it is for cisplatin,[53] and other transition metal anticancer complexes.[57-59]

3.4.5 Catalytic oxidation of NADH to NAD^+

The potential for complexes [(η^5-Cp*)Ir(2-(4'-fluorophenyl)pyridine)Cl] **2**, [(η^5-Cp*)Ir(2-phenyl-5-fluoropyridine)Cl] **4**, [(η^5-Cp*)Ir(2-(4'-hydroxyphenyl)-pyridine)Cl] **11** and [(η^5-Cp*)Ir(2-phenyl-5-hydroxypyridine)Cl] **12** to modulate the NAD^+/NADH ratio in cells catalytically was examined. All complexes exhibited catalytic activity towards the conversion of NADH to NAD^+ by first order reaction kinetics with respect to [NADH]. Complex **11** exhibits the best catalytic activity with a TON of 28 and TOF of 3.2 h^{-1} ([NADH] = 146 μM) while **2** and **4** have the lowest TON of 22 and TOF of 1.2 and 1.1 h^{-1}, respectively (Table 3.5). The presence of the hydroxyl group in **11** and **12** seems to enhance the catalytic activity. Complexes **11** and **12** also exhibited an unusual kinetic profile for the first 3 h of reaction time, followed by the expected first order kinetics (Figure 3.8). The hydroxyl group on complex [(η^5-Cp*)Ir(2-phenyl-6-hydroxypyridine)Cl] has been previously reported to be important for the catalytic activity towards the dehydrogenative oxidation of organic compounds,[60] which implies that the hydroxyl group may be involved in the catalytic cycle. Although the position of the hydroxyl group in **11** and **12** is further from the metal centre than in [(η^5-Cp*)Ir(2-phenyl-6-hydroxypyridine)Cl], the unusual kinetics observed may indicate that it is initially playing a role in the

catalytic activity. It has been suggested that the rate-limiting step in this catalytic reaction is the formation of the Ir-NADH adduct leading to first-order reaction kinetics with respect to [NADH],[32] therefore the unusual kinetic profile of **11** and **12** may be a result of participation by the hydroxyl groups. The involvement of the ligand in the oxidation of NADH in half-sandwich iridium(III) complexes has not been previously observed.

It has been well documented that half-sandwich iridium(III) complexes can form iridium-hydride species in the presence of a hydride source like sodium borohyride, which allows the complex to partake in a range of catalytic reactions. The oxidation of NADH proceeds via formation of an Ir-H species as observed in the ^{1}H NMR spectrum (Figure 3.9), in agreement with previous work on related complexes,[31,61] showing that the H4 protons in NADH can be accessed as a hydride donor.

Further studies into the catalytic cycle of complex **2** with NADH involved determination of the by-product of the reaction. It has been previously demonstrated that both hydrogen gas and hydrogen peroxide can be formed in these reactions,[32,42,61] by protonation of the Ir-H species or by direct hydride transfer to molecular oxygen, respectively. Under the experimental conditions used, neither H_2 or H_2O_2 was detected. This may be a result of the low concentration of complex **2** (250 μM) used. It was found that increasing the concentration resulted in precipitation of the complex upon addition of NADH and inhibited the catalytic reaction. The precipitation may be the result of an increase in ionic strength of the solution upon addition of NADH which was used as the di-potassium salt.

As these complexes can convert NADH to NAD^+ catalytically, it may be possible to disrupt this important redox couple in cells, which could have implications for cell metabolism, including lactate dehydrogenase-catalysed lactate-pyruvate

conversions,[62] enhancement of ROS levels,[42,63] as well as reducing the concentration of one of the major electron-donors in the electron transport chain.

3.4.6 Antiproliferative Activity

The antiproliferative activity of the seventeen complexes covered a wide range, from 1 to 60 μM in A2780, 3.7 to 54.3 μM in HCT-116, 3.7 to 47 μM in MCF-7 and 2.1 to 89 μM in A549 cells, showing that the substituent on the chelating ligand has a significant effect on the antiproliferative activity of the complex (Table 3.6). Complexes **2**, **8**, **13** and **15** are all just as, or more, potent than the previously reported phenyl-extended Cp^{xPh} complex **17** (IC_{50} = 2.14 μM) towards A2780 cells, showing that the addition of functional groups to the 2-PhPy ligand can provide a strategy for increasing potency rather than functionalising the Cp^{x} capping ligand. In contrast, complexes **3**, **4**, **7**, **9**, **10** and **11** are less active towards A2780 cells than the parent complex [(η^5-Cp*)Ir(2-PhPy)Cl]. It is apparent that the presence of hydroxymethyl groups in complexes **9** and **10** decreases the antiproliferative activity. However, the presence of methyl groups enhances the activity, making them potentially interesting for further study. Methyl groups are inherently more likely to contribute to increased lipophilicity than hydroxymethyl groups, perhaps indicating that hydrophobicity is important for high potency.

The fluoro complexes **1** and **2**, in which the fluorine atom is situated on the phenyl ring, have promising activity of 2.7 and 4.4 μM, respectively, whereas complexes **3** and **4** in which the fluorine substituent is on the pyridyl ring have IC_{50} values of >50 μM, demonstrating the contrasting biological activity of the structural isomers. This difference in activity for isomers is also observed for complexes **11** (IC_{50} = 47.3 μM) and **12** (IC_{50} = 13.29 μM) which contain hydroxyl groups on the phenyl and pyridyl

ring, respectively. Similarly for the nitro-containing complexes **7** (IC_{50} = 24.73 μM) and **8** (IC_{50} = 2.7 μM). Therefore, not only is the type of substituent important, but also where it is situated on the chelating ligand. It has been demonstrated in half-sandwich iridium(III) complexes bearing picolinamide chelating ligands that the inclusion of a substituent atom in the arene ring of the chelating ligand increases the activity over the un-functionalized complex.[19] A further increase in activity was observed upon the introduction of a second chlorine atom depending on its position. However, the contrasting activities between structural isomers observed in this work are much greater than in the picolinamide complexes.

3.4.7 Correlations Between Hydrophobicity, Iridium-Cellular Accumulation and Potency

The complexes studied here are all neutral chlorido species in the presence of biologically relevant concentrations of chloride. Hydrophobicity can promote interaction with the lipophilic cell membrane[64] and promote hydrophobic interactions with protein targets.[65] In general, the accumulation and potency of organometallic complexes in cells increases with an increase in their hydrophobicity.[43,59,66,67] The relative hydrophobicity of complexes **2**, **4**, **7**, **8** and **11-14** (4 pairs of structural isomers) was determined by RP-HPLC (Table 3.7). As RP-HPLC relies on the relative interaction between the hydrophilic mobile phase and hydrophobic stationary phase, determination of the relative hydrophobicity of a series of complexes can be based on retention times. It was found that the nature of the substituent on the 2-PhPy ligand can dictate the hydrophobicity of the complex, with hydroxyl complexes **11** and **12** being the least lipophilic, while complexes **13** and **14** bearing methyl groups are the most. Intriguingly, complex **12** appeared to be

much more hydrophobic than the corresponding structural isomer **11** with retention times of 17.8 and 15.1 min, respectively (Figure 3.11). It is apparent that not only the type of substituent but also its position governs the hydrophobicity of the complex.

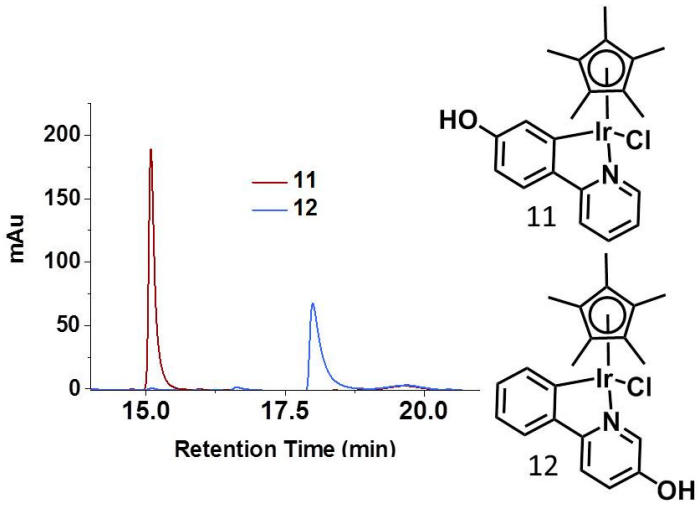

Figure 3.11. RP-HPLC traces of complexes **11** and **12**. Retention times: **11** - 15.1 min and **12** - 17.8 min, showing that the position of the hydroxyl group on the 2-PhPy ligand affects the hydrophobicity of the complexes.

To examine if structural isomers accumulate in cells to a different extent, the cellular-iridium accumulation in A2780 cells of **2**, **4**, **7**, **8** and **11-14** was determined at equipotent (IC_{50}) concentrations (Table 3.8). For isomers **2/4** and **13/14** the levels of cellular-iridium accumulation are similar, with only small differences between them. Isomers **7/8** show no difference between their respective iridium accumulations. However, isomers **11/12** show contrasting levels of cellular-iridium accumulation, with **12** being accumulated 6× more than **11** (10.2 vs. 1.6 ng Ir/10^6 A2780 cells).

The hydrophobicity measurements were correlated with cellular-iridium accumulation in A2780 cells in order to investigate if hydrophobicity is important in their ability to enter cells (Figure 3.12 a-b). There is a clear relationship between a higher hydrophobicity and an increase in cellular accumulation ($R^2 = 0.969$). Isomers

13 and **14** are the most hydrophobic complexes and accumulate in A2780 cells to the highest extent, while complex **11** with the lowest hydrophobicity showed the lowest accumulation. It was recently demonstrated that the structurally similar iridium(III) complex [(η^5-Cp*)Ir(7,8-benzoquinoline)Cl] is transported into cells by both energy-independent passive diffusion and energy-dependent pathways.[68] Since an increase in hydrophobicity results in an increase in cellular accumulation, it is likely that passive diffusion plays at least a part in the mechanism of cellular accumulation for these complexes, making hydrophobicity an important design feature.

The cellular-iridium accumulation was correlated with antiproliferative activity in A2780 cells, which shows that a pattern exists between enhanced accumulation and increase in potency (Figure 3.12 c). Complex **11** exhibits the lowest cellular accumulation and second lowest potency (1.58 ng Ir/10^6 cells, 47.3 μM) and complex **13** exhibits the highest cellular accumulation and potency (18.46 ng Ir/10^6 cells, 1.18 μM). In the case of structural isomers **11** and **12**, the difference in hydrophobicity of the complexes as a consequence of changing the position of the hydroxyl group on the 2-PhPy ligand results in enhanced cellular-accumulation for the more hydrophobic complex **12** which leads to a more potent complex. Interestingly, although **2** and **8** exhibit low IC_{50} values (2.7 μM) they show similar levels of cellular accumulation to their less potent structural isomers **4** (IC_{50} > 60 μM) and **7** (IC_{50} = 24.73 μM). As the iridium accumulation is performed at IC_{50} concentrations, this may indicate that the mechanism involved in the antiproliferative activity of complexes **2** and **8** is more efficient over their counterparts **4** and **7**.

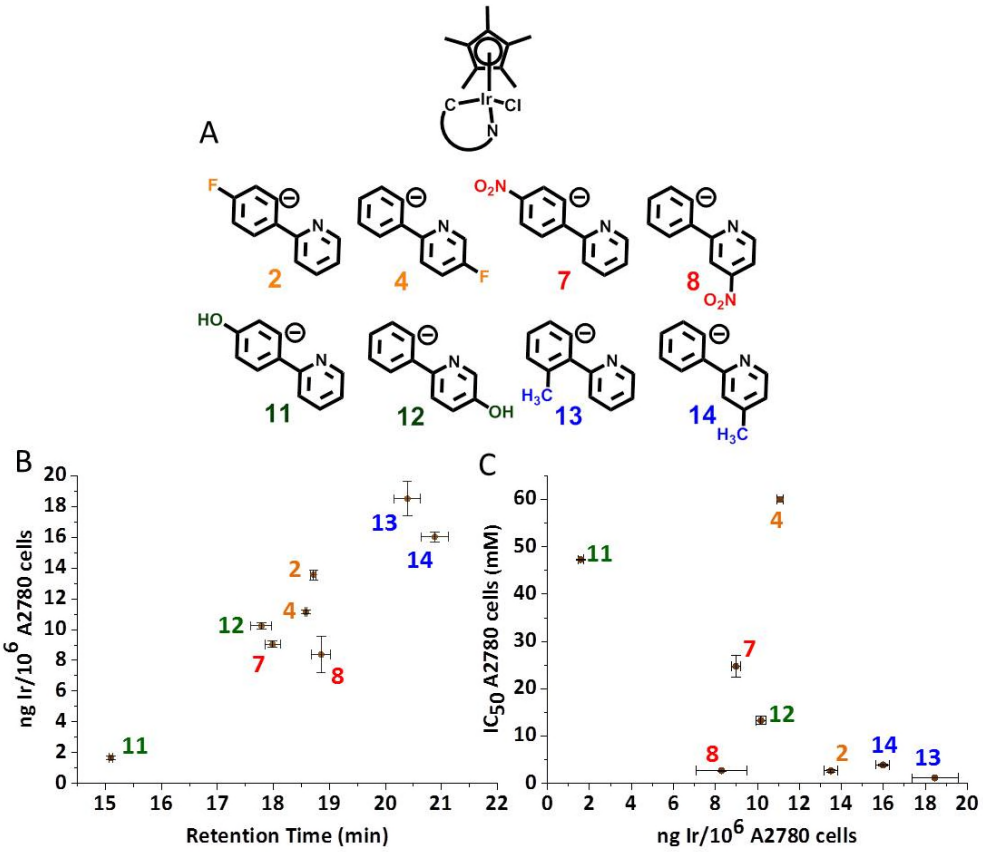

Figure 3.12. (a) Structures of complexes studied. (b) Relative hydrophobicity as indicated by retention times on RP-HPLC against cellular accumulation of iridium at IC_{50} concentrations in A2780 cells after exposure to complexes **2**, **4**, **7**, **8** and **11-14** showing a dependence on hydrophobicity for cellular accumulation. (c) Comparison of cellular accumulation of iridium and antiproliferative activity of complexes **2**, **4**, **7**, **8** and **11-14** in A2780 cells showing a general pattern of higher cellular accumulation resulting in more potent complexes.

3.4.8 Cellular-Iridium Distribution of Isomers 2 and 4

The distribution of iridium in A2780 human ovarian cancer cells after exposure to structural isomers [(η^5-Cp*)Ir(2-(4'-fluorophenyl)pyridine)Cl] **2** and [(η^5-Cp*)Ir(2-phenyl-5-fluoropyridine)Cl] **4** follows the order of localisation: cytosol > cell membrane and particulate > nucleus > cytoskeleton (Figure 3.10). Although both isomers followed the same trend, they do so to different extents. Complex **4** localises in the cytosol to a greater extent than **2** (69.2% vs. 51.4%), whereas **2** localises in the

cell membrane and particulate to a greater extent than **4** (28.4% vs. 17.9%). The variations in localisation preference arising from this small structural change may reflect the differences observed in antiproliferative activity.[69,70] For example, if the biological target of these complexes is in the cell membrane and particulate fraction then that may explain why isomer **2** is more active than **4**. As the isomers exhibit dramatically different IC_{50} values yet both bind to guanine and accumulate in the nucleus to similar extents, DNA may not be the main biological target. It has also been shown that halogen-bonding interactions could be important in rational drug design,[71] therefore the position of fluorine within the ligand may influence the way the complexes interact with biomolecules, leading ultimately to variations in activity.

3.5 Conclusions

Interest in iridium(III) half-sandwich complexes as anticancer agents is increasing, with new complexes being reported and novel mechanisms of action being discovered.[17,19,30,42,72] This work has focussed on the effects of electron-donating and electron-withdrawing substituents on *C,N*-chelating 2-PhPy ligands on the chemical, physio-chemical and biological activity of their complexes, with notable differences arising between structural isomers.

DFT calculations show that the nature and position of the substituent has minimal effect on the electronic charge at the iridium centre, Cp* or chlorido ligands, but exerts localised changes in the electrostatic potential surface and overall electron density of the chelating ligand.

The separation of enantiomers of the complexes was attempted and showed that the chiral resolution using HPLC allows isolation of enantiomerically pure complexes.

However, studies into the stability of the enantiomers once isolated showed that they epimerise back to a racemic mixture.

All complexes hydrolysed rapidly at 310 K, but almost complete suppression of aquation can be achieved with 4 mM NaCl implying that under physiological conditions the complexes would exist as the neutral chlorido species. All complexes bind strongly to the nucleobase 9-EtG, even in the presence of 4 mM NaCl. The catalytic oxidation of NADH that was demonstrated is a potential reaction that could occur in cells, which is an interesting property of some iridium(III) half-sandwich anticancer complexes.[31,32,73,74] The catalytic activity showed a small dependence on the substituent present on the 2-PhPy ligand, whereby hydroxyl groups slightly enhanced the catalytic ability of the complex compared to fluorine, which may be due to a secondary interaction between the hydroxyl groups with NADH. The oxidation of NADH appears to be mediated through the formation of Ir-H species, as detected by ^{1}H NMR spectroscopy.

The antiproliferative activity of the complexes is strongly dependent on the type of substituent and its position on the chelating ligand, giving rise to contrasting activities between structural isomers despite exhibiting similar chemical behaviour. The presence of substituents on the 2-PhPy ligand can in some cases generate complexes that are more potent than those bearing the extended Cp^{xPh} ligand, thus providing an alternative strategy for increasing potency in these systems.

Further physicochemical analysis of these complexes showed that both the nature and position of substituent can determine their hydrophobicity, and consequently affect the accumulation of Ir in A2780 cells. Correlation analysis showed that an increase in hydrophobicity results in an increase in cellular-Ir accumulation, which generally results in an increase in potency. Cellular-Ir distribution in A2780 cells of

a pair of structural isomers that exhibit contrasting biological activity yet similar levels of Ir-accumulation showed that the position of the substituent can affect the extent of localisation in cellular compartments.

This study shows that small changes in the functionalisation of the chelating ligands in half-sandwich iridium(III) complexes can have a profound effect on the biological activity of the complexes. Importantly, it also highlights that the inclusion of substituents in 2-PhPy ligands can provide complexes with enhanced potency without the use of extended cyclopentadienyl capping ligands, a strategy that could be beneficial for the development of this class of complexes.

3.6 References

(1) Garbutcheon-Singh, K. B. G., M.P.; Harper, B.W.; Krause-Heuer, A.M.; Manohar, M.; Orkey, N.; Aldrich-Wright, J.R. *Curr. Top. Med. Chem.* **2011**, *11*, 521.

(2) Sava, G.; Bergamo, A.; Dyson, P. J. *Dalton Trans.* **2011**, *40*, 9069.

(3) Hartinger, C. G.; Metzler-Nolte, N.; Dyson, P. J. *Organometallics.* **2012**, *31*, 5677.

(4) Ma, D.-L.; Chan, D. S.-H.; Leung, C.-H. *Acc. Chem. Res.* **2014**, *47*, 3614.

(5) Chow, M. J.; Licona, C.; Yuan Qiang Wong, D.; Pastorin, G.; Gaiddon, C.; Ang, W. H. *J. Med. Chem.* **2014**, *57*, 6043.

(6) Tripathy, S. K.; De, U.; Dehury, N.; Pal, S.; Kim, H. S.; Patra, S. *Dalton Trans.* **2014**, *43*, 14546.

(7) Romero-Canelón, I.; Salassa, L.; Sadler, P. J. *J. Med. Chem.* **2013**, *56*, 1291.

(8) Furrer, M. A.; Garci, A.; Denoyelle-Di-Muro, E.; Trouillas, P.; Giannini, F.; Furrer, J.; Clavel, C. M.; Dyson, P. J.; Süss-Fink, G.; Therrien, B. *Chem. Eur. J.* **2013**, *19*, 3198.

(9) Köpf, H.; Köpf-Maier, P. *Angew. Chem. Int. Ed. Eng.* **1979**, *18*, 477.

(10) Lümmen, G.; Sperling, H.; Luboldt, H.; Otto, T.; Rübben, H. *Cancer Chemother. Pharmacol.* **1998**, *42*, 415.

(11) Kröger, N.; Kleeberg, U. R.; Mross, K.; Edler, L.; Hossfeld, D. K. *Onkologie* **2000**, *23*, 60.

(12) Raja, M. U.; Tauchman, J.; Therrien, B.; Süss-Fink, G.; Riedel, T.; Dyson, P. J. *Inorg. Chim. Acta* **2014**, *409, Part B*, 479.

(13) Kandioller, W.; Balsano, E.; Meier, S. M.; Jungwirth, U.; Goschl, S.; Roller, A.; Jakupec, M. A.; Berger, W.; Keppler, B. K.; Hartinger, C. G. *Chem. Commun.* **2013**, *49*, 3348.

(14) Bugarcic, T.; Habtemariam, A.; Deeth, R. J.; Fabbiani, F. P. A.; Parsons, S.; Sadler, P. J. *Inorg. Chem.* **2009**, *48*, 9444.

(15) Habtemariam, A.; Melchart, M.; Fernández, R.; Parsons, S.; Oswald, I. D. H.; Parkin, A.; Fabbiani, F. P. A.; Davidson, J. E.; Dawson, A.; Aird, R. E.; Jodrell, D. I.; Sadler, P. J. *J. Med. Chem.* **2006**, *49*, 6858.

(16) Scolaro, C.; Bergamo, A.; Brescacin, L.; Delfino, R.; Cocchietto, M.; Laurenczy, G.; Geldbach, T. J.; Sava, G.; Dyson, P. J. *J. Med. Chem.* **2005**, *48*, 4161.

(17) Novohradsky, V.; Zerzankova, L.; Stepankova, J.; Kisova, A.; Kostrhunova, H.; Liu, Z.; Sadler, P. J.; Kasparkova, J.; Brabec, V. *Metallomics* **2014**, *6*, 1491.

(18) Ludwig, G.; Ranđelović, I.; Maksimović-Ivanić, D.; Mijatović, S.; Bulatović, M. Z.; Miljković, D.; Korb, M.; Lang, H.; Steinborn, D.; Kaluđerović, G. N. *ChemMedChem* **2014**, *9*, 1586.

(19) Almodares, Z.; Lucas, S. J.; Crossley, B. D.; Basri, A. M.; Pask, C. M.; Hebden, A. J.; Phillips, R. M.; McGowan, P. C. *Inorg. Chem.* **2014**, *53*, 727.

(20) Payne, R.; Govender, P.; Therrien, B.; Clavel, C. M.; Dyson, P. J.; Smith, G. S. *J. Organomet. Chem.* **2013**, *729*, 20.

(21) Hearn, J. M.; Romero-Canelón, I.; Qamar, B.; Liu, Z.; Hands-Portman, I.; Sadler, P. J. *ACS Chem. Biol.* **2013**, *8*, 1335.

(22) Lucas, S. J.; Lord, R. M.; Wilson, R. L.; Phillips, R. M.; Sridharan, V.; McGowan, P. C. *Dalton Trans.* **2012**, *41*, 13800.

(23) Gupta, G.; Kumar, J.; Garci, A.; Nagesh, N.; Therrien, B. *Molecules* **2014**, *19*, 6031.

(24) Li, Y.; Tan, C.-P.; Zhang, W.; He, L.; Ji, L.-N.; Mao, Z.-W. *Biomaterials* **2015**, *39*, 95.

(25) Ruiz, J.; Vicente, C.; de Haro, C.; Bautista, D. *Inorg. Chem.* **2013**, *52*, 974.

(26) Liu, Z.; Habtemariam, A.; Pizarro, A. M.; Fletcher, S. A.; Kisova, A.; Vrana, O.; Salassa, L.; Bruijnincx, P. C. A.; Clarkson, G. J.; Brabec, V.; Sadler, P. J. *J. Med. Chem.* **2011**, *54*, 3011.

(27) Liu, Z.; Habtemariam, A.; Pizarro, A. M.; Clarkson, G. J.; Sadler, P. J. *Organometallics* **2011**, *30*, 4702.

(28) Liu, Z.; Salassa, L.; Habtemariam, A.; Pizarro, A. M.; Clarkson, G. J.; Sadler, P. J. *Inorg. Chem.* **2011**, *50*, 5777.

(29) Wirth, S.; Rohbogner, C.; Cieslak, M.; Kazmierczak-Baranska, J.; Donevski, S.; Nawrot, B.; Lorenz, I.-P. *J. Biol. Inorg. Chem.* **2010**, *15*, 429.

(30) Ruiz, J.; Rodriguez, V.; Cutillas, N.; Samper, K. G.; Capdevila, M.; Palacios, O.; Espinosa, A. *Dalton Trans.* **2012**, *41*, 12847.

(31) Liu, Z.; Deeth, R. J.; Butler, J. S.; Habtemariam, A.; Newton, M. E.; Sadler, P. J. *Angew. Chem. Int. Ed.* **2013**, *52*, 4194.

(32) Betanzos-Lara, S.; Liu, Z.; Habtemariam, A.; Pizarro, A. M.; Qamar, B.; Sadler, P. J. *Angew. Chem. Int. Ed.* **2012**, *51*, 3897.

(33) Romero-Canelón, I.; Sadler, P. J. *Inorg. Chem.* **2013**, *52*, 12276.

(34) Geldmacher, Y.; Splith, K.; Kitanovic, I.; Alborzinia, H.; Can, S.; Rubbiani, R.; Nazif, M.; Wefelmeier, P.; Prokop, A.; Ott, I.; Wölfl, S.; Neundorf, I.; Sheldrick, W. *J. Biol. Inorg. Chem.* **2012**, *17*, 631.

(35) Steunenberg, P.; Ruggi, A.; van den Berg, N. S.; Buckle, T.; Kuil, J.; van Leeuwen, F. W. B.; Velders, A. H. *Inorg. Chem.* **2012**, *51*, 2105.

(36) Djukic, J.-P.; Iali, W.; Pfeffer, M.; Le Goff, X.-F. *Chem. Eur. J* **2012**, *18*, 6063.

(37) Hwang, T. L.; Shaka, A. J. *J. Magn. Reson.* **1995**, *112*, 275.

(38) Adamo, C.; Barone, V. *J. Chem. Phys.* **1999**, *110*, 6158.

(39) Hay, P. J.; Wadt, W. R. *J. Chem. Phys.* **1985**, *82*, 270.

(40) McLean, A. D.; Chandler, G. S. *J. Chem. Phys.* **1980**, *72*, 5639.

(41) M. J. Frisch, G. W. T., H. B. Schlegel, G. E. Scuseria, ; M. A. Robb, J. R. C., J. A. Montgomery, Jr., T. Vreven, ; K. N. Kudin, J. C. B., J. M. Millam, S. S. Iyengar, J. Tomasi, ; V. Barone, B. M., M. Cossi, G. Scalmani, N. Rega, ; G. A. Petersson, H. N., M. Hada, M. Ehara, K. Toyota, ; R. Fukuda, J. H., M. Ishida, T. Nakajima, Y. Honda, O. Kitao, ; H. Nakai, M. K., X. Li, J. E. Knox, H. P. Hratchian,

J. B. Cross, ; V. Bakken, C. A., J. Jaramillo, R. Gomperts, R. E. Stratmann, ; O. Yazyev, A. J. A., R. Cammi, C. Pomelli, J. W. Ochterski, ; P. Y. Ayala, K. M., G. A. Voth, P. Salvador, J. J. Dannenberg, ; V. G. Zakrzewski, S. D., A. D. Daniels, M. C. Strain, ; O. Farkas, D. K. M., A. D. Rabuck, K. Raghavachari, ; J. B. Foresman, J. V. O., Q. Cui, A. G. Baboul, S. Clifford, ; J. Cioslowski, B. B. S., G. Liu, A. Liashenko, P. Piskorz, ; I. Komaromi, R. L. M., D. J. Fox, T. Keith, M. A. Al-Laham, ; C. Y. Peng, A. N., M. Challacombe, P. M. W. Gill, ; B. Johnson, W. C., M. W. Wong, C. Gonzalez, and J. A. Pople *Gaussian 03, Revision D.02* **2004**, *Gaussian, Inc., Wallingford CT*.

(42) Liu, Z.; Romero-Canelón, I.; Qamar, B.; Hearn, J. M.; Habtemariam, A.; Barry, N. P. E.; Pizarro, A. M.; Clarkson, G. J.; Sadler, P. J. *Angew. Chem. Int. Ed.* **2014**, *53*, 3941.

(43) van Rijt, S. H.; Mukherjee, A.; Pizarro, A. M.; Sadler, P. J. *J. Med. Chem.* **2009**, *53*, 840.

(44) Babak, M. V.; Meier , S. M.; Legin, A. A.; Adib Razavi, M. S.; Roller, A.; Jakupec , M. A.; Keppler , B. K.; Hartinger , C. G. *Chem. Eur. J* **2013**, *19*, 4308.

(45) Lau, J. S.-Y.; Lee, P.-K.; Tsang, K. H.-K.; Ng, C. H.-C.; Lam, Y.-W.; Cheng, S.-H.; Lo, K. K.-W. *Inorg. Chem.* **2009**, *48*, 708.

(46) Park-Gehrke, L. S.; Freudenthal, J.; Kaminsky, W.; DiPasquale, A. G.; Mayer, J. M. *Dalton Trans.* **2009**, 1972.

(47) Li, L.; Brennessel, W. W.; Jones, W. D. *Organometallics* **2009**, *28*, 3492.

(48) Burgoyne, N. J.; Jackson, R. M. *Bioinformatics* **2006**, *22*, 1335.

(49) Therapontos, C.; Erskine, L.; Gardner, E. R.; Figg, W. D.; Vargesson, N. *Proc. Nat. Acad. Sci. USA* **2009**, *106*, 8573.

(50) Brunner, H. *Eur. J. Inorg. Chem.* **2001**, *2001*, 905.

(51) Dadci, L.; Elias, H.; Frey, U.; Hoernig, A.; Koelle, U.; Merbach, A. E.; Paulus, H.; Schneider, J. S. *Inorg. Chem.* **1995**, *34*, 306.

(52) Helm, L.; Merbach, A. E. *Coord. Chem. Rev.* **1999**, *187*, 151.

(53) Takahara, P. M.; Rosenzweig, A. C.; Frederick, C. A.; Lippard, S. J. *Nature* **1995**, *377*, 649.

(54) Pizarro, A. M.; Sadler, P. J. *Biochimie* **2009**, *91*, 1198.

(55) Liu, H.-K.; Berners-Price, S. J.; Wang, F.; Parkinson, J. A.; Xu, J.; Bella, J.; Sadler, P. J. *Angew. Chem.* **2006**, *118*, 8333.

(56) Pullman, B.; Pullman, A. *Biochim. Biophys. Acta* **1959**, *36*, 343.

(57) Fu, Y.; Romero, M. J.; Habtemariam, A.; Snowden, M. E.; Song, L.; Clarkson, G. J.; Qamar, B.; Pizarro, A. M.; Unwin, P. R.; Sadler, P. J. *Chem. Sci.* **2012**, *3*, 2485.

(58) Betanzos-Lara, S.; Salassa, L.; Habtemariam, A.; Novakova, O.; Pizarro, A. M.; Clarkson, G. J.; Liskova, B.; Brabec, V.; Sadler, P. J. *Organometallics* **2012**, *31*, 3466.

(59) Ruiz, J.; Rodríguez, V.; Cutillas, N.; Espinosa, A.; Hannon, M. J. *Inorg. Chem.* **2011**, *50*, 9164.

(60) Fujita, K.-i.; Yoshida, T.; Imori, Y.; Yamaguchi, R. *Org. Lett.* **2011**, *13*, 2278.

(61) Maenaka, Y.; Suenobu, T.; Fukuzumi, S. *J. Am. Chem. Soc.* **2011**, *134*, 367.

(62) Ying, W. *Antioxid. Redox Signaling* **2007**, *10*, 179.

(63) Dougan, S. J.; Habtemariam, A.; McHale, S. E.; Parsons, S.; Sadler, P. J. *Proc. Nat. Acad. Sci. U.S.A.* **2008**, *105*, 11628.

(64) Kerns, E. H.; Di, L. In *Drug-like Properties: Concepts, Structure Design and Methods*; Academic Press: San Diego, 2008, p 43.

(65) Hansch, C.; Maloney, P. P.; Fujita, T.; Muir, R. M. *Nature* **1962**, *194*, 178.

(66) Mendoza-Ferri, M.-G.; Hartinger, C. G.; Eichinger, R. E.; Stolyarova, N.; Severin, K.; Jakupec, M. A.; Nazarov, A. A.; Keppler, B. K. *Organometallics* **2008**, *27*, 2405.

(67) Hanif, M.; Nazarov, A. A.; Hartinger, C. G.; Kandioller, W.; Jakupec, M. A.; Arion, V. B.; Dyson, P. J.; Keppler, B. K. *Dalton Trans.* **2010**, *39*, 7345.

(68) Novohradsky, V.; Liu, Z.; Vojtiskova, M.; Sadler, P. J.; Brabec, V.; Kasparkova, J. *Metallomics* **2014**, *6*, 682.

(69) Capobianco, J. O.; Zakula, D.; Frost, D. J.; Goldman, R. C.; Li, L.; Klein, L. L.; Lartey, P. A. *Antimicrob. Agents Chemother.* **1998**, *42*, 389.

(70) Shaul, P.; Frenkel, M.; Goldstein, E. B.; Mittelman, L.; Grunwald, A.; Ebenstein, Y.; Tsarfaty, I.; Fridman, M. *ACS Med. Chem. Lett.* **2013**, *4*, 323.

(71) Lu, Y.; Shi, T.; Wang, Y.; Yang, H.; Yan, X.; Luo, X.; Jiang, H.; Zhu, W. *J. Med. Chem.* **2009**, *52*, 2854.

(72) Liu, Z.; Romero-Canelón, I.; Habtemariam, A.; Clarkson, G. J.; Sadler, P. J. *Organometallics* **2014**.

(73) Liu, Z.; Sadler, P. J. *Inorg. Chem. Front.* **2014**, *1*, 668.

(74) Liu, Z.; Sadler, P. J. *Acc. Chem. Res.* **2014**, *47*, 1174.

Chapter 4

Influence of Chlorido and Pyridyl Monodentate Ligands on the Properties of the Anticancer Complex $[(\eta^5\text{-Cp*})\text{Ir}(2\text{-}(2'\text{-methylphenyl})\text{pyridine})\text{X}]^{0/+}$

4.1 Introduction

The most widely employed monodentate ligand in chelated half-sandwich "piano-stool" complexes is chloride. This is largely as a consequence of the synthetic route from the metal arene/Cp^x dimer using the readily available metal salt $MCl_3.nH_2O$ (M = Ru(III), Os(III), Ir(III), Rh(III)).[1]

Varying the different monodentate ligands in half-sandwich anticancer complexes bearing three monodentate ligands has led to the development of a vast library of complexes with various activities.[2-6] Well known examples being the [(η^6-arene)Ru(1,3,5-triaza-7-phosphatricyclo[3.3.1.1]decane)$(Cl)_2$] RAPTA series of complexes by Dyson *et al.*[7-10] which has yielded complexes showing promising activity towards metastatic cancers.

The effect of substituting the chlorido monodentate ligand in chelated half-sandwich complexes has not been so widely explored.[11] Work performed with ruthenium complexes of the type [(η^6-arene)Ru(ethylenediamine)X]$^{0/+}$ (X=halide, pseudo-halide, pyridine, thiolate) showed that the ability of the monodentate ligand to undergo hydrolysis was closely linked to cytotoxic activity, with stable monodentate adducts commonly leading to inactive complexes.[12] Aquation is believed to be a key activation step for clinical metallodrug cisplatin, allowing it to bind to its proposed target DNA.[13] Osmium complexes of the type [(η^6-arene)Os(phenyliminopyridine)X]PF_6^+ (X = Cl^- or I^-) have shown that the change in halide has little effect on the cytotoxicity of the complex,[14] in contrast to the structurally similar [(η^6-arene)Os(phenylazopyridine)X]PF_6 (X = Cl^- or I^-) complexes in which the presence of the iodido ligand resulted in more potent complexes than the chlorido analogues.[15] Intriguingly, these iodido complexes do

not hydrolyse, yet exhibit superior antiproliferative activity. As well as affecting chemical reactivity, it has also been suggested that the monodentate ligand can affect the transport mechanism in which Ru(II) half-sandwich complexes enter cells.[16]

The contrasting behaviour of the different monodentate ligands in chelated half-sandwich iridium(III) complexes has led to the study of pyridine derivatives in place of the chloride. In contrast to Ru(II) arene complexes, substitution of the chlorido ligand in complex [(η^5-Cp^{xBiPh})Ir(2-PhPy)Cl] with pyridine ([(η^5-Cp^{xBiPh})Ir(2-PhPy)pyridine]PF_6) resulted in an increase in potency and selectivity towards A2780 human ovarian cancer cells over MRC5 human fibroblasts (healthy cells).[17] This increase in activity upon introduction of pyridine monodentate ligands was also observed in the corresponding Cp^{xPh} complex.[18] These pyridine complexes exhibited enhanced aqueous stability, with little to no aquation at the monodentate site, suggesting that enhanced stability could be an important design feature.

This Chapter seeks to investigate the chemical and biological properties that may lead to enhanced potency in anticancer iridium(III) complexes of the type [(η^5-Cp*)Ir(2-PhPy)Cl] by replacement of the chlorido ligand in the most potent complex discussed in Chapter 3 [(η^5-Cp*)Ir(2-(2'-methylphenyl)pyridine)Cl] **13**, (IC_{50} – 1.18 ± 0.08 μM against A2780 cells) with pyridine derivatives (Chart 4.1). The effect these pyridine derivatives can have on the aqueous chemistry (including hydrolysis, 9-EtG binding, NADH oxidation and reaction with GSH) and biological behaviour has been investigated, and compared with the parent chlorido complex. The lability of the monodentate ligand has also been probed by using pyridine derivatives bearing either an electron-donating (-NMe_2) or electron-withdrawing group (-CF_3).

Chart 4.1. Ir(III) complexes studied in this Chapter.

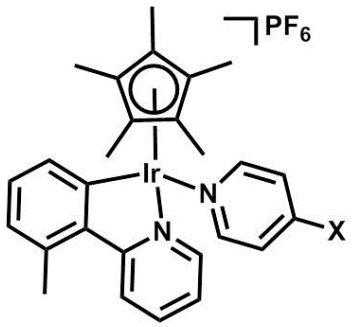

18 X = H
19 X = NMe_2
20 X = CF_3

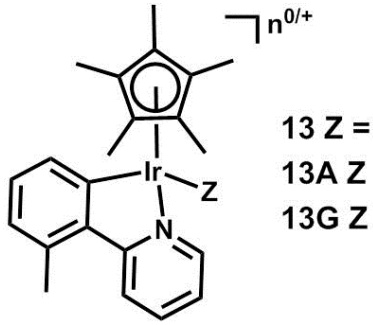

13 Z = Cl^- n = 0
13A Z = D_2O/OD n = 1^+/0
13G Z = 9-EtG n = 1^+

4.2 Experimental Section

4.2.1 Materials

4-(Dimethylamino)pyridine (≥99%), 4-(trifluoromethyl)pyridine (97%), ammonium hexafluorophosphate (95%), 9-ethylguanine (≥98%), *β*-nicotinamide adenine dinucleotide - reduced dipotassium salt (NADH) (≥95%) and L-glutathione reduced (GSH) (≥98%) were purchased from Sigma-Aldrich (UK). Pyridine was purchased from Fisher Scientific (UK). Solvents used for synthesis were of laboratory grade and used without further purification. Solvents for HPLC purity examination (water and acetonitrile) were of HPLC grade with added trifluoroacetic acid which was purchased from Sigma-Aldrich (UK). Complex **13** was prepared as described in Chapter 3.

4.2.2 Synthesis

[(η^5-Cp*)Ir(2-(2'-methylphenyl)pyridine)pyridine]PF_6 (18) [(η^5-Cp*)Ir(2-(2'-methylphenyl)pyridine)Cl] (**13**) (50 mg, 0.094 mmol) was dissolved in MeOH (20 mL) and H_2O (10 mL); silver nitrate (15 mg, 0.092 mmol) was added, the flask was wrapped in foil and the reaction mixture was heated under reflux and N_2 for 1 h. After cooling to ambient temperature, the reaction mixture was placed in a centrifuge (9000 RPM, 282 K, 30 min) and the solution was carefully decanted off, leaving behind an off-white solid. Pyridine (372 mg, 380 μL, 4.7 mmol) was added to the solution, the flask wrapped in foil and the reaction left stirring under N_2 at ambient temperature for 18 h. Ammonium hexafluorophosphate (76 mg, 0.47 mmol) was then added and the solvent was allowed to slowly evaporate at ambient temperature and pressure, yielding the product as a yellow precipitate which was isolated by filtration under reduced pressure and washed with Et_2O (27 mg, 40%). **^{1}H NMR** (300 MHz, acetone-d_6) δ = 9.33 (d, 1H, J = 4.2 Hz), 8.61 (dd, 2H, J = 6.5, 1.5 Hz), 8.28 (d, 1H, J = 8.4 Hz), 8.07 (td, 1H, J = 7.6, 1.6 Hz), 7.97 (d, 1H, J = 7.3 Hz), 7.90 (tt, 1H, J = 7.7, 1.4 Hz), 7.61-7.56 (m, 1H), 7.42-7.38 (m, 2H), 7.28 (t, 1H, J = 7.5 Hz), 7.01 (d, 1H, J = 7.3 Hz), 2.66 (s, 3H), 1.66 (s, 15H). **ESI-MS** (MeOH) m/z = 575.2 $[M\text{-}PF_6]^+$. **CHN analysis** calc. for $C_{27}H_{30}N_2F_6IrP$ C – 45.06%, H – 4.20%, N – 3.89%. Found C – 44.90%, H – 4.10%, N – 3.84%. **HPLC Purity** 254 nm – 99.0 %.

[(η^5-Cp*)Ir(2-(2'-methylphenyl)pyridine)4-(dimethylamino)pyridine]PF_6 (19) As for **18** using 4-(dimethylamino)pyridine (574 mg, 4.7 mmol) in place of pyridine. Slow evaporation yielded yellow needle crystals (41 mg, 57%). **^{1}H NMR** (400 MHz, acetone-d_6) δ = 9.26 (dd, 1H, J = 5.7, 1.3 Hz), 8.27 (d, 1H, J = 8.4 Hz), 8.04 (td, 1H, J = 7.5, 1.6 Hz), 7.92 (d, 1H, J = 7.5 Hz), 7.86 (d, 2H, J = 7.4 Hz), 7.54 (ddd, 1H, J = 7.2, 5.7, 1.3 Hz), 7.24 (t, 1H, J = 7.5 Hz), 6.99 (d, 1H, J = 7.4 Hz), 6.44 (d, 2H, J =

7.4 Hz), 2.99 (s, 6H), 2.67 (s, 3H), 1.66 (s, 15H). **ESI-MS** (MeOH) m/z = 618.1 [M-PF_6]$^+$. **CHN analysis** calc. for $C_{29}H_{35}N_3F_6IrP$ C – 45.66%, H – 4.63%, N – 5.51%. Found C – 45.53%, H – 4.54%, N – 5.52%. **HPLC Purity** 254 nm – 99.0 %. Crystals suitable for X-ray diffraction were obtained from a methanol/ether solution at 278 K.

[(η^5-Cp*)Ir(2-(2'-methylphenyl)pyridine)4-(trifluoromethyl)pyridine]PF_6 (20)

As for **18** using 4-(trifluoromethyl)pyridine (691 mg, 544 μL, 4.7 mmol) in place of pyridine. Slow evaporation yielded yellow crystals (30 mg, 41%). **^{1}H NMR** (400 MHz, acetone-d_6) δ = 9.35 (dd, 1H, J = 5.7, 1.3 Hz), 8.95 (d, 2H, J = 6.6 Hz), 8.30 (d, 1H, J = 8.4 Hz), 8.09 (ddd, 1H, J = 8.9, 7.5, 1.6 Hz), 7.98 (d, 1H, J = 7.5 Hz), 7.72 (d, 2H, J = 6.6 Hz), 7.60 (ddd, 1H, J = 7.2, 5.7, 1.3 Hz), 7.30 (t, 1H, J = 7.5 Hz), 7.03 (d, 1H, J = 7.4 Hz), 2.66 (s, 3H), 1.67 (s, 15H). **ESI-MS** (MeOH) m/z = 643.1 [M-PF_6]$^+$. **CHN analysis** calc. for $C_{28}H_{29}N_2F_9IrP$ C – 42.69%, H – 3.71%, N – 3.56%. Found C – 42.46%, H – 3.65%, N – 3.54%. **HPLC Purity** 254 nm – 98.5 %.

4.2.3 Methods

4.2.3.1 X-ray Crystallography

The structure of complex **19** was solved by Dr. Guy Clarkson (Department of Chemistry, University of Warwick) as described in Chapter 2 (section 2.2.8).

4.2.3.2 HPLC Purity Measurements

HPLC purity determination of complexes **18-20** (ca. 100 μM 10% MeOH/90% H_2O (v/v)) were performed as described in Chapter 2 (section 2.2.5.1).

4.2.3.3 Aqueous Stability

The stability of complexes **18-20** (ca. 500 μM) in aqueous solution and in the presence of chloride concentrations representative of blood plasma (104 mM), the cytoplasm (23 mM) and cell nucleus (4 mM) were determined by ^{1}H NMR spectroscopy over 24 h. Briefly, complexes were dissolved in 26.7% MeOD-d_4/73.3% D_2O (v/v) by dissolution of complexes in MeOD-d_4 followed by rapid dilution with D_2O at 310 K and NMR spectra recorded at various time intervals. All spectra were internally referenced to 1,4-dioxane (3.75 ppm) and water suppression was performed using Shaka techniques. Calculation of the stability was made by peak integrations.

4.2.3.4 Reaction with 9-Ethylguanine

The reaction of complexes **18-20** (ca. 500 μM) with 9-EtG (ca. 500 μM) were studied by ^{1}H NMR spectroscopy. Typically, one mol equiv. of 9-EtG in D_2O was added to a solution of complex in MeOD-d_4/D_2O to give a final complex concentration of ca. 500 μM in 26.7% MeOD-d_4/73.3% D_2O (v/v). All spectra were internally referenced to 1,4-dioxane (3.75 ppm) and water suppression was performed using Shaka techniques. ^{1}H NMR spectra were recorded at various time intervals at 310 K and samples incubated at this temperature during the course of the reaction. Percentage binding was based on peak integrations.

4.2.3.5 Reaction with Reduced L-glutathione (GSH)

Complexes **13** and **18-20** were assessed for stability in the presence of GSH by RP-HPLC and LC-MS. The complex was dissolved in MeOH (1.5 mM) and an aliquot of 100 μL was diluted by addition of H_2O (790 μL), 0.5 M Na_2HPO_4/NaH_2PO_4 buffer at pH 7.5 (10 μL) and 4.5 mM GSH in H_2O (100 μL) to give a final complex

concentration of 150 μM (1 mol eq.) and GSH concentration of 450 μM (3 mol eq.) in 5 mM phosphate buffer at pH 7.5, 10% MeOH/90% H_2O. Samples were incubated at 310 K for 24 h. HPLC measurements were made at 1, 4, 8 and 24 h, LC-MS measurement was taken at 24 h. The instrumentation for LC-MS is described in Chapter 2 (section 2.2.6). HPLC/LC measurements were made using the Agilent 1200 system with a VWD and 100 μL loop. The column use was an Agilent Zorbax Eclipse Plus C18, 150 × 4.6 mm with a 5 μm pore size. The mobile phase was H_2O 0.1% TFA and CH_3CN 0.1% TFA, with a flow rate of 1 mL min^{-1}. The detection wavelength was set at 254 nm and the reference wavelength at 360 nm. Sample injections were half the loop volume (50 μL) for HPLC measurements and either 5 or 25 μL for LC-MS, with needle washes of MeOH and H_2O between injections. The gradient used is shown in Figure 4.1.

Time (min)	%B
0	2
5	2
10	20
20	40
25	40
35	80
40	80
42	2
57	2

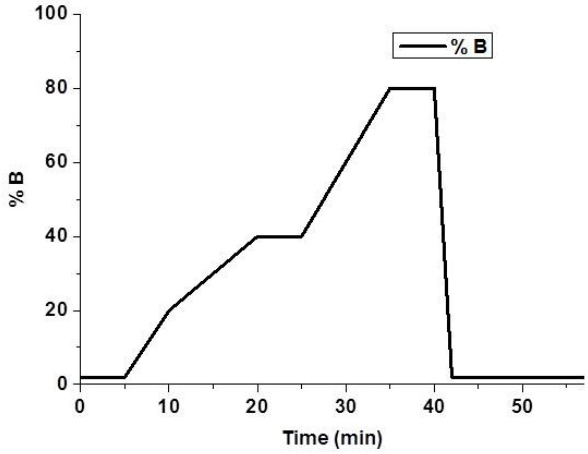

Figure 4.1. HPLC/LC method used for analysis of GSH reactions using H_2O 0.1% TFA (solvent A) and CH_3CN 0.1% TFA (solvent B).

4.2.3.6 Catalytic Oxidation of NADH

Complexes **13** and **19** were evaluated for the catalytic oxidation of NADH to NAD^+ by UV-Visible spectroscopy over a 24 h period in 0.5% MeOH/99.5% H_2O at 310 K

in 5 mM Na_2HPO_4/NaH_2PO_4 buffer, pH 7.5. The complex concentration was 2.5 μM with an NADH concentration of 127 μM. The conversion of NADH to NAD^+ was followed by absorption at 339 nm (ε_{NADH} = 6220 cm^{-1} M^{-1}) to allow evaluation of kinetic data.

4.2.3.7 Antiproliferative Activity

Antiproliferative activity assays were performed by Dr. Isolda Romero-Canelón (Department of Chemistry, University of Warwick) as described in Chapter 2 (section 2.2.14.2). Complexes **18-20** were evaluated for activity in the A2780 human ovarian cancer cell line and compared with complex **13** from Chapter 3. All complexes were also evaluated for activity in the MRC5 human fibroblast cell line.

4.2.3.8 Total ROS Production in A2780 Cancer Cells

Flow cytometry analysis of total reactive oxygen species (ROS) induction in A2780 cells caused by exposure to complexes **13** and **18-20** was carried out using the Total ROS/ detection kit (Enzo-life sciences) according to the supplier's instructions. This was performed by Dr. Isolda Romero-Canelón (Department of Chemistry, University of Warwick). Briefly, 1.0×10^6 A2780 cells per well were seeded in a 6-well plate. Cells were pre-incubated in drug-free media at 310 K for 24 h in a 5% CO_2 humidified atmosphere, and then drugs were added to triplicates at concentrations of IC_{50}. After 24 h of drug exposure, supernatants were removed by suction and cells were washed and harvested. Staining was achieved by re-suspending the cell pellets in buffer containing the green fluorescent reagent. Cells were analysed in a Becton Dickinson FACScan Flow Cytometer using FL1 channel Ex/Em: 490/525nm. Data were processed using Flowjo software. Positive controls for comparison purposes were obtained by exposing A2780 cells to pyocyanin for 24 h.

4.2.3.9 Induction of Apoptosis in A2780 Cancer Cells

Flow cytometry analysis of apoptotic populations of A2780 cells caused by exposure to complexes **13** and **18-20** with 0 h and 24 h cell recovery time, was carried out using the Annexin V-FITC Apoptosis Detection Kit (Sigma Aldrich) according to the supplier's instructions. This was performed by Dr. Isolda Romero-Canelón (Department of Chemistry, University of Warwick). Briefly, 1.0×10^6 A2780 cells per well were seeded in a 6-well plate. Cells were pre-incubated in drug-free media at 310 K for 24 h, after which drugs were added at equipotent concentrations equal to IC_{50} and 2 x IC_{50}. After 24 h of drug exposure, supernatants were removed by suction and cells were washed with PBS. Finally, cells were harvested using trypsin-EDTA. Sample staining was achieved by re-suspending the cell pellets in buffer containing Annexin V-FITC and PI. For positive-apoptosis controls, A2780 cells were exposed to staurosporine (1 μg mL^{-1}) for 2 h. Cells for apoptosis studies were used with no previous fixing procedure as to avoid non-specific binding of the annexin V-FITC conjugate.

4.2.3.10 ICP-OES Analysis

ICP-OES analysis of sample stocks used for biological studies was carried out as described in Chapter 2 (section 2.2.10).

4.3 Results

4.3.1 Synthesis and Characterisation

Complexes **18-20** bearing pyridyl monodentate ligands were synthesised from the chlorido complex **13** by reaction with 0.98 mol equiv. of $AgNO_3$ in $MeOH/H_2O$ under reflux, removing the chlorido ligand by precipitation as AgCl and forming the

corresponding aqua complex. After removal of the AgCl, either 50 mol equiv. of pyridine (Py), 4-(dimethylamino)pyridine (Py-NMe_2) or 4-(trifluoromethyl)pyridine (Py-CF_3) was added to form the desired complex bearing a pyridyl monodentate ligand. All complexes were isolated as PF_6 salts. The complexes were fully characterised by ^{1}H NMR spectroscopy, ESI-MS, CHN analysis and purity also determined by HPLC. Complex **13** was prepared as described in Chapter 3. Its chemical and biological properties are compared with **18-20** in this Chapter.

Analysis of the ^{1}H NMR spectra of complexes **18-20** showed no differences between the observed chemical shifts of the methyl protons (on the 2-(2'-methylphenyl)pyridine and Cp* capping ligand) for each complex and little difference among the aromatic protons on the chelating ligand. The proton adjacent to the bonding nitrogen on the pyridyl ring of 2-(2'-methylphenyl)pyridine ligand showed the greatest variation in chemical shift, ranging from 9.26 ppm to 9.35 ppm.

The X-ray crystal structure of complex **19** was determined and shows the expected pseudo-octahedral half-sandwich geometry with the iridium bound to the η^5-pentamethylcyclopentadienyl ring (Ir – ring centroid 1.840 Å), the 2-(2'-methylphenyl)pyridine chelating ligand (Ir – C 2.045(5) Å, Ir – N 2.083(4) Å) and the Py-NMe_2 monodentate ligand (Ir – N 2.106(4) Å). The structure and atom numbering scheme are shown in Figure 4.2, crystallographic data are shown in Table 4.1 and selected bond angles and lengths shown in Table 4.2. No π-π stacking features were observed in the X-ray crystal structure.

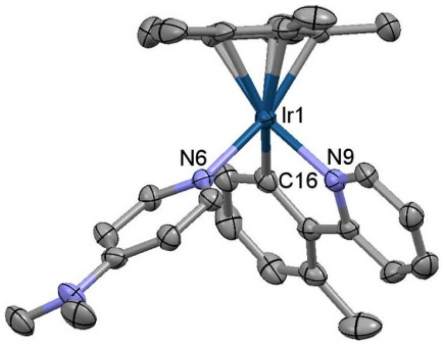

Figure 4.2. X-ray crystal structure with atom numbering scheme for complex [(η^5-Cp*)Ir(2-(2'-methylphenyl)pyridine)4-(dimethylamino)pyridine]PF_6 **19** with thermal ellipsoids drawn at 50%. Hydrogen atoms and PF_6 counterion have been removed for clarity.

Table 4.1. Selected X-ray crystallographic data (left) and selected bond lengths (Å) and bond angles (°) (right) for complex [(η^5-Cp*)Ir(2-(2'-methylphenyl)pyridine)4-(dimethylamino)pyridine]PF_6 **19**.

	19
Formula	$C_{29}H_{35}F_6IrN_3P$
MW	762.77
Crystal Colour	Yellow
Cryst size (mm)	0.12 x 0.10 x 0.04
λ (Å)	0.71073
Temp (K)	150
Cryst system	Monoclinic
Space group	P2(1)/n
a (Å)	10.1080(2)
b (Å)	19.8098(4)
c (Å)	14.8637(3)
α (°)	90
β (°)	95.0570(19)
γ (°)	90
Vol (Å^3)	2964.66(11)
Z	4
$R(Fo^2)$	0.0426
$Rw(Fo^2)$	0.0802
GOF	1.096

Bond/angle	**19**
Ir-C (Cp* ring)	2.263(5)
	2.242(5)
	2.173(5)
	2.174(5)
	2.175(5)
Ir-C (centroid)	1.840
Ir-C	2.045(5)
Ir-N9 (2-PhPy)	2.083(4)
Ir-N16 (monodentate)	2.106(4)
C-Ir-N 9	77.44(19)
C-Ir-N16 (monodentate)	86.24(18)
N9-Ir-N16 (monodentate)	86.18(16)

4.3.2 Aqueous Stability

The aqueous stability of complexes **18-20** (ca. 500 μM) was examined by ^{1}H NMR spectroscopy in 26.6% MeOD-d_4/73.3% D_2O (v/v) at 310 K over 24 h. The stability could be determined as a function of pyridine release, which was confirmed by the addition of the relevant pyridyl ligand to the NMR sample. The greatest stability was observed for complex **18** with 85% of the complex still bearing the pyridyl ligand, and the lowest for complex **20** with 76% of complex still bearing the pyridyl ligand (Figure 4.3) after 24 h. The release of the pyridine ligand is slow, in comparison to **13** where the extent of hydrolysis reaches equilibrium within 15 min. A new set of peaks could be observed in the low-field region which were assumed to be due to the formation of the aqua species [(η^5-Cp*)Ir(2-(2'-methylphenyl)pyridine)OD_2]$^+$ (**13A**). However, comparison to the ^{1}H NMR of the chlorido complex **13** under the same conditions shows that the new peaks do not share the same chemical shift as the assigned adduct **13A** (Figure 4.3).

Analysis of the ESI-MS of solutions of **18-20** after 24 h showed only peaks associated with [M-PF_6]$^+$ (575.1, 618.1 and 643.1 for **18**, **19** and **20**, respectively) where the pyridyl ligand is still bound, and the [M-PF_6-Pyridyl]$^+$ (496.1) species was also observed. No aqua species was detected, but this was also the case for complex **13**, which exhibits an m/z of 496.1 being the species [M-Cl]$^+$ or [M-OD_2]$^+$. Free chelating ligand was not detected, neither was a peak associated with a hydroxido-bridge dimers that can occur for half-sandwich metal complexes in aqueous solution.[19,20]

The pH* of each solution was measured at 0 h and 24 h to assess if the pyridyl ligand can change the pH* of the unbuffered solution. Aqua complexes can be sensitive to changes in pH. The pH* at 0 h was found to be between 7.3-7.5, which

changed to 7.5-7.6 after 24 h for complexes **18-20** compared to pH* 7.5 for complex **13**, making the reason for the chemical shifts differing due to a shift in the aqua complex resonances from changes in pH* unlikely.

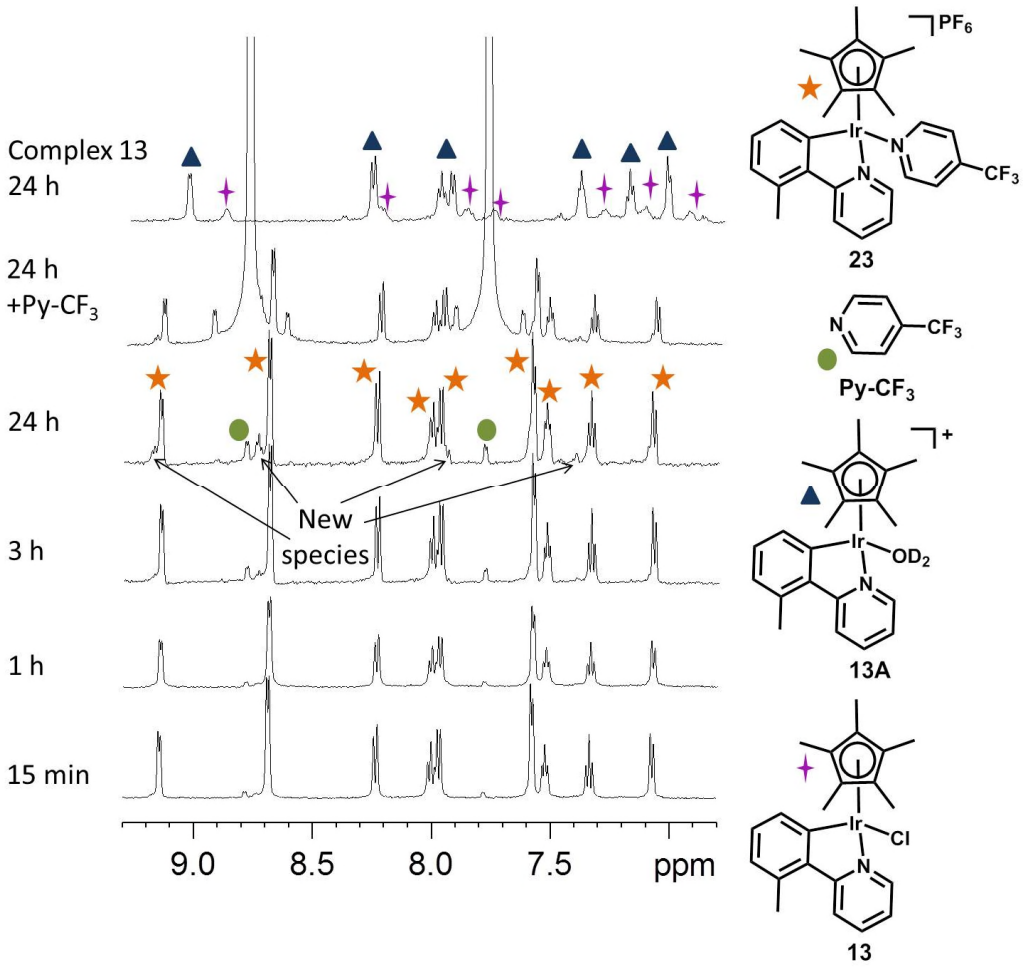

Figure 4.3. ^{1}H NMR (600 MHz) spectra of complex [(η^5-Cp*)Ir(2-(2'-methylphenyl)pyridine)4-(trifluoromethyl)pyridine]PF_6 **20** (ca. 500 µM) in 26.6% MeOD-d_4/73.3% D_2O (v/v), 310 K at 15 min, 1 h, 3 h, 24 h and 24 h + large excess of Py-4-CF_3. Comparison with complex **13** under the same conditions, showing no formation of expected aqua adduct **13A**. Complex **20** = ★,Py-4-CF_3 = ●, **13A** = ▲ and ✦ = **13**.

Table 4.3. Percentage of complex (determined by ^{1}H NMR, 600 MHz, 310 K) found to exhibit either the chloride (**13**) or pyridyl (**18-20**) monodentate ligand in solution after incubation in 26.6% MeOD-d_4/73.3% D_2O (v/v)) after 24 h.

Complex	Monodentate ligand	% Ir-Cl/Pyridyl (24 h)
13	Cl^-	28[a]
18	Py	85
19	Py-NMe_2	81
20	Py-CF_3	76

[a]Determined in Chapter 3.

The stability of complexes **18-20** (ca. 500 μM) was also examined at biologically relevant concentrations of chloride, representing blood plasma (104 mM), the cytoplasm (23 mM) and the cell nucleus (4 mM) by ^{1}H NMR spectroscopy in 26.6% MeOD-d_4/73.3% D_2O (v/v) at 310 K over 24 h (Figure 4.4). No changes in the ^{1}H NMR spectra were observed for all complexes, indicating no conversion to the chlorido complex **13.**

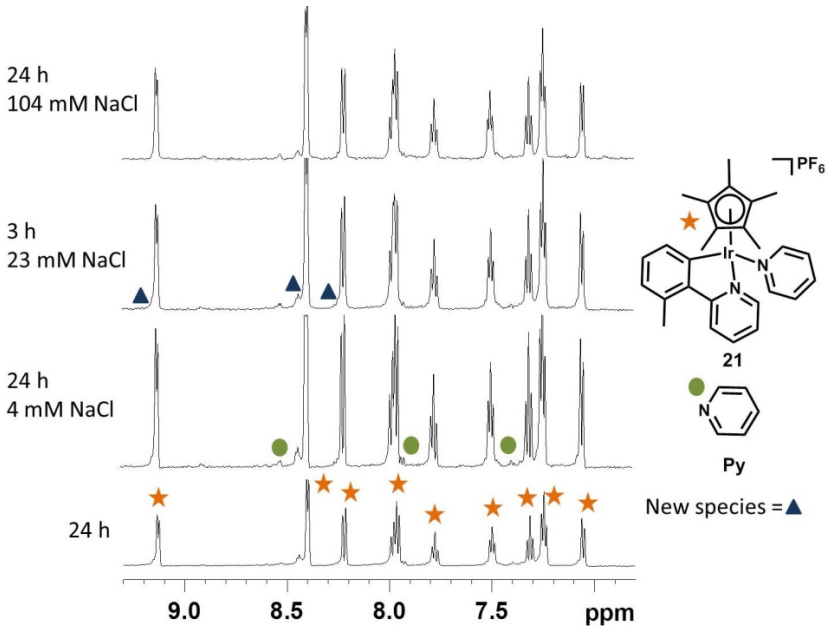

Figure 4.4. ^{1}H NMR (600 MHz) spectra of complex [(η^5-Cp*)Ir(2-(2'-methylphenyl)pyridine)pyridine]PF_6 **18** (ca. 500 μM) in 26.6% MeOD-d_4/73.3% D_2O (v/v), 310 K at 24 h with either 0 mM, 4 mM, 23 mM or 104 mM NaCl. Complex **18** = ★, Py = ● and new species = ▲.

4.3.3 Reaction with Nucleobase 9-Ethylguanine

To assess the reactivity of complexes **18-20** (ca. 500 μM) towards potential biological targets, the reaction with DNA nucleobase 9-EtG (ca. 500 μM) was examined by ^{1}H NMR spectroscopy in 26.6% MeOD-d_4/73.3% D_2O (v/v) at 310 K over 24 h (Figure 4.5 and Table 4.4). After 15 min, a new set of peaks were observed and assigned as the 9-EtG adduct (**13G**) along with the release of the monodentate pyridyl ligands. Between 22-38% of **13G** formed during the reaction. The proton adjacent to the binding nitrogen on the pyridyl ring of the chelating ligand is shifted downfield by ca. 0.40 ppm upon binding of 9-EtG, whereas the H8 proton of 9-EtG is shifted upfield by ca. 0.45 ppm compared to free 9-EtG. After 24 h no further changes in the spectra were observed, indicating equilibrium between complexes **18-20** and **13G** had been reached within 15 min. ESI-MS of the reaction mixtures indicated a peak of 675.3 which corresponds to $[M\text{-}Py\text{-}PF_6\text{+}9\text{-}EtG]^+$ (calculated m/z = 675.24), confirming binding of the nucleobase.

Table 4.4. Extent of binding of complexes **13** and **18-20** (500 μM) to 9-EtG (500 μM) to form complex **13G** as measured by ^{1}H NMR spectroscopy (600 MHz, 26.6% MeOD-d_4/73.3% D_2O (v/v), 310 K).

Complex	Monodentate ligand	% binding to 9-EtG (24 h)[a]
13	Cl^-	100[b]
18	Py	24
19	Py-NMe_2	22
20	Py-CF_3	38

[a]Calculated from peak integral ratios of **13G**/(**13** or **18-20**). [b]Determined in Chapter 3.

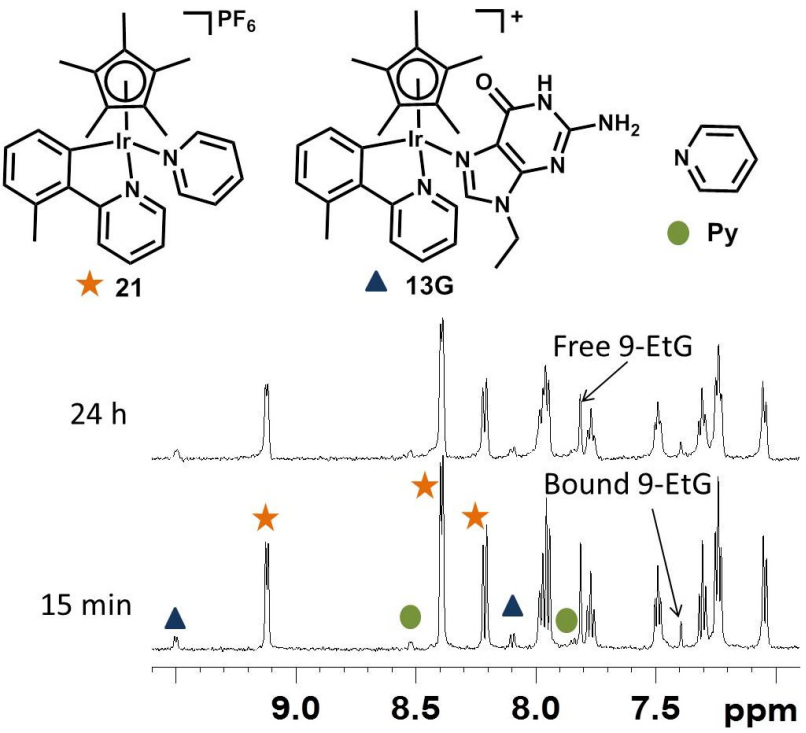

Figure 4.5. 600 MHz ^{1}H NMR spectra of the reaction between complex [(η^5-Cp*)Ir(2-(2'-methylphenyl)pyridine)pyridine]PF_6 **18** (*ca.* 500 μM) and 9-EtG (ca. 500 μM) in 26.6% MeOD-d_4/73.3% D_2O (v/v), 310 K after 15 min and 24 h. Complex **18** = ★, **13G** = ▲ and Py = ●.

4.3.4 Reaction with GSH

The interaction of metal-based drugs with GSH can cause deactivation as in the case of cisplatin, by inhibiting the metal from reacting with biological targets and by cellular-efflux mechanisms of metal-GSH adducts.[13,21] Complexes **13** and **18-20** were investigated for their reaction with GSH in order to determine if the extent of reaction is modulated by the type of monondentate ligand bound to the iridium centre. The reactions of complexes **13** and **18-20** (150 μM) with GSH (450 μM) in 10% MeOH/90% H_2O, 5 mM Na_2HPO_4/Na_2HPO_4 (pH = 7.5), 310 K were monitored at different time points by RP-HPLC and the chromatograms are shown in Figure 4.6. Within 1 h, all complexes had begun to react with GSH, as was evident by the formation of new peaks in the HPLC traces. The new species continued to increase

in intensity during the next 23 h. With the exception of the peaks corresponding to release of Py, Py-NMe_2 and Py-CF_3 (**18** – t_R =2.45min , **19** – t_R = 9.80 min and **20** – t_R = 14.04 min, respectively), the reaction with complexes **13** and **18-20** resulted in traces with almost identical t_R. This indicates that the new species formed are likely to be the same for all complexes.

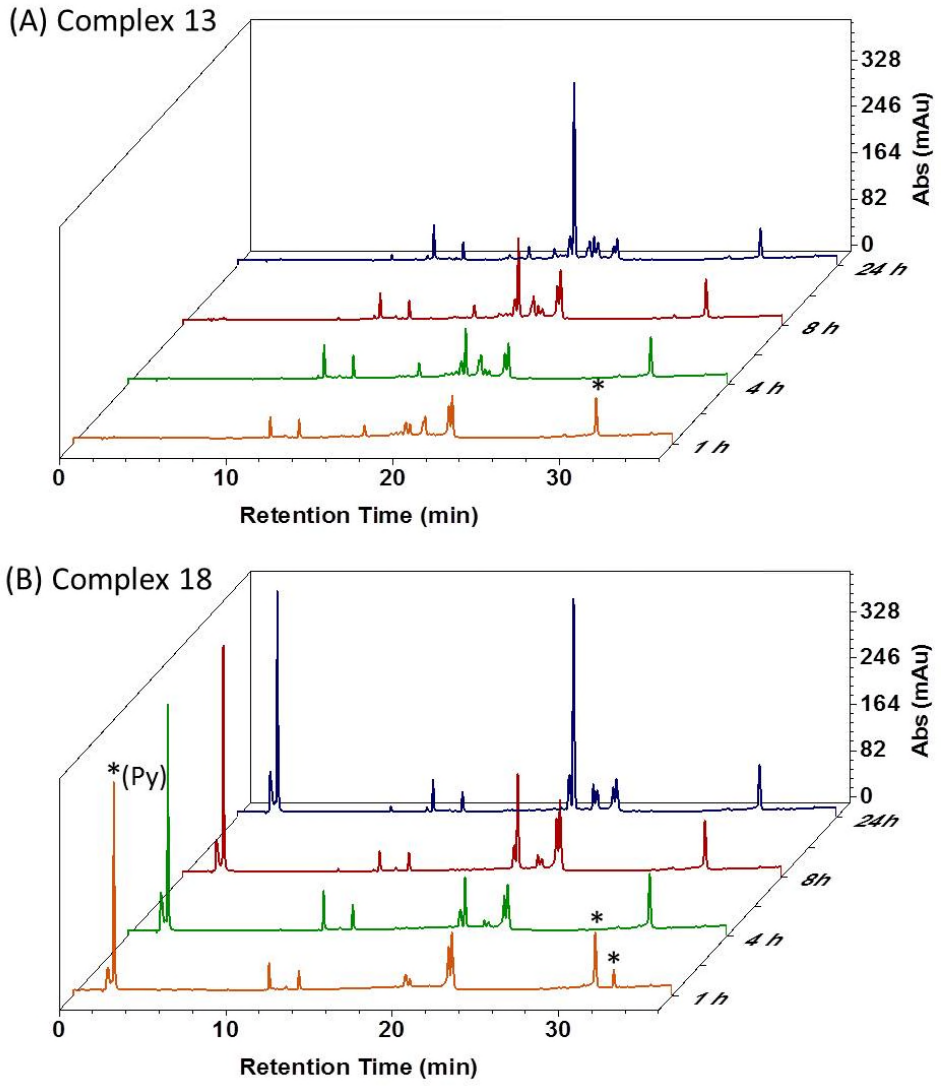

Figure 4.6. RP-HPLC (H_2O 0.1% TFA/ CH_3CN 0.1% TFA, λ = 254 nm) traces for the reaction of complexes **13** (A), **18** (B), **19** (C) and **20** (D) (150 μM) with GSH (450 μM) in 10% MeOH/90% H_2O, 5 mM Na_2HPO_4/Na_2HPO_4 (pH = 7.5), 310 K at various time intervals. Asterisks (*) indicate peaks that are present for each complex before incubation with GSH.

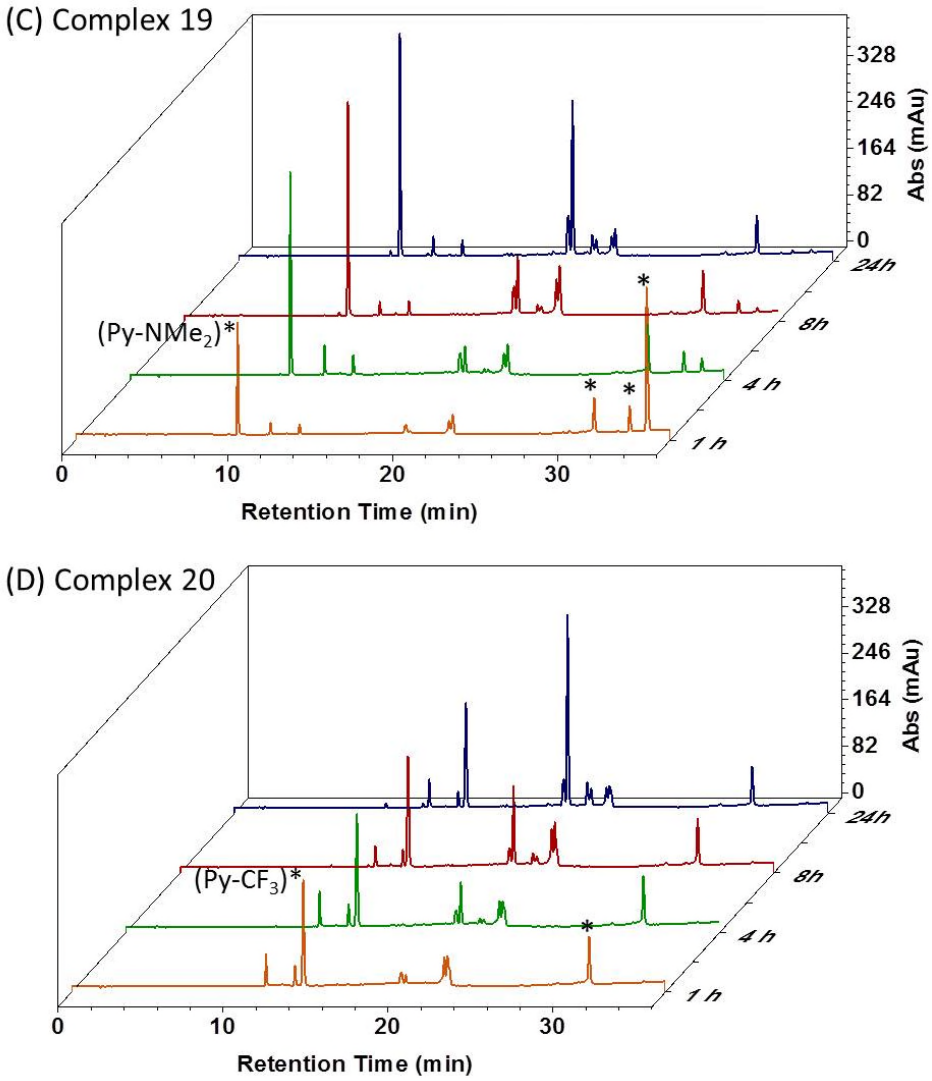

Figure 4.6. RP-HPLC (H_2O 0.1% TFA/ CH_3CN 0.1% TFA, λ = 254 nm) traces for the reaction of complexes **13** (A), **18** (B), **19** (C) and **20** (D) (150 μM) with GSH (450 μM) in 10% MeOH/90% H_2O, 5 mM Na_2HPO_4/Na_2HPO_4 (pH = 7.5), 310 K at various time intervals. Asterisks (*) indicate peaks that are present for each complex before incubation with GSH.

Determination of the products between the reaction of complex **13** and GSH after 24 h was performed by LC-MS and is shown in Figure 4.7 and Table 4.5. Two of the peaks (4 and 7) showed no m/z signal that could be identified as either an Ir-containing species or relevant organic fragment. Peak 8 had an m/z of 817.18 that

contained the Ir isotopic pattern but could not be assigned. Peak 9 (m/z = 496.12) corresponds to unreacted complex **13** (calculated m/z {[(η^5-Cp*)Ir(2'-methylphenyl)pyridine)]}$^+$ = 496.16).

Oxidised GSH (GSSG) was observed as peak 1 (m/z 613.17, calculated m/z {GSSH+H}$^+$ = 613.16). Peak 2 (m/z = 787.58) was assigned as an iridium GSH bridged dimer, where three molecules of deprotonated GSH (thiolate sulphur atom deprotonated, forming GS$^-$) bridge two Ir centres which still bear the Cp* capping ligand ([(η^5-Cp*)Ir(μ-SG)$_3$Ir(η^5-Cp*)]$^{2-}$, calculated m/z {[(η^5-Cp*)Ir(μ-SG)$_3$Ir(η^5-Cp*)]+4H}$^{2+}$ = 787.70). The free bidentate ligand that would be released from the formation of this dimer was detected as peak 3 (m/z = 169.86, calculated m/z {2'-methylphenyl)pyridine+H}$^+$ = 170.10). Interestingly, peaks 5 (m/z = 819.19) and 6 (m/z = 835.24) were identified to be Ir-SG monodentate adducts where the chelating ligand is still bound, however, they correspond to the sulfur-oxidised adducts [(η^5-Cp*)Ir(2'-methylphenyl)pyridine)(S-O)G]$^-$ (sulfenate) (calculated m/z {[(η^5-Cp*)Ir(2'-methylphenyl)pyridine)(S-O)G]+2H}$^+$ = 819.24) and [(η^5-Cp*)Ir(2'-methylphenyl)pyridine)(S-O$_2$)G]$^-$ (sulfinate) (calculated m/z {[(η^5-Cp*)Ir(2'-methylphenyl)pyridine)(S-O$_2$)G]+2H}$^+$ = 835.24). The unoxidised Ir-SG adduct was not detected.

Integration of each peak that contains an iridium species (as evident from the isotopic pattern) to determine the change in the amount of that species over time is shown for complexes **13** and **19** in Figure 4.8. It can be seen that [(η^5-Cp*)Ir(μ-SG)$_3$Ir(η^5-Cp*)]$^{2-}$ remains relatively constant over time, and the extent of formation is less for the reaction with **19** compared to **13**. The reaction of **19** with GSH is shown to be slower than **13** during the first 8 h, as evident by the higher percentage of peaks associated with unreacted **19** compared with **13**. Complexes **18** and **20**

showed little difference in rate of formation of products compared to **13**. After 24 h, the percentage of [(η^5-Cp*)Ir(2'-methylphenyl)pyridine)(S-O)G]$^-$, [(η^5-Cp*)Ir(2'-methylphenyl)pyridine)(S-O_2)G]$^-$ and the unidentified new Ir species is relatively the same for both **13** and **19**.

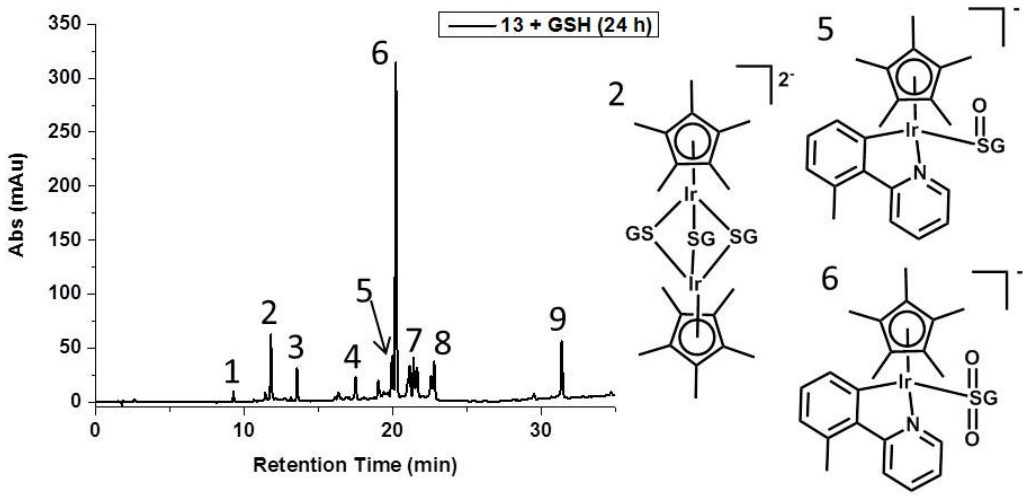

Figure 4.7. Peak assignments from LC-MS data of the reaction of complex **13** (150 μM) with GSH (450 μM) in 10% MeOH/90% H_2O, 5 mM Na_2HPO_4/Na_2HPO_4 (pH = 7.5), 310 K at 24. Structures of important Ir-containing species are shown with relevant peak numbers.

Table 4.5. LC-MS analysis for the reaction between complex **13** (1 mol equiv.) and GSH (3 mol equiv.) under argon after 24 h, 310 K.

Peak	m/z	Assigned species	Calculated m/z
1	613.17	{GSSG+H}$^+$	613.16
2	787.58	{[(η^5-Cp*)Ir(μ-SG)$_3$Ir(η^5-Cp*)]+4H}$^{2+}$	787.70
3	169.86	{2-(2'-methylphenyl)pyridine+H}$^+$	170.10
4	n.d.	n.d.	n.d.
5	819.19	{[(η^5-Cp*)Ir(2'-methylphenyl)pyridine)(S-O)G]+2H}$^+$	819.24
6	835.24	{[(η^5-Cp*)Ir(2'-methylphenyl)pyridine)(S-O_2)G]+2H}$^+$	835.24
7	n.d.	n.d.	n.d.
8	817.18	unknown	n/a
9	496.12	{[(η^5-Cp*)Ir(2'-methylphenyl)pyridine)]}$^+$	496.16

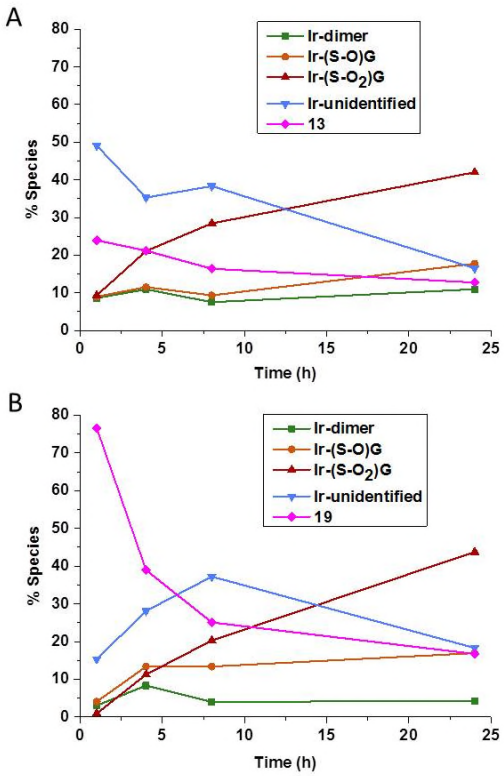

Figure 4.8. Percentage of each iridium species after various time intervals upon the reaction of (A) **13** + GSH and (B) **19** + GSH (complex (150 μM), GSH (450 μM) in 10% MeOH/90% H_2O, 5 mM Na_2HPO_4/Na_2HPO_4 (pH = 7.5), 310 K. Data obtained by integration of HPLC peaks. The structures of Ir-dimer (green), Ir-(S-O)G (orange) and Ir-(S-O_2)G (red) are shown in Figure 4.7.

The oxidation of the sulfur atom was investigated by performing the reaction of complex **13** under argon (including degassing solvent under argon), to elucidate whether the oxygen is coming from O_2 present in the atmosphere. The reaction was left for 24 h and analysed by LC-MS (Figure 4.9 and Table 4.6). Formation of the $[(\eta^5\text{-Cp*})\text{Ir}(\mu\text{-SG})_3\text{Ir}(\eta^5\text{-Cp*})]^{2-}$ dimer (peak 1) occurred alongside release of the chelating ligand (peak 2). Interestingly, a small peak corresponding to the species [(η^5-Cp*)Ir(2-(2'-methylphenyl)pyridine)(S-O)G] was observed (peak 6), and no formation of [(η^5-Cp*)Ir(2-(2'-methylphenyl)pyridine)(S-O_2)G] was detected. Two new peaks (3 and 5) were observed with an m/z of 801.13 (1+) and 401.13 (2+), which could correspond to the unoxidised GSH adduct

[(η^5-Cp*)Ir(2-(2'-methylphenyl)pyridine)SG]$^-$. However, {[(η^5-Cp*)Ir(2-(2'-methylphenyl)pyridine)SG]+2H}$^+$ has a calculated m/z of 803.24. Within the same peak, m/z of 496.12 and 308.11 were observed which correspond to [(η^5-Cp*)Ir(2-(2'-methylphenyl)pyridine)]$^+$ and free GSH, respectively.

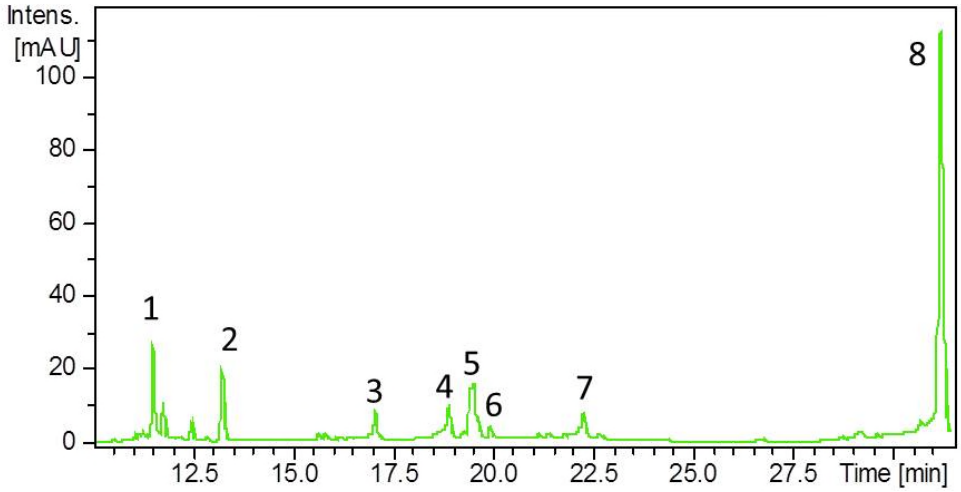

Figure 4.9. LC-MS traces of the reaction of complex **13** (150 μM) with GSH (450 μM) in 10% MeOH/90% H_2O, 5 mM Na_2HPO_4/Na_2HPO_4 (pH = 7.5), 310 K at 24 h under argon.

Table 4.6. LC-MS analysis for the reaction between complex **13** (150 μM) with GSH (450 μM) in 10% MeOH/90% H_2O, 5 mM Na_2HPO_4/Na_2HPO_4 (pH = 7.5), 310 K at 24 h under argon.

Peak	m/z	Assigned species	Calculated m/z
1	787.58	{[(η^5-Cp*)Ir(μ-SG)$_3$Ir(η^5-Cp*)]+4H}$^{2+}$	787.70
2	169.84	{2-(2'-methylphenyl)pyridine+H}$^+$	170.10
3	801.13	{[(η^5-Cp*)Ir(2-(2'-methylphenyl)pyridine)SG]+2H}$^+$	803.25
4	n.d.	n.d.	n.d.
5	801.13	{[(η^5-Cp*)Ir(2-(2'-methylphenyl)pyridine)SG]+2H}$^+$	803.25
	401.13	{[(η^5-Cp*)Ir(2-(2'-methylphenyl)pyridine)SG]+3H}$^{2+}$	402.13
	496.13	{[(η^5-Cp*)Ir(2'-methylphenyl)pyridine)]}$^+$	496.16
	308.11	{GSH+H}$^+$	308.09
6	819.12	{[(η^5-Cp*)Ir(2'-methylphenyl)pyridine)(S-O)G]+2H}$^+$	819.24
7	496.15	{[(η^5-Cp*)Ir(2'-methylphenyl)pyridine)]}$^+$	496.16
8	496.08	{[(η^5-Cp*)Ir(2'-methylphenyl)pyridine)]}$^+$	496.16

4.3.5 Catalytic Oxidation of NADH to NAD^+

Disruption of the NADH/NAD^+ ratio in cells appears to be of importance to the mechanism of action of iridium(III) half-sandwich complexes.[17,22] The ability to catalytically oxidise NADH (127 μM) to NAD^+ was examined for complexes **13** and **19** (2.5 μM) by UV-Vis spectroscopy in 0.5% MeOH/99.5% H_2O (v/v) in 5 mM Na_2HPO_4/Na_2HPO_4 (pH = 7.5) at 310 K over a 24 h period. The conversion to NAD^+ was followed by the decrease of the band at 339 nm which corresponds to NADH (ε_{NADH} = 6220 cm^{-1} M^{-1}) which allowed the calculation of the turn over number (TON) and turn over frequency (TOF) (h^{-1}) of the reaction (Figure 4.10). Both **13** and **19** showed mild catalytic activity, although intriguingly, both complexes exhibited a TON of 16 and TOF of 1.4 h^{-1}.

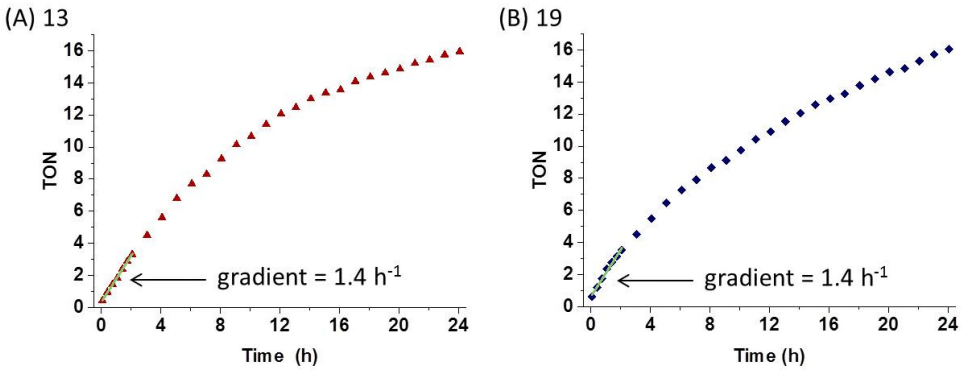

Figure 4.10. Plot of TON vs. Time for the reaction of complexes **13** (A) and **19** (B) (2.5 μM) with NADH (127 μM) in 0.5% MeOH/99.5% H_2O (v/v) in 5 mM Na_2HPO_4/Na_2HPO_4 (pH = 7.5) at 310 K. TOF (h^{-1}) calculated from the initial gradient (first 2 h) of TON vs. Time.

4.3.6 Antiproliferative Activity

The antiproliferative activity of complexes **18-20** in A2780 human ovarian cancer cells was evaluated and compared to complex **13**, Table 4.7. The importance of cell

recovery time was also evaluated by measuring the cell viability after 0 h and 72 h recovery time (after the initial 24 h drug incubation period). It is evident from Table 4.7 that the complexes exhibit antiproliferative activity rapidly and within 24 h, with IC_{50} values ranging from 0.65 – 4.4 μM. With 72 h recovery time, the IC_{50} values for complexes **18** and **20** remain virtually the same. For the chlorido complex **13**, the 72 h recovery time results in enhanced potency by almost 4 × compared with 0 h recovery time. In contrast, the potency of complex **19** appears to be slightly reduced with the 72 h cell recovery time, with the IC_{50} value increasing from 0.65 to 1.4 μM.

All of the complexes were also evaluated for activity against MRC5 human fibroblasts, which is representative of healthy, rapidly dividing cells, after 72 h recovery time. The selectivity factor (SF) of each complex was calculated as the ratio between $IC_{50\ MRC5}/IC_{50\ A2780}$ where a higher SF is indicative of a more selective complex towards A2780 human ovarian cancer cells over healthy fibroblasts MRC5 (Table 4.7). Small variations in activity were observed in the MRC5 cell line, with IC_{50} values ranging from 2.4 – 4.6 μM. The selectivity factor index for complex **13** is the highest showing the best selectivity (SF = 3.6), while complex **20** exhibits the least selectivity with an SF of 0.9.

Table 4.7. Inhibition of growth of A2780 human ovarian cancer cells and MRC5 human fibroblast cells (72 h recovery time only) by complexes **13** and **18-**. Selectivity factor (SF) calculated as the ratio between $IC_{50\ MRC5}/IC_{50\ A2780}$ after 72 h recovery time.

Complex	Monodentate Ligand	A2780 IC_{50} (μM)		MRC5 IC_{50} (μM)	SF
		0 h recovery	72 h recovery		
13	Cl^-	4.4 ± 0.4	1.18 ± 0.08[a]	4.6 ± 0.1	3.9
18	Py	2.00 ± 0.06	2.1 ± 0.3	2.4 ± 0.1	1.1
19	Py-NMe_2	0.65 ± 0.05	1.4 ± 0.3	2.98 ± 0.04	2.1
20	Py-CF_3	3.9+ ± 0.2	4.1 ± 0.9	3.6 ± 0.2	0.9

[a]Evaluated in Chapter 3.

4.3.7 Induction of ROS

The induction of high levels of ROS in cancer cells may be related to the mechanism of action of some anticancer metal complexes,[23-25] where an increase of cellular ROS levels ultimately leads to oxidative stress and cell death. The ability of complexes **13**, **18**, **19** and **20** to induce ROS in A2780 cells (IC_{50} values, 24 h incubation, 0 h recovery time) was measured by flow cytometry and is shown in Figure 4.11. All complexes induce high levels of ROS (as indicated by high fluorescence in the FL-1 channel reading green fluorescence) compared with untreated cells. Little difference was observed between the parent complex **13** and pyridyl adducts **18-20**. The elevation of ROS levels is likely to contribute to the antiproliferative mechanism of these complexes.

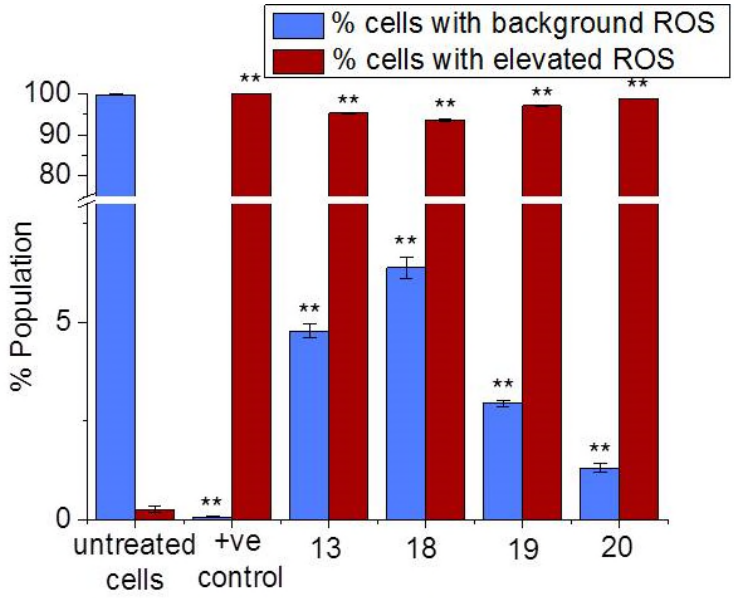

Figure 4.11. Induction of total ROS in A2780 cells upon incubation with complexes **13**, **18**, **19** and **20** (IC_{50} concentrations, 24 h incubation, 0 h recovery time) as measured by flow cytometry. Percentage of cells exhibiting normal levels of ROS in each experiment are indicated by blue bars. Percentage of cells exhibiting enhanced levels of ROS compared to normal levels are indicated by red bars. The positive control was pyocyanin. Students t-test for percentage of fluorescence compared with untreated cells (** indicates $p < 0.01$)

4.3.8 Induction of Apoptosis

Induction of programmed cell death (apoptosis) in A2780 cells upon exposure to complexes **13** and **18-20** at IC_{50} and 2 × IC_{50} values for 24 h was determined by flow cytometry, with either 0 h or 24 h cell recovery time (Figure 4.12). At 0 h recovery time, a very small population of cells was found to be apoptotic, with the vast majority being viable. After 24 h recovery time, a significant number of apoptotic cells were detected from cells incubated with complexes **18** and **19** at IC_{50} concentrations. At 2 × IC_{50} concentrations, the percentage of apoptotic cells vastly increases for **18** and **20**. A2780 cells incubated with complex **13** show no significant induction of apoptosis at either 0 h or 24 h recovery time.

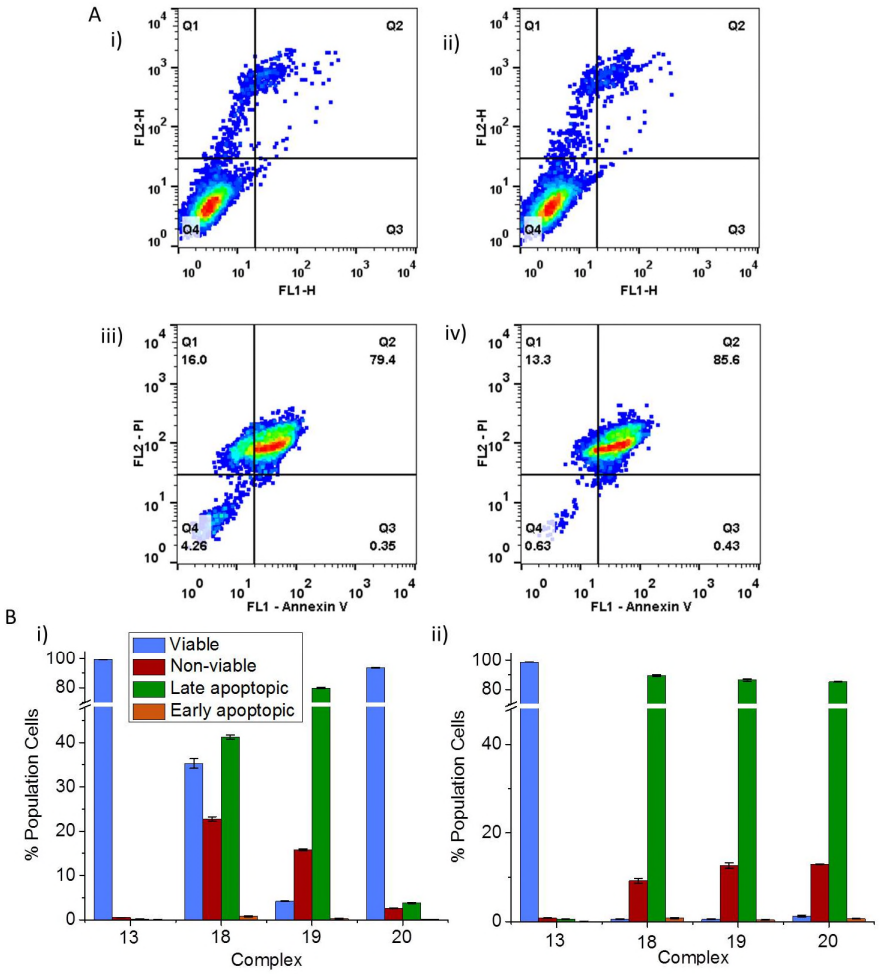

Figure 4.12. (A) – Flow cytometry dot plots of A2780 cells after exposure to complex **19** with 0 h recovery time (i – IC_{50} and ii – 2 × IC_{50}) and 24 h recovery time (iii – IC_{50} and iv – 2 × IC_{50}). Q1 = non-viable cells, Q2 = late-apoptotic cells, Q3 = early-apoptotic cells and Q4 = viable cells. FL-1 channel = Annexin V fluorescence and FL-2 channel = propidium iodide fluorescence. (B) Percentage of cells in each quadrant after exposure to complexes **13** and **18-20** for 24 h at (i) IC_{50} and (ii) 2 × IC_{50} values with 24 h cell recovery time.

4.4 Discussion

4.4.1 X-ray Crystal Structure of Complex 19

The X-ray crystal structure of [(η^5-Cp*)Ir(2-(2'-methylphenyl)pyridine)4-(dimethylamino)pyridine]PF_6 **19** shows the expected "piano-stool" conformation for

pseudo-octahedral half-sandwich complexes, with no notable π-stacking features observed in the crystal lattice.

A search of the Cambridge Crystallographic Database showed that this is the first example of an iridium(III) Cp* complex with a *C,N*-chelating ligand also bearing a monondentate pyridine ligand. The Ir – ring centroid (1.840 Å), 2-(2'-methylphenyl)pyridine chelating ligand (Ir – C 2.045(5) Å, Ir – N 2.083(4) Å) and the 4-dimethylaminopyridine monodentate ligand (Ir – N 2.106(4) Å) bond lengths are similar to the previous examples of 2-PhPy with extended Cp^{xPh} and Cp^{xBiPh} with pyridine monodentate ligands.[17,18] Comparison with the X-ray crystal structures of [(η^5-Cp*)Ir(2-PhPy)Cl] complexes from Chapter 3 show that **19** exhibits similar Ir – ring centroid and Ir – C/N bond lengths with the chelated 2-PhPy ligand, demonstrating that little change to the solid-state structure of these complexes occurs upon the introduction of a pyridyl ligand in place of chloride.

4.4.2 Aqueous Stability

The formation of aqua adducts in half-sandwich metal complexes is believed to be in many cases an activation step, enabling the metal to bind covalently to possible biological target sites *via* the substitution of the relatively more labile M-OH_2 (M = metal) bond.[26-28] Previous studies on the aqueous behaviour of half-sandwich iridium(III) complexes have predominantly focussed on complexes bearing chlorido ligands.[19,29] These have shown that the Ir-Cl bond is surprisingly labile, with fast rates of ligand exchange with water observed compared to their non-"piano-stool" octahedral counterparts.[30] The fast rate of hydrolysis of complex [(η^5-Cp*)Ir(2-(2'-methylphenyl)pyridine)Cl] **13** was demonstrated in Chapter 3, with 72% formation

of the corresponding aqua adduct [(η^5-Cp*)Ir(2-(2'-methylphenyl)pyridine)D_2O]$^+$ **13A** within 15 min, remaining unchanged after 24 h.

The replacement of chlorido with pyridyl ligands in [(η^5-Cp*)Ir(2-(2'-methylphenyl)pyridine)pyridine]PF_6 **18**, Py-NMe_2 [(η^5-Cp*)Ir(2-(2'-methylphenyl)pyridine)4-(dimethylamino)pyridine]PF_6 **19** and Py-CF_3 [(η^5-Cp*)Ir(2-(2'-methylphenyl)pyridine)4-(trifluoromethyl)pyridine]PF_6 **20**, results in an increase in the stability towards hydrolysis, with between 76-85% of the species remaining as the pyridyl adduct over 24 h.

Ruthenium complexes containing *N,N*-chelating ligands, such as [(η^6-hexamethylbenzene)Ru(ethylenediamine)pyridine]$(PF_6)_2$[12] and [(η^6-p-cymene)Ru(2,2'-bipyrimidine)(4-methyl)pyridine]$(PF_6)_2$[31] show no formation of their corresponding aqua adducts, although they also exhibit a decrease in antiproliferative activity compared to Ru(II) complexes bearing chlorido ligands. The iridium complex [(η^5-Cp^{xPh})Ir(2-phenylpyridine)pyridine]PF_6 also shows no aquation,[18] whereas the biphenyl complex [(η^5-Cp^{xBiPh})Ir(2-phenylpyridine)pyridine]PF_6 does show a small degree of hydrolysis over 24 h.[17] This suggests that the capping Cp^x ligand plays a role in governing the stability of the pyridine adducts in Ir(III) half-sandwich complexes.

Interestingly, the formation of the expected aqua adduct **13A** was not observed (Figure 4.3). Initially, it was considered that the release of Py, Py-NMe_2 and Py-CF_3 could make the unbuffered aqueous solution more basic, hence resulting in a shift in the proton resonances corresponding to the aqua complex. Py and Py-NMe_2 exhibit pKa values of 5.2 and 9.7,[32] respectively. Analysis of the pH* of the solutions showed little change compared to complex **13**. Ultimately, the species could not be

identified with certainty using NMR or MS, however, it is clear the complexes remain predominantly as their initial Ir-pyridyl adducts over 24 h.

The stability of the pyridine complexes **18-20** in the presence of chloride concentrations representative of the cell nucleus (4 mM), cytoplasm (23 mM) and blood plasma (104 mM) was also examined to investigate if conversion to parent complex **13** would occur in biological systems. Complexes **18-20** all showed complete stability, with no formation of complex **13** detected and the same degree of the unidentified species observed. This contradicts previous studies of similar complexes,[17] where chloride adducts were formed presumably from the aqua species formed *via* hydrolysis rather than by direct substitution of the pyridyl monodentate ligand. It was found in Chapter 3 that precipitation of the chloride complex could occur above concentrations of 4 mM NaCl under the conditions studied, which may result in not detecting the formation of **13**. However, no precipitation was observed, further supporting that conversion to the chloride complex had not occurred.

Complex **20** which exhibits the least aqueous stability (within the pyridyl series) bears the electron-withdrawing $-CF_3$ group para to the binding nitrogen on the pyridine ligand. This is likely to increase the lability of the bond between the nitrogen and iridium centre by electron-withdrawal, leading to enhanced pyridyl loss. The presence of the electron-donating $-NMe_2$ group para to the binding nitrogen on the pyridine ligand has the opposite effect, increasing the electron-donating ability of the pyridine and increasing the stability between the iridium-nitrogen bond.

4.4.3 Reactions with Biomolecules

4.4.3.1 9-Ethylguanine

Since DNA is considered a major target of metal-based anticancer compounds, reactivity towards 9-EtG was examined as a model for guanine binding in DNA. All complexes formed the 9-EtG adduct **13G**, with complex **13** exhibiting 100% binding within 15 min. This is consistent with previous reports of similar complexes.[19] The pyridyl complexes **18-20** show a decrease in the ability to bind to 9-EtG, with only 22-38% formation of **13G** after 24 h. This may indicate that pyridyl complexes **18-20** are less likely to bind to DNA in the cell compared to complex **13** due to the more stable Ir-N bond.[18,31]

The electron donating -NMe_2 group on the pyridine ligand in complex **19** stabilises the Ir-N(pyridyl) bond, reducing the reactivity of the complex with 9-EtG. The opposite effect was observed for complex **20** which bears the electron-withdrawing –CF_3 group, resulting in a greater extent of binding to 9-EtG. The observed reactivity towards 9-EtG parallels the expected reactivity of each complex **13** > **20** > **18** > **19** showing that modulation of activity towards DNA nucleobases can be achieved by careful selection of the monodentate ligand.

4.4.3.2 GSH

The concentration of GSH in cells is high, ranging from 0.5 – 10 mM in mammalian cells.[33] The interaction of metallodrugs with GSH can lead to inactivation as in the case with cisplatin where binding of GSH results in the drug being pumped out of the cell by specific membrane transport systems,[34] while thiolate adducts of cisplatin exhibit reduced reactivity towards biological targets such as DNA.[35] It has also been demonstrated that glutathione S-transferase π (GSTπ) may play a role in the

detoxification of cisplatin by GSH.[36] In some cases, reaction of metal complexes with GSH may be integral to their antiproliferative activity, as in the case for some octahedral Pt(IV)[37] and Ru(III)[38] complexes. The half-sandwich ruthenium(II) complex [(η^6-pcym)Ru(azpy)I]PF_6 (azpy = *N,N*-dimethylphenyl- or hydroxyphenyl-azopyridine) undergoes ligand-centred catalytic oxidation of GSH to GSSG resulting in enhanced levels of ROS, where coordination of the azpy chelating ligand to the ruthenium activates its catalytic activity.[39] It is believed that adducts of GSH with iridium complexes such as [(η^5-Cp^x)Ir(2-PhPy)SG] may also be less reactive, resulting in the decreased attack on potential biological targets.[17] This may be modulated by the type of monodentate ligand present on the complex.

Within the pyridyl series, the order of stability in the presence of GSH followed from most to least stable **19** > **18** ~ **20** (Figures 4.6 and 4.8). Complexes **18** and **20** exhibit a similar degree of reactivity towards GSH compared to chlorido complex **13**. Modulation of reactivity by pyridyl ligands is observed only in the case of **19** indicating that the electron-donating –NMe_2 group is essential for enhanced stability in the presence of GSH. In contrast, the iridium complex [(η^5-Cp^{xBiPh})Ir(2-PhPy)Py]PF_6 shows markedly enhanced stability in the presence of GSH compared to its chlorido analogue [(η^5-Cp^{xBiPh})Ir(2-PhPy)Cl].[17] This may indicate that the presence of the extended cyclopentadienyl capping ligand also plays a role in the reactivity of the pyridine complex towards GSH. This could be due to steric hindrance caused by the biphenyl rings compared with the Cp* ligand studied in this work. It has been previously demonstrated that the use of Cp^{xPh} and Cp^{xBiPh} capping ligands in some half-sandwich iridium(III) complexes leads to slower rates of hydrolysis for chlorido complexes.[29] This may also result in more stable pyridine monodentate for Cp^{xBiPh} complexes compared with Cp* complexes.

The reaction of complexes **13** and **18-20** with GSH resulted in HPLC traces with peaks having almost identical retention times (Figure 4.6), indicating that the reaction products are independent from the nature of the monodentate ligand. LC-MS analysis of the reaction between complex **13** and GSH resulted in the identification of several reaction products (Figure 4.7 and Table 4.5). The identification of the glutathione bridged Ir dimer $[(\eta^5\text{-Cp*})\text{Ir}(\mu\text{-SG})_3\text{Ir}(\eta^5\text{-Cp*})]^{2-}$ was supported by a peak corresponding to free chelating ligand 2-(2'-methylphenyl)pyridine. Analysis of the formation of products over time suggests that the bridged species forms quickly and its concentration stays constant over the 24 h period. This may suggest that $[(\eta^5\text{-Cp*})\text{Ir}(\mu\text{-SG})_3\text{Ir}(\eta^5\text{-Cp*})]^{2-}$ is a kinetic product of the reaction.

In the presence of air, the Ir-GSH adducts $[(\eta^5\text{-Cp*})\text{Ir}(2'\text{-methylphenyl})\text{pyridine})(\text{S-O})\text{G}]^-$ (sulfenate) and $[(\eta^5\text{-Cp*})\text{Ir}(2'\text{-methylphenyl})\text{pyridine})(\text{S-O}_2)\text{G}]^-$ (sulfinate) were observed, but no $[(\eta^5\text{-Cp*})\text{Ir}(2'\text{-methylphenyl})\text{pyridine})\text{SG}]^-$ was found. The Ir-(S-O)G and Ir-(S-O_2)G adducts appear to increase over time. As the extinction coefficient for each species is unknown, the definitive concentration of each species in solution cannot be determined; however, it can be deduced which species increase/decrease in concentration during the course of the reaction in relation to the other species present.

An unidentified Ir-containing species was also observed, which appears to be an intermediate species, as exemplified in Figure 4.8 for the reaction between **19** and GSH. Its concentration in solution increases during the first 8 h of reaction, but then decreases after 24 h. The concentration of this species also decreases over time for the reaction between **13** and GSH, but initially forms quickly due to the faster reaction of **13** compared to **19**.

Intriguingly, binding of GSH to the iridium may result in oxidation of the sulfur atom by dioxygen. This was further examined by performing the reaction under argon (Figure 4.9 and Table 4.6). LC-MS analysis identified two new peaks that could correspond to the adduct [(η^5-Cp*)Ir(2-(2'-methylphenyl)pyridine)SG]$^-$. The peaks contained m/z species including [(η^5-Cp*)Ir(2-(2'-methylphenyl)pyridine)]$^+$ and free GSH, which may be dissociating during the ionisation process. An m/z of 801.13 was detected which is the exact mass of [(η^5-Cp*)Ir(2-(2'-methylphenyl)pyridine)SG]$^-$. As the LC-MS was run in positive mode, this species is 2 Daltons lower than the detectable species {[(η^5-Cp*)Ir(2-(2'-methylphenyl)pyridine)SG]+2H}$^+$ (calculated m/z of 803.25). Therefore, it cannot be determined with certainty that the unoxidised Ir-SG adduct has been detected. The Ir-(S-O)G adduct was detected as a minor species and no Ir-(S-O_2)G was observed, indicating that the presence of O_2 gas is likely to promote the oxidation of the bound sulfur atom. The small presence of Ir-(S-O)G may be a consequence of the exposure of the reaction mixture to air upon injection into the LC-MS. These oxidised species have not been previously reported for half-sandwich Ir(III) complexes unless coupled with another reaction. Such an oxidation was demonstrated for the iridium complex [(η^5-Cp^{xBiPh})Ir(2-PhPy)Py]PF_6, but only when coupled to the catalytic oxidation of NADH to NAD$^+$ to produce H_2O_2 where oxidation of the sulfur atom then occurs.[40] Further addition of H_2O_2 was required to produce the glutathione-sulfinate adduct.

The Ru(II) arene complex [(η^6-biphenyl)Ru(ethylenediamine)Cl]PF_6 was shown to bind to GSH through the thiolate sulfur atom and was oxidised to the sulfenate complex by dioxygen, although further oxidation to the sulfinate was not observed.[28] This resulted in a Ru-(S-O)G adduct that then facilitated the binding to guanine,

while the Ru-SG adduct did not. Performing the same reaction under argon supressed the formation of the sulfenate complex. Therefore, it can be postulated that if complexes **13** and **18-20** are capable of forming these oxidised GSH adducts, their reactivity may not be severely decreased as the adducts formed may be more labile than the Ir-SG adduct.

4.4.3.3 Catalytic Oxidation of NADH

The use of platinum-group chelated metal half-sandwich complexes for the catalytic oxidation of NADH to NAD^+[22,41,42] and NAD^+ to NADH[43-45] has been well documented, where the catalytic activity appears to take place at the monodentate site. The catalytic oxidation of NADH to NAD^+ may be an important feature of half-sandwich iridium(III) complexes,[46] and could potentially occur in cells.[22] The catalytic activity of [(η^5-Cp*)Ir(2-PhPy)Cl] complexes was evaluated in Chapter 3. They can oxidise NADH, potentially contributing to the mechanism of action responsible for the antiproliferative activity.

The chlorido complex **13** and the less reactive Py-NMe_2 complex **19** were investigated for their catalytic activity towards the oxidation of NADH to NAD^+. Intriguingly, both **13** and **19** exhibited similar catalytic activity, with a TON after 24 h of 16 and TOF of 1.4 h^{-1} at an NADH concentration of 127 μM (Figure 4.10). This implies that under the conditions used, the monodentate ligand has little effect on the catalytic activity of the complex, despite these complexes exhibiting different reactivities towards aquation, 9-EtG binding and GSH stability. The use of pyridyl monodentate ligands in place of chloride may protect the complex from possible deactivation by other reactions that can occur inside the cell (e.g. with GSH,

proteins), whilst potentially allowing the complex to modulate the ratio of $NADH/NAD^+$.[17,18]

4.4.4 Antiproliferative Activity, ROS and Cell Death

The antiproliferative activity of complexes **18-20** was evaluated and compared to parent complex **13** in the A2780 human ovarian cancer cell line at both 0 h and 72 h recovery times, Table 4.7.

For pyridyl complexes **18** and **20**, the potency of the complexes remains unchanged for both 0 h and 72 h recovery times. Both complexes induce high levels of ROS in A2780 cells within 24 h of exposure (Figure 4.11) but show no induction of apoptosis within this time frame. Therefore, the induction of ROS could activate another mode of cell death, such as necrosis[47,48] or autophagy.[49,50] However, it is also possible that the compounds have arrested cell division during the 24 h incubation (compared to control cells) without causing cell death, hence no detection of dying/dead cells. Intriguingly, after 24 h cell recovery time, both **18** and **20** induce apoptotic cell death (Figure 4.12). This could imply that the ROS induced within the first 24 h is activating a delayed apoptosis, or, the complexes are exhibiting another mechanism of antiproliferative action with a delayed response that can activate apoptotic cell death. Similar wave-like behaviour has been observed by the platinum complex *trans*-$[PtCl_2(NH_3)$thiazole] where non-apoptotic cell death was followed by a prolonged period of growth arrest, then induction of apoptosis in the remaining viable cells.[51]

Complex **19** which has been shown to be the most chemically stable complex studied in this work exhibits an IC_{50} value of 650 nM against A2780 cells after 24 h incubation time. This remarkably high activity is accompanied by induction of ROS

and no apoptosis, as in the case of complexes **18** and **20**. The activation of apoptosis was only observed after 24 h of cell recovery during which cells were not exposed to the complex. In contrast to the other pyridyl complexes, the IC_{50} value after 72 h recovery time increases from 0.65 to 1.4 μM. This may imply that the cellular damage or cell arrest incurred within the first 24 h is "reversible" and hence the cells are able to recover and proliferate.

The parent chlorido complex **13** exhibits an IC_{50} value of 4.4 μM with 0 h recovery time and 1.18 μM after 72 h recovery time. Complex **13** also induces high levels of ROS after 24 h incubation period, but does not show any induction of apoptosis at either 0 h or 24 h cell recovery time, in contrast to the pyridyl complexes **18-20**. This may imply that apoptosis is not activated in the mechanism of **13**, or that the apoptosis is even further delayed. As the potency of complex **13** increases with time, this suggests that it is slower at exhibiting its antiproliferative activity than pyridyl complexes **18-20**. This implies that the greater stability of the pyridyl complexes initially results in more potent systems and may show faster cytotoxic activity, which may be a result of protection from deactivating reactions that may occur.

These results indicate that replacement of the chlorido ligand with pyridyl derivatives can result in the enhancement of potency, where the potency at 0 h recovery time after 24 h incubation with the Ir complexes is related to the stability of the monodentate ligand (**19** > **18** > **20** > **13**) and appears to be independent of the activation of apoptosis, potentially demonstrating cytostatic activity rather than cytotoxic activity. Therefore, the monodentate ligand can play a dramatic role in the biological behaviour of these half-sandwich iridium(III) complexes.

4.4.5 Selectivity of Complexes Towards A2780 Cancer Cells

The selectivity towards A2780 cells over healthy cells for the pyridyl complexes followed the order **19** > **18** > **20** (SF = 2.1, 1.1 and 0.9, respectively). There is a trend in selectivity with greater stability of the pyridyl monodentate ligand resulting in a more selective complex. However, parent chloride complex **13** showed the best selectivity (SF = 3.9), despite containing the more labile chlorido ligand. Therefore, no enhancement in selectivity occurs by replacement of the chlorido ligand with the more stable pyridyl ligands, in contrast to iridium complex [(η^5-Cp^{xBiPh})Ir(2-PhPy)pyridine]PF_6 *vis-a-vis* its chloride analogue (SF of 13 vs 4).[17] This may indicate that the presence of the Cp^{xBiPh} capping ligand may play a role in governing the selectivity of the complex in parallel with the choice of monodentate ligand.

4.5 Conclusions

The importance of incorporating different monodentate ligands in chelated half-sandwich complexes is evident, with not only modulation of reactivity[18,31] but also cell transport mechanisms being affected.[16]

In this Chapter, the monodentate ligands pyridine, 4-(dimethylamino)pyridine and 4-(trifluoromethyl)pyridine were used to replace the chlorido ligand in the potent complex [(η^5-Cp*)Ir(2-(2'-methylphenyl)pyridine)Cl] **13** to investigate the effects on aqueous stability, reactivity towards potential biological targets and biological behaviour, with the aim of increasing potency and selectivity.

The pyridyl containing complexes **18-20** all exhibit enhanced stability in aqueous solution (76-85%) compared to parent chlorido complex **13** (28%) with respect to the release of the monodentate ligand. The rate at which the pyridyl ligands dissociate from the complexes are also dramatically slowed compared to the quickly reached

(within 15 min) equilibrium between Ir-Cl and Ir-OD_2/OD for **13**. Upon release of the pyridyl ligand, the formation of the aqua complex **13A** does not appear to be the new species (as determined by ^{1}H NMR spectroscopy), although the identity of the new species was not determined. The pyridyl complexes also resist conversion to the parent complex in concentrations of chloride mimicking biologically relevant conditions.

Complexes **18-20** show less binding to the guanine derivative 9-EtG (22-38%) than the chlorido complex (100%), and an electron-donating -NMe_2 substituent on the pyridine ligand enhances the stability towards reaction with GSH. The general trend in stability follows the order of **19** (Py-NMe_2) > **18** (Py)> **20** (Py-CF_3)> **13** (Cl^-), which correlates with the type of monodentate ligand present on the complex. The electron-donating -NMe_2 group in **19** stabilises the bonding of the monodentate ligand, whereas the electron-withdrawing –CF_3 group in **20** decreases the stability of the bond. This shows that modulation of chemical reactivity at the monodentate site can be achieved by careful selection of the ligands used.

Although the products of the reaction with GSH are independent of the monondentate ligand, these complexes show the interesting property of promoting the oxidation of the sulfur atom in the presence of O_2. The formation of glutathione sulfenate and glutathione sulfinate adducts, which have been shown to be more labile than metal-SG adducts in Ru(II) arene systems,[28] may allow the complex to perform its antiproliferative mechanism without being deactivated.

Replacement of the chlorido ligand with pyridine derivatives can result in the enhancement of antiproliferative activity.[17,18] In this work, the potency after 0 h recovery time is directly related to the stability of the Ir bond to the monodentate ligand (**19** > **18** > **20** > **13**) and appears to be independent on the activation of

apoptosis, potentially demonstrating cytostatic activity. The activity after 72 h recovery time shows no correlation with stability. The generation of ROS is likely to be a contributing factor to the antiproliferative activity of all of the complexes during the initial 24 h incubation. The cell recovery time does not affect the potency of complexes **18** and **20**, but prolonged recovery decreases the activity of **19** and enhances the activity of **13**. Induction of apoptosis is only observed after 24 h for **18-20**, suggesting that they cause cell death at a faster rate than the parent complex **13**. Therefore, these monodentate ligands can play a dramatic role in the biological behaviour of half-sandwich iridium(III) complexes.

Intriguing differences in the biological behaviour observed for these structurally similar Cp* iridium(III) complexes arise from the use of different monodentate ligands. The antiproliferative activity can be partially rationalised by the greater stability of the pyridyl complexes, but further study is warranted to understand fully the biological behaviour of these complexes.

4.6 References

(1) Tönnemann, J.; Risse, J.; Grote, Z.; Scopelliti, R.; Severin, K. *Eur. J. Inorg. Chem.* **2013**, *2013*, 4558.

(2) Babak, M. V.; Meier , S. M.; Legin, A. A.; Adib Razavi, M. S.; Roller, A.; Jakupec , M. A.; Keppler , B. K.; Hartinger , C. G. *Chem. Eur. J* **2013**, *19*, 4308.

(3) Mitra, R.; Das, S.; Shinde, S.; Sinha, S.; Somasundaram, K.; Samuelson, A. G. *Chem. Eur. J* **2012**, *18*, 12278.

(4) Ludwig, G.; Ranđelović, I.; Maksimović-Ivanić, D.; Mijatović, S.; Bulatović, M. Z.; Miljković, D.; Korb, M.; Lang, H.; Steinborn, D.; Kaluđerović, G. N. *ChemMedChem* **2014**, *9*, 1586.

(5) Ludwig, G.; Mijatović, S.; Ranđelović, I.; Bulatović, M.; Miljković, D.; Maksimović-Ivanić, D.; Korb, M.; Lang, H.; Steinborn, D.; Kaluđerović, G. N. *Eur. J. Med. Chem.* **2013**, *69*, 216.

(6) Kilpin, K. J.; Crot, S.; Riedel, T.; Kitchen, J. A.; Dyson, P. J. *Dalton Trans.* **2014**, *43*, 1443.

(7) Govender, P.; Sudding, L. C.; Clavel, C. M.; Dyson, P. J.; Therrien, B.; Smith, G. S. *Dalton Trans.* **2013**, *42*, 1267.

(8) Renfrew, A. K.; Juillerat-Jeanneret, L.; Dyson, P. J. *J. Organomet. Chem.* **2011**, *696*, 772.

(9) Vock, C. A.; Scolaro, C.; Phillips, A. D.; Scopelliti, R.; Sava, G.; Dyson, P. J. *J. Med. Chem.* **2006**, *49*, 5552.

(10) Scolaro, C.; Bergamo, A.; Brescacin, L.; Delfino, R.; Cocchietto, M.; Laurenczy, G.; Geldbach, T. J.; Sava, G.; Dyson, P. J. *J. Med. Chem.* **2005**, *48*, 4161.

(11) Kurzwernhart, A.; Kandioller, W.; Enyedy, E. A.; Novak, M.; Jakupec, M. A.; Keppler, B. K.; Hartinger, C. G. *Dalton Trans.* **2013**, *42*, 6193.

(12) Wang, F.; Habtemariam, A.; van der Geer, E. P. L.; Fernández, R.; Melchart, M.; Deeth, R. J.; Aird, R.; Guichard, S.; Fabbiani, F. P. A.; Lozano-Casal, P.; Oswald, I. D. H.; Jodrell, D. I.; Parsons, S.; Sadler, P. J. *Proc. Nat. Acad. Sci. USA* **2005**, *102*, 18269.

(13) Lippert, B. *Cisplatin: chemistry and biochemistry of a leading anticancer drug*; Helvetica Chimica Acta: Würzburg, 1999.

(14) Fu, Y.; Romero, M. J.; Habtemariam, A.; Snowden, M. E.; Song, L.; Clarkson, G. J.; Qamar, B.; Pizarro, A. M.; Unwin, P. R.; Sadler, P. J. *Chem. Sci.* **2012**, *3*, 2485.

(15) Fu, Y.; Habtemariam, A.; Basri, A. M. B. H.; Braddick, D.; Clarkson, G. J.; Sadler, P. J. *Dalton Trans.* **2011**, *40*, 10553.

(16) Romero-Canelon, I.; Pizarro, A. M.; Habtemariam, A.; Sadler, P. J. *Metallomics* **2012**, *4*, 1271.

(17) Liu, Z.; Romero-Canelón, I.; Qamar, B.; Hearn, J. M.; Habtemariam, A.; Barry, N. P. E.; Pizarro, A. M.; Clarkson, G. J.; Sadler, P. J. *Angew. Chem. Int. Ed.* **2014**, *53*, 3941.

(18) Liu, Z.; Romero-Canelón, I.; Habtemariam, A.; Clarkson, G. J.; Sadler, P. J. *Organometallics* **2014**, *33*, 5324.

(19) Liu, Z.; Habtemariam, A.; Pizarro, A. M.; Clarkson, G. J.; Sadler, P. J. *Organometallics* **2011**, *30*, 4702.

(20) Peacock, A. F. A.; Habtemariam, A.; Fernández, R.; Walland, V.; Fabbiani, F. P. A.; Parsons, S.; Aird, R. E.; Jodrell, D. I.; Sadler, P. J. *J. Am. Chem. Soc.* **2006**, *128*, 1739.

(21) Berners-Price, S. J.; Kuchel, P. W. *J. Inorg. Biochem.* **1990**, *38*, 327.

(22) Betanzos-Lara, S.; Liu, Z.; Habtemariam, A.; Pizarro, A. M.; Qamar, B.; Sadler, P. J. *Angew. Chem. Int. Ed.* **2012**, *51*, 3897.

(23) Jungwirth, U.; Kowol, C. R.; Keppler, B. K.; Hartinger, C. G.; Berger, W.; Heffeter, P. *Antioxid. Redox Signaling* **2011**, *15*, 1085.

(24) Kandioller, W.; Balsano, E.; Meier, S. M.; Jungwirth, U.; Goschl, S.; Roller, A.; Jakupec, M. A.; Berger, W.; Keppler, B. K.; Hartinger, C. G. *Chem. Commun.* **2013**, *49*, 3348.

(25) Liu, Y.; Zhang, X.; Zhang, R.; Chen, T.; Wong, Y.-S.; Liu, J.; Zheng, W.-J. *Eur. J. Inorg. Chem.* **2011**, *2011*, 1974.

(26) Peacock, A. F. A.; Habtemariam, A.; Moggach, S. A.; Prescimone, A.; Parsons, S.; Sadler, P. J. *Inorg. Chem.* **2007**, *46*, 4049.

(27) Pizarro, A.; Habtemariam, A.; Sadler, P. In *Medicinal Organometallic Chemistry*; Jaouen, G., Metzler-Nolte, N., Eds.; Springer Berlin Heidelberg: 2010; Vol. 32, p 21.

(28) Wang, F.; Xu, J.; Habtemariam, A.; Bella, J.; Sadler, P. J. *J. Am. Chem. Soc.* **2005**, *127*, 17734.

(29) Liu, Z.; Habtemariam, A.; Pizarro, A. M.; Fletcher, S. A.; Kisova, A.; Vrana, O.; Salassa, L.; Bruijnincx, P. C. A.; Clarkson, G. J.; Brabec, V.; Sadler, P. J. *J. Med. Chem.* **2011**, *54*, 3011.

(30) Helm, L.; Merbach, A. E. *Coord. Chem. Rev.* **1999**, *187*, 151.

(31) Betanzos-Lara, S.; Salassa, L.; Habtemariam, A.; Novakova, O.; Pizarro, A. M.; Clarkson, G. J.; Liskova, B.; Brabec, V.; Sadler, P. J. *Organometallics* **2012**, *31*, 3466.

(32) Hassner, A. In *Encyclopedia of Reagents for Organic Synthesis*; John Wiley & Sons, Ltd: 2001.

(33) Hwang, C.; Sinskey, A.; Lodish, H. *Science* **1992**, *257*, 1496.

(34) Heffeter, P.; Jungwirth, U.; Jakupec, M.; Hartinger, C.; Galanski, M.; Elbling, L.; Micksche, M.; Keppler, B.; Berger, W. *Drug. Resist. Update.* **2008**, *11*, 1.

(35) Reedijk, J. *Proc. Nat. Acad. Sci. USA* **2003**, *100*, 3611.

(36) Goto, S.; Iida, T.; Cho, S.; Oka, M.; Kohno, S.; Kondo, T. *Free Radical Res.* **1999**, *31*, 549.

(37) Wexselblatt, E.; Gibson, D. *J. Inorg. Biochem.* **2012**, *117*, 220.

(38) Schluga, P.; Hartinger, C. G.; Egger, A.; Reisner, E.; Galanski, M.; Jakupec, M. A.; Keppler, B. K. *Dalton Trans.* **2006**, 1796.

(39) Dougan, S. J.; Habtemariam, A.; McHale, S. E.; Parsons, S.; Sadler, P. J. *Proc. Nat. Acad. Sci. U.S.A.* **2008**, *105*, 11628.

(40) Liu, Z.; Sadler, P. J. *Inorg. Chem. Front.* **2014**, *1*, 668.

(41) Liu, Z.; Deeth, R. J.; Butler, J. S.; Habtemariam, A.; Newton, M. E.; Sadler, P. J. *Angew. Chem. Int. Ed.* **2013**, *52*, 4194.

(42) Maenaka, Y.; Suenobu, T.; Fukuzumi, S. *J. Am. Chem. Soc.* **2011**, *134*, 367.

(43) Soldevila-Barreda, J. J.; Bruijnincx, P. C. A.; Habtemariam, A.; Clarkson, G. J.; Deeth, R. J.; Sadler, P. J. *Organometallics* **2012**, *31*, 5958.

(44) Yan, Y.; Melchart, M.; Habtemariam, A.; Peacock, A. A.; Sadler, P. *J. Biol. Inorg. Chem.* **2006**, *11*, 483.

(45) Fish, R. H. *Aust. J. Chem.* **2010**, *63*, 1505.

(46) Liu, Z.; Sadler, P. J. *Acc. Chem. Res.* **2014**, *47*, 1174.

(47) Halliwell, B. In *eLS*; John Wiley & Sons, Ltd: 2001.

(48) Morgan, M. J.; Kim, Y.-S.; Liu, Z.-g. *Cell Res.* **2008**, *18*, 343.

(49) Chen, Y.; Azad, M. B.; Gibson, S. B. *Cell Death Differ.* **2009**, *16*, 1040.

(50) Chen, Y.; McMillan-Ward, E.; Kong, J.; Israels, S. J.; Gibson, S. B. *J. Cell Sci.* **2007**, *120*, 4155.

(51) Farrell, N.; Povirk, L. F.; Dange, Y.; DeMasters, G.; Gupta, M. S.; Kohlhagen, G.; Khan, Q. A.; Pommier, Y.; Gewirtz, D. A. *Biochem. Pharmacol.* **2004**, *68*, 857.

Chapter 5

Conjugation of the Anticancer Complex [(η^5-Cp*)Ir(2-phenyl-5-pyridinecarboxaldehyde)Cl] to Amines

5.1 Introduction

The conjugation of organic molecules to metal complexes for biological use can bestow new properties on the resulting complex, such as enhanced aqueous solubility, selectivity towards cancer cells (receptor mediated delivery),[1] and delivery of the complex to a particular organelle.[2] This has been widely demonstrated with Pt(II) and Pt(IV) anticancer complexes.[3,4] It has also been demonstrated that peptides can be conjugated to metal complexes which can enhance specific uptake[5-7] and for example, localise preferentially into the cell nucleus by attachment of nuclear localisation sequence (NLS) peptides.[8]

Half-sandwich iridium(III) complexes have shown great promise as anticancer agents.[9,10] More specifically, complexes of the type [(η^5-Cp^x)Ir(2-PhPy)Cl] (Cp^x = Cp*, Cp^{xPh}, Cp^{xBiPh}) have shown potent activity against A2780 human ovarian cancer cells.[11-13] The functionalisation of these complexes could allow further exploration of their biological behaviour (i.e. fluorescent studies) and could further enhance their suitability as potential drug candidates *via* enhancing their selectivity through targeted delivery. Ruiz *et al.* demonstrated the functionalisiation of half-sandwich complexes through addition of the levonorgestrel group to 2-PhPy by Sonogashira coupling, followed by metallation of the functionalised 2-PhPy chelating ligand to form the corresponding *C,N*-chelated Ru(II), Rh(III) and Ir(III) piano-stool complexes.[14,15] This "pre-modification" route has the advantage of not interfering with the chemistry that the metal centre can exhibit, particularly at the more labile monodentate site. However, the disadvantage is that each complex has to be made from different functionalised chelating ligands.

The alternative "post-modification" route requires a functional group on the metal complex that would react specifically with the moiety being conjugated, minimising any side-reactions that could occur. Previous examples of this have been shown by Metzle-Nolte *et al.* using Sonogashira coupling[16] and "click chemistry"[17] in ferrocene and octahedral complexes. An approach which has gained some interest is the exploitation of the reactivity of aldehydes with primary amino groups to form Schiff base complexes, which has been demonstrated in square-planar Pt(II)[18] and octahedral Ir(III)[19] complexes. In both cases, reduction of the imine bond to the secondary amine was achieved using a hydride source, forming hydrolytically stable compounds.

This chapter aims to explore the post-modification of chelated half-sandwich Ir(III) complexes by exploiting the reactivity of an aldehyde moiety on the chelating ligand as a proof-of-concept. The reaction of a range of primary aliphatic and aromatic amines (including a fluorescent dansyl derivative) with complex [(η^5-Cp*)Ir(2-phenyl-5-pyridinecarboxaldehyde)Cl] **6** has been performed using microwave-assisted chemistry. The high reactivity of amines with aldehydes should result in reduced binding of the amines toward the metal centre. The new conjugates were characterised by ^{1}H NMR spectroscopy, ESI-MS/HRMS and combustion analysis. The reaction of an amine with an aldehyde results in imine bonds which are known to be hydrolytically unstable, especially at low pH. The synthesis of a water stable fluorescent secondary amine conjugate has been investigated using different reduction techniques, which has led to the study of the fluorescence of the complex in A2780 human ovarian cancer cells. Finally, an investigation into the reaction of the aldehyde moiety with lysine residues in the peptides Substance P and [Lys-3]-bombesin to form Ir-peptide conjugates is described. The new conjugates have been

characterised by ultra-high resolution Fourier Transform – Ion Cyclotron Resonance (FT-ICR) MS/MS techniques. The outline of the work performed in this Chapter is shown in Scheme 5.1.

Scheme 5.1. Outline of the work carried out in this chapter, involving the synthesis of new Schiff base conjugates arising from complex [(η^5-Cp*)Ir(2-phenyl-5-pyridinecarboxaldehyde)Cl] **6** with primary amines. Investigations include aqueous stability, reduction to the secondary amine derivative and evaluating potential applications of a fluorescent conjugate. Evaluation of the reaction of complex **6** with lysine-containing peptides by FT-ICR-MS is also performed.

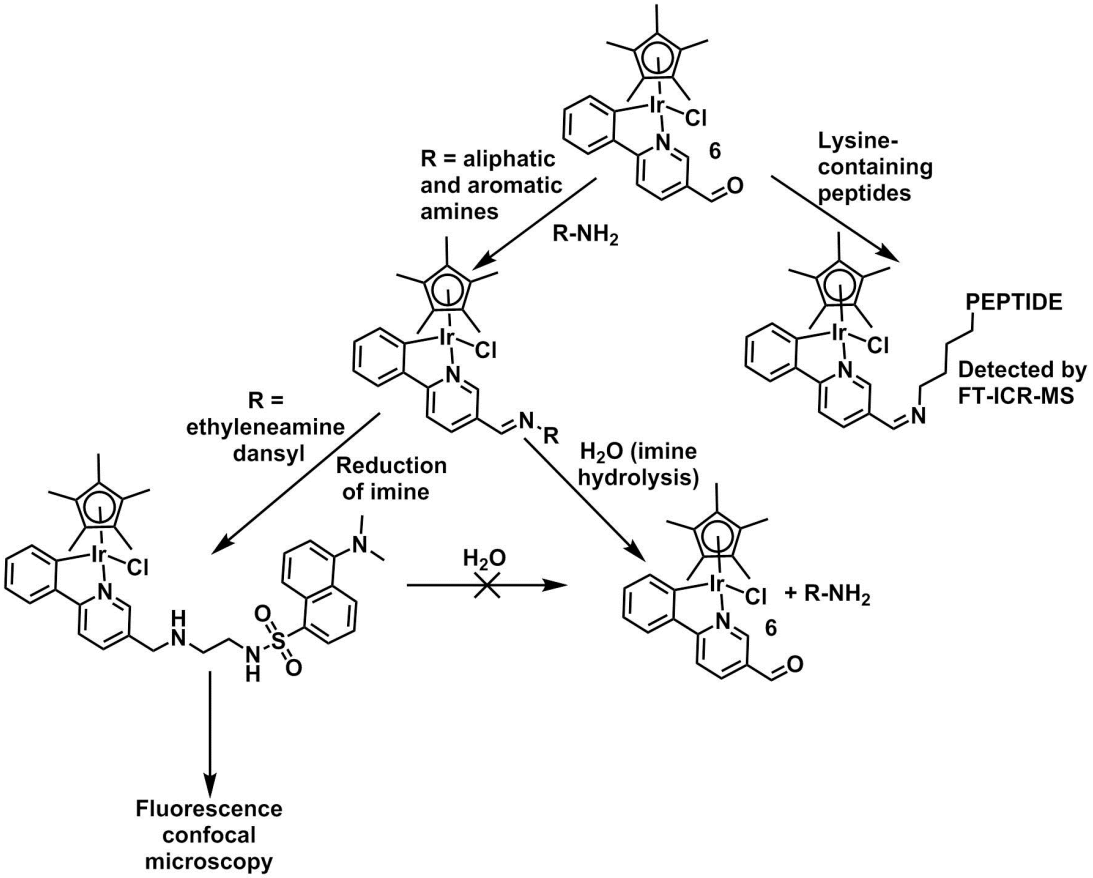

5.2 Experimental Section

5.2.1 Materials

2-Aminophenol (99%), 4-aminophenol (≥98%), 4-(4-aminophenyl)-butyric acid (95%), 2-aminoethanol (99%), 2-aminoethanesulfonic acid (≥99%), tyramine (99%), ethylenediamine, dansyl chloride (≥99%), triethylsilane (99%), $Pd(OAc)_2$ (≥99%) Substance P and [Lys-3]-bombesin were purchased from Sigma-Aldrich (UK). 2-Methoxyethylamine was purchased from VWR International (UK). Solvents used for synthesis were of laboratory grade and used without further purification. Solvents for HPLC purity test and peptide incubations (water and acetonitrile) were of HPLC grade with added trifluoroacetic acid or ammonium acetate which was purchased from Sigma-Aldrich (UK). The synthesis of *N*-(2-aminoethyl)-5-(dimethylamino)naphthalene-1-sulfonamide was performed according to a literature procedure.[20] Complex [(η^5-Cp*)Ir(2-phenyl-5-pyridinecarboxaldehyde)Cl] **6** was synthesised as described in Chapter 3.

5.2.2 Synthesis

[(η^5-Cp*)Ir(4-(((6-phenylpyridin-3-yl)methylene)amino)phenol)Cl] (21)

Complex **6** (25 mg, 0.0458 mmol) was dissolved in acetone (5 mL) in a microwave vial, followed by addition of 4-aminophenol (6 mg, 0.055 mmol). The solution was stirred for 5 min to ensure complete dissolution before being placed in the microwave instrument (393 K, 150 W, 250 psi, 5 min). The reaction mixture was then transferred to a round bottom flask and evaporated to dryness on a rotary evaporator. MeOH (1 mL) was added and the solution was sonicated for 30 s resulting in the formation of an orange precipitate. This was collected by filtration under reduced pressure and washed with hexane yielding the product as an orange

solid (15 mg, 51%). **^{1}H NMR** (400 MHz, acetone-d_6) δ = 9.28 (d, 1H, J = 1.2 Hz), 8.78 (s, 1H), 8.66 (bs, 1H), 8.32 (dd, 1H, J = 8.5, 1.5 Hz), 8.12 (d, 1H, J = 8.3 Hz), 7.85-7.81 (m, 2H), 7.33 (d, 2H, J = 8.6 Hz), 7.15 (t, 1H, J = 7.8 Hz), 7.01 (t, 1H, J = 7.6 Hz), 6.92 (d, 2H, J = 8.6 Hz), 1.71 (s, 15H). **ESI-MS** (MeOH) m/z = 601.2 $[M-Cl]^+$. **CHN analysis** calc. for $C_{28}H_{28}N_2ClIrO.CH_3OH$ C – 52.12%, H – 4.83%, N – 4.19%. Found C – 51.98%, H – 4.39%, N – 4.33%.

[(η^5-Cp*)Ir(4-(4-(((6-phenylpyridin-3-yl)methylene)amino)phenyl)butanoic acid)Cl] (22) As for **21** using complex **6** (30 mg, 0.055 mmol), $CHCl_3$ (10 mL), 4-(4-aminophenyl)butyric acid (12 mg, 0.066 mmol) (dissolution aided by brief sonication). The product was collected by filtration under reduced pressure and washed with hexane yielding the product as an orange solid (15 mg, 39%). **^{1}H NMR** (400 MHz, dmso-d_6) δ = 12.18 (bs, 1H), 9.18 (s, 1H), 8.85 (s, 1H), 8.33 (d, 1H J = 8.6 Hz), 8.22 (d, 1H, J = 8.6 Hz), 7.89 (d, 1H, J = 7.7 Hz), 7.75 (d, 1H, J = 7.7 Hz), 7.33 (d, 2H, J = 8.2 Hz), 7.28 (d, 2H, J = 8.2 Hz), 7.16 (t, 1H, J = 7.6 Hz), 7.03 (t, 1H, J = 7.5 Hz), 2.63 (t, 2H, J = 7.4 Hz), 2.24 (t, 2H, J = 7.3 Hz), 1.82 (quin, 2H, J = 7.6 Hz), 1.64 (s, 15H). **ESI-MS** (MeOH) m/z = 671.2 $[M-Cl]^+$. **CHN analysis** calc. for $C_{32}H_{34}N_2ClIrO_2$ C – 54.42%, H – 4.85%, N – 3.97%. Found C – 54.10%, H – 4.91%, N – 3.92%.

[(η^5-Cp*)Ir(2-(((6-phenylpyridin-3-yl)methylene)amino)ethan-1-ol)Cl] (23) As for **21** using complex **6** (50 mg, 0.0917 mmol), $CHCl_3$ (8 mL), ethanolamine (6.72 mg, 6.64 μL, 0.11 mmol). The product was collected by filtration under reduced pressure and washed with hexane yielding the product as an orange solid (30 mg, 56%). **^{1}H NMR** (400 MHz, dmso-d_6) δ = 9.02 (s, 1H), 8.49 (s, 1H), 8.15 (bs, 2H), 7.85 (d, 1H, J = 7.5 Hz), 7.72 (d, 1H, J = 7.6 Hz), 7.14 (t, 1H, J = 7.5 Hz), 7.01 (t, 1H, J = 7.5 Hz), 4.70 (t, 1H, J = 5.0 Hz), 3.70 (bs, 4H), 1.61 (s, 15H). **ESI-MS**

(MeOH) m/z = 553.2 $[M\text{-}Cl]^+$. **CHN analysis** calc. for $C_{24}H_{28}N_2ClIrO.0.1CHCl_3$ C – 48.24%, H – 4.72%, N – 4.67%. Found C – 48.06%, H – 4.68%, N – 4.64%.

[(η^5-Cp*)Ir(*N*-(2-methoxyethyl)-1-(6-phenylpyridin-3-yl)methanimine)Cl] (24) As for **21** using complex **6** (50 mg, 0.0917 mmol), $CHCl_3$ (8 mL), 2-methoxyethylamine (8.26 mg, 9.56 μL, 0.11 mmol). The product was collected by filtration under reduced pressure and washed with hexane yielding the product as an orange solid (26 mg, 47%).**^{1}H NMR** (400 MHz, dmso-d_6) δ = 9.01 (s, 1H), 8.51 (s, 1H), 8.16 (bs, 2H), 7.85 (d, 1H, J = 7.5 Hz), 7.73 (d, 1H, J = 7.4 Hz), 7.15 (t, 1H, J = 7.2 Hz), 7.01 (t, 1H, J = 7.3 Hz), 3.79 (bs, 2H), 3.64 (bs, 1H), 3.28 (s, 3H), 1.61 (s, 15H). **ESI-MS** (MeOH) m/z = 567.2 $[M\text{-}Cl]^+$. **CHN analysis** calc. for $C_{25}H_{30}N_2ClIrO$ C – 49.86%, H – 5.02%, N – 4.65%. Found C – 49.55%, H – 4.92%, N – 4.49%.

[(η^5-Cp*)Ir(4-(2-(((6-phenylpyridin-3-yl)methylene)amino)ethyl)phenol)Cl] (25) As for **21** using complex **6** (50 mg, 0.0917 mmol), $CHCl_3$ (8 mL), tyramine (15 mg, 0.11 mmol). The product was collected by filtration under reduced pressure and washed with hexane yielding the product as an orange solid (30 mg, 49%). **^{1}H NMR** (400 MHz, acetone-d_6) δ = 9.09 (s, 1H), 8.33 (s, 1H), 8.13 (d, 1H, J = 8.5 Hz), 8.05 (d, 1H, J = 8.3 Hz), 7.81 (d, 1H, J = 7.3 Hz), 7.79 (d, 1H, J = 7.2 Hz), 7.13 (t, 1H, J = 7.6 Hz), 7.09 (d, 1H, J = 8.3 Hz), 6.99 (t, 1H, J = 7.5 Hz), 6.75 (d, 2H, J = 8.4Hz), 3.92-3.82 (m, 2H), 2.94-2.90 (m, 2H), 1.68 (s, 15H). **ESI-MS** (MeOH) m/z = 629.2 $[M\text{-}Cl]^+$. **CHN analysis** calc. for $C_{30}H_{32}N_2ClIrO.0.25$hexane C – 55.17%, H – 5.22%, N – 4.08%. Found C – 55.31%, H – 5.22%, N – 4.20%.

[(η^5-Cp*)Ir(5-(dimethylamino)-N-(2-(((6-phenylpyridin-3-yl)methylene)amino)ethyl)naphthalene-1-sulfonamide)Cl] (26) As for **21** using complex **6** (60 mg, 0.110 mmol), $CHCl_3$ (10 mL), *N*-(2-aminoethyl)-5-

(dimethylamino)naphthalene-1-sulfonamide (39 mg, 0.132 mmol). The product was collected by filtration under reduced pressure and washed with hexane yielding the product as an orange solid (65 mg, 72%).**^{1}H NMR** (400 MHz, acetone-d_6) δ = 8.99 (d, 1H, J = 1.2 Hz), 8.56 (d, 1H, J = 8.4 Hz), 8.35 (d, 1H, J = 8.6 Hz), 8.26 (dd, 1H, J = 7.3, 0.9 Hz), 8.12 (s, 1H), 8.01 (d, 1H, J = 8.5 Hz), 7.90 (dd, 1H, J = 8.4, 1.7 Hz), 7.82-7.79 (m, 2H), 7.64 (t, 1H, J = 8.0 Hz), 7.52 (t, 1H, J = 8.2 Hz), 7.23 (d, 1H, J = 7.4 Hz), 7.14 (td, 1H, J = 7.5, 0.9 Hz), 7.00 (t, 1H, J = 7.3 Hz), 6.84 (t, 1H, J = 6.2 Hz), 3.59 (m, 2H), 3.34 (q, 2H, J = 6.1 Hz), 2.87 (s, 6H), 1.68 (s, 15H). **ESI-MS** (MeOH) m/z = 785.2 $[M\text{-}Cl]^+$. **HR-MS** (MeOH) calc. for $C_{36}H_{40}N_4IrO_2S^+$ m/z – 785.2496. Found m/z – 785.2512. **CHN analysis** calc. for $C_{36}H_{40}N_4ClIrO_2S$ C – 52.70%, H – 4.91%, N – 6.83%. Found C –52.36%, H – 5.23%, N – 6.47%.

5-(dimethylamino)-N-(2-(((6-phenylpyridin-3-yl)methylene)amino)ethyl)naphthalene-1-sulfonamide (**L26**) 2-Phenyl-5-pyridinecarboxaldehyde (130 mg, 0.71 mmol) was dissolved in $CHCl_3$ (14 mL) in a microwave vial. *N*-(2-aminoethyl)-5-(dimethylamino)naphthalene-1-sulfonamide (208 mg, 0.71 mmol) was added and stirred for 5 min, then placed in the microwave instrument (393 K, 150 W, 250 psi, 5 min). The reaction mixture was concentrated to dryness to yield the product which was used without further purification (310 mg, 95%). **^{1}H NMR** (400 MHz, acetone-d_6) δ = 8.68 (s, 1H), 8.54 (d, 1H, J = 8.5 Hz), 8.35 (d, 1H, J = 8.9 Hz), 8.27 (d, 1H, J = 7.2 Hz), 8.17 (d, 2H, J = 7.6 Hz), 7.93 (bs, 3H), 7.62 (t, 1H, J = 7.8 Hz), 7.53-7.45 (m, 4H), 7.18 (d, 1H, J = 7.4 Hz), 6.87 (t, 1H, J = 4.8 Hz), 3.54 (t, 2H, J = 5.8 Hz), 3.35 (q, 2H, J = 5.4 Hz), 2.84 (s, 6H). Purity = 98.8% based on ^{1}H NMR. **ESI-MS** (MeOH) m/z = 459.2 $[M+H]^+$.

[(η^5-Cp*)Ir(5-(dimethylamino)-N-(2-(((6-phenylpyridin-3-yl)methyl)amino)ethyl)naphthalene-1-sulfonamide)Cl] (27) Complex **26** (60 mg, 0.073 mmol) was dissolved in EtOH (25 mL) under an N_2 atmosphere, followed by addition of triethylsilane (13 mg, 17.52 μL, 0.1097 mmol) and stirring for 5 min. $Pd(OAc)_2$ (1.64 mg, 0.0073 mmol) was added and the reaction mixture was stirred at ambient temperature for 30 min. The solution was evaporated to dryness on a rotary evaporator, the crude mixture was dissolved in DCM (10 mL) and purified by automated flash silica chromatography using the conditions as described in the methods section of this chapter (section 5.2.3.2). Product fractions were combined and evaporated to dryness on a rotary evaporator, yielding a yellow solid (20 mg, 33%). **^{1}H NMR** (400 MHz, acetone-d_6) δ = 8.66 (s, 1H), 8.56 (d, 1H, J = 8.7 Hz), 8.40 (d, 1H, J = 8.7 Hz), 8.24 (d, 1H, J = 7.3 Hz), 7.87 (d, 1H, J = 8.4 Hz), 7.75 (d, 1H, J = 7.6 Hz), 7.72 (d, 1H, J = 7.7 Hz), 7.65-7.57 (m, 3H), 7.25 (d, 1H, J = 7.6 Hz), 7.09 (t, 1H, J = 7.2 Hz), 6.96 (t, 1H, J = 7.2 Hz), 6.70 (bs, 1H), 3.63 (s, 2H), 3.04 (t, 2H, J = 5.9 Hz), 2.85 (s, 6H), 2.64 (q, 2H, J = 5.6 Hz), 1.63 (s, 15H). **ESI-MS** (MeOH) m/z = 787.2 $[M\text{-}Cl]^+$. **HR-MS** (MeOH) calc. for $C_{36}H_{42}N_4IrO_2S^+$ m/z – 787.2652. Found m/z – 787.2649. **CHN analysis** calc. for $C_{36}H_{42}N_2ClIrO.0.5CH_2Cl_2$ C – 50.69%, H – 5.01%, N – 6.48%. Found C – 50.43%, H – 4.90%, N – 6.43%.

5.2.3 Methods

5.2.3.1 Automated Flash Silica Chromatography

Purification of complex **27** was carried out using the Biotage Isolera One instrument, fitted with a UV-vis detector (detection λ = 254 nm) and running the Spektra package employing dichloromethane and methanol as elution solvents on a SNAP KP-Sil 25g column. Briefly, the following conditions were used; equilibration of

column (4 column volumes (CVs)) with 100 % of dichloromethane, elution of product with a gradient of 0 % methanol to 10 % methanol over 10 CVs and then holding at 10 % methanol for 4 CVs.

5.2.3.2 HPLC Purity Measurement

HPLC purity measurement of complex **27** (100 μM, 10% MeCN/90% H_2O v/v) was performed as described in Chapter 2 (section 2.2.5.1).

5.2.3.3 Aqueous Stability

The stability of complexes **21-27** (ca. 500 μM) in aqueous solution was determined by ^{1}H NMR spectroscopy at 298 K. Briefly, complexes were dissolved in 10% dmso-d_6/90% D_2O (v/v) by dissolution of complexes in dmso-d_6 (5 mM) followed by rapid dilution with D_2O at either pH 7.5, 6.2 or 4.1. All spectra were internally referenced to 1,4-dioxane (3.75 ppm) and water suppression was performed using Shaka techniques.[21] Percentage of hydrolysis of the imine/secondary amine bond was based on peak integrations.

5.2.3.4 UV-Vis Spectroscopy

The UV-vis spectra of complexes **6**, **26** and **27** and *N*-(2-aminoethyl)-5-(dimethylamino)naphthalene-1-sulfonamide in DCM and 10% MeOH/90% H_2O v/v (50 μM) were acquired as described in Chapter 2 (section 2.2.7).

5.2.3.5 Fluorescence Measurements

Fluorescence emission spectra of complexes **6**, **26** and **27** (50 μM) and *N*-(2-aminoethyl)-5-(dimethylamino)naphthalene-1-sulfonamide (5 μM) in DCM and 10% MeOH/90% H_2O (v/v) for **27** and *N*-(2-aminoethyl)-5-(dimethylamino)naphthalene-1-sulfonamide (50 μM) were recorded on a Jasco FP-6500 fluorimeter using quartz

cuvettes. Spectra were acquired using the excitation wavelengths reported in section 5.3.8, using excitation and emission slits at 3 nm and 5 nm, respectively. The response time was set at 0.5 s, sensitivity to medium, and scanning speed of 500 nm min^{-1}.

5.2.3.6 Antiproliferative Activity

Antiproliferative activity assays for complex **27** against A2780 human ovarian cancer cells were performed by Dr. Isolda Romero-Canelón (Department of Chemistry, University of Warwick) as described in Chapter 2 (section 2.2.14.2). The concentration of the stock solution was determined by ICP-OES measurements.

5.2.3.7 Epifluorescence Microscopy of A2780 Cells

This work was performed by Dr. Carlos Sanchez-Cano (Department of Chemistry, University of Warwick). A2780 ovarian carcinoma cells were seeded on 4-well microscopy chambers (10000 cells/well; 500 μL supplemented RPMI 1640 medium), left to attach for 24 h, and then treated with 2 x IC_{50} of complex **27** for another 24 h. After treatment, medium was removed, cells washed twice with PBS and fixed with 4% paraformaldehyde solution (20 min at RT). Cell nuclei were stained using Propidium Iodide (0.1mg mL^{-1}; 10 min at RT; λ_{ex} = 535 nm/λ_{em} = 617 nm) followed by two washes with PBS. Cells were imaged in an IX71 Olympus microscope using a 100 x objective.

5.2.3.8 ICP-OES Analysis

ICP-OES analyses were carried out as described in Chapter 2. Calibrants were freshly prepared at concentrations of 1000, 800, 600, 400, 200 and 100 ppb which were spiked with NaCl to match the salt content of the samples being analysed.

5.2.3.9 Reactions of Complex 6 with Peptides

Complex **6** (250 μM, MeCN) was incubated with either Substance P or [Lys-3]-bombesin (1 mM, H_2O) at 310 K for 24 h. The reaction solution was then analysed by UHR-MS (section 5.2.3.10).

RP-HPLC was employed on the incubation of **6** with [Lys-3]-bombesin, using the Agilent 1200 system with a VDW and 100 μL loop. The column used was an Agilent ZORBAX Eclipse Plus C18, 150 × 4.6 mm with a 5 μm pore size. Mobile phase used was 2 mM NH_4OAc H_2O/ MeCN. Flow rate was 1 mL min^{-1} and the detection wavelength was set at 254 nm with the reference wavelength at 360 nm. Sample injections were half the loop volume (50 μL). Solvent gradient used was as described for purity determination (section 2.2.5.1).

5.2.3.10 Ultra-High Resolution - Mass Spectrometry (UHR-MS)

Analysis of the reactions between complex **6** and peptides Substance P and [Lys-3]-bombesin were performed using Fourier Transform Ion Cyclotron Resonance Mass Spectrometry (FT-ICR-MS) by Mr. Christopher Wootton (Department of Chemistry, University of Warwick).

Nano-spray (nESI) Mass spectrometry was performed on a Bruker SolariX FT-ICR MS fitted with an Apollo II Ion source and a 12 Tesla actively-shielded magnet (Bruker Daltonics, Bremen, Germany). Aqueous Peptide samples (5 μM) were spiked with 0.3% formic acid to aid in effective ionisation during nESI. Ir containing samples were sprayed in ACN with no added acid. Full MS spectra were externally calibrated using a mass spectrum of Agilent tune-mix (Agilent), calibration constants from the tune-mix spectrum were then applied to spectra of interest.

For CAD MS/MS,[22] the species of interest were isolated in the first quadrupole and accelerated into the hexapole collision cell for Collisionally Activated Dissociation (CAD) 10-30 V and continuously accumulated for 0.1-4 s before transfer to the Infinity Cell© for detection.

For ECD MS/MS,[23] the species of interest were isolated in the first quadrupole, externally accumulated in the collision cell for 0.1-7 s and then transferred to the Infinity Cell© for Electron Capture Dissociation (ECD) fragmentation and detection. Ions in the Infinity Cell© were irradiated with 1.3 eV (peptides) - 2.5 eV (Ir adducts) electrons from a 1.5 A hollow cathode dispenser for 50-1200 mS.

The notation used to describe the peptide fragments from both CAD and ECD MS/MS experiments are descried in Scheme 5.2.[24] For CAD, the notation used for the fragments left along the N-C and C-N directions is b*n* an y*n*, respectively, where *n* = number of amino acids left in the peptide. For ECD, the notation used for the fragments left along the N-C and C-N directions is c*n* an z*n*, respectively, where n = number of amino acids left in the peptide.

MS/MS spectra were internally calibrated using the minimal number of unmodified (peptide spectra) or modified (Ir adduct spectra) B/C ions and the charge reduced species $[M+nH]^{n-1+\cdot}$ where possible (species used for calibration are marked) .

Scheme 5.2. Peptide fragmentation notation used for both CAD and ECD MS/MS experiments.

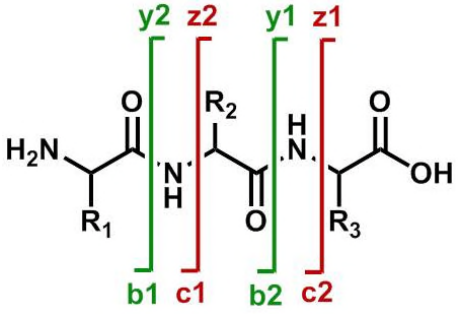

5.3 Results

5.3.1 Reaction of Complex 6 with Ethanolamine

The reactivity of complex [(η^5-Cp*)Ir(2-phenyl-5-pyridinecarboxaldehyde)Cl] **6** bearing an aldehyde on the pyridyl ring towards the formation of the Schiff base conjugate with ethanolamine (ca 1:1 mol equiv.), was examined by ^{1}H NMR spectroscopy in $CDCl_3$ at 298 K over 21 h (Figure 5.1). Within 20 min a new set of peaks had formed, which continued to grow in intensity over the following 21 h. The formation of the peak at 8.35 ppm is indicative of the *H*-C=N proton in an imine which accompanies the decrease of the C*H*O peak (10.04 ppm) of complex **6**. The formation of the Schiff base results in an overall high-field shift of the 2-PhPy protons, with the H6 proton on the pyridyl ring shifting by 0.15 ppm. ESI-MS analysis of the reaction mixture showed an m/z of 553.3 which corresponds to the Schiff base conjugate [(η^5-Cp*)Ir(2-(((6-phenylpyridin-3-yl)methylene)amino)ethan-1-ol)]$^+$. The reaction was also accompanied by a colour change, from red to orange.

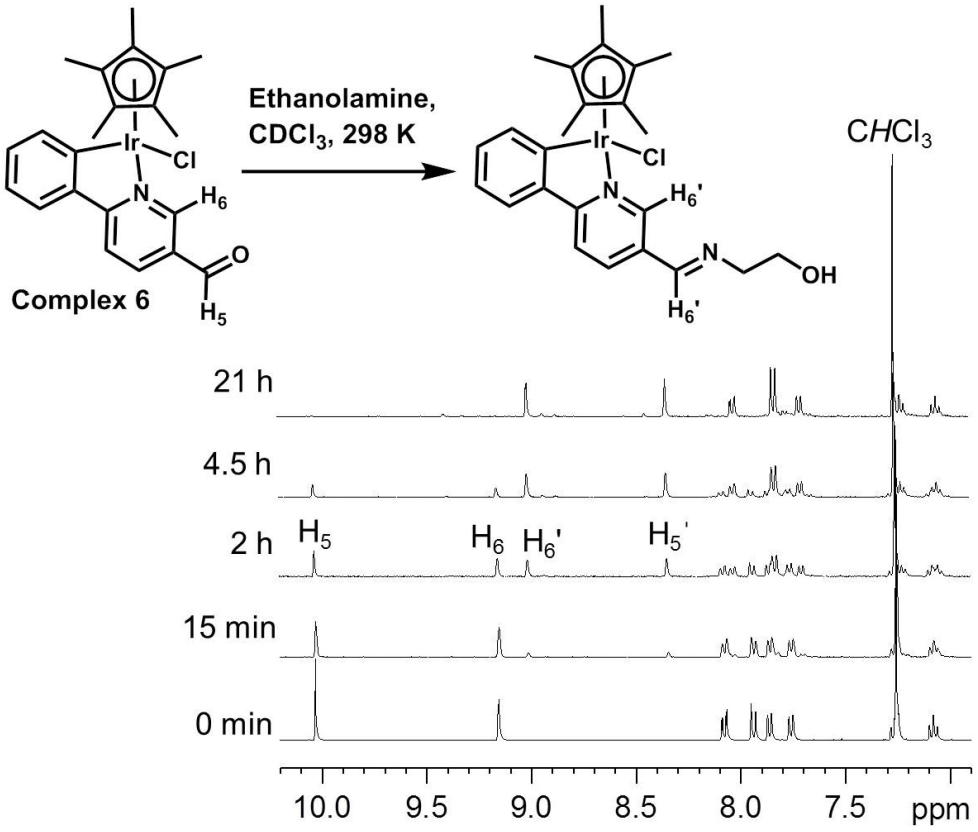

Figure 5.1. Low-field region of the ^{1}H NMR spectum (400 MHz, $CDCl_3$) for the reaction between [(η^5-Cp*)Ir(2-phenyl-5-pyridinecarboxaldehyde)Cl] **6** (1 mol equiv.) and ethanolamine (1 mol equiv.) at 298 K after various times.

5.3.2 Synthesis and Characterisation of Schiff Base Conjugates

The microwave-assisted synthesis of new Schiff base conjugates originating from complex **6** was explored. The organic amines used in the Schiff base reactions along with the reaction conditions and outcomes of each reaction are listed in Table 5.1. The amines were selected to include aliphatic and aromatic amines, as well as to provide a fluorescent tag (dansyl group) to aid in investigation of biologically relevant interactions. These experiments resulted in the isolation and characterisation of six Schiff base conjugates **21**-**26** after 5 min reaction time (Figure 5.2)**.** It was found that purification of the new complexes could be best achieved by evaporating off the solvent to dryness, followed by the addition of ca 1 mL of MeOH with brief

sonication (30 s). This resulted in precipitation of the complexes as orange solids in moderate to good yields ranging from 39-72%.

Only two of the amines attempted did not yield Schiff base conjugates. Reaction of **6** with 2-aminophenol and 2-aminoethanesulfonic acid resulted in no detectable product peaks by either ^{1}H NMR or ESI-MS.

Table 5.1. Amines and reaction conditions used to synthesise Schiff base conjugates of [(η^5-Cp*)Ir(2-phenyl-5-pyridinecarboxaldehyde)Cl] **6** (1 mol equiv.) (microwave power setting of 150 W, 250 psi, 393 K and reaction time of 5 min).

Amine (1.2 mol equiv.)	Solvent	Yield of complex after purification
4-aminophenol	$CHCl_3$	0%
4-aminophenol	acetone	51% (**21**)
2-aminophenol	$CHCl_3$	0%
2-aminophenol	acetone	0%
2-aminophenol	MeOH	0%
4-(4-aminophenyl)butyric acid	$CHCl_3$	39% (**22**)
ethanolamine	MeOH	0%
ethanolamine	$CHCl_3$	56% (**23**)
2-methoxyethylamine	$CHCl_3$	47% (**24**)
tyramine	$CHCl_3$	49% (**25**)
N-(2-aminoethyl)-5-(dimethylamino)naphthalene-1-sulfonamide	$CHCl_3$	72% (**26**)
2-aminoethanesulfonic acid	$CHCl_3$	0%
2-aminoethanesulfonic acid	DMF	0%
2-aminoethanesulfonic acid	MeOH	0%

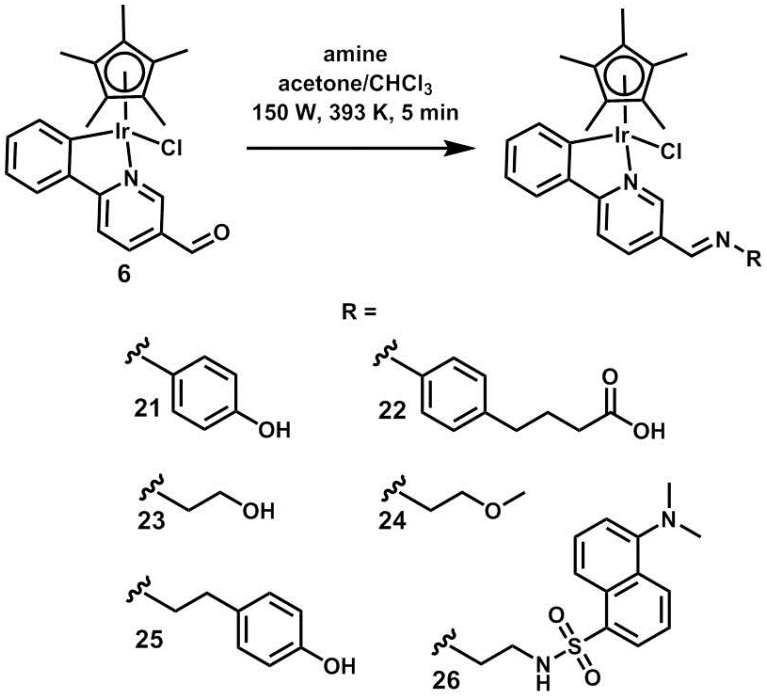

Figure 5.2. Scheme for reaction of complex **6** with the corresponding amines using microwave-assisted synthesis (150 W, 250 psi, 393 K, 5 min) and the structures of the isolated Schiff base conjugates **21-26**.

Proton assignments were made using ^{1}H-^{1}H COSY measurements, that provided a near complete assignment of the spectrum as demonstrated for complex [(η^5-Cp*)Ir(5-(dimethylamino)-N-(2-(((6-phenylpyridin-3-yl)methylene)amino)-ethyl)naphthalene-1-sulfonamide)Cl] **26** in Figure 5.3. Coupling of the aliphatic protons Hj to NHk was observed. The Hi protons in complex **26** exhibit a complicated splitting pattern that can be assigned as two overlapping doublet of triplets of doublets (dtd), where each Hi proton appears magnetically inequivalent, resulting in ^{2}J (13.9 Hz), ^{3}J (5.6 Hz) and ^{4}J (1.2 Hz) coupling to the Hi, Hj and Hh protons, respectively, as shown in Figure 5.3 b. This was not observed for complexes **21-25**.

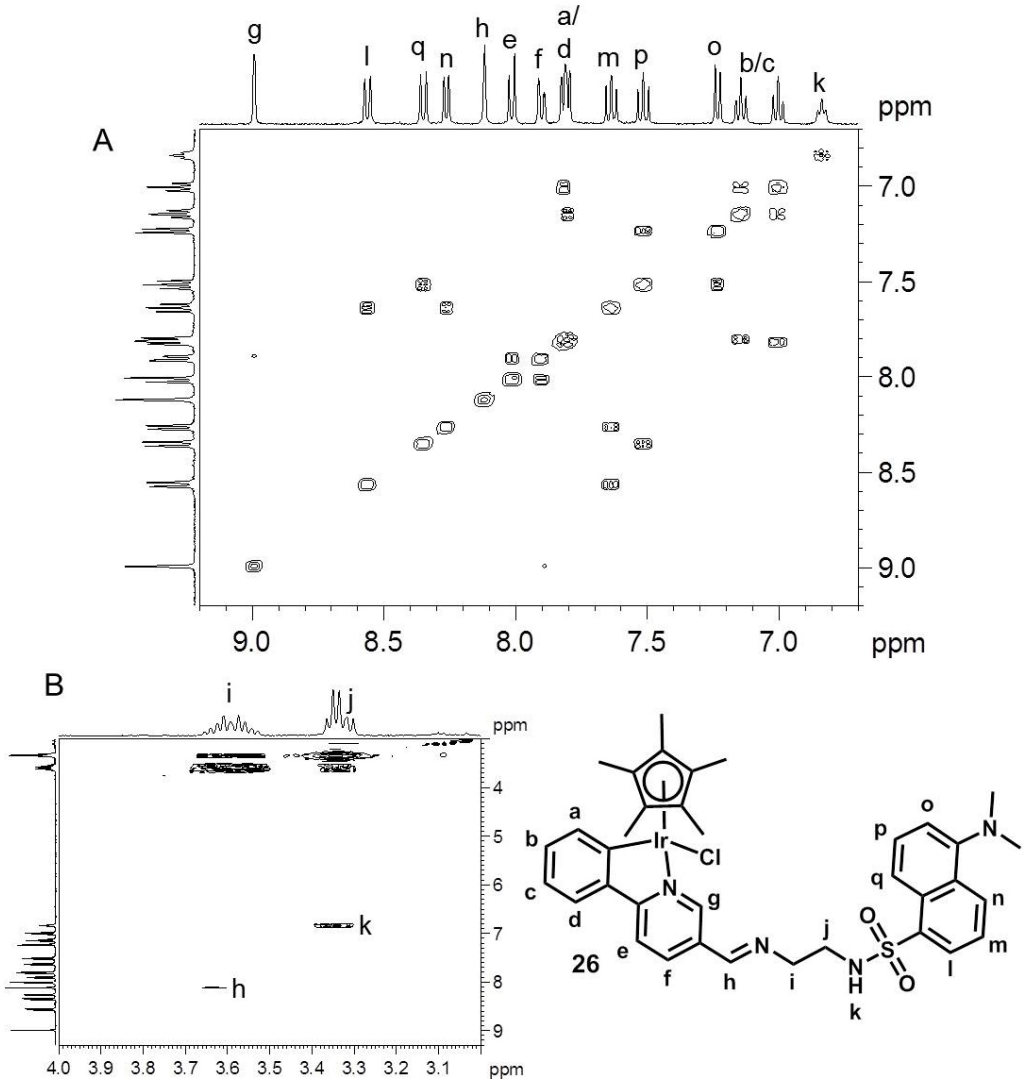

Figure 5.3. (A) Low-field region and (B) high-field region of ^{1}H-^{1}H COSY assignment (400 MHz, acetone-d_6) for [(η^5-Cp*)Ir(5-(dimethylamino)-N-(2-(((6-phenylpyridin-3-yl)methylene)amino)ethyl)naphthalene-1-sulfonamide)Cl] **26**.

The synthesis of complex **26** was also attempted *via* a "pre-functionalisation" route by reaction of [(η^5-Cp*)$IrCl_2$]$_2$ with the dansyl-conjugated 2-PhPy chelating ligand (**L26**) using the same conditions as described in Chapter 3 (Figure 5.4 a) The synthesis of **L26** was performed using the same synthetic procedure as for complex **26**. Evaporating the solvent to dryness yielded **L26** with a purity of 98.8% based on ^{1}H NMR spectroscopy and was used without further purification. After the reaction between [(η^5-Cp*)$IrCl_2$]$_2$ and **L26**, the crude reaction mixture was analysed by ^{1}H

NMR. Multiple species were present in solution based on the ^{1}H NMR spectrum (Figure 5.4 b), including multiple Cp* peaks, indicating multiple binding modes. Comparison to the ^{1}H NMR spectrum of complex **26** showed little similarities in chemical shift, implying that the desired complex had not formed during the reaction to any appreciable extent.

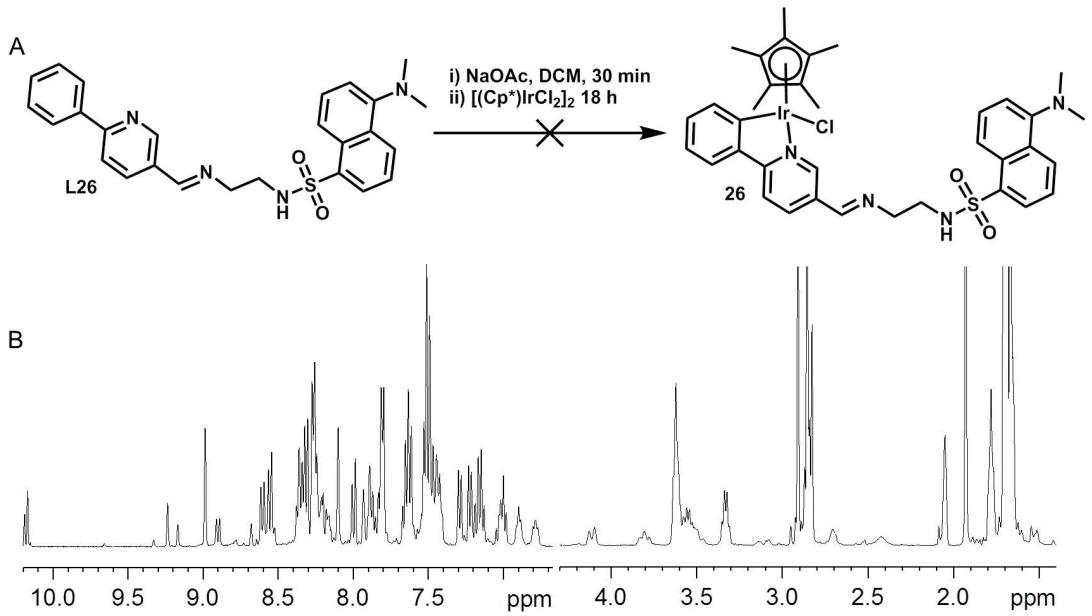

Figure 5.4. (A) – Reaction scheme for the synthesis of complex **26** using **L26**. (B) ^{1}H NMR (400 MHz, acetone-d_6) of products formed from the reaction indicating multiple Ir containing species.

5.3.3 Aqueous Stability of Schiff Base Conjugates

The stability of complexes **21-26** (500 μM) was investigated by ^{1}H NMR spectroscopy in 10% dmso-d_6/90% D_2O at pH* 7.5 (5 mM Na_2HPO_4/NaH_2PO_4), pH* 6.2 and pH* 4.1 (not buffered) at 298 K over 24 h. Hydrolysis at the metal centre appears to be supressed in the presence of high concentrations of dmso, allowing for direct study of the stability of the imine bond. The hydrolysis of the imine bond in complex [(η^5-Cp*)Ir(4-(((6-phenylpyridin-3-yl)methylene)amino)-

phenol)Cl] **21** at pH* 7.5 is shown in Figure 5.5 and the percentage of hydrolysis for each complex at various time periods and at different pH* values are shown in Figure 5.6.

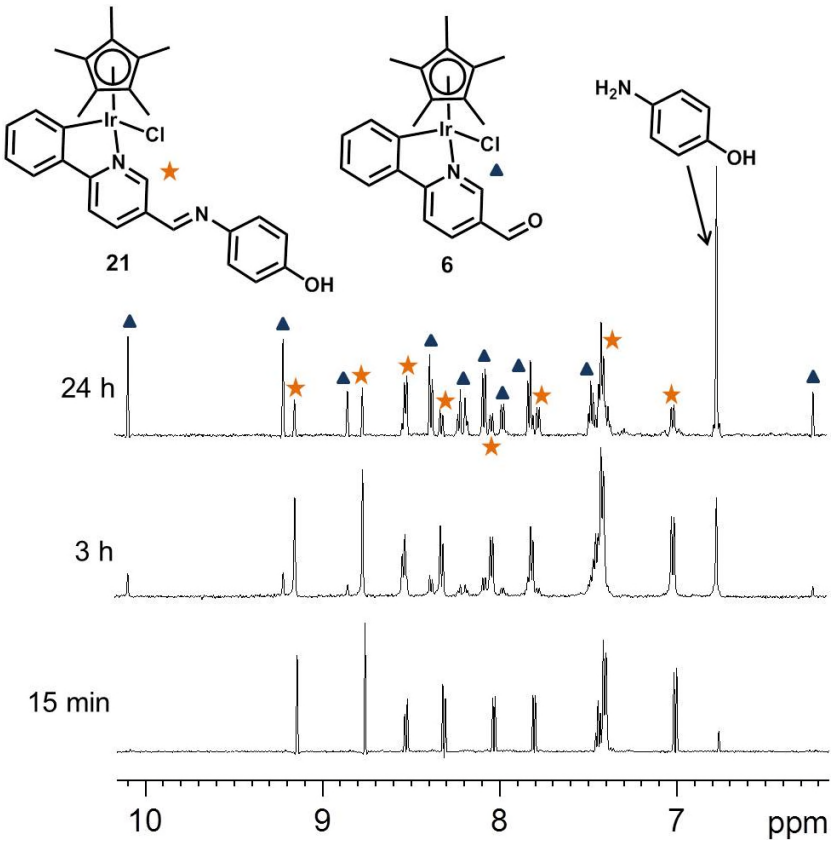

Figure 5.5. ^{1}H NMR spectrum (600 MHz, 10% dmso-d_6/90% D_2O) of [(η^5-Cp*)Ir(4-(((6-phenylpyridin-3-yl)methylene)amino)phenol)Cl] **21** (ca. 500 μM) in 5 mM Na_2HPO_4/NaH_2PO_4 buffer, pH* 7.5 after various times, indicating hydrolysis of the imine bond in **21** forming aldehyde complex **6** and free 4-aminophenol (appears as a converging AB system so only one chemical shift).

On decreasing the pH*, the percentage of hydrolysis products generally increases after 15 min reaction time. After 3 h, complexes **23-26** which contain aliphatic amine conjugates exhibit the greatest extent of hydrolysis at pH* 7.5, which was also the case at 24 h. For complexes **21** and **22** which were synthesised from aromatic amines, the rate of hydrolysis is greatest at more acidic pH* over the 24 h reaction time. In particular, complex **22** showed greatly enhanced hydrolysis at pH* 6.2 and

4.1 after just 15 min, with over 97% of imine hydrolysis occurring. Analysis of the pH* of each solution after 24 h showed that in the unbuffered solutions the pH* of complexes **23-26** had shifted from 4.1 and 6.2 to between 9.4-10.2, while for complexes **21** and **22** the pH* had shifted to 7.5 and 5.7, respectively.

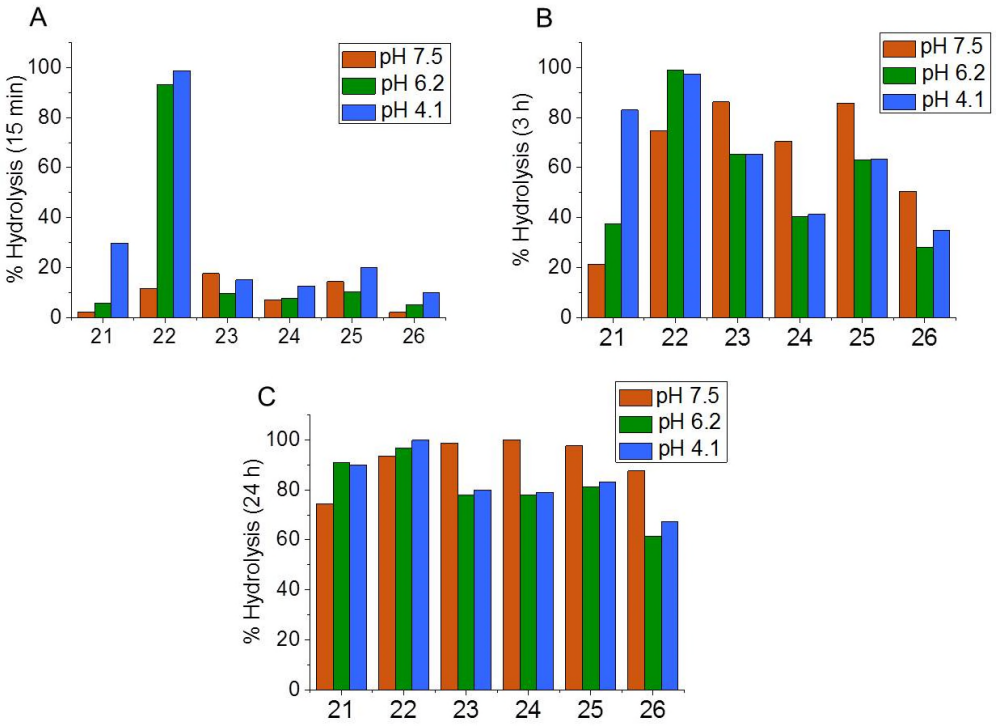

Figure 5.6. Percentage of imine bond hydrolysis for complexes **21-26** as determined by ^{1}H NMR spectroscopy (600 MHz, 10% dmso/90% H_2O) at pH* 7.5 (5 mM Na_2HPO_4/NaH_2PO_4) - orange, 6.2 - green and 4.1 - blue. A – 15 min, B – 3 h and C – 24 h

5.3.4 Reduction of Schiff Base 26 to Secondary Amine 27

Reduction of Schiff base complex [(η^5-Cp*)Ir(5-(dimethylamino)-N-(2-(((6-phenylpyridin-3-yl)methylene)amino)ethyl)naphthalene-1-sulfonamide)Cl] **26** to the corresponding secondary amine was performed to stabilise the fluorescent tag towards hydrolysis. The traditional method for reducing imines to the corresponding

secondary amine generally involves using a hydride source such as $NaBH_4$ or $NaCNBH_3$. Reduction using the milder $NaCNBH_3$ (10 mol equiv) was attempted on complex **26** in THF under N_2 at ambient temperature for 1 d. Purification by precipitation of a $CHCl_3$ solution with hexane resulted in many products and was deemed unsuitable for this system.

An alternative route was attempted for the reduction using triethylsilane (1.5 mol equiv) with $Pd(OAc)_2$ (10% cat.) in EtOH at ambient temperature under N_2, where the reduction of organic imines to secondary amines has been reported to occur within 20 min reaction time.[25] Within 30 min, complete reduction of complex **26** to [(η^5-Cp*)Ir(5-(dimethylamino)-N-(2-(((6-phenylpyridin-3-yl)methyl)amino)ethyl)-naphthalene-1-sulfonamide)Cl] **27** had occurred as monitored by ESI-MS.

Purification of complex **27** was attempted by recrystallisation from acetone/ether, MeOH/ether, $CHCl_3$/hexane, DCM/hexane and THF/pentane mixtures at different temperatures, but pure **27** was not isolated. Purification by silica column chromatography was attempted which yielded purified product as determined by ^{1}H NMR spectroscopy, HR-MS, and HPLC (94%). A comparison of the ^{1}H NMR spectra of complexes **26** and **27** are shown in Figure 5.7 alongside the HR-MS spectra for each complex. The RP-HPLC trace of complex **27** (100 μM in 10% MeCN/90% H_2O) is shown in Figure 5.8. Upon reduction, the imine proton resonance of **26** (8.12 ppm) was no longer visible and a singlet at 3.63 ppm with an integration of two H was present in **27**, corresponding to the reduced CH_2 (Hh). The pyridyl protons Hg and Hf are also shifted to high-field by 0.33 and ca. 0.40 ppm, respectively. The reduction of **26** to **27** was also confirmed by HR-MS (m/z = $[M-Cl]^+$) where a 2 Dalton shift was observed (785.2512 and 787.2649 for complexes **26** and **27**, respectively).

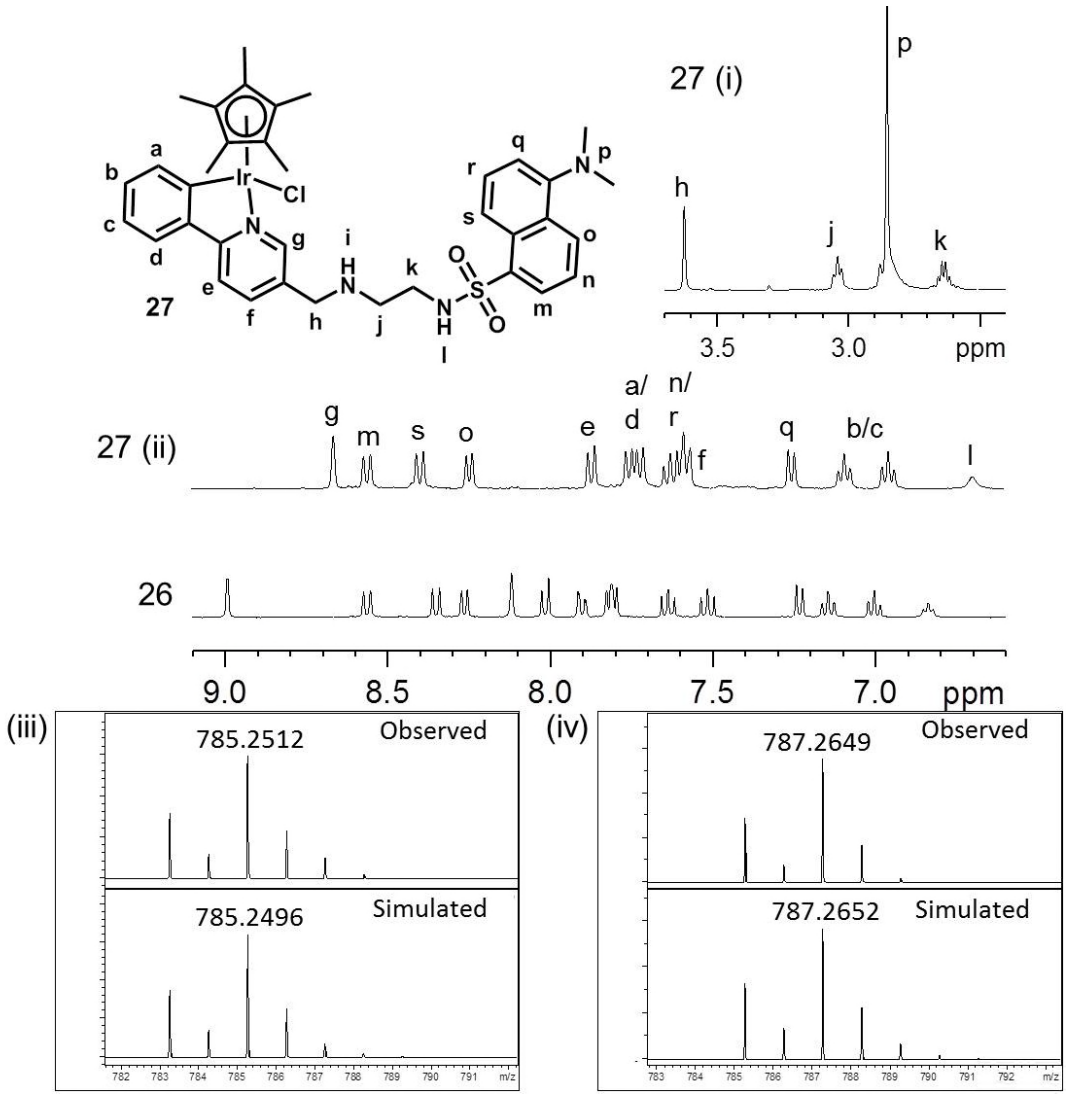

Figure 5.7. ^{1}H NMR spectra (400 MHz, acetone-d_6) of complexes **26** and **27** with assignments of protons for complex **27** based on a ^{1}H-^{1}H COSY experiment (i – high-field region and ii – low field region of complex **27**). HR-MS of complexes (iii) **26** and (iv) **27** showing that the reduction of the imine bond to the secondary amine has occurred. Top trace shows observed MS and bottom trace shows simulated MS trace for $[M\text{-}Cl]^{+}$.

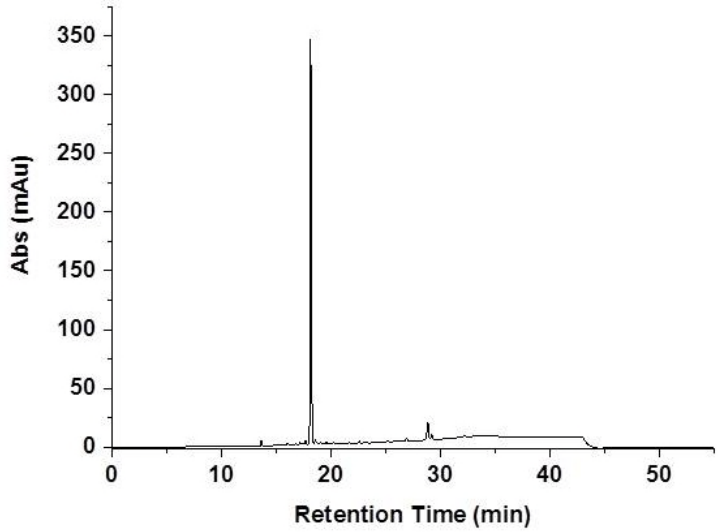

Figure 5.8. RP-HPLC trace of complex **27** (100 μM) in 10% MeCN/90% H_2O v/v (purity = 94%).

5.3.5 Reaction between Complex 26 and Et_3SiH

As Et_3SiH can act as a hydride donor, with the potential to form an Ir-H species with **26**, the stability of **26** in the presence of Et_3SiH was also examined without the $Pd(OAc)_2$ catalyst. After 2 h, ESI-MS confirmed that reduction to the secondary amine complex **27** had occurred. The crude ^1H NMR of the reaction indicated that the same species had formed when compared with the product isolated using the Pd(II) catalyst (Figure 5.9 a). The reaction mixture also contained a new set of peaks for the triethylsilyl species (0.95 (Ha) and 0.59 (Hb) ppm), along with a quartet (Hc) at 3.68 ppm which appears to couple to a proton (Hd) (as observed in the ^1H-^1H COSY spectrum, Figure 5.9 b) which overlaps with the residual ethanol solvent (triplet, 1.12 ppm).[26] The ^1H-^1H COSY NMR spectrum also showed two different proton environments are present at around 1.12 ppm both coupled to two different quartet peaks. Integration of the CH_3 peaks in the new triethylsilyl species to nine results in the integration of 2H for the new quartet peak at 3.68 ppm. This could

indicate that the new triethylsilyl species is the ethoxy species Et_3SiOEt. Assignment of the new silyl species was attempted by positive mode ESI-MS (50-500 MW) but no mass peak was detected that could correspond to a silyl species.

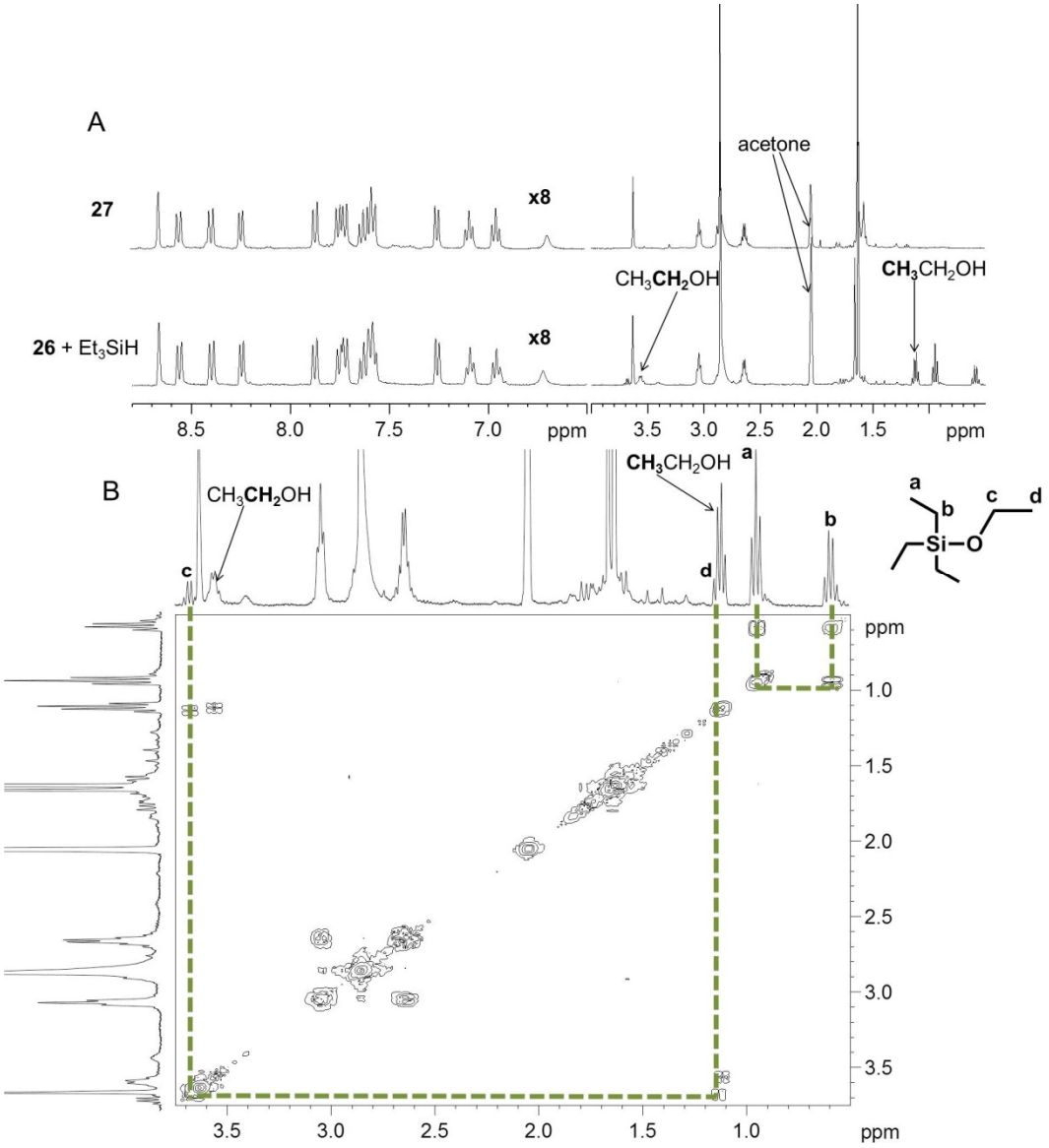

Figure 5.9. (A) ^{1}H NMR (400 MHz, acetone-d_6) spectra of the crude reaction mixture between complex **26** (1 mol equiv.) and Et_3SiH (1.5 mol equiv.) at ambient temperature for 2 h and comparison to the reaction of complex **26** with Et_3SiH and cat. $Pd(OAc)_2$ (**27**) showing the same product is formed. (B) ^{1}H-^{1}H COSY NMR spectrum of the crude reaction mixture, showing the identification of a new ethyl species which may correspond to Et_3SiOEt.

The reaction was also followed by ^{1}H NMR spectroscopy (600 MHz, 298 K, ethanol-d_6) for complex **26** and **13** (control – no reducible bond) (Figure 5.10 and 5.11, respectively). The reduction of complex **26** was complete within 10 min, as monitored by the disappearance of the original set of peaks for **26**. No iridium-hydride species was detected throughout the reaction. Another set of peaks also formed after reduction of the imine bond had occurred, along with a slight down-field shift in the original product peaks. Et_3SiH is almost fully converted to the new species after 30 min, as observed by the small high-field shift in the ethyl protons (Figure 5.10 b). No peaks formed which correspond to the new siliyl adduct, which may be due to the formation of $Et_3SiOCD_2CD_3$ as the ethanol present in the reaction is deuterated.

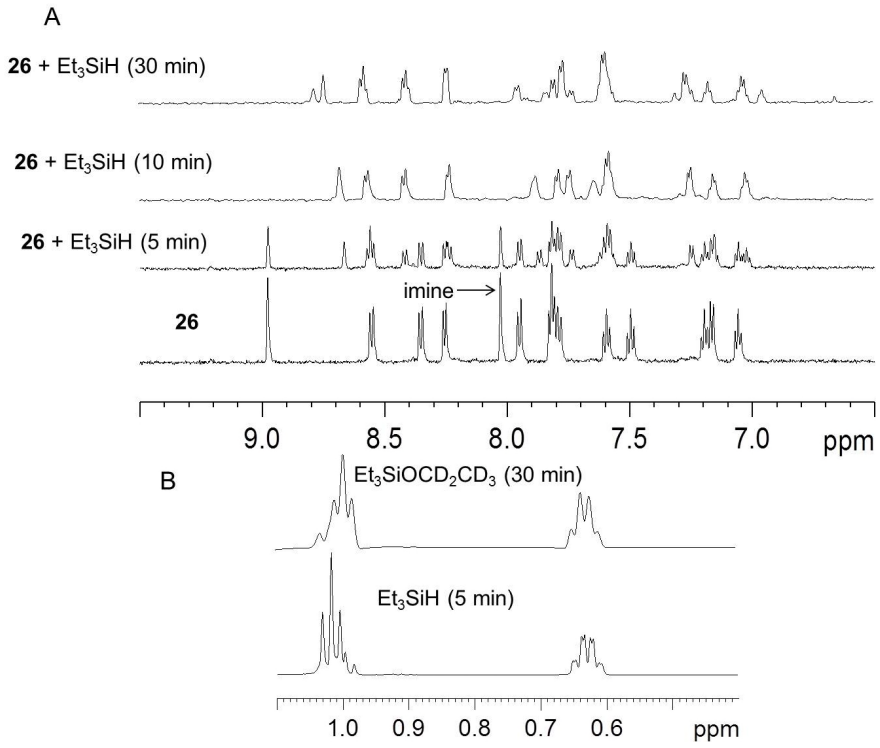

Figure 5.10. (A) Low field region of the ^{1}H NMR spectrum (600 MHz, ethanol-d_6, 298 K) of complex **26** (1 mol equiv.) with Et_3SiH (1.5 mol equiv.) at various time intervals. (b) High field region of reaction showing the conversion of Et_3SiH to another silyl species.

In contrast, incubation of complex **13** with Et_3SiH resulted in an iridium-hydride peak at -12.46 ppm together with the corresponding new peaks for the Cp* and 2-PhPy chelating ligand, were also visible within the time taken to acquire the first spectrum (5 min) (Figure 5.11). As observed with **26**, Et_3SiH appears to be almost fully converted to the hypothesised $Et_3SiOCD_2CD_3$ species.

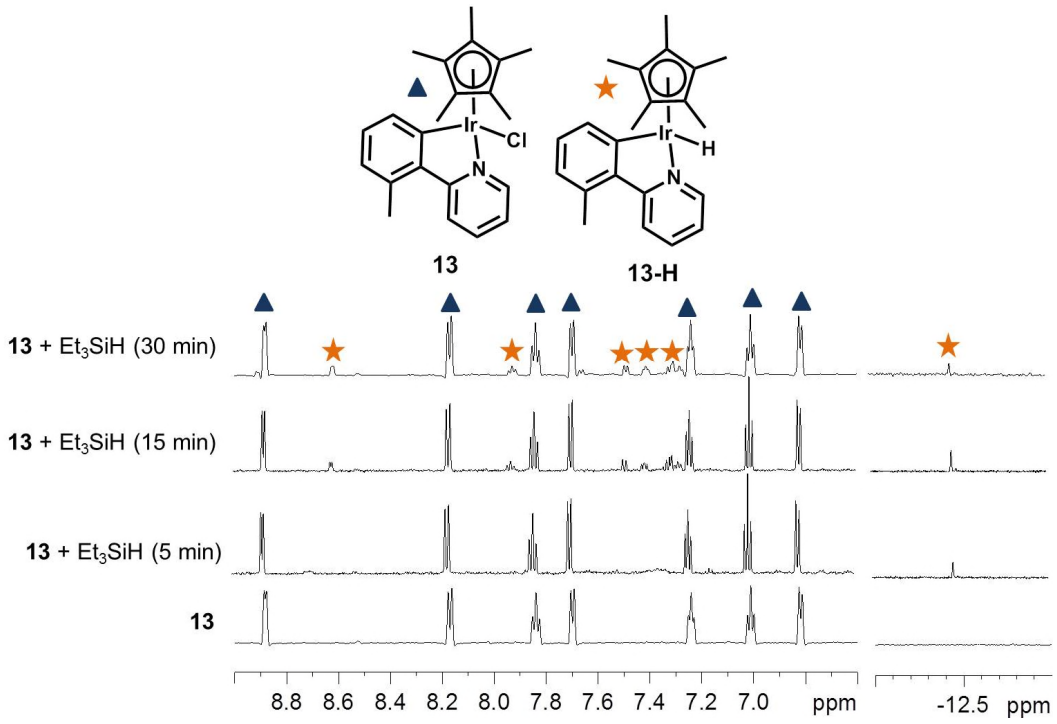

Figure 5.11. ^{1}H NMR spectrum (600 MHz, ethanol-d_6, 298 K) at various times during the reaction between complex **13** and Et_3SiH (1.5 mol equiv.), showing the formation of the Ir-H complex **13-H** after 5 min.

The reduction of the imine bond in **L26** was attempted using 10% mol cat. of complex **13** with Et_3SiH (1.5 mol equiv) in ethanol at ambient temperature to determine if **13** can catalytically reduce imine bonds in the presence of Et_3SiH. The reduction of **L26** was also examined using $Pd(OAc)_2$ (10% mol cat.) with Et_3SiH (1.5 mol equiv) and also in the presence of just Et_3SiH. After 30 min, the reduction of **L26** in the presence of complex **13** was complete as monitored by ESI-MS and ^{1}H NMR spectroscopy (Figure 5.12). Intriguingly, no reduction had occurred in the

presence of the Pd catalyst, even after 24 h, whereas partial reduction of **L26** by just Et_3SiH was observed after 24 h.

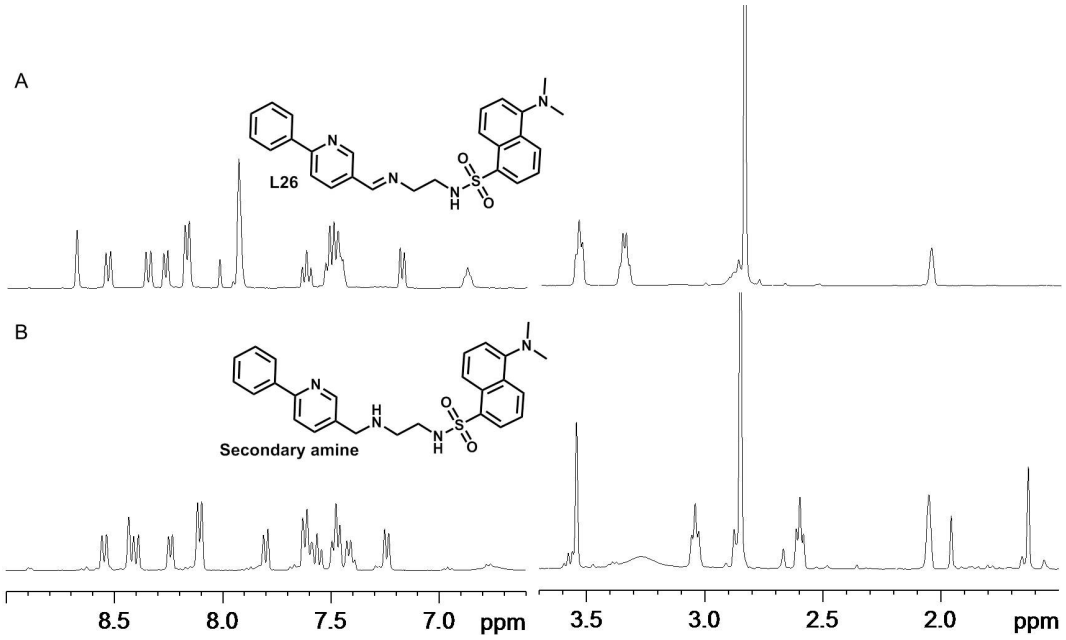

Figure 5.12. ^{1}H NMR (400 MHz, acetone-d_6) spectra of (A) **L26** and (B) reaction between **L26** + 10% mol cat. **13** + Et_3SiH (1.5 mol equiv) in ethanol at ambient temperature after 30 min.

5.3.6 Aqueous Stability of Complex 27

The aqueous stability of the secondary amine bond in complex **27** was monitored at 15 min, 24 h and 21 d in 5 mM Na_2HPO_4/NaH_2PO_4 buffer, pH 7.5, ambient temperature by ^{1}H NMR spectroscopy (10% dmso-d_6/90% D_2O), Figure 5.13. No change in the spectrum was observed after 24 h and only minimal change after 21 d compared to the first spectra taken (15 min), indicating that complex **27** exhibits the expected aqueous stability compared to the hydrolytically unstable imine bond of **26**. The small changes in the spectra are likely due to competition between dmso and aqua adducts over time.

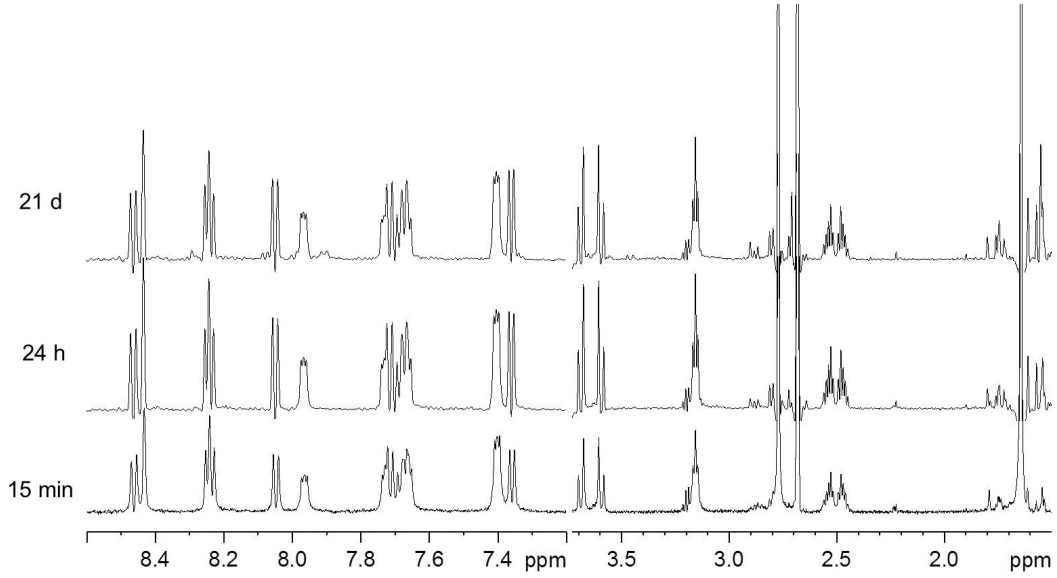

Figure 5.13. Stability of complex **27** monitored by ^{1}H NMR spectroscopy (10% dmso-d_6/90% D_2O) in 5 mM Na_2HPO_4/NaH_2PO_4 buffer, pH 7.5 after 15 min, 24 h and 21 d.

5.3.7 Fluorescence of Complexes 6, 26 and 27

The luminescence properties of complexes **6**, **26** and **27** were investigated in DCM and compared to the free dansyl-amine tag (*N*-(2-aminoethyl)-5-(dimethylamino)naphthalene-1-sulfonamide). UV-Vis spectra of all the compounds (50 μM, 298 K) were recorded and the observed bands used to excite the compounds to measure for fluorescence. The excitation wavelengths that produced the most intense fluorescence for each compound are indicated on the UV-vis spectra in Figure 5.14 a, where the observed fluorescence (Figure 5.14 b) and the resulting normalised fluorescence emission spectra (Figure 5.14 c) for each compound at 5 μM for the dansyl-amine tag and 50 μM for complexes **26** and **27** are shown. Both complexes **26** and **27** exhibited fluorescence, where the emission maximum (em λ_{max}) was the same at 503 nm, while the em λ_{max} for the dansyl-amine was found at 490 nm. The complexes exhibit markedly reduced fluorescence compared to the free dansyl-amine. No fluorescence was observed for complex **6**.

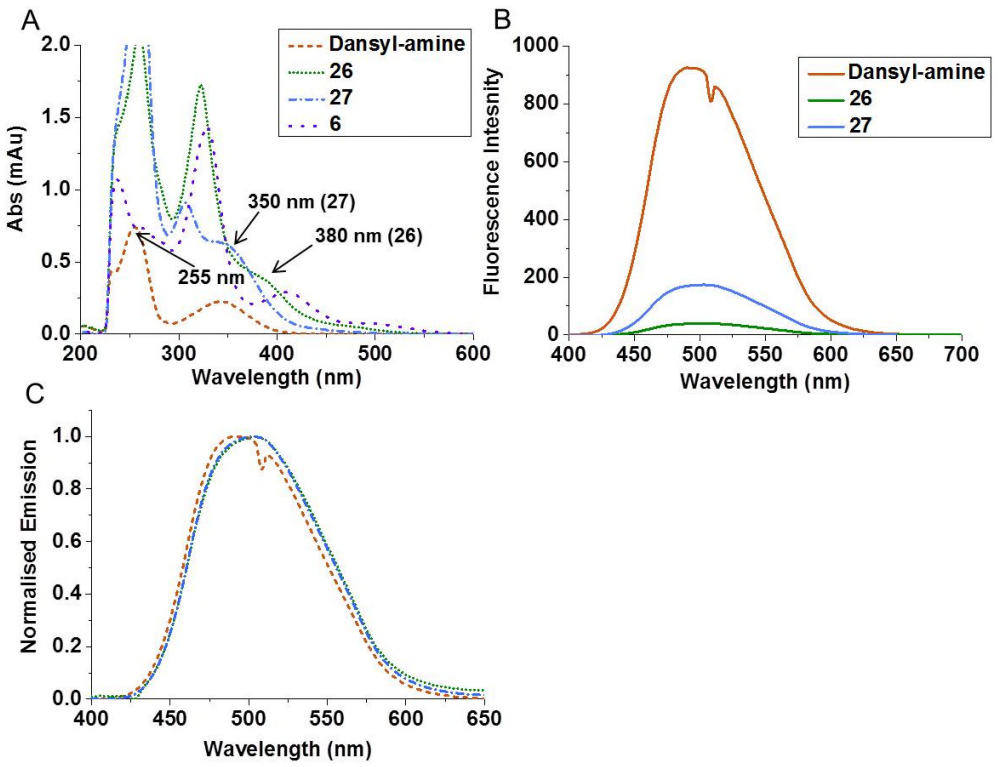

Figure 5.14. (a) UV-Vis spectra of dansyl-amine (orange dash) and complexes **26** (green dot), **27** (blue dash-dot) and **6** (purple dash) in DCM at (50 µM, 298 K) with labelled bands being responsible for the most intense fluorescence when used to excite the compounds. (b) Fluorescence emission spectra of dansyl-amine (5 µM) and complexes **26** and **27** (50 µM) in DCM, 298 K (after subtraction from the DCM blank). (c) Normalised fluorescence emission of dansyl-amine (5 µM) and complexes **26** and **27** (50 µM).

The intensity of fluorescence for complex **27** and dansyl-amine (ca. 50 µM) were recorded in aqueous solution (10% MeOH, 90% H_2O) and are shown in Figure 5.15, where the excitation wavelengths used for **27** and dansyl-amine were 252 nm and 246 nm, respectively. Both the dansyl-amine and **27** exhibited markedly reduced fluorescence in aqueous solution in comparison to DCM, where the fluorescence of **27** is almost completely quenched.

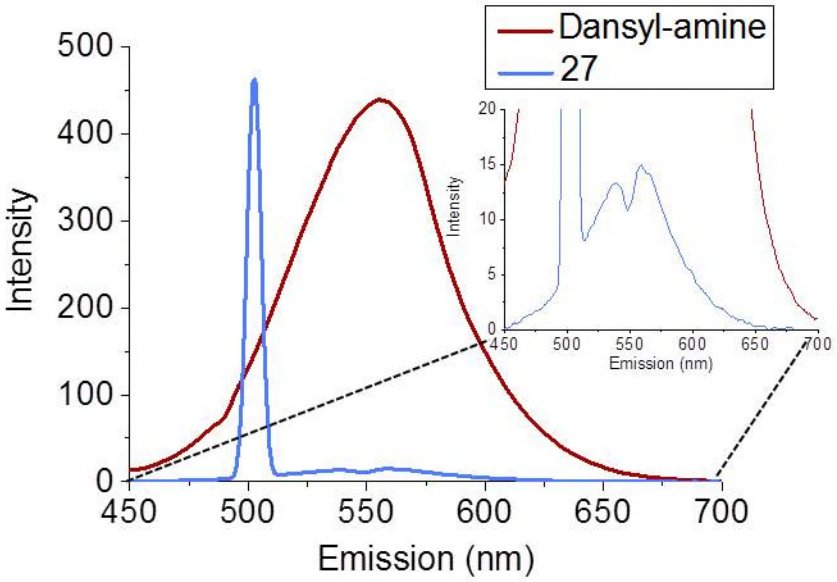

Figure 5.15. Fluorescence emission spectra of dansyl-amine (red) and complex **27** (blue) at 50 μM in 10% MeOH/90% H_2O. Emission at 504 nm for complex **27** due to excitation at 252 nm ($2\times\lambda_{ex}$).

5.3.8 Epifluorescence Microscopy of A2780 Cancer Cells

The ability to track complex **27** in A2780 human ovarian cancer cells was investigated by epifluorescence microscopy. The antiproliferative activity for **27** was determined, with an IC_{50} of 4.9 ± 0.2 μM, making it a reasonably potent complex. The cells were exposed to **27** at 2 × IC_{50} for 24 h, followed by fixing, staining with propidium iodide (PI, nuclear stain) then imaging, Figure 5.16. Only autofluorescence was observed upon excitation under UV light, demonstrating no fluorescence due to complex **27**. The control propidium iodide (PI) fluoresced upon excitation under green light showing PI binding to DNA.

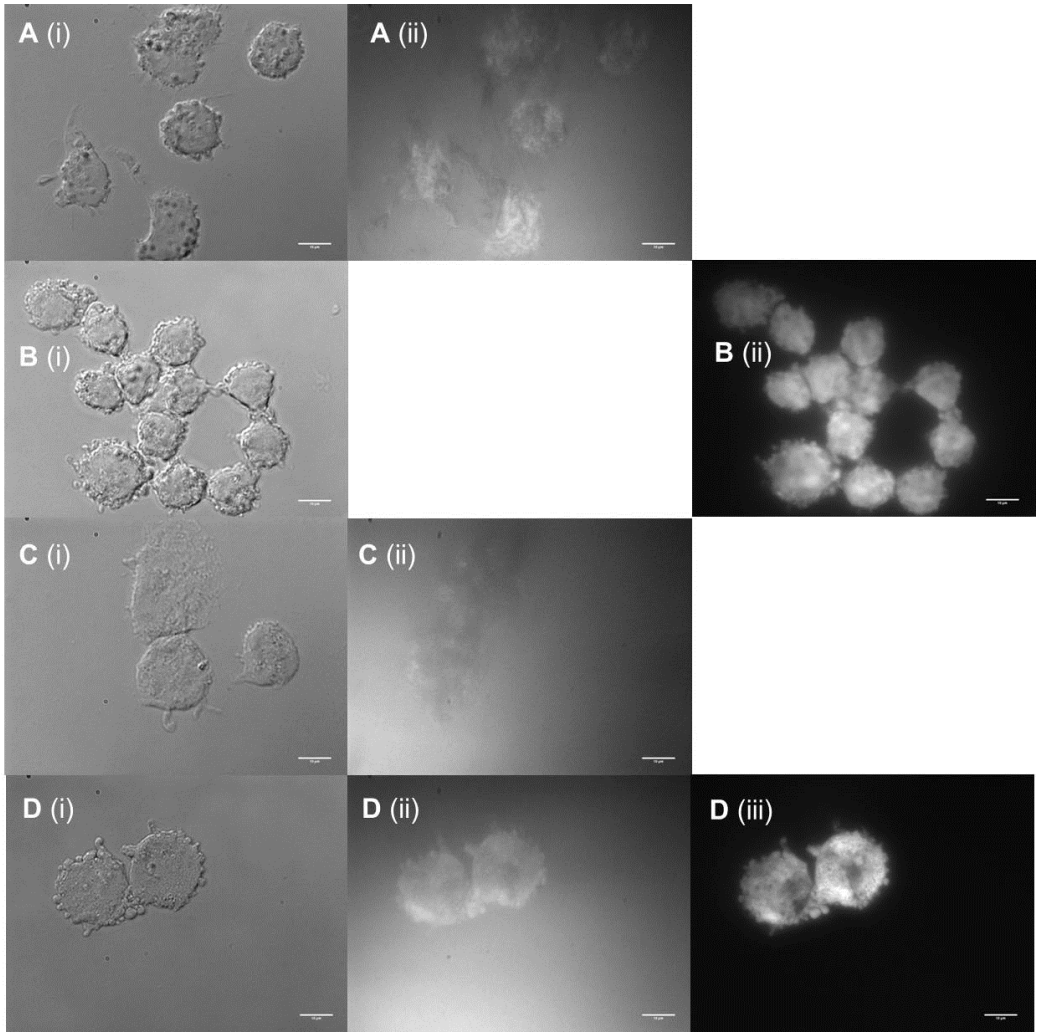

Figure 5.16. A – control A2780 cells imaged as (i) brightfield and (ii) λ_{ex} = UV where autofluoresence was observed. B – A2780 cells stained with PI (i) brightfield and (ii) λ_{ex} = green light exhibiting fluorescence in the nucleus. C – A2780 cells incubated with complex **27** at 2 × IC_{50} for 24 h (i) brightfield and (ii) λ_{ex} = UV exhibiting autofluorescence. D – A2780 cells incubated with complex **27** followed by PI (i) brightfield, (ii) λ_{ex} = UV and (iii) λ_{ex} = green light. Bar = 10 microns. Only autofluorescence was observed in cells incubated with **27** indicating no fluorescence due to **27**.

5.3.9 Reactions with Lysine-Containing Peptides

Organic compounds bearing aldehyde functional groups can react with peptides and proteins which contain lysine residues, forming Schiff base conjugates.[27,28] The reaction of Substance P (SubP) and [Lys-3]-bombesin (L3BBS) (as model peptides

containing lysine residues) with complex **6** after 24 h (310 K) was studied by Fourier Transform-Ion Cyclotron Resonance (FT-ICR), using Collisionally Activated Dissociation (CAD)[22] and Electron Capture Dissociation (ECD)[23] MS/MS techniques to determine the binding sites on each peptide. In all cases, the molecular ion peak obtained involved the loss of the chlorido monodentate ligand in detection of the species [(η^5-Cp*)Ir(2-phenyl-5-pyridinecarboxaldehyde)Cl] **6**, Schiff base modifications of complex **6**, and when direct binding of the peptide at the monodentate site occurs. The denotations used to describe the species analysed are shown in Table 5.2. Potential binding sites on Substance P and [Lys-3]-bombesin upon reaction with metal complexes are highlighted in Figure 5.17a and include histidine[29,30] and methionine[31] residues, which bind at the metal centre, as well as the proposed reaction of lysine to the aldehyde functional group. The structures of potential Ir-peptide conjugates are shown in Figure 5.17b.

Table 5.2. The denotations used to describe the species analysed by FT-ICR-MS in the forthcoming MS spectra.

Species	Denotation	Species	Denotation
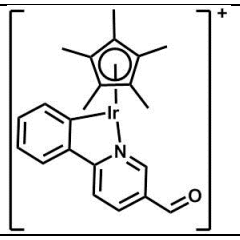	[**6***]$^+$	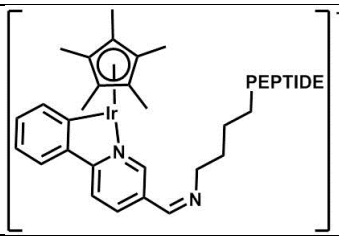	[Peptide+**6***-H_2O]$^+$
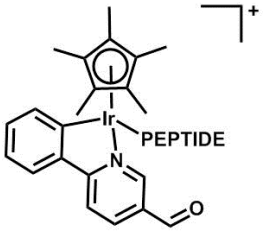	[Peptide+**6***]$^+$	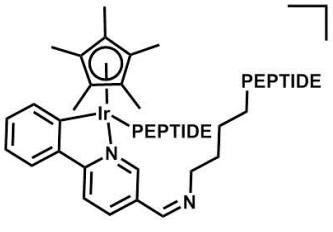	[(2×Peptide) +**6***-H_2O]$^+$

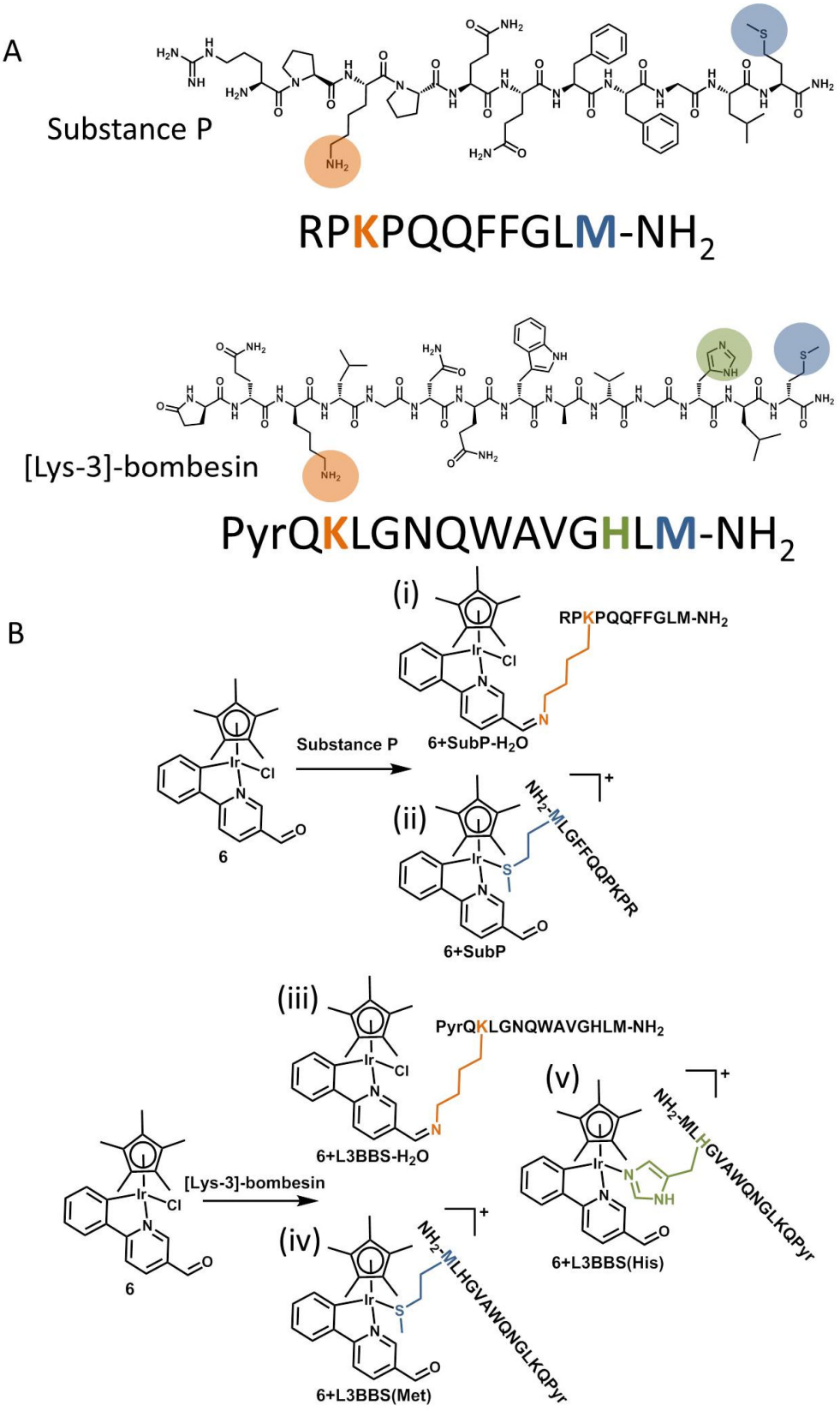

Figure 5.17. (a) Substance P and [Lys-3]-bombesin. Potential binding sites are highlighted on the peptide and in bold in the amino acid letter code. (b) Structures of the possible Ir-peptide conjugates upon reaction with complex **6**.

Incubation of complex **6** (165 μM, MeCN, 66% v/v) with Substance P (330 μM, H_2O, 33% v/v) at 310 K after 24 h led to the detection of the species [SubP+**6***-H_2O+H]$^{2+}$ (m/z = 918.92794, calculated m/z = 918.93143). The loss of a water molecule is indicative of a condensation reaction such as Schiff base formation. The Ir-peptide conjugate can be fragmented along the peptide backbone using CAD MS/MS to deduce the binding site of the iridium complex. The notation is described in section 5.2.3.10, where b = number of amino acids left in the peptide along the N-C direction and y = number of amino acids left in the peptide along the C-N direction.[24] When the iridium isotopic pattern and mass of the complex are absent after the fragmentation of a particular amino acid indicates the binding site of the complex on the peptide. The fragmentation of the Ir-peptide conjugate narrows the binding site of the iridium complex to lysine (Figure 5.19, mass table in Appendix Table A1). No adducts were observed for Substance P binding at the monodentate site. Therefore, the Ir-peptide conjugate **6+SubP-H_2O** appears to be the product of the reaction (Figure 5.17 b (i)).

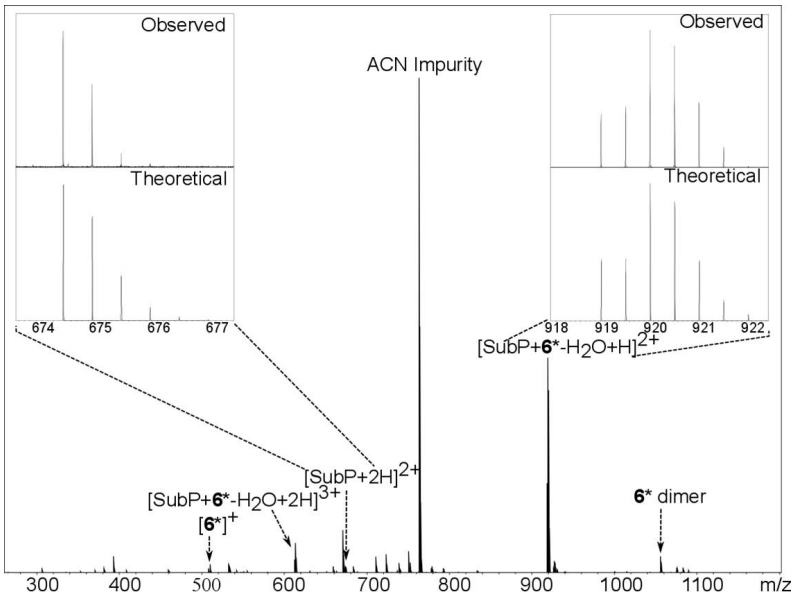

Figure 5.18. nESI-MS of the reaction between complex **6** and Substance P at 310 K after 24 h, indicating that binding of the peptide to complex **6** has occurred.

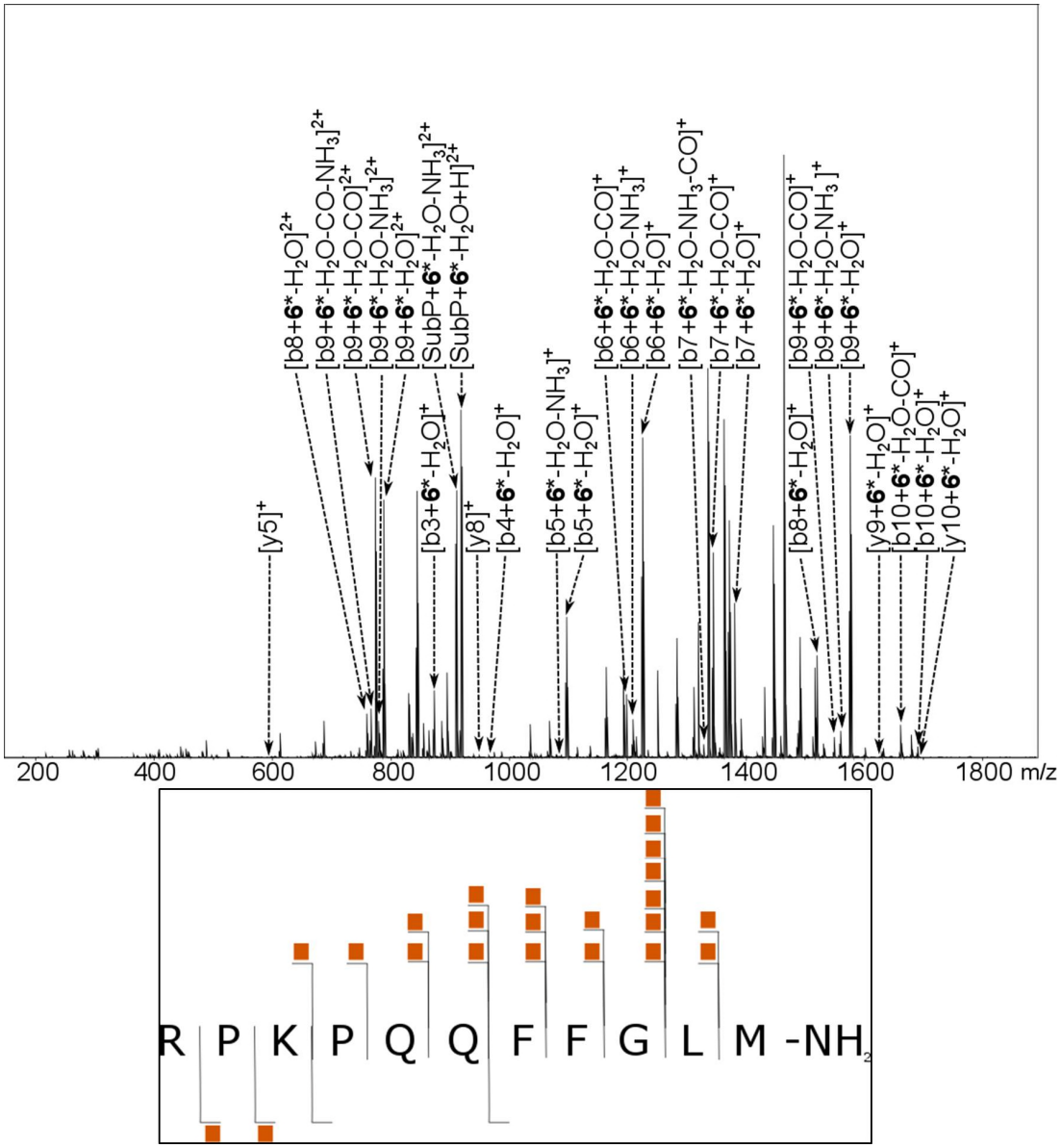

Figure 5.19. FT-ICR CAD MS/MS spectrum of the species [SubP+**6***-H_2O+H]$^{2+}$ showing binding of the peptide *via* the lysine (K) residue as a consequence of Schiff base formation with complex **6**. The Ir-peptide conjugate is fragmented along the peptide backbone, where b = number of amino acids left in the peptide along the N-C direction and y = number of amino acids left in the peptide along the C-N direction, allowing for precise determination of the binding site. The orange boxes in the fragmentation map indicate the iridiated peptide fragments observed in the MS/MS.

Incubation of complex **6** (165 μM, MeCN, 66% v/v) with [Lys-3]-bombesin (330 μM, H_2O, 33% v/v) at 310 K after 24 h led to a more complicated spectrum (Figure 5.20), with MS peaks corresponding to the condensation product [L3BBS+**6***-H_2O+H]$^{2+}$ (m/z = 1040.96930, calculated m/z = 1040.97182) as well as the [L3BBS+**6***+H]$^{2+}$ species (m/z = 1049.97710, calculated m/z = 1049.97406), indicating binding to the complex in two different ways. FT-ICR CAD MS/MS was used to assign the species [L3BBS+**6***-H_2O+H]$^{2+}$ which is bound *via* the lysine residue (Figure 5.21, mass table in Appendix Table A2) as expected. Therefore, one of the products from the reaction is likely to be **6+L3BBS-H_2O** (Figure 5.17 b (iii)).

Assignment of the binding site for the species [L3BBS+**6***+H]$^{2+}$ proved difficult for the incubated sample, due to the presence of unreacted peptide. Separation of the species present was attempted using RP-HPLC (Figure 5.22 a). The peak in the chromatogram which contained the highest degree of metal-peptide species [L3BBS+**6***-H_2O+H]$^{2+}$ and [L3BBS+**6***+H]$^{2+}$ (with minimal free L3BBS, as determined using nESI-MS) was used to analyse the [L3BBS+**6***+H]$^{2+}$ binding mode. Analysis of the [L3BBS+**6**+H]$^{2+}$ species by FT-ICR-ECD MS/MS showed binding *via* the histidine residue (Figure 5.22 b, mass table in Appendix Table A3), therefore, the species is likely to be **6*+L3BBS(His)** (Figure 5.17 b (v)). Similarly to CAD, the fragments in ECD are labelled as such; c = number of amino acids left in the peptide along the N-C direction and z = number of amino acids left in the peptide along the C-N direction.[24]

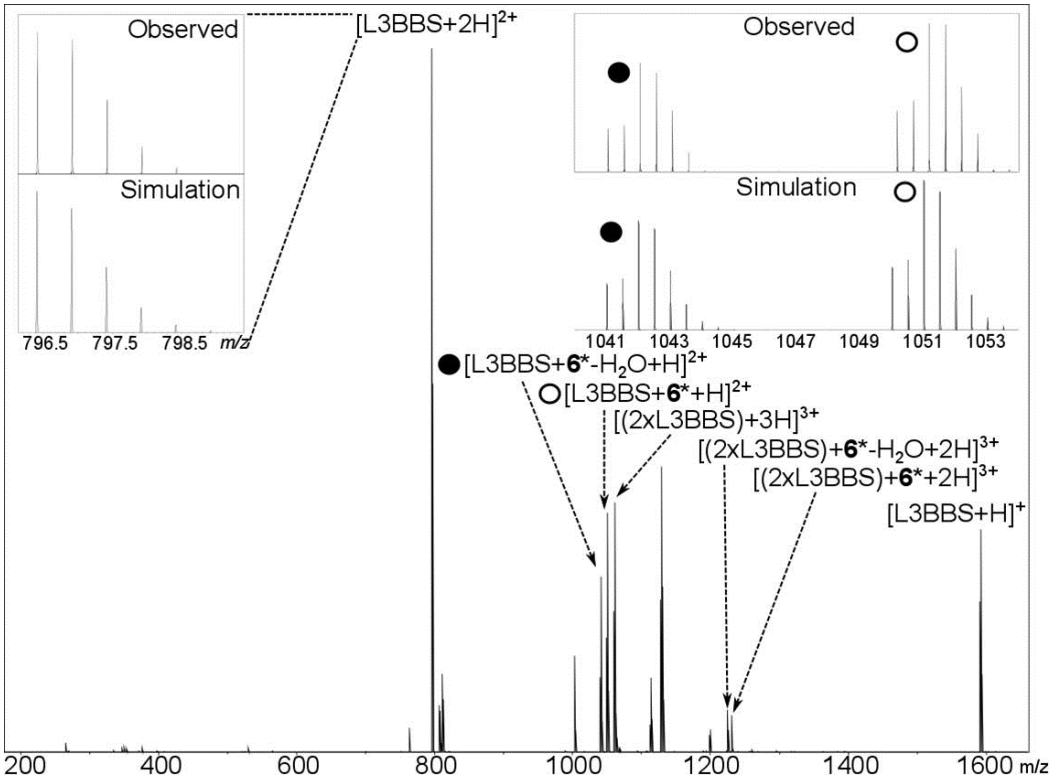

Figure 5.20. nESI-MS of the reaction between complex **6** and [Lys-3]-bombesin at 310 K after 24 h, indicating that more than one binding mode to complex **6** has occurred.

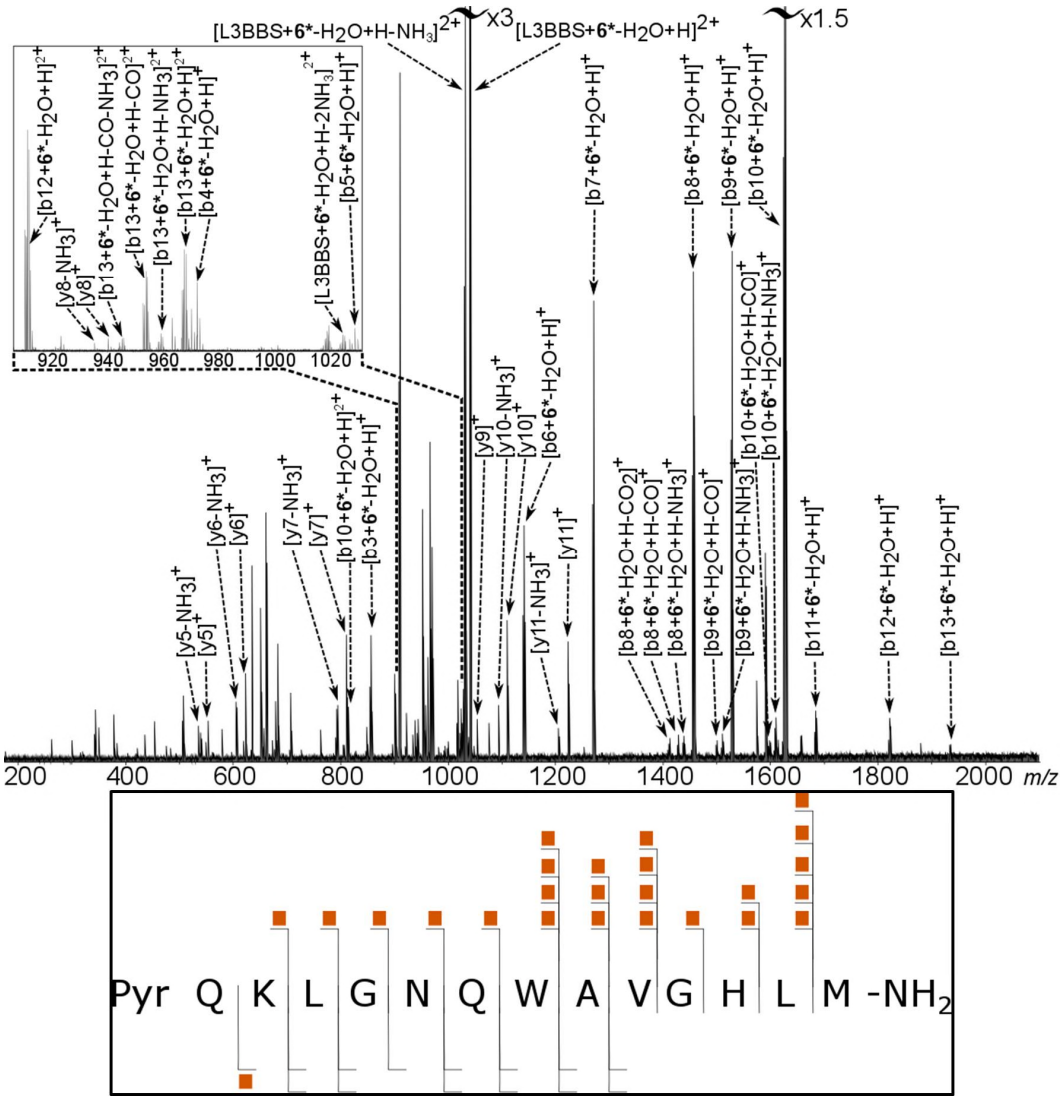

Figure 5.21. FT-ICR CAD MS/MS spectrum of the species [L3BBS+**6***-H_2O+H]$^{2+}$ showing binding of the peptide *via* the lysine (K) residue as a consequence of Schiff base formation with complex **6**. The Ir-peptide conjugate is fragmented along the peptide backbone, where b = number of amino acids left in the peptide along the N-C direction and y = number of amino acids left in the peptide along the C-N direction, allowing for precise determination of the binding site. The orange boxes in the fragmentation map indicate the iridiated peptide fragments observed in the MS/MS.

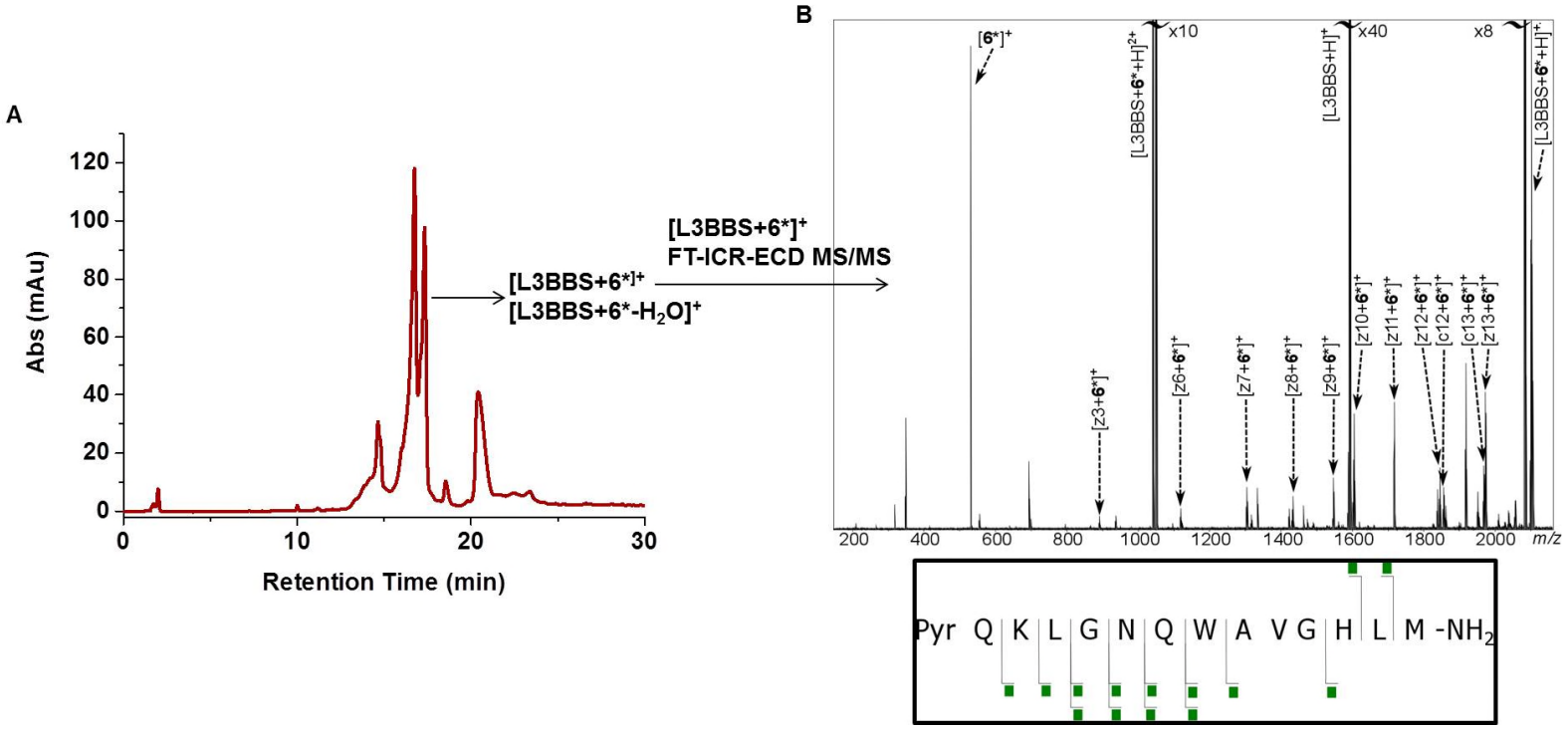

Figure 5.22. (A) RP-HPLC (2 mM NH_4OAc H_2O/MeCN, sig = 254 nm) of the reaction between complex **6** and L3BBS after 24 h. (B) FT-ICR ECD MS/MS spectrum of the species [L3BBS+**6***+H]$^{2+}$ as isolated by HPLC, showing binding of the peptide *via* the histidine (H) residue as a consequence of binding at the monodentate site on complex **6**. The Ir-peptide conjugate is fragmented along the peptide backbone, where c = number of amino acids left in the peptide along the N-C direction and z = number of amino acids left in the peptide along the C-N direction, allowing for precise determination of the binding site. The green boxes in the fragmentation map indicate the iridiated peptide fragments observed in the MS/MS.

5.4 Discussion

5.4.1 Synthesis and Characterisation of Complexes 21-26

The use of complex [(η^5-Cp*)Ir(2-phenyl-5-pyridinecarboxaldehyde)Cl] **6** as a "chemical platform" for modification *via* formation of Schiff bases with amines was assessed using microwave-assisted chemistry. Microwave synthesis allows reactions to proceed at a faster rate than traditional laboratory techniques, which has been attributed to the capacity to reach higher temperatures, as well as the ability to induce increased solvent molecular vibrations.[32]

The reaction of **6** (1 mol equiv.) with amines (1.2 mol equiv., Table 5.1) produced six novel Schiff base conjugates from both aromatic and aliphatic primary amines within 5 min reaction time. Using traditional laboratory techniques, the formation of imine conjugates is relatively straightforward, however, reaction times can range from 1 – 24 h. $CHCl_3$ and acetone were found to be the most suitable solvents examined.

Sonication of a concentrated methanolic solution resulted in precipitation of the desired product, with yields ranging from 39-72%. The biggest loss of yield appeared to be in the purification step, where some product may remain in the sonicated MeOH solution. Attempts to purify the complexes using crystallisation from $CHCl_3$/hexane, acetone/Et_2O and THF/pentane always resulted in immediate precipitation upon addition of the anti-solvent, which did not yield products of good purity. This also resulted in difficulty obtaining crystals suitable for X-ray diffraction.

The ^{1}H NMR spectra of complexes **21-26** all exhibited the characteristic imine peak alongside the loss of the low-field aldehyde peak. ESI-MS showed peaks

corresponding to the loss of the chloride ligand, alongside the addition of the organic amine with loss of a H_2O molecule, which confirms that the condensation reaction has taken place. Elemental analysis of the reaction products was generally in good agreement with the expected values.

An alternative route to form complex **26** was investigated by reaction of $[(\eta^5\text{-Cp*})IrCl_2]_2$ with the already dansyl-conjugated 2-PhPy chelating ligand (**L26**), Figure 5.4. The reaction was performed using the previously described route to synthesise *C,N*-chelated half-sandwich complexes. It was found that many different products were formed, and the desired complex **26** could not be identified. Therefore, the post-modification method is required rather than functionalising the chelating ligand before complexation. This is presumably due to multiple binding modes that the **L26** can exhibit when reacting with $[(\eta^5\text{-Cp*})IrCl_2]_2$ in the presence of a base.

5.4.2 Imine Reduction in Complex 26

As Schiff bases are susceptible to hydrolysis, investigations into stabilising the bond by formation of the secondary amine were carried out. This was of particular importance in the case of complex **26** (Figure 5.2) where a stable bond may allow tracking of the complex *via* fluorescence microscopy. The reduction of imines to the corresponding secondary amines is a well-established reaction. Most reduction of imine bonds involves using a reducing agent which acts a hydride donor. It has also been documented that chelated half-sandwich Ir(III) complexes can reduce imines *via* transfer hydrogenation in the presence of a hydride source.[33]

The reaction of complex **26** with $NaCNBH_3$ (which is a milder reducing agent than $NaBH_4$), resulted in the formation of many different products based on the ^1H NMR

spectrum. An alternative route involving Et_3SiH and the catalyst $Pd(OAc)_2$ was investigated.[25] The catalytic cycle has been proposed to involve *in situ* reduction of Pd(II) to Pd(0) by Et_3SiH, followed by oxidative addition of Et_3SiH then reductive elimination by reaction with ethanol to form H_2 gas and the silyether Et_3SiOEt (Figure 5.23).[34] The H_2 gas may be absorbed onto the surface of the Pd(0) to enable hydrogenation of the imine to occur,[35] although this was originally proposed for the hydrogenation of 1-alkenes where the same catalytic process was then applied to imines.[25] Following the experimental protocol, and purification by flash silica chromatography, the secondary amine complex **27** was isolated in 33% yield.

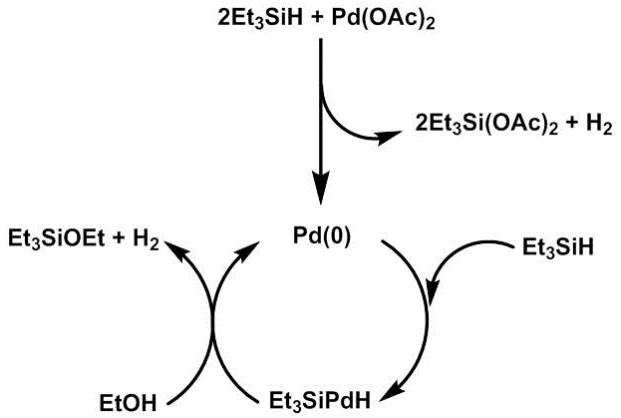

Figure 5.23. Catalytic cycle for the *in situ* production of H_2 by the reaction of Et_3SiH with $Pd(OAc)_2$ in ethanol to reduce imine bonds.[34]

Most reports on the reaction of Et_3SiH with Ir complexes are based on octahedral pincer complexes.[36-38] Intriguingly, the imine moiety in complex **26** was able to be reduced to generate complex **27** in the presence of Et_3SiH without the need for the Pd catalyst as is required for organic transformations, implying involvement of the Ir complex in the reduction process. Analysis of the crude reaction mixture (by ^1H NMR spectroscopy, Figure 5.9) showed that the product was the same as from the reaction using the Pd catalyst. As the method used involves stirring complex **26** with

Et_3SiH for 5 min prior to adding the $Pd(OAc)_2$, it is likely that the reduction to form **27** has already been initiated.

The reaction of complex **26** with Et_3SiH (1.5 mol equiv) was followed by ^1H NMR spectroscopy, but showed no formation of an Ir-H species. (Figure 5.10). However, complex **13** which has no reducible functional groups exhibited an Ir-H resonance at -12.46 ppm within 5 min (Figure 5.11). Interestingly, the catalytic reduction of **L26** to the secondary amine could be performed using 10% mol catalyst of complex **13** with Et_3SiH (Figure 5.12), while in the presence of the Pd catalyst no reduction occurred. This could imply that the ability to form an Ir-H species may be responsible for the reduction of the imine bond in **26** and the presence of the Pd catalyst is not necessary. The work reported here appears to be the first finding of the reduction of a bond within an organo-iridium complex that is initiated *via* the complex itself.

Recently, it was reported that the complex [(η^5-Cp*)Ir(2-phenylpyridine)Cl] could reduce imines to secondary amines in the presence of Et_3SiH, although good yields were only found upon removal of the chloride ligand using an additive such as $NaBArF_{24}$. The mechanism of hydrosilylation was not confirmed, but a possible route hypothesised was *via* formation of the Ir-H species.[39]

During the reaction with complex **26**, the loss of the hydride from Et_3SiH appears to result in the formation of ethoxy silyl species Et_3SiOEt, as is evident from the appearance of a new set of peaks which integrate to an ethoxy species in the ^1H NMR spectrum (Figure 5.9). At first, the Et_3SiCl species would seem the most plausible by-product, *via* substitution with the chlorido monodentate ligand. However, as shown in the reaction of Et_3SiH with complex **13**, the chloride adduct remains dominant in solution whilst the consumption of Et_3SiH takes place. It has

been reported that reaction of Et_3SiH with $InCl_3$ in the presence of MeOH to reduce iminium bonds results in the formation of the methoxy silyl species Et_3SiOMe, rather than the presumed chloride species.[40]

A possible reduction mechanism is shown in Figure 5.24 based on the ^1H NMR experiments on **26** and **13** with Et_3SiH in ethanol. Formation of an Ir-H species of **26** occurs through reaction with Et_3SiH, alongside the formation of Et_3SiOEt by reaction with EtOH, followed with production of HCl (**A**). Protonation of the imino nitrogen of another molecule of **26** activates the imine towards nucleophilic attack by the Ir-H species, forming the secondary amine complex **27** (**B**), where association of the chloride with the 16 electron complex $[(\eta^5\text{-Cp*})\text{Ir(2-PhPy)}]^+$ re-forms **26** (**C**). Due to the position of the imine bond it is unlikely that intramolecular hydride transfer can occur, therefore, intermolecular transfer is more likely. The fast reduction of the imine bond may be responsible for the lack of Ir-H peak observed during the reaction with **26**. Another possible mechanism could involve a sacrificial amount of complex **26** being converted to the Ir-H species, which upon hydride transfer, immediately forms more Ir-H upon reaction with Et_3SiH, rather than re-association with the chloride.

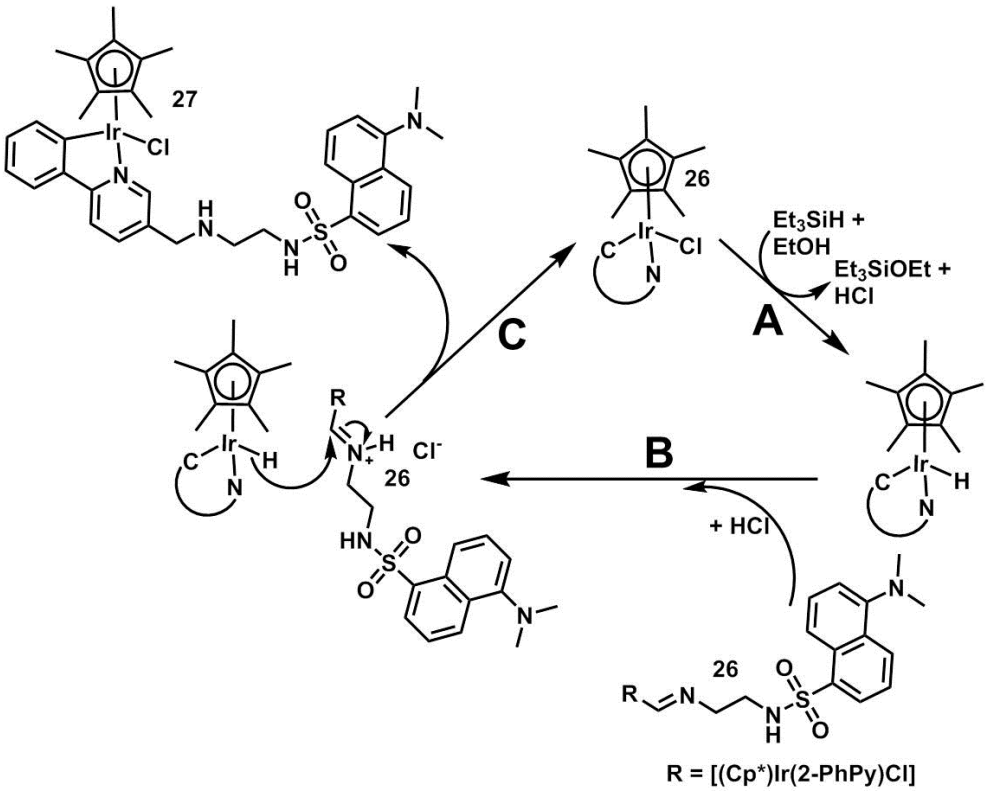

Figure 5.24. Proposed reaction scheme for the reduction of complex **26** to **27** using Et_3SiH.

5.4.3 Aqueous Stability of Complexes 21-27

Imine bonds are known to be unstable in aqueous solution, and the extent of hydrolysis tends to increase as the pH of the solution is decreased. Having a labile bond which is pH-sensitive may be advantageous where a tag that has been used as a targeting moiety (e.g. folic acid for uptake into FR^+ cells), or possibly another cytotoxic agent, is cleaved in the acidic microtumour environment (pH < 6.5).[41] This concept was examined with the imine conjugates **21-26** by studying the stability of the imino bond at various pH values.

After 15 min at pH 7.5 (buffered), complexes **21-26** showed between 2-18% hydrolysis of the imine bond, which increased to 21-86% after 3 h. There appears to be no correlation between the type of amine conjugate (aliphatic vs. aromatic) and

the extent of imine hydrolysis. At more acidic pH*, the extent of hydrolysis increased after 15 min. The decrease in the extent of hydrolysis after 3 h for complexes **23-26** at lower pH* can be attributed to the release of the aliphatic amine in an unbuffered solution. The pK_a of aliphatic amines is around 10,[42] therefore release of basic amines will increase the pH* of the solution, which was also observed experimentally after 24 h. This may result in a decrease in the rate of hydrolysis. The pK_a of aromatic amines is lower, at around 4.5 for aniline, which results in a less pronounced effect on the basicity of the unbuffered aqueous solution. Therefore, it is possible that under the acidic microtumour environment, an enhancement of imine hydrolysis may occur which could make these conjugates suitable for cleavage inside cancer cells.

The secondary amine complex **27** exhibited excellent stability in aqueous solution, showing that the reduction of the imine bond can yield conjugates are stable in aqueous solution, making it more suitable for tracking the complex by fluorescence microscopy than the imine complex **26**.

5.4.4 Fluorescence of Complexes 26 and 27

The addition of a fluorescent moiety to metal complexes can be a useful strategy for assessing the compartmentalisation of the complex and hence the study of possible biological targets. Complexes **26** and **27** (50 μM) which bear the fluorescent dansyl-amine tag showed fluorescence in DCM (Figure 5.14) while the parent aldehyde complex **6** exhibited no emission, demonstrating that the presence of the fluorescent chromophore is required. It is evident that a reduction in the fluorescence intensity is observed upon conjugation of the fluorophore to the complexes, although causes of this reduction were not investigated further.

The reduced fluorescence in aqueous solution compared to organic solvents (Figure 5.15) is a common phenomenon observed for both the dansyl-amine tag and complex **27** (10% MeOH, 90% H_2O v/v). Oxygen gas is also known to be an effective collisional quencher of fluorescence,[43] which may play a greater role in aqueous solution over DCM. Fluorescent compounds such as PI exhibit weak fluorescence in aqueous solution, but upon intercalation between DNA base pairs (which leads to the fluorophore being in a more hydrophobic environment), its fluorescence increases around 30-fold.[44] Octahedral Ir(III) complexes of the type $[Ir(2\text{-}PhPy)_2(N,N)]^+$ (N,N = dpq, dpqa, dppz, dppn) also show this behaviour, where binding to CT-DNA results in an increase in luminescence intensity in comparison to aqueous buffered solutions,[45,46] which has been attributed to reduced hydrogen bonding between the chelating ligand and water molecules when bound to DNA. The fluorescence was examined for complex **27** in A2780 cells (Figure 5.16) which showed only autofluorescence (fluorescence exhibited naturally by cells from proteins). As **27** exhibits vastly reduced fluorescence in aqueous solution this may mean that **27** does not interact with biological molecules that can provide a sufficiently hydrophobic environment. Another possible factor might be the extent of accumulation of **27** in A2780 cells is too low to provide a fluorescence signal.

Although complex **27** appears to be unsuitable for fluorescence microscopy, it has been demonstrated that a fluorophore can be successfully conjugated to complex **6**, which may result in the exploration of other fluorescent molecules (e.g. PI, EtBr) that can be conjugated and studied for their potential as fluorescent probes for Ir(III) half-sandwich complexes.

5.4.5 Reactions of Complex 6 with Lysine-Containing Peptides

There is great interest in the attachment of peptides to metal complexes, which can be beneficial for specific uptake in cancer cells through processes such as receptor recognition.[47] The conjugation of peptides to metal complexes can be achieved *via* click chemistry[48] or even palladium cross-coupling,[49] although an artificial peptide is required that contains the required functional group, such as an alkyne or iodine substituent. Traditional peptide coupling techniques using Fmoc protected amino acids have also been demonstrated for the half-sandwich Os(II) complex [(η^5-biphenyl)Os(picolinate)Cl].[5]

Complex **6** reacted with the lysine residue in the peptides Substance P (SubP) (Figures 5.18-5.19) and [Lys-3]-bombesin (L3BBS) (Figures 5.20-5.21) *via* the aldehyde group on the chelating ligand, forming an imine conjugate as determined by FT-ICR MS. It is worth noting that SubP is an important neuropeptide in pain perception and inflammatory disease,[50] and bombesin (similar in structure to L3BBS, in which the lysine residue is originally arginine in bombesin) is a tumour marker for small cell lung carcinoma.[51] The ability to conjugate SubP to complex **6** could lead to a new method for studying pain perception (by the ability to analyse concentration/location of iridium using MS/ICP techniques).

With further investigation, this highlights that the reaction could be the basis of a new metal-peptide conjugation system. Interestingly, multiple binding modes can be exhibited with peptides when histidine is present, as in the case with L3BBS. Incubation of complex **6** with L3BBS led to two conjugates as determined by MS. FT-ICR ECD MS/MS showed that the secondary binding mode involved iridium binding to the histidine residue (Figure 5.22), based on the fragmentation of the peptide backbone. Therefore, if a synthetic methodology were to be developed, it

may be necessary to use a peptide that does not contain histidine. It appears that sulfur-containing methionine (which has been previously been shown to bind to metal complexes)[31] does not bind in this system, however, cysteine sulfur may bind in a similar fashion to GSH as observed for complex **13** in Chapter 4.

The conjugation of BSA (which contains surface lysine residues) at pH 8.7 to octahedral Ir(III) complexes bearing the aldehyde *C,N*- chelating ligand (2-quinolyl)benzaldehyde has been reported with the reduction of the imine being performed using $NaCNBH_3$ in order to make a stable Ir-BSA conjugate.[19] Although the incubations performed in this study were purely a proof-of-concept work, the aqueous instability of the imine conjugate would require a reducing agent to form the stable secondary amine, as purification of metal-peptide conjugates requires the use of RP-HPLC. $NaCNBH_3$ appears to be incompatible with the half-sandwich Ir(III) complexes studied here. Therefore, future work into the conjugation of lysine-containing peptides under alternative conditions (i.e. DMF) followed by reduction using the more complex-friendly Et_3SiH reducing agent may lead to new iridium-peptide conjugates.

5.5 Conclusions

A conjugation strategy for the post-modification of the half-sandwich Ir(III) anticancer complex [(η^5-Cp*)Ir(2-phenyl-5-pyridinecarboxaldehyde)Cl] **6** bearing an aldehyde functional group has been devised, whereby aliphatic and aromatic amines can be conjugated to form new Schiff base complexes. Using microwave-assisted chemistry, new conjugates were synthesised in ca. 5 min, compared with other coupling techniques such as copper click chemistry, or palladium Sonogashira

coupling which require catalysts, longer reaction times and oxygen-free reaction conditions.

Aqueous stability studies showed that hydrolysis of the imine bond in Schiff base complexes **21-26** can increase at more acidic pH, although, release of aliphatic amines in unbuffered solutions effectively decreases the extent of hydrolysis as a consequence of increasing the pH of the solution. This may make these conjugates suitable for cleavage inside cancer cells where the pH is generally slightly acidic. Further study is warranted on the possibility of exploiting this for delivery of other cytotoxic agents, or for the cleavage of a tag that has been used for targeted delivery of the Ir(III) complex.

Studies on stabilising the imine bond towards hydrolysis using the mild reducing reagent Et_3SiH with catalytic amounts of $Pd(OAc)_2$ showed that the secondary amine complex **27** could be synthesised from the corresponding Schiff base complex **26**. Intriguingly, studies into the reactivity of complex **26** with Et_3SiH without the Pd catalyst showed that reduction to **27** could be performed giving the same product as identified by ^1H NMR spectroscopy. Hence, the reduction of the imine bond is independent on the use of the Pd catalyst. Preliminary studies into the possible mechanism of reduction have revealed that an Ir-H species may be involved, which can reduce the imine bond of another molecule of **26**, effectively exploiting the catalytic ability of chelated half-sandwich Ir(III) complexes to initiate the reduction.

The addition of the fluorescent dansyl group resulted in complexes that showed fluorescence in chlorinated solvents (**26** and **27**), but minimal fluorescence in aqueous media (**27**). Complex **27** also showed that no fluorescence in A2780 cells, which may be as a consequence of either not residing in a sufficiently hydrophobic environment (i.e. cytosol) or the cellular accumulation of **27** was too low for a

fluorescence signal. However, the successful conjugation of a fluorophore to a half-sandwich Ir(III) anticancer complex has been performed demonstrating the proof-of principle.

Finally, the reaction of complex **6** with the lysine-containing peptides Substance P and [Lys-3]-bomesin revealed that new Schiff bases conjugates can be formed *via* reaction with lysine residues, as determined by FT-ICR-MS (MS/MS) techniques which can accurately pinpoint the site of conjugation. This may lead to the development of a conjugation strategy for forming iridium-peptide complexes using mild conditions.

5.6 References

(1) Babak, M. V.; Plażuk, D.; Meier, S. M.; Arabshahi, H. J.; Reynisson, J.; Rychlik, B.; Błauż, A.; Szulc, K.; Hanif, M.; Strobl, S.; Roller, A.; Keppler, B. K.; Hartinger, C. G. *Chem. Eur. J* **2015**, *21*, 5110.

(2) Morrison, D. E.; Aitken, J. B.; de Jonge, M. D.; Ioppolo, J. A.; Harris, H. H.; Rendina, L. M. *Chem. Commun.* **2014**, *50*, 2252.

(3) Wang, X.; Guo, Z. *Chem. Soc. Rev.* **2013**, *42*, 202.

(4) Pathak, R. K.; McNitt, C. D.; Popik, V. V.; Dhar, S. *Chem. Eur. J* **2014**, *20*, 6861.

(5) Van Rijt, S. H.; Kostrhunova, H.; Brabec, V.; Sadler, P. J. *Bioconjugate Chem.* **2011**, *22*, 218.

(6) Kuil, J.; Steunenberg, P.; Chin, P. T. K.; Oldenburg, J.; Jalink, K.; Velders, A. H.; van Leeuwen, F. W. B. *ChemBioChem* **2011**, *12*, 1897.

(7) Gandioso, A.; Shaili, E.; Massaguer, A.; Artigas, G.; Gonzalez-Canto, A.; Woods, J. A.; Sadler, P. J.; Marchan, V. *Chem. Commun.* **2015**, *51*, 9169.

(8) Noor, F.; Kinscherf, R.; Bonaterra, G. A.; Walczak, S.; Wölfl, S.; Metzler-Nolte, N. *ChemBioChem* **2009**, *10*, 493.

(9) Liu, Z.; Sadler, P. J. *Acc. Chem. Res.* **2014**, *47*, 1174.

(10) Medici, S.; Peana, M.; Nurchi, V. M.; Lachowicz, J. I.; Crisponi, G.; Zoroddu, M. A. *Coord. Chem. Rev.* **2015**, *284*, 329.

(11) Novohradsky, V.; Liu, Z.; Vojtiskova, M.; Sadler, P. J.; Brabec, V.; Kasparkova, J. *Metallomics* **2014**, *6*, 682.

(12) Liu, Z.; Salassa, L.; Habtemariam, A.; Pizarro, A. M.; Clarkson, G. J.; Sadler, P. J. *Inorg. Chem.* **2011**, *50*, 5777.

(13) Liu, Z.; Habtemariam, A.; Pizarro, A. M.; Clarkson, G. J.; Sadler, P. J. *Organometallics* **2011**, *30*, 4702.

(14) Ruiz, J.; Rodriguez, V.; Cutillas, N.; Samper, K. G.; Capdevila, M.; Palacios, O.; Espinosa, A. *Dalton Trans.* **2012**, *41*, 12847.

(15) Ruiz, J.; Rodríguez, V.; Cutillas, N.; Espinosa, A.; Hannon, M. J. *Inorg. Chem.* **2011**, *50*, 9164.

(16) Hoffmanns, U.; Metzler-Nolte, N. *Bioconjugate Chem.* **2006**, *17*, 204.

(17) Gasser, G.; Pinto, A.; Neumann, S.; Sosniak, A. M.; Seitz, M.; Merz, K.; Heumann, R.; Metzler-Nolte, N. *Dalton Trans.* **2012**, *41*, 2304.

(18) Chtchigrovsky, M.; Eloy, L.; Jullien, H.; Saker, L.; Ségal-Bendirdjian, E.; Poupon, J.; Bombard, S.; Cresteil, T.; Retailleau, P.; Marinetti, A. *J. Med. Chem.* **2013**.

(19) Lee, P.-K.; Liu, H.-W.; Yiu, S.-M.; Louie, M.-W.; Lo, K. K.-W. *Dalton Trans.* **2011**, *40*, 2180.

(20) Wang, J.; Pham, D.-T.; Kee, T. W.; Clafton, S. N.; Guo, X.; Clements, P.; Lincoln, S. F.; Prud'homme, R. K.; Easton, C. J. *Macromolecules* **2011**, *44*, 9782.

(21) Hwang, T. L.; Shaka, A. J. *J. Magn. Reson.* **1995**, *112*, 275.

(22) Jennings, K. R. *Int. J. Mass. Spectrom. Ion. Phys.* **1968**, *1*, 227.

(23) Zubarev, R. A.; Kelleher, N. L.; McLafferty, F. W. *J. Am. Chem. Soc.* **1998**, *120*, 3265.

(24) Roepstorff, P.; Fohlman, J. *Biol. Mass Spectrom.* **1984**, *11*, 601.

(25) Mirza-Aghayan, M.; Boukherroub, R.; Rahimifard, M. *Appl. Organomet. Chem.* **2013**, *27*, 174.

(26) Gottlieb, H. E.; Kotlyar, V.; Nudelman, A. *J. Org. Chem* **1997**, *62*, 7512.

(27) Uchida, K. *Free Radical Biol. Med.* **2000**, *28*, 1685.

(28) Kergonou, J.-F.; Marais, D.; Lafite, C.; Pennacino, I.; Ducousso, R. *Biochimie* **1987**, *69*, 1153.

(29) Hu, W.; Luo, Q.; Wu, K.; Li, X.; Wang, F.; Chen, Y.; Ma, X.; Wang, J.; Liu, J.; Xiong, S.; Sadler, P. J. *Chem. Commun.* **2011**, *47*, 6006.

(30) Qi, Y.; Liu, Z.; Li, H.; Sadler, P. J.; O'Connor, P. B. *Rapid Commun. Mass Spectrom.* **2013**, *27*, 2028.

(31) Williams, J. P.; Brown, J. M.; Campuzano, I.; Sadler, P. J. *Chem. Commun.* **2010**, *46*, 5458.

(32) Lidström, P.; Tierney, J.; Wathey, B.; Westman, J. *Tetrahedron* **2001**, *57*, 9225.

(33) Hopmann, K. H.; Bayer, A. *Coord. Chem. Rev.* **2014**, *268*, 59.

(34) Mirza-Aghayan, M.; Boukherroub, R.; Bolourtchian, M. *Appl. Organomet. Chem.* **2006**, *20*, 214.

(35) Mandal, P. K.; McMurray, J. S. *J. Org. Chem.* **2007**, *72*, 6599.

(36) Yang, J.; Brookhart, M. *Adv. Synth. Catal.* **2009**, *351*, 175.

(37) Yang, J.; Brookhart, M. *J. Am. Chem. Soc.* **2007**, *129*, 12656.

(38) Lai, R.-Y.; Lee, C.-I.; Liu, S.-T. *Tetrahedron* **2008**, *64*, 1213.

(39) Corre, Y.; Iali, W.; Hamdaoui, M.; Trivelli, X.; Djukic, J. P.; Agbossou-Niedercorn, F.; Michon, C. *Catal. Sci. Tech.* **2015**, *5*, 1452.

(40) Lee, O.-Y.; Law, K.-L.; Ho, C.-Y.; Yang, D. *J. Org. Chem* **2008**, *73*, 8829.

(41) Fukamachi, T.; Chiba, Y.; Wang, X.; Saito, H.; Tagawa, M.; Kobayashi, H. *Cancer Lett.* **2010**, *297*, 182.

(42) Brown, W.; Foote, C.; Iverson, B.; Anslyn, E. *Organic Chemistry*; Cengage Learning, 2011.

(43) Lakowicz, J. R.; Weber, G. *Biochemistry* **1973**, *12*, 4161.

(44) Meurant, G. *Methods in Cell Biology: Fluorescence Microscopy of Living Cells in Culture*; Elsevier Science, 1989; Vol. 30.

(45) Lo, K. K.-W.; Li, S. P.-Y.; Zhang, K. Y. *New J. Chem.* **2011**, *35*, 265.

(46) Lo, K. K.-W.; Chung, C.-K.; Zhu, N. *Chem. Eur. J* **2006**, *12*, 1500.

(47) Metzler-Nolte, N. *CHIMIA* **2007**, *61*, 736.

(48) Köster, S. D.; Dittrich, J.; Gasser, G.; Hüsken, N.; Henao Castañeda, I. C.; Jios, J. L.; Della Védova, C. O.; Metzler-Nolte, N. *Organometallics* **2008**, *27*, 6326.

(49) Pfeiffer, H.; Rojas, A.; Niesel, J.; Schatzschneider, U. *Dalton Trans.* **2009**, 4292.

(50) O'Connor, T. M.; O'Connell, J.; O'Brien, D. I.; Goode, T.; Bredin, C. P.; Shanahan, F. *J. Cell. Physiol.* **2004**, *201*, 167.

(51) Bostwick, D. G.; Roth, K. A.; Evans, C. J.; Barchas, J. D.; Bensch, K. G. *Am. J. Pathol.* **1984**, *117*, 195.

Chapter 6

Phenyliminopyridyl Half-sandwich Iridium(III) Complexes: Characterisation, Solution Chemistry and Biological Activity

6.1 Introduction

The success of cisplatin and its second generation counterparts carboplatin and oxaliplatin for the treatment of cancers including testicular, ovarian and bladder has led to a wide variety of different metals being studied as potential anticancer agents.[1] Chelated piano stool complexes of Ru(II), Os(II) and Ir(III) have shown promise, in which greater potency and selectivity than cisplatin has been observed in some cases.[2,3] Properties such as hydrophobicity can be tuned *via* the capping ligand[4] and functionality on the chelating ligand (as demonstrated in Chapter 3). Reactivity at the metal centre towards biomolecules can be controlled by careful selection of the type of chelating ligand[5] (i.e. hydrogen bonding sites for enhanced interaction with nucleobases) and monodentate ligands.[6,7]

Despite the increasing rise in antibacterial resistance, very little research has been undertaken on half-sandwich metal complexes as antibacterial agents,[8-10] where Ru(II) complexes have been the most widely studied.[8,11-13] The mode of antibacterial action has not been fully elucidated, although Ru(II) complexes of the type [(η^5-*p*-cymene)Ru(2-methoxyphenyl-bis(3,5-dimethylpyrazol-1-yl)methane)OH_2]$(ClO_4)_2$ appear to bind to DNA *in vitro* in *E. coli*.[10] This mechanism is similar to that proposed for some chelated Ru(II) half-sandwich anticancer complexes.[14,15]

The use of Ir(III) half-sandwich complexes as antibacterial agents is limited to only a few studies. Previously reported neutral *N,O*-chelated half-sandwich complexes [(η^5-Cp*)M(quinolin-8-olate)Cl] (M = Ir(III) or Rh(III)) showed good activity for the Rh(III) complex against Gram-positive bacteria while the Ir(III) analogue was less effective.[9] Half-sandwich Ir(III) aminoacidato complexes have also been evaluated as antibacterial agents against Mycobaterium, where the presence of hydrophobic

side-chains (i.e. proline, valine, phenylalanine) promoted high activity.[16] The mechanism of action of these complexes has not been investigated and so desirable properties for piano-stool Ir(III) complexes as antibacterial agents has not been established.

There has been little reported research on the chemical and biological properties of *N*-(pyrid-2-ylmethylene)amine (ImPy) half-sandwich Ir(III) complexes,[17,18] although a common ligand set for Ru(II) piano stool complexes.[19-21] In general, coordination of neutral *N,N*-chelating ligands results in less potent antiproliferative agents towards mammalian cells than anionic *N,N*- or *C,N*-chelating ligands in Ir(III) complexes,[22,23] presumably as a consequence of increased hydrophobicity leading to enhanced cellular accumulation. This may be advantageous for the design of antibacterial agents, where reduced cytotoxicity towards mammalian cells is desirable.

A set of ImPy ligands was used to synthesise novel Ir(III) Cp*, Cp^{xPh} and Cp^{xBiPh} complexes (Chart 6.1). The synthesis, characterisation and solution chemistry are presented, with preliminary investigations into the effect on the nature of the chelating ligand and Cp^{x} capping ligand on antibacterial activity against Gram positive *S. aureus*, Gram negative *E. coli*, and their anticancer activity against A2780 human ovarian cancer cells.

Chart 6.1. Half-sandwich iridium(III) complexes bearing phenyliminopyridine ligands synthesised and studied in this chapter.

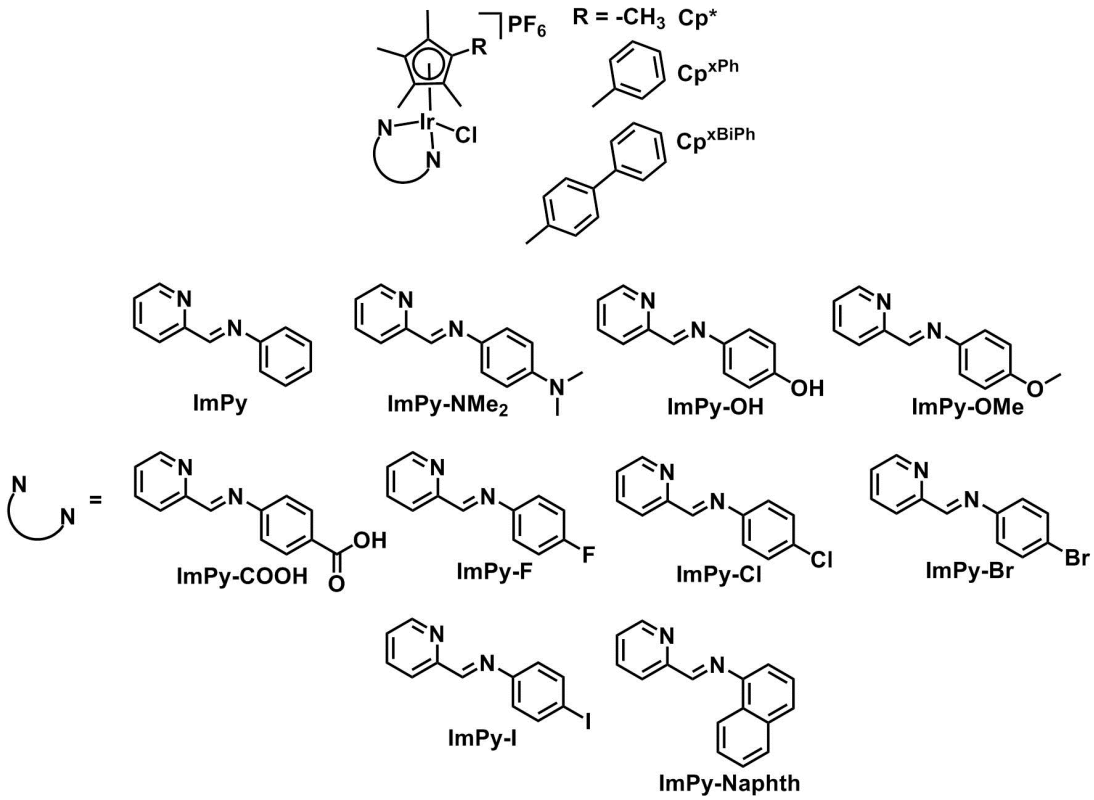

Complex	Chelating Ligand	Cp^x	Complex	Chelating Ligand	Cp^x
28	ImPy	Cp*	**37**	ImPy-F	Cp*
29	ImPy-NMe_2	Cp*	**38**	ImPy-Cl	Cp*
30	ImPy-NMe_2	Cp^{xPh}	**39**	ImPy-Br	Cp*
31	ImPy-NMe_2	Cp^{xBiPh}	**40**	ImPy-I	Cp*
32	ImPy-OH	Cp*	**41**	ImPy-I	Cp^{xPh}
33	ImPy-OH	Cp^{xPh}	**42**	ImPy-I	Cp^{xBiPh}
34	ImPy-OH	Cp^{xBiPh}	**43**	ImPy-Naphth	Cp*
35	ImPy-OMe	Cp*	**44**	ImPy-Naphth	Cp^{xPh}
36	ImPy-COOH	Cp*	**45**	ImPy-Naphth	Cp^{xBiPh}

6.2 Experimental Section

6.2.1 Materials

$IrCl_3.3H_2O$ (99%) was purchased from Precious Metals Online (Australia). 1,2,3,4,5-Pentamethylcyclopentadiene (95%), 2,3,4,5-tetramethyl-2-cyclopentenone (95%), 4-bromobiphenyl (98%), n-butyllithium (1.6 M in hexanes), phenyllithium (1.6 M in dibutylether), 2-pyridinecarboxaldehyde (99%), aniline (98%), *N*-*N*-dimethyl-*p*-phenylenediamine (97%), 4-aminophenol (≥98%), *p*-anisidine (≥99%), 4-aminobenzoic acid (≥99%), 4-fluoroaniline (99%), 4-chloroaniline (98%), 4-bromoaniline (97%), 4-iodoaniline (98%), 2-naphthylamine (≥99%), ammonium hexafluorophosphate (≥95%) and NaCl (>99.999%) were purchased from Sigma-Aldrich (UK). Solvents used for synthesis were of laboratory grade and used without further purification. Solvents for HPLC purity examination and relative hydrophobicity determination (water and acetonitrile) were of HPLC grade with added trifluoroacetic acid or NaCl which was purchased from Sigma-Aldrich (UK). The synthesis of dimers $[(\eta^5\text{-Cp*})IrCl_2]_2$, $[(\eta^5\text{-Cp}^{xPh})IrCl_2]_2$ and $[(\eta^5\text{-Cp}^{xBiPh})IrCl_2]_2$ is described in Chapter 2.

6.2.2 Syntheses

6.2.2.1 Synthesis of Iminopyridine Ligands

***N*-(2-Pyridylmethylene)-benzenamine (ImPy-H)** 2-Pyridinecarboxaldehyde (287 mg, 255 µL, 2.68 mmol) was dissolved in MeCN (25 mL) followed by addition of aniline (250 mg, 245 µL, 2.68 mmol) and heated at reflux under N_2 for 18 h. The reaction mixture was cooled to ambient temperature and solvent removed under reduced pressure to yield the product as a brown oil, with no

further purification performed (401 mg, 82%). **^{1}H NMR** (400 MHz, dmso-d_6) δ = 8.72 (dq, 1H, J = 4.8, 1.0 Hz), 8.59 (s, 1H), 8.16 (dt, 1H, J = 7.8, 1.0 Hz), 7.94 (td, 1H, J = 7.6, 1.8 Hz), 7.52 (ddd, 1H, J = 7.4, 4.8, 1.3 Hz), 7.46-7.41 (m, 2H), 7.34-7.27 (m, 3H). **ESI-MS** (MeOH) m/z = 183.1 $[M+H]^+$.

***N,N*-Dimethyl-*N*-(2-pyridylmethylene)-1,4-benzenediamine (ImPy-NMe$_2$)** As for **ImPy-H** using 2-pyridinecarboxaldehyde (197 mg, 175 μL, 1.84 mmol), MeCN (25 mL) and *N*-*N*-dimethyl-*p*-phenylenediamine (250 mg, 1.84 mmol). The product was isolated as a green solid (299 mg, 90%). **^{1}H NMR** (400 MHz, dmso-d_6) δ = 8.66 (dq, 1H, J = 4.8, 1.0 Hz), 8.62 (s, 1H), 8.11 (dt, 1H, J = 8.0, 0.9 Hz), 7.90 (td, 1H, J = 7.7, 1.6 Hz), 7.45 (ddd, 1H, J = 7.4, 4.8, 1.2 Hz), 7.36 (d, 2H, J = 9.0 Hz), 6.77 (d, 2H, J = 9.0 Hz), 2.95 (s, 6H). **ESI-MS** (MeOH) m/z = 226.1 $[M+H]^+$.

4-[(2-Pyridylmethylene)amino]-phenol (ImPy-OH) As for **ImPy-H** using 2-pyridinecarboxaldehyde (245 mg, 218 μL, 2.29 mmol), MeCN (25 mL) and 4-aminophenol (250 mg, 2.29 mmol). The reaction mixture was cooled to ambient temperature where a light green solid formed; this was isolated by filtration under reduced pressure and washed with hexane (310 mg, 68%). **^{1}H NMR** (400 MHz, dmso-d_6) δ = 9.67 (bs, 1H), 8.68 (dq, 1H, J = 4.8, 1.0 Hz), 8.60 (s, 1H), 8.11 (dt, 1H, J = 7.9, 1.0 Hz), 7.92 (td, 1H, J = 7.6, 1.4 Hz), 7.48 (ddd, 1H, J = 7.4, 4.8, 1.2 Hz), 7.29 (d, 2H, J = 8.8 Hz), 6.83 (d, 2H, J = 8.8 Hz). **ESI-MS** (MeOH) m/z = 221.0 $[M+Na]^+$.

4-Methoxy-*N*-(2-pyridylmethylene)-benzenamine (ImPy-OMe) As for **ImPy-H** using 2-pyridinecarboxaldehyde (217 mg, 193 μL, 2.03 mmol), MeCN (25 mL) and *p*-anisidine (250 mg, 2.03 mmol). The product isolated as a brown oil (332

mg, 77%). **^{1}H NMR** (400 MHz, $CDCl_3$) δ = 8.68 (dq, 1H, J = 4.8, 1.0 Hz), 8.62 (s, 1H), 8.17 (dt, 1H, J = 7.9, 1.0 Hz), 7.78 (td, 1H, J = 7.7, 1.7 Hz), 7.34-7.30 (m, 3H), 6.94 (d, 2H, J = 8.9 Hz), 3.82 (s, 3H). **ESI-MS** (MeOH) m/z = 213.0 $[M+H]^+$.

4-[(2-Pyridylmethylene)amino]-benzoic acid (ImPy-COOH) As for **ImPy-H** using 2-pyridinecarboxaldehyde (195 mg, 173 µL, 1.82 mmol), MeCN (25 mL) and 4-aminobenzoic acid (250 mg, 1.82 mmol). The reaction mixture was cooled to ambient temperature where the pale yellow solid formed which was isolated by filtration under reduced pressure and washed with hexane (325 mg, 79%). **^{1}H NMR** (400 MHz, dmso-d_6) δ = 12.92 (bs, 1H), 8.75 (dq, 1H, J = 4.8, 1.0 Hz), 8.59 (s, 1H), 8.17 (dt, 1H, J = 7.9, 0.9 Hz), 8.02-7.96 (m, 3H), 7.57 (ddd, 1H, J = 7.5, 4.8, 1.2 Hz), 7.38 (d, 2H, J = 8.6 Hz). **ESI-MS** (MeOH) m/z = 249.0 $[M+Na]^+$.

4-Fluoro-*N*-(2-pyridylmethylene)-benzenamine (ImPy-F) As for **ImPy-H** using 2-pyridinecarboxaldehyde (240 mg, 214 µL, 2.25 mmol), MeCN (25 mL) and 4-fluoroaniline (250 mg, 2.25 mmol). The product isolated as a brown solid (400 mg, 89%). **^{1}H NMR** (400 MHz, dmso-d_6) δ = 8.72 (dq, 1H, J = 4.8, 1.0 Hz), 8.60 (s, 1H), 8.14 (dt, 1H, J = 7.9, 0.9 Hz), 7.95 (td, 1H, J = 7.8, 1.7 Hz), 7.53 (ddd, 1H, J = 7.5, 4.8, 1.2 Hz), 7.44-7.39 (m, 2H), 7.30-7.24 (m, 2H). **ESI-MS** (MeOH) m/z = 201.0 $[M+H]^+$.

4-Chloro-*N*-(2-pyridylmethylene)-benzenamine (ImPy-Cl) As for **ImPy-H** using 2-pyridinecarboxaldehyde (210 mg, 186 µL, 1.96 mmol), MeCN (25 mL) and 4-chloroaniline (250 mg, 1.96 mmol). The product isolated as a brown solid (370 mg, 87%). **^{1}H NMR** (400 MHz, dmso-d_6) δ = 8.73 (dq, 1H, J = 4.8, 1.0 Hz), 8.60 (s, 1H), 8.15 (dt, 1H, J = 7.9, 1.0 Hz), 7.96 (td, 1H, J = 7.6, 1.7 Hz), 7.54

(ddd, 1H, J = 7.5, 4.8, 1.2 Hz), 7.49 (d, 2H, J = 8.7 Hz), 7.37 (d, 2H, J = 8.7 Hz). **ESI-MS** (MeOH) m/z = 217.0 $[M+H]^+$.

4-Bromo-*N*-(2-pyridylmethylene)-benzenamine (ImPy-Br) As for **ImPy-H** using 2-pyridinecarboxaldehyde (156 mg, 138 μL, 1.45 mmol), MeCN (25 mL) and 4-bromoaniline (250 mg, 1.45 mmol). The product isolated as a brown solid (230 mg, 61%). **^{1}H NMR** (400 MHz, dmso-d_6) δ = 8.72 (dq, 1H, J = 4.8, 1.0 Hz), 8.59 (s, 1H), 8.14 (dt, 1H, J = 7.9, 0.9 Hz), 7.95 (td, 1H, J = 7.6, 1.6 Hz), 7.61 (d, 2H, J = 8.6 Hz), 7.54 (ddd, 1H, J = 7.5, 4.8, 1.2 Hz), 7.30 (d, 2H, J = 8.6 Hz). **ESI-MS** (MeOH) m/z = 260.9 $[M+H]^+$.

4-Iodo-*N*-(2-pyridylmethylene)-benzenamine (ImPy-I) As for **ImPy-H** using 2-pyridinecarboxaldehyde (122 mg, 109 μL, 1.14 mmol), MeCN (25 mL) and 4-iodoaniline (250 mg, 1.14 mmol). The product isolated as a brown solid (278 mg, 79%). **^{1}H NMR** (400 MHz, dmso-d_6) δ = 8.73 (dq, 1H, J = 4.8, 1.0 Hz), 8.58 (s, 1H), 8.15 (dt, 1H, J = 7.9, 1.0 Hz), 7.96 (td, 1H, J = 7.8, 1.7 Hz), 7.78 (d, 2H, J = 8.6 Hz), 7.55 (ddd, 1H, J = 7.5, 4.8, 1.2 Hz), 7.16 (d, 2H, J = 8.6 Hz). **ESI-MS** (MeOH) m/z = 308.9 $[M+H]^+$.

***N*-(2-Pyridnylmethylene)-1-naphthalenamine (ImPy-Naphth)** As for **ImPy-H** using 2-pyridinecarboxaldehyde (187 mg, 166 μL, 1.76 mmol), MeCN (25 mL) and 2-naphthylamine (250 mg, 1.76 mmol). The reaction mixture was cooled to ambient temperature and solvent removed under yielding a dark brown oil. (350 mg, 85%). **^{1}H NMR** (300 MHz, acetone-d_6) δ = 8.75 (d, 1H, J = 4.8Hz), 8.72 (s, 1H), 8.43-8.38 (m, 2H), 7.99-7.90 (m, 2H), 7.82 (d, 1H, J = 8.2 Hz), 7.59-7.47 (m, 4H), 7.26 (d, 1H, J = 7.3 Hz). **ESI-MS** (MeOH) m/z = 233.3 $[M+H]^+$.

6.2.2.2 Synthesis of [(η^5-Cp^x)Ir(ImPy)Cl]PF$_6$ Complexes

[(η^5-Cp*)Ir(ImPy-H)Cl]PF$_6$ (28) To [(η^5-Cp*)IrCl$_2$]$_2$ (66 mg, 0.083 mmol), MeOH (20 mL) was added to form a suspension which was stirred at ambient temperature under N_2 for 10 min. ImPy-NMe$_2$ (30 mg, 0.166 mmol) was added and the reaction mixture stirred at ambient temperature under N_2 for 15 h. The solution was concentrated to ca. 10 mL on a rotary evaporator followed by addition of NH_4PF_6 (67 mg, 0.415 mmol) which resulted in a precipitate. This was isolated *via* filtration under reduced pressure and washed with cold MeOH and hexane. The solid was then dissolved in acetone and filtered through celite, where the filtrate was concentrated to dryness and further dried under vacuum, yielding the product as an orange crystalline solid (95 mg, 83%). **^{1}H NMR** (400 MHz, dmso-d$_6$) δ =9.39 (s, 1H), 9.06 (d, 1H, J = 5.2 Hz), 8.42 (dd, 1H, J = 7.6, 1.1 Hz), 8.35 (td, 1H, J = 7.7, 1.2 Hz), 7.95 (ddd, 1H, J = 7.4, 5.6, 1.7 Hz), 7.70-7.62 (m, 4H), 7.55 (tt, 1H, J = 7.1, 1.6 Hz), 1.42 (s, 15H). **ESI-MS** (MeOH) m/z = 545.0 [M-PF$_6$]$^+$. **CHN analysis** calc. for $C_{22}H_{25}N_2ClF_6IrP$ C – 38.29%, H – 3.65%, N – 4.06%. Found C – 38.44%, H – 3.61%, N – 3.94%. **HPLC Purity** 254 nm – 96.8 %.

[(η^5-Cp*)Ir(ImPy-NMe$_2$)Cl]PF$_6$ (29) As for **28** using [(η^5-Cp*)IrCl$_2$]$_2$ (66 mg, 0.083 mmol), MeOH (20 mL), ImPy-NMe$_2$ (37 mg, 0.166 mmol) and NH_4PF_6 (67 mg, 0.415 mmol). The product isolated as a dark red crystalline solid (108 mg, 89%). **^{1}H NMR** (400 MHz, dmso-d$_6$) δ =9.18 (s, 1H), 8.98 (d, 1H, J = 5.4 Hz), 8.34-8.26 (m, 2H), 7.87 (ddd, 1H, J = 7.4, 5.6, 1.8 Hz), 7.56 (d, 2H, J = 9.0 Hz), 6.86 (d, 2H, J = 9.0 Hz), 3.03 (s, 6H), 1.44 (s, 15H). **ESI-MS** (MeOH) m/z = 588.1 [M-PF$_6$]$^+$. **CHN analysis** calc. for $C_{24}H_{30}N_3ClF_6IrP$ C – 39.32%,

H – 4.12%, N – 5.73%. Found C – 38.72%, H – 4.04%, N – 5.49%. **HPLC Purity** 254 nm – 99.5 %. Crystals suitable for X-ray diffraction were obtained by slow evaporation of a methanol/acetone solution at ambient temperature.

[(η^5-Cp^{xPh})Ir(ImPy-NMe$_2$)Cl]PF$_6$ (30) As for **28** using [(η^5-Cp^{xPh})IrCl$_2$]$_2$ (30 mg, 0.0326 mmol), MeOH (15 mL), ImPy-NMe$_2$ (15 mg, 0.0652 mmol) and NH_4PF_6 (26 mg, 0.163 mmol). The product isolated as a dark red solid (25 mg, 48%). **^{1}H NMR** (400 MHz, dmso-d$_6$) δ =9.24 (s, 1H), 8.65 (d, 1H, J = 5.4 Hz), 8.36 (d, 1H, J = 7.6 Hz), 8.28 (t, 1H, J = 7.6), 7.78 (d, 1H, J = 6.0 Hz), 7.55 (d, 2H, J = 8.9 Hz), 7.47-7.41 (m, 3H), 7.35 (d, 2H, J = 7.0 Hz), 6.77 (d, 2H, J = 9.0 Hz), 3.00 (s, 6H), 1.62 (s, 3H), 1.58 (s, 3H), 1.49 (s, 3H), 1.25 (s, 3H). **ESI-MS** (MeOH) m/z = 650.1 [M-PF$_6$]$^+$. **CHN analysis** calc. for $C_{29}H_{32}N_3ClF_6IrP.H_2O$ C – 42.83%, H – 4.21%, N – 5.28%. Found C – 42.95%, H – 3.96%, N – 5.17%. **HPLC Purity** 254 nm – 99.2 %.

[(η^5-Cp^{xBiPh})Ir(ImPy-NMe$_2$)Cl]PF$_6$ (31) As for **28** using [(η^5-Cp^{xBiPh})IrCl$_2$]$_2$ (70 mg, 0.0652 mmol), MeOH (25 mL), ImPy-NMe$_2$ (30 mg, 0.1305 mmol) and NH_4PF_6 (53 mg, 0.326 mmol). The product isolated as a dark red solid (80 mg, 70%). **^{1}H NMR** (400 MHz, acetone-d$_6$) δ =9.23 (s, 1H), 8.83 (d, 1H, J = 5.5 Hz), 8.45, (d, 1H, J = 7.9 Hz), 8.32 (td, 1H, J = 7.8, 1.3 Hz), 7.83 (ddd, 1H, J = 7.4, 5.5, 1.5 Hz), 7.78-7.72 (m, 4H), 7.68 (d, 2H, J = 9.1 Hz), 7.64 (d, 2H, J = 8.4 Hz), 7.53-7.49 (m, 2H), 7.43 (tt, 1H, J = 6.5, 1.2 Hz), 6.85 (d, 2H, J = 9.1 Hz), 3.06 (s, 6H), 1.82 (s, 3H), 1.71 (s, 3H), 1.54 (s, 3H), 1.52 (s, 3H). **ESI-MS** (MeOH) m/z = 726.1 [M-PF$_6$]$^+$. **CHN analysis** calc. for $C_{35}H_{36}N_3ClF_6IrP$ C – 48.25%, H – 4.16%, N – 4.82%. Found C – 47.74%, H – 4.12%, N – 4.66%. **HPLC Purity** 254 nm – 99.4%.

[(η^5-Cp*)Ir(ImPy-OH)Cl]PF_6 (32) As for **28** using [(η^5-Cp*)$IrCl_2$]$_2$ (66 mg, 0.083 mmol), MeOH (20 mL), ImPy-OH (33 mg, 0.166 mmol) and NH_4PF_6 (67 mg, 0.415 mmol). The product isolated as an orange solid (83 mg, 71%). **^{1}H NMR** (400 MHz, dmso-d_6) δ =9.25 (s, 1H), 9.01 (d, 1H, J = 5.4 Hz), 8.38-8.30 (m, 2H), 7.91 (ddd, 1H, J = 7.4, 5.6, 1.7 Hz), 7.53 (d, 2H, J = 8.8 Hz), 6.96 (d, 2H, J = 8.8 Hz), 1.44 (s, 15H). **ESI-MS** (MeOH) m/z = 561.0 [M-PF_6]$^+$. **CHN analysis** calc. for $C_{22}H_{25}N_2ClF_6IrOP$ C – 37.42%, H – 3.57%, N – 3.97%. Found C – 37.59%, H – 3.62%, N – 3.85%. **HPLC Purity** 254 nm – 99.6 %. Crystals suitable for X-ray diffraction were obtained by slow evaporation of a methanol/acetone solution at ambient temperature.

[(η^5-Cp^{xPh})Ir(ImPy-OH)Cl]PF_6 (33) As for **28** using [(η^5-Cp^{xPh})$IrCl_2$]$_2$ (30 mg, 0.0326 mmol), MeOH (15 mL), ImPy-OH (13 mg, 0.0652 mmol) and NH_4PF_6 (26 mg, 0.163 mmol). The product isolated as an orange solid (20 mg, 40%). **^{1}H NMR** (400 MHz, dmso-d_6) δ =9.31 (s, 1H), 8.63 (d, 1H, J = 5.4 Hz), 8.41 (d, 1H, J = 7.7 Hz), 8.30 (t, 1H, J = 7.7 Hz), 7.82 (t, 1H, J = 6.3 Hz), 7.52-7.38 (m, 7H), 6.88 (d, 2H, J = 8.5 Hz), 1.63 (s, 3H), 1.56 (s, 3H), 1.42 (s, 3H), 1.23 (s, 3H). **ESI-MS** (MeOH) m/z = 623.0 [M-PF_6]$^+$. **CHN analysis** calc. for $C_{27}H_{27}N_2ClF_6IrOP$ C – 42.22%, H – 3.54%, N – 3.65%. Found C – 42.10%, H – 3.69%, N – 3.82%. **HPLC Purity** 254 nm – 99.7 %.

[(η^5-Cp^{xBiPh})Ir(ImPy-OH)Cl]PF_6 (34) As for **28** using [(η^5-Cp^{xBiPh})$IrCl_2$]$_2$ (70 mg, 0.0652 mmol), MeOH (25 mL), ImPy-OH (26 mg, 0.1305 mmol) and NH_4PF_6 (53 mg, 0.326 mmol). The product isolated as an orange solid (50 mg, 45%). **^{1}H NMR** (400 MHz, acetone-d_6) δ =9.34 (s, 1H), 9.10 (bs, 1H), 8.84 (d, 1H, J = 5.3 Hz), 8.52 (d, 1H, J = 7.0 Hz), 8.36 (td, 1H, J = 7.8, 1.4 Hz), 7.88 (ddd,

1H, J = 7.4, 5.6, 1.5 Hz), 7.80-7.74 (m, 4H), 7.69-7.65 (m, 4H), 7.53-7.49 (m, 2H), 7.43 (tt, 1H, J = 6.5, 1.2 Hz), 7.03 (d, 2H, J = 8.8 Hz), 1.83 (s, 3H), 1.70 (s, 3H), 1.54 (s, 3H), 1.48 (s, 3H). **ESI-MS** (MeOH) m/z = 698.8 $[M\text{-}PF_6]^+$. **CHN analysis** calc. for $C_{33}H_{31}N_2ClF_6IrOP.0.5H_2O$ C – 46.45%, H – 3.78%, N – 3.28%. Found C – 46.51%, H – 3.76%, N – 3.17%. **HPLC Purity** 254 nm – 99.6 %.

[(η^5-Cp*)Ir(ImPy-OMe)Cl]PF_6 (35) As for **28** using $[(\eta^5\text{-Cp*})IrCl_2]_2$ (66 mg, 0.083 mmol), MeOH (20 mL), ImPy-OMe (35 mg, 0.166 mmol) and NH_4PF_6 (67 mg, 0.415 mmol). The product isolated as an orange solid (90 mg, 75%). **^{1}H NMR** (400 MHz, dmso-d_6) δ =9.30 (s, 1H), 9.03 (d, 1H, J = 5.4 Hz), 8.40-8.31 (m, 2H), 7.92 (ddd, 1H, J = 7.4, 5.6, 1.7 Hz), 7.65 (d, 2H, J = 8.9 Hz), 7.18 (d, 2H, J = 8.9 Hz), 3.86 (s, 3H), 1.44 (s, 15H). **ESI-MS** (MeOH) m/z = 575.0 $[M\text{-}PF_6]^+$. **CHN analysis** calc. for $C_{23}H_{27}N_2ClF_6IrOP$ C – 38.36%, H – 3.78%, N – 3.89%. Found C – 38.34%, H – 3.70%, N – 3.80%. **HPLC Purity** 254 nm – 98.3 %.

[(η^5-Cp*)Ir(ImPy-COOH)Cl]PF_6 (36) As for **28** using $[(\eta^5\text{-Cp*})IrCl_2]_2$ (66 mg, 0.083 mmol), MeOH (20 mL), ImPy-COOH (38 mg, 0.166 mmol) and NH_4PF_6 (67 mg, 0.415 mmol). The product isolated as an orange solid (102 mg, 84%). **^{1}H NMR** (400 MHz, dmso-d_6) δ =9.45 (s, 1H), 9.08 (d, 1H, J = 5.5 Hz), 8.45 (d, 1H, J = 6.8 Hz), 8.36 (td, 1H, J = 7.7, 1.2 Hz), 8.18 (d, 2H, J = 8.5 Hz), 7.97 (ddd, 1H, J = 7.4, 5.6, 1.7 Hz), 7.76 (d, 2H, J = 8.5 Hz), 1.43 (s, 15H). **ESI-MS** (MeOH) m/z = 589.0 $[M\text{-}PF_6]^+$. **CHN analysis** calc. for $C_{23}H_{25}N_2ClF_6IrO_2P$ C – 37.63%, H – 3.43%, N – 3.82%. Found C – 37.75%, H – 3.44%, N – 3.63%. **HPLC Purity** 254 nm – 98.5 %.

[(η^5-Cp*)Ir(ImPy-F)Cl]PF_6 (37) As for **28** using $[(\eta^5\text{-Cp*})IrCl_2]_2$ (66 mg, 0.083 mmol), MeOH (20 mL), ImPy-F (33 mg, 0.166 mmol) and NH_4PF_6 (67 mg, 0.415

mmol). The product isolated as an orange solid (96 mg, 82%). **^{1}H NMR** (400 MHz, dmso-d_6) δ =9.38 (s, 1H), 9.06 (d, 1H, J = 5.4 Hz), 8.42 (d, 1H, J = 6.9 Hz), 8.35 (td, 1H, J = 7.7, 1.1 Hz), 7.96 (ddd, 1H, J = 7.3, 5.6, 1.4 Hz), 7.77-7.71 (m, 2H), 7.54-7.49 (m, 2H), 1.44 (s, 15H). **ESI-MS** (MeOH) m/z = 563.0 $[M\text{-}PF_6]^+$. **CHN analysis** calc. for $C_{22}H_{24}N_2ClF_7IrP$ C – 37.32%, H – 3.42%, N – 3.96%. Found C – 37.01%, H – 3.32%, N – 3.84%. **HPLC Purity** 254 nm – 98.0 %.

[(η^5-Cp*)Ir(ImPy-Cl)Cl]PF_6 (38) As for **28** using [(η^5-Cp*)$IrCl_2$]$_2$ (66 mg, 0.083 mmol), MeOH (20 mL), ImPy-Cl (36 mg, 0.166 mmol) and NH_4PF_6 (67 mg, 0.415 mmol). The product isolated as an orange solid (94 mg, 78%). **^{1}H NMR** (400 MHz, dmso-d_6) δ =9.39 (s, 1H), 9.06 (d, 1H, J = 5.4 Hz), 8.43 (d, 1H, J = 7.3 Hz), 8.35 (td, 1H, J = 7.7, 1.1 Hz), 7.96 (ddd, 1H, J = 7.3, 5.6, 1.4 Hz), 7.76-7.70 (m, 4H), 1.44 (s, 15H). **ESI-MS** (MeOH) m/z = 579.0 $[M\text{-}PF_6]^+$. **CHN analysis** calc. for $C_{22}H_{24}N_2Cl_2F_6IrP$ C – 36.47%, H – 3.34%, N – 3.87%. Found C – 36.62%, H – 3.32%, N – 3.77 %. **HPLC Purity** 254 nm – 99.0 %.

[(η^5-Cp*)Ir(ImPy-Br)Cl]PF_6 (39) As for **28** using [(η^5-Cp*)$IrCl_2$]$_2$ (66 mg, 0.083 mmol), MeOH (20 mL), ImPy-Br (43 mg, 0.166 mmol) and NH_4PF_6 (67 mg, 0.415 mmol). The product isolated as an orange solid (98 mg, 77%). **^{1}H NMR** (400 MHz, dmso-d_6) δ =9.39 (s, 1H), 9.06 (d, 1H, J = 5.4 Hz), 8.43 (d, 1H, J = 7.4 Hz), 8.35 (td, 1H, J = 7.7, 1.2 Hz), 7.96 (ddd, 1H, J = 7.3, 5.6, 1.4 Hz), 7.87 (d, 2H, J = 8.7 Hz), 7.64 (d, 2H, J = 8.7 Hz), 1.44 (s, 15H). **ESI-MS** (MeOH) m/z = 623.1 $[M\text{-}PF_6]^+$. **CHN analysis** calc. for $C_{22}H_{24}N_2BrClF_6IrP$ C – 34.36%, H – 3.15%, N – 3.64%. Found C – 34.44%, H – 3.10%, N – 3.49%. **HPLC Purity** 254 nm – 99.3 %.

[(η^5-Cp*)Ir(ImPy-I)Cl]PF_6 (40) As for **28** using [(η^5-Cp*)$IrCl_2$]$_2$ (66 mg, 0.083 mmol), MeOH (20 mL), ImPy-I (51 mg, 0.166 mmol) and NH_4PF_6 (67 mg, 0.415 mmol). The product isolated as an orange solid (114 mg, 84%). **^{1}H NMR** (400 MHz, dmso-d_6) δ =9.37 (s, 1H), 9.06 (d, 1H, J = 5.4 Hz), 8.43 (d, 1H, J = 7.8 Hz), 8.35 (td, 1H, J = 7.7, 1.2 Hz), 8.03 (d, 2H, J = 8.6 Hz), 7.96 (ddd, 1H, J = 7.3, 5.6, 1.5 Hz), 7.48 (d, 2H, J = 8.6 Hz), 1.43 (s, 15H). **ESI-MS** (MeOH) m/z = 671.1 [M-PF_6]$^+$. **CHN analysis** calc. for $C_{22}H_{24}N_2ClF_6IIrP.H_2O$ C – 31.68%, H – 3.14%, N – 3.36%. Found C – 31.72%, H – 2.86%, N – 3.24%. **HPLC Purity** 254 nm – 99.5 %.

[(η^5-Cp^{xPh})Ir(ImPy-I)Cl]PF_6 (41) As for **28** using [(η^5-Cp^{xPh})$IrCl_2$]$_2$ (30 mg, 0.0326 mmol), MeOH (15 mL), ImPy-I (20 mg, 0.0652 mmol) and NH_4PF_6 (26 mg, 0.163 mmol). The product isolated as an orange solid (35 mg, 61%). **^{1}H NMR** (400 MHz, dmso-d_6) δ =9.43 (s, 1H), 8.64 (d, 1H, J = 5.3 Hz), 8.46 (d, 1H, J = 7.5 Hz), 8.34 (t, 1H, J = 7.9 Hz), 7.95 (d, 2H, J = 8.2 Hz), 7.86 (t, 1H, J = 6.3 Hz), 7.51-7.38 (m, 7H), 1.64 (s, 3H), 1.54 (s, 3H), 1.38 (s, 3H), 1.30 (s, 3H). **ESI-MS** (MeOH) m/z = 732.9 [M-PF_6]$^+$. **CHN analysis** calc. for $C_{27}H_{26}N_2ClF_6IIrP.H_2O$ C – 36.19%, H – 3.15%, N – 3.13%. Found C – 36.19%, H – 2.94%, N – 3.20%. **HPLC Purity** 254 nm – 99.2 %. Crystals suitable for X-ray diffraction were obtained by slow evaporation of a methanol/acetone solution at ambient temperature.

[(η^5-Cp^{xBiPh})Ir(ImPy-I)Cl]PF_6 (42) As for **28** using [(η^5-Cp^{xBiPh})$IrCl_2$]$_2$ (70 mg, 0.0652 mmol), MeOH (25 mL), ImPy-I (40 mg, 0.1305 mmol) and NH_4PF_6 (53 mg, 0.326 mmol). The product isolated as an orange solid (50 mg, 40%). **^{1}H NMR** (400 MHz, acetone-d_6) δ =9.48 (s, 1H), 8.88 (d, 1H, J = 5.4 Hz), 8.59 (d,

1H, J = 6.9 Hz), 8.40 (td, 1H, J = 7.8, 1.3 Hz), 8.01 (d, 2H, J = 8.6 Hz), 7.93 (ddd, 1H, J = 7.6, 5.6, 1.5 Hz), 7.79 (d, 2H, J = 8.3 Hz), 7.76-7.73 (m, 2H), 7.66 (d, 2H, J = 8.3 Hz), 7.59 (d, 2H, J = 8.5 Hz), 7.53-7.50 (m, 2H), 7.44 (tt, 1H, J = 7.4, 1.2 Hz), 1.84 (s, 3H), 1.71 (s, 3H), 1.58 (s, 3H), 1.45 (s, 3H). **ESI-MS** (MeOH) m/z = 809.0 $[M\text{-}PF_6]^+$. **CHN analysis** calc. for $C_{33}H_{30}N_2ClF_6IIrP$ C – 41.54%, H – 3.17%, N – 2.94%. Found C – 41.31%, H – 3.19%, N – 2.78%. **HPLC Purity** 254 nm – 98.4 %. Crystals suitable for X-ray diffraction were obtained by slow evaporation of a methanol/acetone solution at 278 K.

Complexes **43-45** were characterised by ^{1}H NMR spectroscopy at 353 K due to dynamic behaviour observed in solution. This is discussed further in section 6.3.2.

[(η^5-Cp*)Ir(ImPy-Naphth)Cl]PF_6 (43) As for **28** using [(η^5-Cp*)$IrCl_2$]$_2$ (66 mg, 0.083 mmol), MeOH (20 mL), ImPy-Naphth (39 mg, 0.166 mmol) and NH_4PF_6 (67 mg, 0.415 mmol). The product isolated as an orange solid (77 mg, 63%). **^{1}H NMR** (600 MHz, dmso-d_6, 353 K) δ =9.63 (s, 1H), 9.09 (d, 1H, J = 5.3 Hz), 8.47 (d, 1H, J = 7.8 Hz), 8.37 (t, 1H, J = 7.8 Hz), 8.14 (d, 1H, J = 7.8 Hz), 8.10 (d, 1H, J = 8.3 Hz), 8.01 (t, 1H, J = 6.7 Hz), 7.81 (bs, 2H), 7.75-7.69 (m, 2H), 7.66-7.63 (m, 1H), 1.32 (s, 15H). **ESI-MS** (MeOH) m/z = 595.1 $[M\text{-}PF_6]^+$. **CHN analysis** calc. for $C_{26}H_{27}N_2ClF_6IrP$ C – 42.19%, H – 3.68%, N – 3.78%. Found C – 41.98%, H – 3.65%, N – 3.70%. **HPLC Purity** 254 nm – 98.3%. Crystals suitable for X-ray diffraction were obtained by slow evaporation of a methanol/acetone solution at 278 K.

[(η^5-Cp^{xPh})Ir(ImPy-Naphth)Cl]PF_6 (44) As for **28** using [(η^5-Cp^{xPh})$IrCl_2$]$_2$ (30 mg, 0.0326 mmol), MeOH (15 mL), ImPy-Naphth (15 mg, 0.0652 mmol) and NH_4PF_6 (26 mg, 0.163 mmol). The product isolated as an orange crystalline solid

(29 mg, 55%). **^{1}H NMR** (600 MHz, dmso-d_6, 353 K) δ =9.68 (s, 1H), 8.75 (d, 1H, J = 5.7 Hz), 8.52 (d, 1H, J = 7.8 Hz), 8.39 (t, 1H, J = 7.8 Hz), 8.10 (d, 1H, J = 8.1 Hz), 8.05 (d, 1H, J = 8.5 Hz), 7.94 (t, 1H, J = 6.70 Hz), 7.67-7.63 (m, 2H), 7.56 (t, 1H, J = 7.6 Hz), 7.49 (t, 1H, J = 7.3 Hz), 7.44-7.39 (m, 4H), 6.89 (bs, 2H), 1.60 (s, 3H), 1.36 (s, 3H), 1.20 (s, 3H), 1.12 (s, 3H). **HR-MS** (MeOH) **ESI-MS** (MeOH) m/z = 657.1 $[M\text{-}PF_6]^+$. **CHN analysis** calc. for $C_{31}H_{29}N_2ClF_6IrP$ C – 46.41%, H – 3.64%, N – 3.49%. Found C – 46.22%, H – 3.21%, N – 3.51%. **HPLC Purity** 254 nm – 98.5%. Crystals suitable for X-ray diffraction were obtained by slow evaporation of a methanol/acetone solution at 278 K.

[(η^5-Cp^{xBiPh})Ir(ImPy-Naphth)Cl]PF$_6$ (45) As for **28** using [(η^5-Cp^{xBiPh})$IrCl_2$]$_2$ (70 mg, 0.0652 mmol), MeOH (25 mL), ImPy-Naphth (31 mg, 0.1305 mmol) and NH_4PF_6 (53 mg, 0.326 mmol). The product isolated as an orange solid (64 mg, 56%). **^{1}H NMR** (600 MHz, dmso-d_6) δ =9.69 (s, 1H), 8.82 (d, 1H, J = 5.7 Hz), 8.54 (d, 1H, J = 7.5 Hz), 8.40 (t, 1H, J = 7.7 Hz), 8.10 (d, 1H, J = 8.2 Hz), 8.06 (d, 1H, J = 8.2 Hz), 7.96 (d, 2H, J = 6.8 Hz), 7.74-7.72 (m, 4H), 7.66 (t, 1H, J = 7.3 Hz), 7.57-7.49 (m, 5H), 7.43 (t, 1H, J = 7.4 Hz), 6.87 (bs, 2H), 1.65 (s, 3H), 1.40 (s, 3H), 1.21 (s, 6H). **ESI-MS** (MeOH) m/z = 733.2 $[M\text{-}PF_6]^+$. **CHN analysis** calc. for $C_{37}H_{33}N_2ClF_6IrP.H_2O$ C – 49.58%, H – 3.94%, N – 3.13%. Found C – 49.47%, H – 3.76%, N – 2.93%. **HPLC Purity** 254 nm – 99.0 %.

6.2.3 Methods

6.2.3.1 X-ray Crystallography

The X-ray crystal structures of complexes **29**, **32** and **41-44** were solved by Dr. Guy Clarkson (Department of Chemistry, University of Warwick). The details of the diffraction instrumentation are described in Chapter 2 (section 2.2.8).

6.2.3.2 Computation

DFT calculations were performed using the Guassian 03 package as described in Chapter 2 (section 2.2.9). Electrostatic potential surfaces (EPS) for complexes **29**, **32** and **41-44** where the EPSs are shown in space (with positive and negative regions in blue and red, respectively) and mapped on electron density (isovalue 0.04) of the molecules. The electrostatic potential is represented with a colour scale ranging from red (0.000 au) to blue (+0.450 au).

6.2.3.3 HPLC

6.2.3.3.1 Purity Measurements

HPLC purity measurements on freshly prepared samples of complexes **28-45** (ca. 100 μM, 10% MeOH/90% H_2O) were performed as described in Chapter 2 (2.2.5.1).

6.2.3.3.2 Relative Hydrophobicity Measurements

The relative hydrophobicity of complexes **29**, **32-34**, **40-43** (100 μM, 1:9 MeOH:H_2O in 50 mM NaCl) was determined by RP-HPLC as described in Chapter 2 (section 2.2.5.2).

6.2.3.4 Variable Temperature (VT) ^{1}H NMR

VT-^{1}H NMR measurements on complexes **43-45** were performed using a Bruker AV III 600 NMR spectrometer in acetone-d_6 over a temperature range of 223-328 K.

The rate constant (k_c at coalescence temperature) for the hindered rotation of the naphthyl group in complexes **43-45** (2 mM, acetone-d_6) was calculated using the equations for an unequally populated states[24] based on the imino proton:

$$k_c = \frac{\pi(\nu_a - \nu_b)}{X}$$

where $\nu_a - \nu_b$ is the difference between the two chemical shifts and X is the solution to the polynomial equation[25]:

$$X^6 - 6X^4 + [12 - 27(\Delta p)^2]X^2 - 8 = 0$$

where Δp = population of proton a – population of proton b

The Gibbs free energy of activation ($\Delta G^{\ddagger}$) was calculated using the following equation[25]:

$$\Delta G^{\ddagger} = aT\left[10.319 + \log\left(\frac{T}{k_c}\right)\right]$$

$$a = 1.914 \times 10^{-2} \text{ (for kJ mol}^{-1}\text{)}$$

where T = coalescence temperature (K). The error in the value of $\Delta G^{\ddagger}$ was estimated by evaluating the value of $\Delta G^{\ddagger}$ at ± 2 K from the stated coalescence temperature.

6.2.3.5 Nuclear Overhauser NMR Spectroscopy (NOESY)

Complex **44** (2 mM, acetone-d_6) was analysed by 2D NOESY ^{1}H NMR to determine the conformation of the major species in solution at 223 K using a 0.4 s mixing time. This was performed with the assistance of Dr. Ivan Prokes (Department of Chemistry, University of Warwick).

6.2.3.6 Stability in Aqueous Solution by ^{1}H NMR spectroscopy

The stability of complexes (ca. 500 μM) in aqueous solution and in 4 mM NaCl was monitored by ^{1}H NMR spectroscopy. Briefly, complexes were dissolved in 26.7% MeOD-d_4/73.3% D_2O (v/v) by dissolution of complexes in MeOD-d_4 followed by rapid dilution with D_2O at 310 K and spectra were taken at various time intervals. Stability at different pH* was also investigated using the same method as described above, with D_2O solutions being prepared at differing pH* by addition of either $DClO_4$ or NaOD. All spectra were internally referenced to 1,4-dioxane (3.75 ppm) and water suppression was performed using Shaka techniques.[26] The change in chemical shift arising from the conversion of Ir-OD_2 to Ir-OD as a function of pH* was also assessed to estimate the acidity of the aqua adduct, as described in Chapter 2 (section 2.2.13).

6.2.3.7 Stability in Aqueous Solution and Lysogeny Broth (LB) by LC-MS

The stability of complexes **32** and **42** (ca. 100 μM) was evaluated by LC-MS in the presence of water (10% MeOH/90% H_2O) and LB media (2% dmso/98% H_2O) used for bacterial cell viability experiments. Measurements were performed after 24 h incubation at 310 K. The MS instrumentation used is described in Chapter 2 (section 2.2.6). In both cases, the measurements were performed using the Agilent 1200 system with a VWD and 100 μL loop. The column was an Agilent Zorbax Eclipse Plus C18, 150 × 4.6 mm with a 5 μM pore size. The mobile phase was H_2O 0.1% TFA and CH_3CN 0.1% TFA, with a flow rate of 1

mL min^{-1}. The detection wavelength was set at 254 nm, with sample injections of 5 μL. The gradient was the same used for purity determination (section 2.2.5.1).

6.2.3.8 Antibacterial Activity against *S. aureus* and *E. coli*

Determination of the minimum inhibitory concentration (MIC) and minimum bactericidal concentration (MBC) of complexes **39-45** against *S. aureus* and *E. coli* was performed as described in Chapter 2 (section 2.2.15.2) in collaboration with Dr. Evyenia Shaili (Department of Chemistry, University of Warwick).

6.2.3.9 Membrane Integrity of *S. aureus*

Membrane integrity of *S. aureus* after incubation with complexes **31**, **34**, **42** and **45** was examined using the BacLight DEAD/ALIVE™ Assay (LifeScience Technologies) as described in Chapter 2 (section 2.2.15.3) in collaboration with Dr. Evyenia Shaili (Department of Chemistry, University of Warwick). They were compared to positive (nisin) and negative (vancomycin) controls for the disruption of the cell membrane after short incubation periods (25 min, 310 K).

6.2.3.10 Antiproliferative Activity against Eukaryotic Cells

Antiproliferative activity assays were performed by Dr. Isolda Romero-Canelón (Department of Chemistry, University of Warwick) as described in Chapter 2 (section 2.2.14.2). Complexes **29-45** were evaluated for activity in the A2780 human ovarian cancer cell line and complexes **31**, **34**, **42** and **45** were evaluated for activity in the MRC5 human fibroblast cell lines.

6.2.3.11 ICP-OES Analysis

ICP-OES analysis of stock solutions used for eukaryotic cell work was carried out as described in Chapter 2 (section 2.2.10).

6.3 Results

6.3.1 Synthesis and Characterisation

Eighteen iridium(III) cyclopentadienyl complexes bearing iminopyridine chelating ligands derived from the Schiff base reaction between pyridinecarboxaldehyde and aniline derivatives have been synthesised and characterised by ^{1}H NMR spectroscopy, ESI-MS and elemental analysis. Complexes **29-42** contain para-substituted *N*-(pyrid-2-ylmethylene)phenylamines and complexes **43-45** bear *N*-(2-pyridnylmethylene)-1-naphthalenamine (ImPy-Naphth) as the chelating ligand. Complexes **28**, **29**, **32**, **35-40** and **43** have a η^5-Cp* ring, complexes **30**, **33**, **41** and **44** contain a η^5-Cp^{xPh} ring and complexes **31**, **34**, **42** and **45** bear a η^5-Cp^{xBiPh} as the five coordinate ligand (Chart 6.1). Complexes **30**, **31**, **33**, **34**, **41**, **44**, **44** and **45** are the first examples of ImPy half-sandwich Ir(III) complexes containing an extended cyclopentadienyl ring system to be reported. Complexes **28-45** all contain chloride as the monodentate ligand and were isolated as PF_6 salts.

Complexes **28**, **35** and **38** have been previously prepared[27] but no biological activity has been reported. The complexes synthesised are all chiral at the metal centre resulting in a racemate solution of R and S enantiomers, however, no attempts were made to isolate each enantiomer.

The ImPy ligands were all synthesised by the reaction of 1 mol equivalent of pyridine carboxaldehyde with 1 mol equivalent of aniline derivative in acetonitrile and heated under reflux for 18 h. After either evaporating to dryness or isolating the precipitated ligand, the *N*-(pyrid-2-ylmethylene)amine ligands were isolated in good yields without further purification. Complexes **28-45** were synthesised by the addition of 2 mol equivalents of iminopyridine ligand to 1 mol equivalent of iridium dimer in methanol under nitrogen for 15 h with stirring. Concentration of the reaction mixture followed by addition of ammonium hexafluorophosphate led to the precipitation of the desired complex. Dissolution of the isolated solid in acetone and filtration through celite allowed removal of excess ammonium hexafluorophosphate, where concentrating the solution to dryness followed by further drying on a Schlenk line yielded products of good purity.

The molecular structure of complexes [(η^5-Cp*)Ir(ImPy-NMe_2)Cl]PF_6 **29,** [(η^5-Cp*)Ir(ImPy-OH)Cl]PF_6 **32**, [(η^5-Cp^{xPh})Ir(ImPy-I)Cl]PF_6 **41**, [(η^5-Cp^{xBiPh})Ir(ImPy-I)Cl]PF_6 **42**, [(η^5-Cp^{*})Ir(ImPy-Naphth)Cl]PF_6 **43** and [(η^5-Cp^{xPh})Ir(ImPy-Naphth)Cl]PF_6 **44** were characterised by X-ray crystallography and are shown in Figure 6.1, with selected crystallographic data shown in Table 6.1 and selected bond distances and angles shown in Table 6.2. All complexes exhibit the pseudo-octahedral "piano-stool" structure expected for half-sandwich metal complexes, with Ir – ring centroid distances ranging from 1.785 – 1.796 Å, Ir – N (pyridyl) distances of 2.080 – 2.103 Å, Ir – N (aniline) distances of 2.052 – 2.097 Å and Ir –Cl distances of 2.3704 – 2.4002 Å.

The unit cell of complex [(η^5-Cp^{xPh})Ir(ImPy-Naphth)Cl]PF_6 **44** contained two crystallographically independent molecules (**44a** and **44b**) which possess different

bond lengths/angles and are described separately in Table 6.2. The unit cell of **44** contains 4 molecules where both **44a** and **44b** are represented in a 1:1 ratio, in which **44a** and **44b** contain both R and S enantiomers.

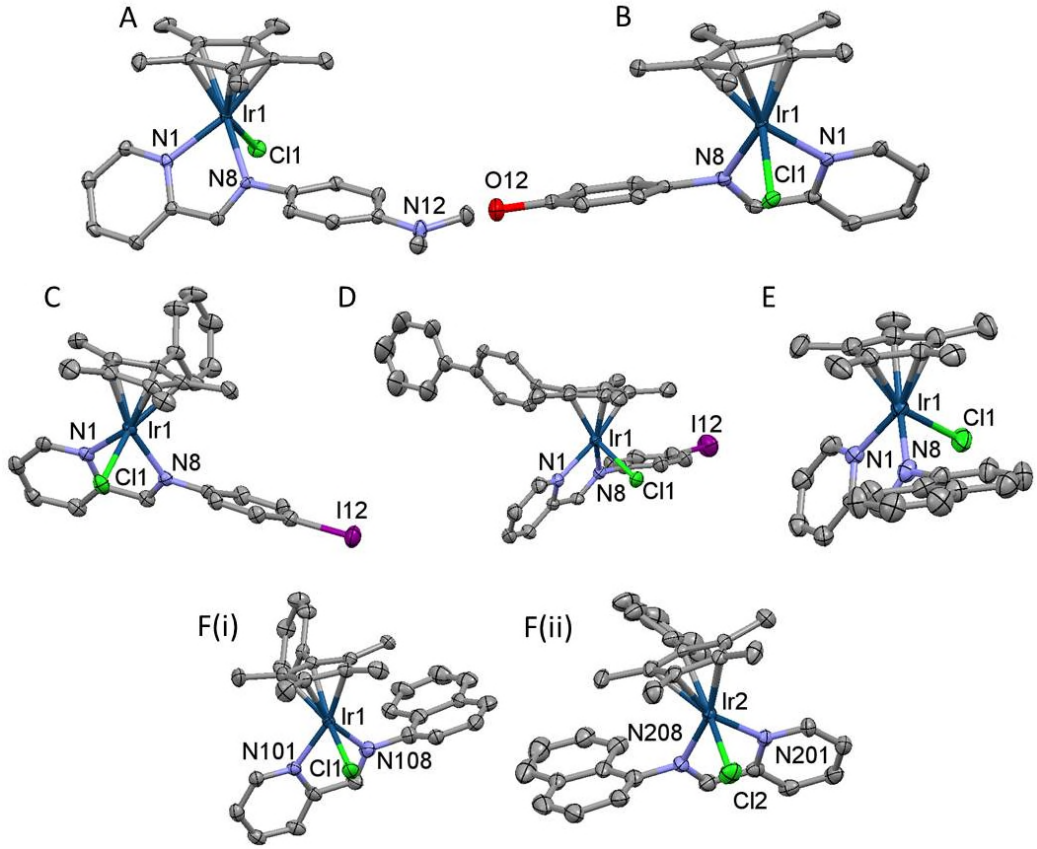

Figure 6.1. X-ray crystal structures with atom numbering scheme for complexes [(η^5-Cp*)Ir(ImPy-NMe_2)Cl]PF_6 **29** (A)**,** [(η^5-Cp*)Ir(ImPy-OH)Cl]PF_6 **32** (B), [(η^5-Cp^{xPh})Ir(ImPy-I)Cl]PF_6 **41** (C), [(η^5-Cp^{xBiPh})Ir(ImPy-I)Cl]PF_6 **42** (D), [(η^5-Cp^{x*})Ir(ImPy-Naphth)Cl]PF_6 **43** (E) and [(η^5-Cp^{BiPh})Ir(ImPy-Naphth)Cl]PF_6 **44a-b** (Fi-ii) with thermal ellipsoids drawn at 50%. Hydrogen atoms, PF_6 counterion and solvent molecules have been omitted for clarity.

Table 6.1. Selected X-ray crystallographic data for complexes [(η^5-Cp*)Ir(ImPy-NMe_2)Cl]PF_6 **29,** [(η^5-Cp*)Ir(ImPy-OH)Cl]PF_6 **32** [(η^5-Cp^{xPh})Ir(ImPy-I)Cl]PF_6, **41** [(η^5-Cp^{xBiPh})Ir(ImPy-I)Cl]PF_6 **42**, [(η^5-Cp^{x*})Ir(ImPy-Naphth)Cl]PF_6 **43** and [(η^5-Cp^{BiPh})Ir(ImPy-Naphth)Cl]PF_6 **44**.

	29	**32**	**41**	**42.1.75H_2O**	**43**	**44**
Formula	$C_{24}H_{30}ClF_6IrN_3P$	$C_{22}H_{25}ClF_6IrN_2OP$	$C_{27}H_{26}ClF_6IIrN_2P$	$C_{33}H_{33.5}ClF_6IIrN_2O_{1.75}P$	$C_{26}H_{27}ClF_6IrN_2P$	$C_{31}H_{29}ClF_6IrN_2P$
MW	733.13	706.06	878.02	985.64	740.11	802.18
Crystal Colour	Red	Orange	Orange	Orange	Orange	Orange
Cryst size (mm)	0.4 x 0.1 x 0.02	0.3 x 0.28 x 0.22	0.2 × 0.2 × 0.01	0.32 x 0.26 x 0.12	0.38 x 0.24 x 0.2	0.22× 0.20 × 0.08
λ (Å)	0.71073	0.71073	0.71073	0.71073	0.71073	0.71073
Temp(K)	100	150	150	150	150	150
Cryst system	Monoclinic	Monoclinic	Triclinic	Triclinic	Monoclinic	Triclinic
Space group	P2(1)/n	P2(1)/n	P-1	P-1	P2(1)/n	P-1
a (Å)	9.9617(4)	8.7481(3)	9.46480(16)	9.70259(18)	10.8265(2)	11.1277(2)
b (Å)	11.4829(3)	20.8057(8)	12.0044(2)	13.8280(2)	11.99174(17)	16.7111(3)
c (Å)	23.0094(7)	13.3561(5)	13.2050(2)	14.8398(2)	20.6677(5)	17.20802(4)
α (°)	90	90	91.4727(14)	113.8378(16)	90	71.8791(16)
β (°)	97.960(3)	95.593(3)	102.6397(15)	91.9104(14)	101.476(2)	72.1957(19)
γ (°)	90	90	100.0312(15)	101.0453(15)	90	80.6946(15)
Vol ($Å^3$)	2606.65(14)	2426.16(16)	1438.41(4)	1773.78(6)	2629.61(9)	2887.71(11)
Z	4	4	2	2	4	4
$R(Fo^2)$	0.0316	0.0295	0.0320	0.046	0.0513	0.0453
$Rw(Fo^2)$	0.0653	0.0577	0.0690	0.1232	0.1222	0.0947
GOF	1.055	1.051	1.029	1.159	1.060	1.031

Table 6.2. Selected bond lengths (Å) and bond angles (°) for complexes [(η^5-Cp*)Ir(ImPy-NMe_2)Cl]PF_6 **29,** [(η^5-Cp*)Ir(ImPy-OH)Cl]PF_6 **32**, [(η^5-Cp^{xPh})Ir(ImPy-I)Cl]PF_6 **41**, [(η^5-Cp^{xBiPh})Ir(ImPy-I)Cl]PF_6 **42,** [(η^5-Cp^{x*})Ir(ImPy-Naphth)Cl]PF_6 **43** and complex [(η^5-Cp^{BiPh})Ir(ImPy-Naphth)Cl]PF_6 **44a** an **44b**.

Bond/angle	**29**	**32**	**41**	**42.1.75H_2O**	**43**	Bond/angle	**44a**		**44b**
Ir-C (Cp ring)	2.177(4)	2.190(4)	2.161(3)	2.155(7)	2.162(6)	Ir1-C (Cp ring)	2.200(4)	Ir2-C (Cp ring)	2.156(4)
	2.195(3)	2.159(3)	2.183(3)	2.190(8)	2.150(6)		2.148(4)		2.188(4)
	2.166(3)	2.162(3)	2.168(3)	2.167(7)	2.171(5)		2.181(5)		2.168(4)
	2.151(3)	2.148(4)	2.172(3)	2.160(7)	2.187(6)		2.164(5)		2.160(4)
	2.154(3)	2.195(4)	2.188(3)	2.188(7)	2.143(6)		2.168(5)		2.177(4)
Ir-C (centroid)	1.789	1.793	1.796	1.796	1.785	Ir1-C (centroid)	1.794	Ir2-C (centroid)	1.790
Ir-N1	2.090(3)	2.095(3)	2.093(3)	2.103(5)	2.080(4)	Ir1-N101	2.099(4)	Ir2-N201	2.081(3)
Ir-N8	2.097(3)	2.094(3)	2.096(3)	2.088(5)	2.052(5)	Ir1-N108	2.067(4)	Ir2-N208	2.078(4)
Ir-Cl	2.3704(8)	2.3948(9)	2.3926(8)	2.3810(15)	2.4002(15)	Ir1-Cl1	2.3878(11)	Ir2-Cl2	2.3806(16)
N1-Ir-N8	76.55(11)	76.22(12)	76.32(10)	76.23(19)	77.06(18)	N101-Ir1-N108	76.18(16)	N201-Ir2-N208	76.71(14)
N1-Ir-Cl	84.45(8)	86.09(8)	84.32(8)	85.01(13)	84.33(13)	N101-Ir1-Cl1	84.21(10)	N201-Ir2-Cl2	83.37(10)
N8-Ir-Cl	84.14(8)	86.75(8)	85.98(7)	87.32(14)	85.55(14)	N108-Ir1-Cl1	85.28(12)	N208-Ir2-Cl2	87.84(12)

The angle between the mean plane of the pyridyl ring connected to the imine carbon and the mean plane of the aniline ring in complexes **29**, **32**, **41** and **44** is similar, ranging from 50.34–58.57° while the angles exhibited in complexes **43** and **44a-b** which bear the naphthyl group are more obtuse, with angles of 63.41, 73.44 and 65.71° for **43**, **44a** and **44b**, respectively.

The propeller twist exhibited by the extended cyclopentadienyl rings between the phenyl and Cp ring in **41** is 65.89° whereas in **42** the twist is 55.31° followed by a further twist between the two phenyl rings at an angle of 32.58°. The propeller twist between the phenyl and Cp ring in **44a** and **44b** is 66.49° and 53.74°, respectively, showing significant difference between the two crystallographically independent molecules.

Weak intermolecular π-π stacking was observed in the crystal structures of complexes **32** and **42** (Figure 6.2) between pyridyl rings of neighbouring molecules, with a centroid – centroid distance of 3.739 and 4.258 Å, respectively. Hydrogen-bonding was also observed in the crystal structure of complex **32** between the –OH on the aniline ring and the F-PF_5 counterion (Figure 6.3) with a OH – F-PF_5 distance of 2.319 Å at an angle of 170.10°.

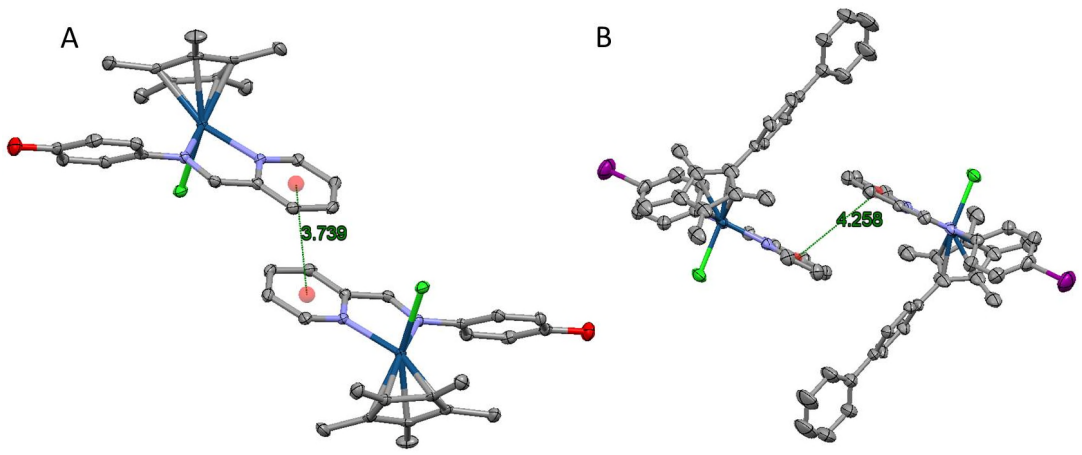

Figure 6.2. The π-π stacking interaction in the X-ray crystal structures of complexes [(η^5-Cp*)Ir(ImPy-OH)Cl]PF_6 **32** (A) and [(η^5-Cp^{xBiPh})Ir(ImPy-I)Cl]PF_6 **42** (B) where the centroid – centroid distance between pyridyl rings of independent molecules is 3.739 and 4.256 Å for **32** and **42**, respectively. Thermal ellipsoids drawn at 50% with hydrogen atoms, PF_6 counterion and solvent molecules omitted for clarity.

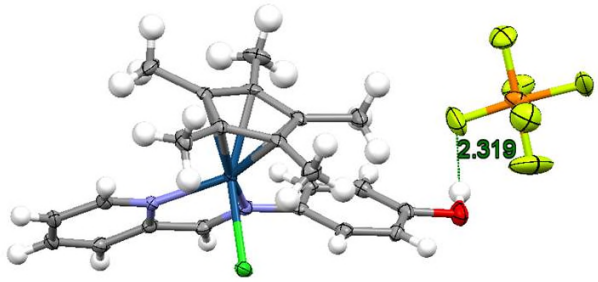

Figure 6.3. The hydrogen-bonding interaction in the X-ray crystal structure of complex [(η^5-Cp*)Ir(ImPy-OH)Cl]PF_6 **32** between the –OH of the aniline ring and the F-PF_5 counterion. The bond distance is 2.319 Å with an OH – F-PF_5 angle of 170.10°. Thermal ellipsoids drawn at 50%.

DFT calculations based on the X-ray crystal structures of complexes **29**, **32** and **41-44** were made at the PBE0/LanL2DZ/6-31+G** level to determine the electrostatic potential surfaces (Figure 6.4). The surfaces of the complexes are relatively non-polar, with an even distribution of electronic charge and no significant differences among the complexes. The phenyl ring in Cp^{xPh} complexes **41** and **44** has a higher

electronic charge density than the Ir – bound cyclopentadienyl ring while the terminal phenyl ring in Cp^{xBiPh} complex **42** has a higher electronic charge density than the first phenyl ring. In most cases, the monodentate chlorido ligand exhibits the most negative electrostatic potential surface, with the exception of complex **32** where the oxygen in the –OH functionalised aniline has a slightly more negative surface.

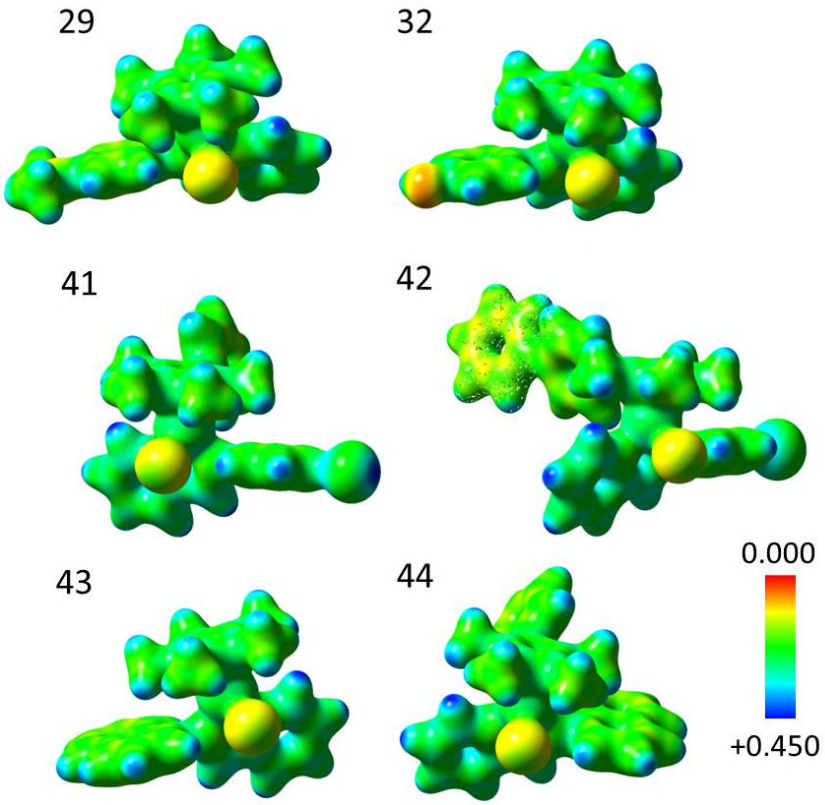

Figure 6.4. Electrostatic potential surfaces of complexes **29**, **32** and **41-44** calculated at the PBE0/LanL2DZ/6-31+G** level using DFT methods. EPS surfaces are shown both in space (with positive and negative regions in blue and red, respectively) and mapped on electron density (isovalue 0.04) of the molecules. The electrostatic potential is represented with a colour scale ranging from red (0.000 au) to blue (+0.450 au).

6.3.2 Dynamic Behaviour of Complexes 43-45 in Solution

Characterisation of complexes **43-45** by ^{1}H NMR spectroscopy in dmso-d_6 at ambient temperature showed that two conformational isomers were present in solution. Upon heating to 353 K, one set of peaks was observed. As rotation around the imino nitrogen – naphthyl carbon (σ-bond) in the ImPy chelating ligand is possible, it is likely that the presence of the bulky naphthyl group results in hindered rotation around this bond, due to steric hindrance by the Cp^{x} rings.

VT-^{1}H NMR was used to investigate this behaviour in acetone-d_6 over a temperature range of 223 – 323 K and is shown for complexes **43** and **44** in Figure 6.5 (**45** exhibits similar behaviour compared with **44**). The imine proton in each complex gave rise to two clearly identifiable species and is shown in Figure 6.5. At 223 K, two clearly defined resonances were observed with a ratio of around 1:2. Upon an increase in temperature, the two imine peaks start to converge. For complexes **44** (Cp^{xPh}) and **45** (Cp^{xBiPh}), the temperature at which the imine peaks coalesce is ca. 300 K whereas for complex **43** (Cp*) the coalescence temperature is ca. 310 K. Above these temperatures the imine peak appears as a singlet which sharpens at higher temperatures. Similar behaviour is observed for the other proton resonances, although it is not as easy to distinguish the point of coalescence.

Thermodynamic parameters were calculated using the equations as described in the experimental section and are shown in Table 6.3. The population of the two species (at 223 K) and all thermodynamic data (including coalescence temperature) were based on the imine proton resonance. It is evident that the Gibbs free energy of activation ($\Delta G^{\ddagger}$) is similar for all complexes, with calculated values ranging from 64-65 kJ mol^{-1}. This shows that the barrier to rotation is relatively independent of the type of cyclopentadienyl ring.

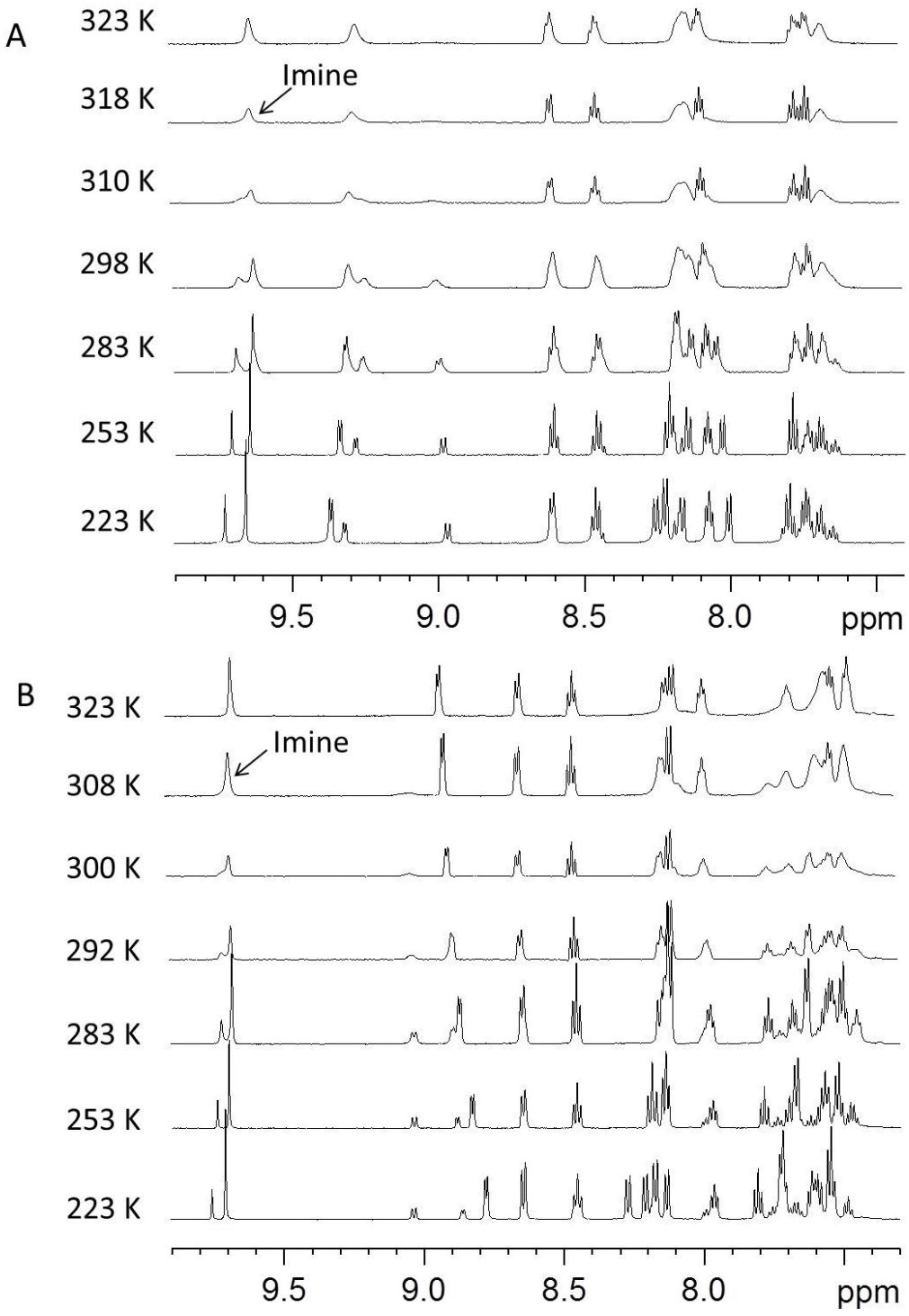

Figure 6.5. Low-field region of ^{1}H NMR (600 MHz, acetone-d_6) of complex **43** (A) and **44** (B) at 2 mM at various temperatures, showing dynamic behaviour due to hindered rotation of naphthyl group.

Table 6.3. Thermodynamic parameters for the rotation of the naphthyl group as calculated from the dynamic NMR spectra of complexes **43-45**. Δv = difference between chemical shifts (at low exchange), T_c = coalescence temperature, k_c = rate constant (coalescence temperature) and $\Delta G^{\ddagger}$ = Gibbs free energy of activation.

Complex	Δv (Hz)	T_c (K)	k_c (s^{-1})	$\Delta G^{\ddagger}$ (kJ mol^{-1})
43	42.6	310 ± 2	60.4	65.4 ± 0.5
44	28.68	300 ± 2	40.7	64.2 ± 0.5
45	21.9	300 ± 2	42.5	64.1 ± 0.5

It can be hypothesised that the two species present in solution belong to two different conformations (C1 – naphthyl group points away from chloride and C2 – naphthyl group points towards chloride) of the naphthylamine ring as demonstrated for complex **43** in Figure 6.6.

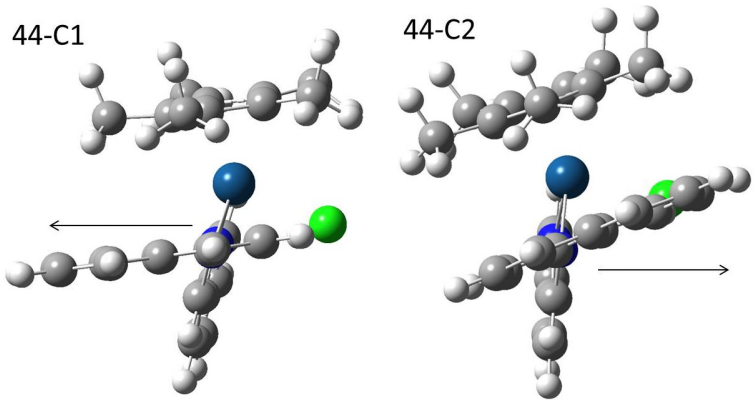

Figure 6.6. Possible conformational isomers (C1 and C2) of complex **43** which differ in the orientation of the naphthyl ring.

2D ^{1}H NMR COSY and NOESY experiments were used to assign the conformation of the major isomer that exists at 223 K for complex **43**, Figure 6.7 a-b and 6.8. The NOESY experiments show cross peaks associated with the imine proton of the major species which appear to be in close proximity to two protons which appear as doublet peaks at 8.60 and 8.24 ppm. The resonance at 8.60 ppm has been assigned as Hd on the pyrdiyl ring of the chelating ligand (Figure 6.8 a). This was based on the

COSY coupling (Figure 6.8 b) which showed that the proton belonged to a ring system bearing four protons, where another proton (doublet) present exhibits two NOE cross peak with Cp* protons of both conformational isomers (Figure 6.7 b) and was assigned as Ha, hence belonging to the pyridyl ring.

The proton at 8.24 ppm (doublet) appears to couple to a proton presenting as a triplet, which is coupled to another proton (triplet) which couples to a proton (doublet), based on COSY assignment. Therefore, the proton at 8.24 ppm presumably belongs to the naphthyl ring which bears four protons and has been assigned as Hf. This would imply that the major isomer in solution is the conformation where the naphthyl group points away from the chloride ligand (C1).

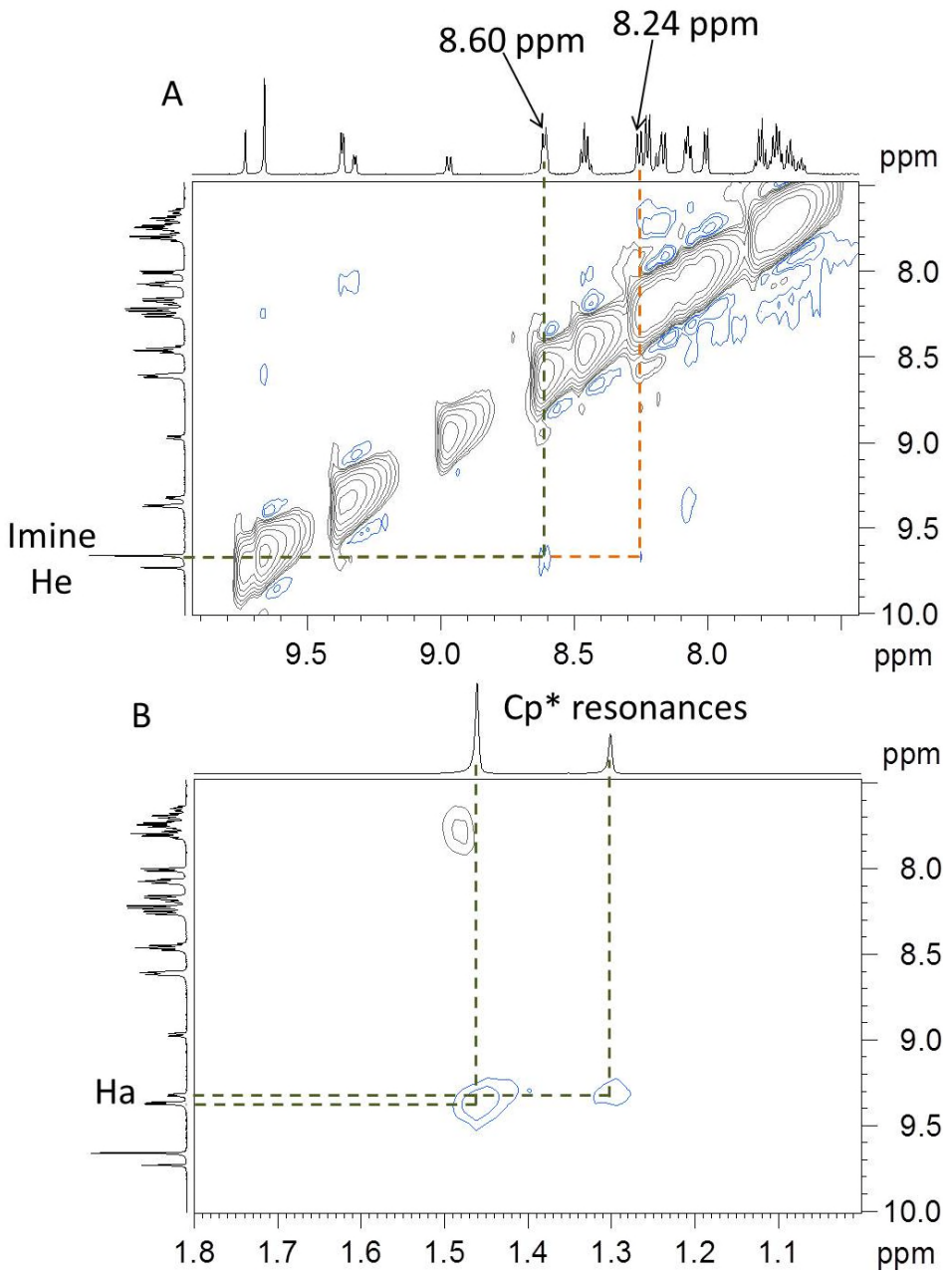

Figure 6.7. (A) Low-field region of ^{1}H NMR 2D NOESY spectrum of complex **43** (600 MHz, 0.4 s mixing time, acetone-d_6) at 223 K, showing cross peaks of the imine proton (He) of the major isomer with two protons at 8.60 and 8.24 ppm. (B) High-field region of ^{1}H NMR NOESY spectrum showing cross peaks with the low-field protons on the pyridyl ring of the chelating ligand (Ha) with the Cp* resonances of the two species.

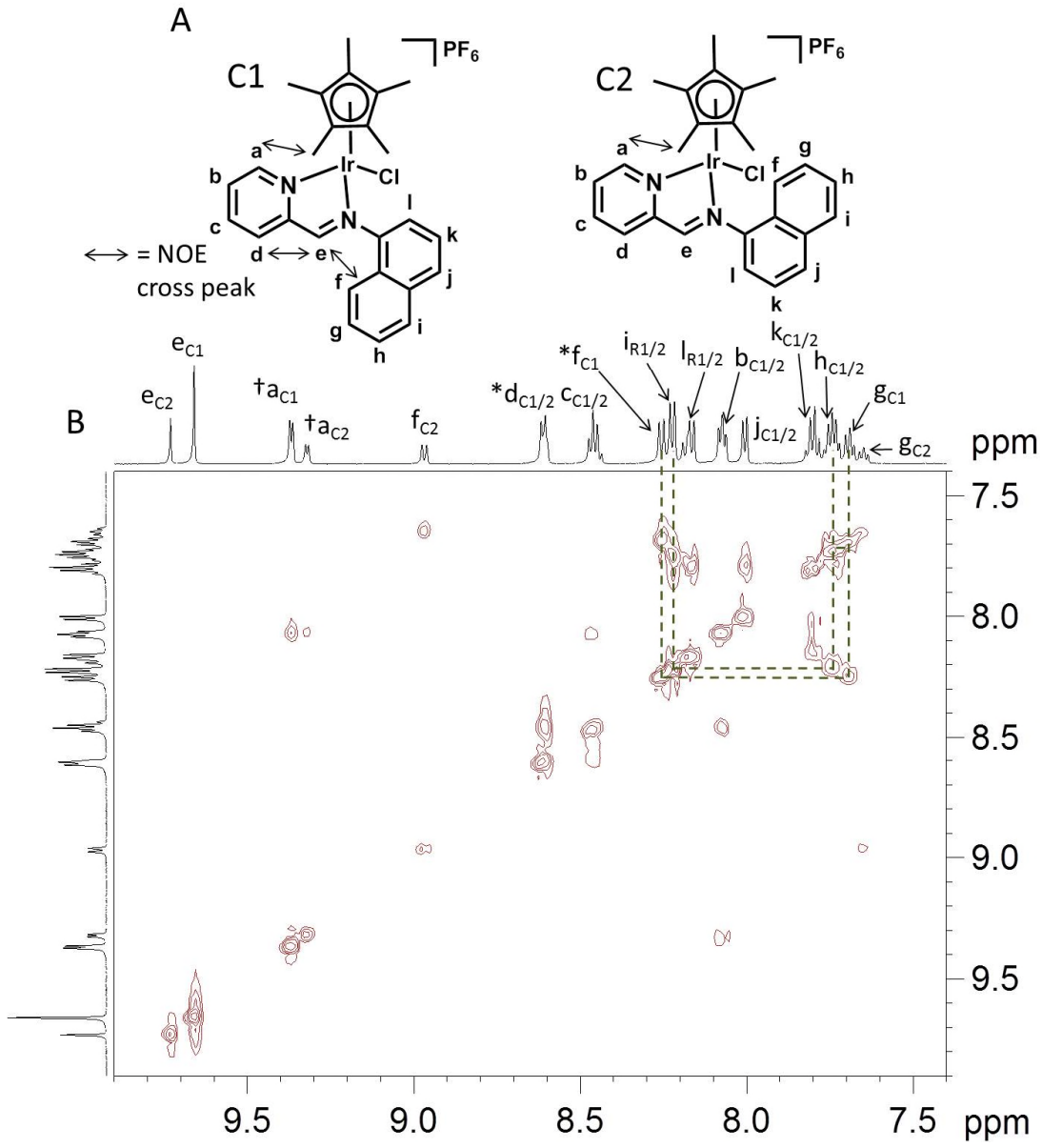

Figure 6.8. (A) Labelling of protons of complex **43** in the two conformations C1 and C2. (B) Assignment of 2D ^{1}H NMR COSY spectrum of complex **43** (600 MHz, acetone-d_6) at 223 K. Major species in solution assigned as conformational isomer C1 where the naphthyl group points away from the chlorido ligand. (* = exhibit NOE cross peaks with imine proton e_{C1} and † = exhibit NOE cross peaks with Cp* protons of C1 and C2).

6.3.3 Aqueous Chemistry

The behaviour of the complexes in aqueous solution was analysed by both ^{1}H NMR spectroscopy and LC-MS to ascertain the species in solution.

6.3.3.1 ^{1}H NMR Spectroscopy

The aqueous solution chemistry of complexes **29-34**, **37** and **40-42** (ca. 500 μM) was investigated by ^{1}H NMR spectroscopy in 26.7% MeOD-d_4/73.3% D_2O (v/v) at 310 K over a 24 h period. They were selected to represent different ImPy chelating ligands and the effect of different Cp^x capping ligands on the behaviour observed.

15 min (first spectra obtained) after dissolution, three sets of peaks were visible in the low-field region for the Cp* complexes, alongside three sets of peaks for the methyl protons on the Cp* ring, as exemplified for complexes [(η^5-Cp*)Ir(ImPy-OH)Cl]PF_6 **32** and [(η^5-Cp*)Ir(ImPy-I)Cl]PF_6 **40** in Figure 6.9 a and 6.10, respectively. In contrast, the Cp^{xPh} (**30**, **33** and **41**) and Cp^{xBiPh} (**31**, **34** and **42**) exhibited two sets of peaks, as exemplified for complex [(η^5-Cp^{xBiPh})Ir(ImPy-OH)Cl]PF_6 **34** in Figure 6.9 b. It is likely that one of the species in all cases is the Ir-OD_2/OD adduct. To confirm that a hydrolysis process had taken place, the ^{1}H NMR spectra were also recorded in 4 mM NaCl. Only one set of peaks were dominant for all complexes, likely belonging to the Ir-Cl adduct, which also had the same chemical shift as the major species in the absence of NaCl. This remained constant over a 24 h period. Therefore, hydrolysis appears to be almost completely supressed in the presence of biologically relevant chloride concentrations. Higher concentrations of NaCl resulted in precipitation of some of the complexes under the conditions studied. The percentage of chloride adduct for each complex after 15 min is shown in Table 6.4. In general, an increase in the substitution of the Cp^x ligand results in less hydrolysis.

After 24 h (in the absence of NaCl), complex [(η^5-Cp*)Ir(ImPy-I)Cl]PF_6 **40** (which appears to hydrolyse to the greatest extent after 15 min) displayed formation of an unidentified new species, as evident by peaks in the high- and low-field region

(Figure 6.10). For all of the other complexes, the formation of a new species after 24 h occurred, but was minor in comparison to **40**. Comparison of the ^{1}H NMR spectra with free chelating ligand showed no similarities in chemical shift. The chloride adduct in all cases appears to remain the dominant species in solution.

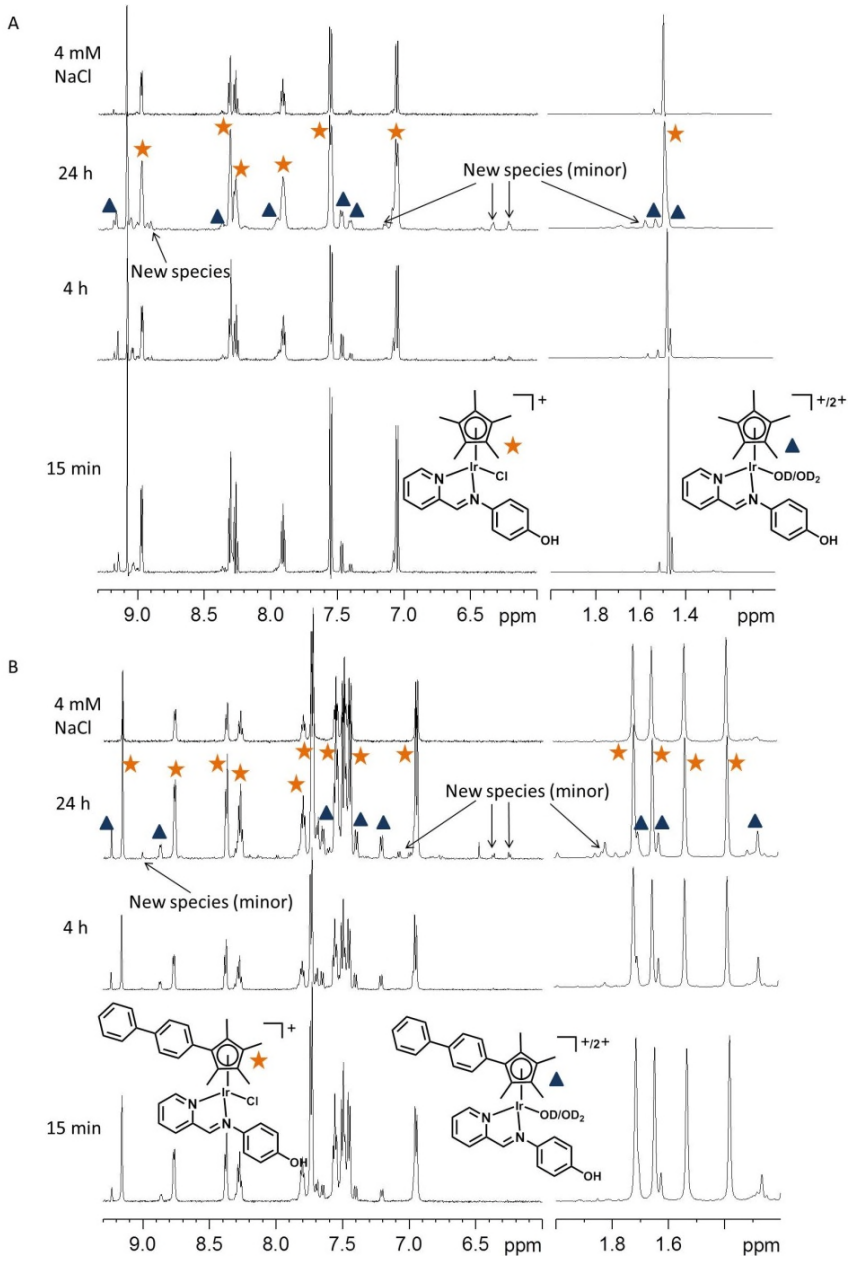

Figure 6.9. ^{1}H NMR spectra of complex [(η^5-Cp*)Ir(ImPy-OH)Cl]PF_6 **32** (A) and [(η^5-Cp^{xBiPh})Ir(ImPy-OH)Cl]PF_6 **34** (B) (ca. 500 μM) in 26.7% MeOD-d_4/73.3% D_2O, 310 K at 15 min, 4 h, 24 h and in the presence of 4 mM NaCl. Star = chloride species and triangle = aqua/hydroxido species. The peaks due to the unidentified new species are highlighted.

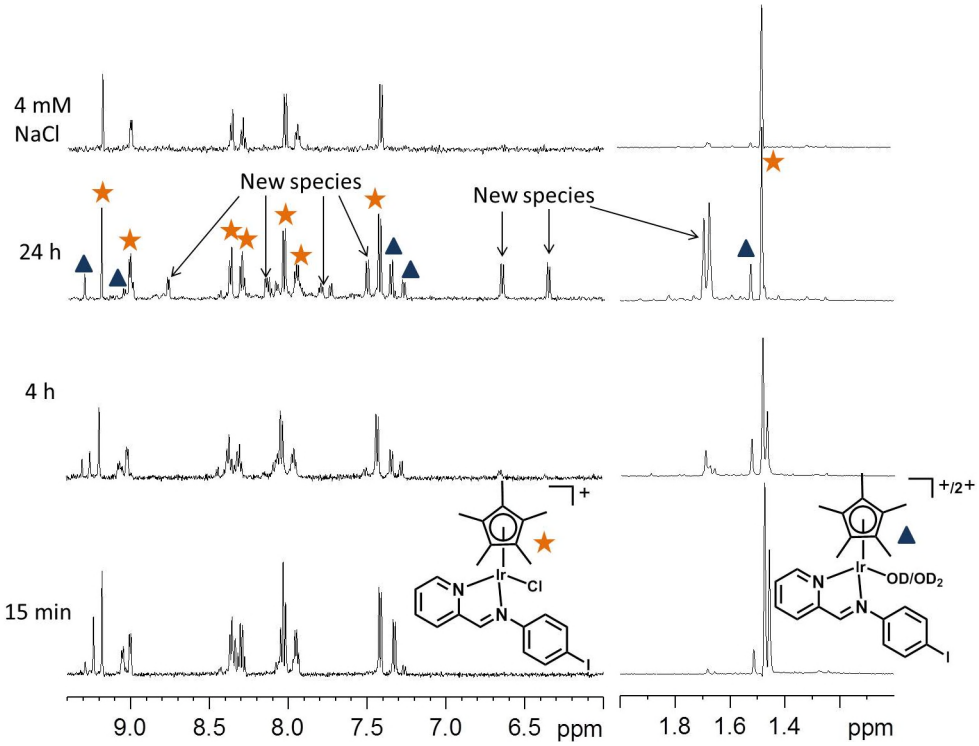

Figure 6.10. ^{1}H NMR spectra of complex [(η^5-Cp*)Ir(ImPy-I)Cl]PF_6 **40** (ca. 500 µM) in 26.7% MeOD-d_4/73.3% D_2O, 310 K at 15 min, 4 h, 24 h and in the presence of 4 mM NaCl. Star = chloride species and triangle = aqua/hydroxido species. The peaks due to the unidentified new species are highlighted.

Table 6.4. Percentage of chloride adduct of complexes **29-34**, **37** and **40-42** (ca. 500 µM) as determined by ^{1}H NMR spectroscopy (600 MHz, 26.7% MeOD-d_4/73.3% D_2O at 310K) after 15 min based on peak integration of the imine proton.

Complex	Cp^x ligand	Chelating ligand	% Ir-Cl
29	Cp*	ImPy-NMe_2	72
30	Cp^{xPh}	ImPy-NMe_2	82
31	Cp^{xPBih}	ImPy-NMe_2	84
32	Cp*	ImPy-OH	81
33	Cp^{xPh}	ImPy-OH	87
34	Cp^{xBiPh}	ImPy-OH	88
37	Cp*	ImPy-F	84
40	Cp*	ImPy-I	56
41	Cp^{xPh}	ImPy-I	58
42	Cp^{xBiPh}	ImPy-I	60

The pH* dependence on the stability of the complexes was also investigated after 24 h. The pH* of the D_2O solution was adjusted, using either $DClO_4$ or NaOD, to give a pH* range of 2.2-8.1 before adding to the concentrated methanolic stock solutions. At low pH* (2.2-4.2), the chlorido adduct appears to be the dominant species, with small peaks associated with aqua/hydroxido species. Upon an increase in pH* (6.2-8.1), the new unidentified species is formed as exemplified for complex [(η^5-Cp*)Ir(ImPy-OH)Cl]PF_6 **32** in Figure 6.11, which increases in intensity as the pH* increases. The formation of the new species appears to be sensitive to the pH* of the solution, which may imply involvement of the coordinated aqua ligand.

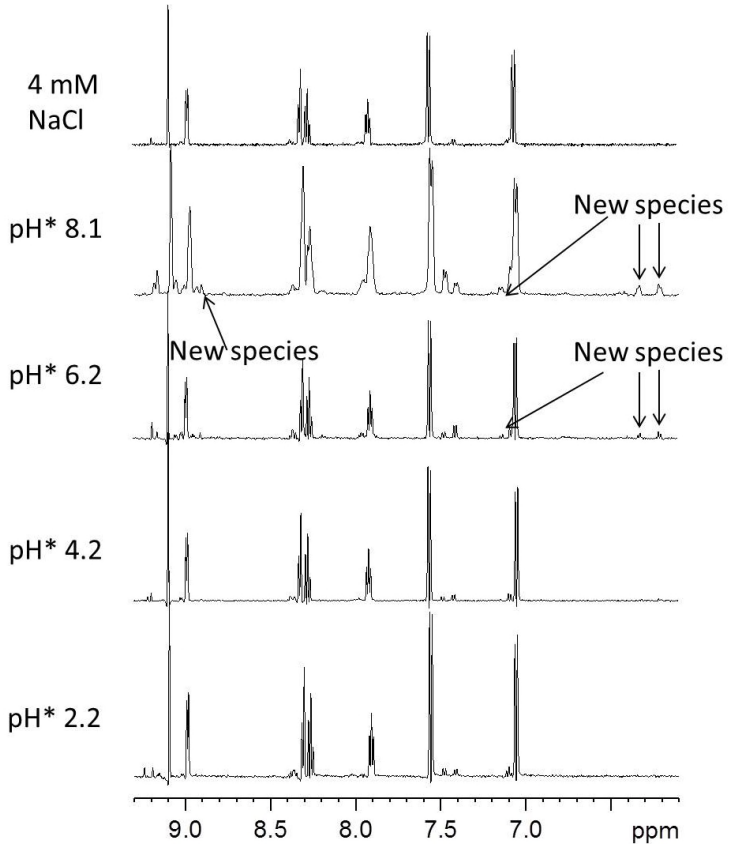

Figure 6.11. Low-field region of ^{1}H NMR spectra of complex [(η^5-Cp*)Ir(ImPy-OH)Cl]PF_6 **32** (ca. 500 μM) in 26.7% MeOD-d_4/73.3% D_2O, 298 K after 24 h over a pH* range of 2.2 – 8.1.

Determination of the pK_a* (pH* at which half of the aqua adducts are deprotonated) of the coordinated aqua ligand was attempted for complexes [(η^5-Cp*)Ir(ImPy-OH)Cl]PF_6 **32** and [(η^5-Cp*)Ir(ImPy-I)Cl]PF_6 **40** (^{1}H NMR, 600 MHz, 26.7% MeOD-d_4/73.3% D_2O, 298K) by preparing aqua complexes from the addition of 0.98 mol equiv. of $AgNO_3$ at pH* 2.0. This resulted in chloride and aqua adducts being present in solution, allowing for detection of any changes in the proton resonances of either species upon a change in pH*. For complex **40** (Figure 6.12 a) fitting the curve to the Henderson-Hasselbalch equation results in a pK_a* value 4.6 ± 0.1, however, the change in chemical shift between pH* 4.1 and 4.9 of the aqua adduct was sharp (9.35-9.25 ppm) and so the error in the pK_a* could be high. As expected, no change in the chloride adduct resonances was observed. The pK_a* of the aqua adduct of complex **32** could not be determined due to complication with the phenolic proton on the chelating ligand, resulting in two pK_a* curves overlapping (Figure 6.12 b). This was confirmed by monitoring the change in shift of the chlorido adduct resonances which showed changes at high pH* presumably due to deprotonation of the phenolic proton. However, it can be estimated that the pK_a* of the aqua adduct is likely to be higher than for complex **40**, as evident by the starting point of the pK_a* curve for **32** (around pH* 5.5).

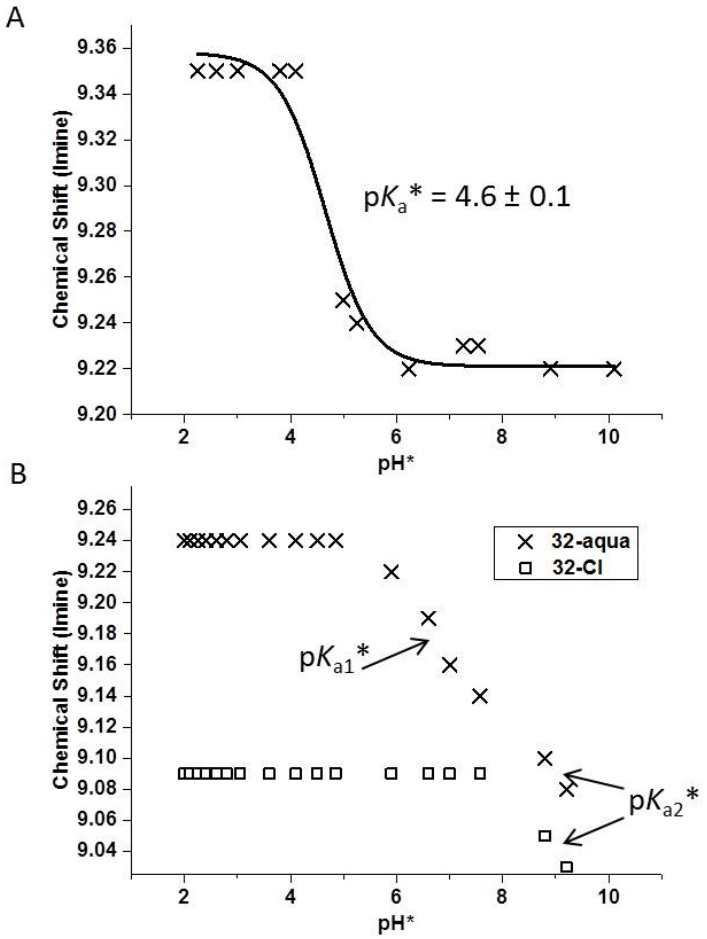

Figure 6.12. pH* titration curves as a function of the imine proton resonance for each species in (A) aqua adduct of complex **40** and (B) aqua and chloride adduct of complex **32**. The two pK_a* curves for complex **32** are due to the aqua ligand (pK_{a1}*) and phenol group (pK_{a2}*).

6.3.3.2 LC-MS

The species present in aqueous solution for complexes [(η^5-Cp*)Ir(ImPy-OH)Cl]PF_6 **32** and [(η^5-Cp^{xBiPh})Ir(ImPy-I)Cl]PF_6 **42** (ca. 100 μM, 10% MeOH/90% H_2O, unbuffered) were also analysed by LC-MS. The LC trace for each complex is shown in Figure 6.13 with assigned peaks corresponding to the MS data obtained (Table 6.5 (**32**) and 6.6 (**42**)). Some peaks in each trace did not show any m/z signal, preventing full assignment of the hydrolysis products (shown as n.d. in the tables). No aqua

adducts were detected for **32** and **42**, only chlorido and TFA adducts (mobile phase contained 0.1% TFA). Intriguingly, both complexes exhibited peaks corresponding to the species $[(Cp^{x})Ir(MeCN)_3]^{2+}$ indicating release of the chelating ligand (H_2O and MeCN were used as mobile phase). Complex **32** exhibited an m/z peak containing the iridium isotopic distribution an m/z of 634.17 that was not assignable. Release of the chelating ligand in aqueous solution was detected as peak 1 for complex **42**.

Table 6.5. LC-MS analysis of complex $[(\eta^5\text{-Cp*})Ir(ImPy\text{-}OH)Cl]PF_6$ **32** (ca. 100 μM, 10% MeOH/90% H_2O).

Peak	m/z	Assigned species	Calculated m/z
1	639.10	$[(\eta^5\text{-Cp*})Ir(ImPy\text{-}OH)O\text{-}(C=O)CF_3]^+$	639.14
2	450.10	$([(\eta^5\text{-Cp*})Ir(MeCN)_3])\text{-}H^+$	450.15
3	634.17	Unassignable	n/a
4	n.d.	n.d.	n.d.
5	561.09	$[(\eta^5\text{-Cp*})Ir(ImPy\text{-}OH)Cl]^+$	561.13

Table 6.6. LC-MS analysis of complex $[(\eta^5\text{-}Cp^{xBiPh})Ir(ImPy\text{-}I)Cl]PF_6$ **42** (ca. 100 μM, 10% MeOH/90% H_2O).

Peak	m/z	Assigned species	Calculated m/z
1	308.09	$[ImPy\text{-}I+H]^+$	308.99
2	588.12	$([(\eta^5\text{-}Cp^{xBiPh})Ir(MeCN)_3])\text{-}H^+$	588.20
3	887.05	$[(\eta^5\text{-}Cp^{xBiPh})Ir(ImPy\text{-}I)\ O\text{-}(C=O)CF_3]^+$	887.09
4	n.d.	n.d.	n.d.
5	809.04	$[(\eta^5\text{-}Cp^{xBiPh})Ir(ImPy\text{-}I)Cl]^+$	809.08

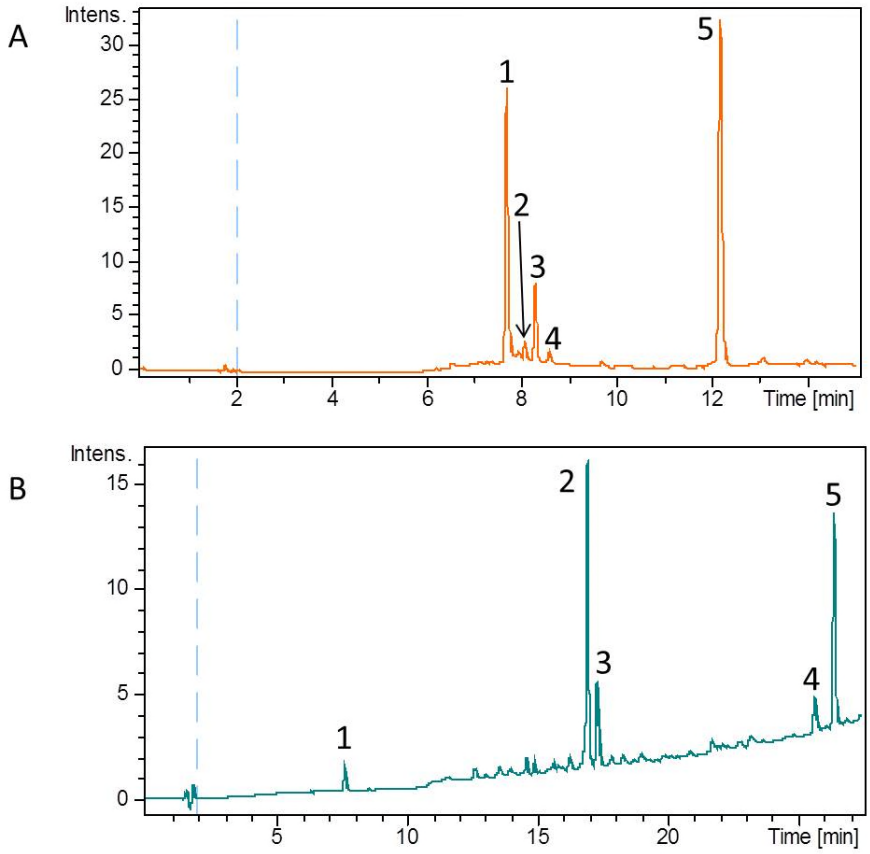

Figure 6.13. LC (λ = 254 nm) traces of complexes [(η^5-Cp*)Ir(ImPy-OH)Cl]PF_6 **32** (A) and [(η^5-Cp^{xBiPh})Ir(ImPy-I)Cl]PF_6 **42** (B) (100 μM) after 24 h incubation at 310 K in 10% MeOH/90% H_2O. Peak numbers indicate species analysed by LC-MS.

The stability of complex [(η^5-Cp^{xBiPh})Ir(ImPy-I)Cl]PF_6 **42** (ca. 100 μM) in LB media (2% dmso/98% LB) which is used in antibacterial assays was also determined after 24 h incubation at 310 K by LC-MS. The peaks in the first 10 min are due to the LB media and so were not analysed. Only two peaks were observed after 10 min which both contained m/z peaks containing the iridium isotopic pattern (see section 1.4) and are indicated in Figure 6.14 and Table 6.7. Peak 1 contained dmso and TFA adducts of **42** and peak 2 was assigned as the chlorido adduct.

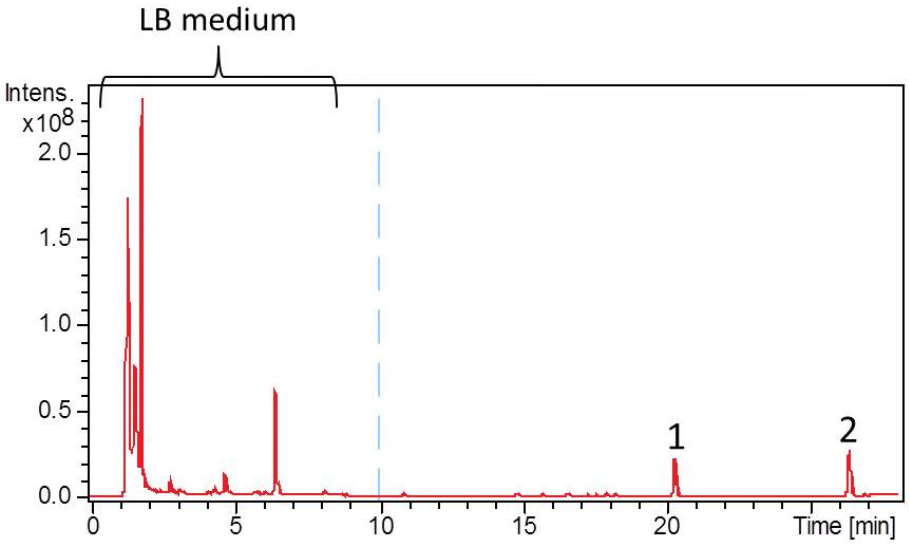

Figure 6.14. LC trace of complex $[(\eta^5\text{-Cp}^{\text{xBiPh}})\text{Ir(ImPy-I)Cl}]\text{PF}_6$ **42** (ca. 100 μM, 2% dmso/98% LB media) after 24 h incubation at 310 K.

Table 6.7. LC-MS analysis of complex $[(\eta^5\text{-Cp}^{\text{xBiPh}})\text{Ir(ImPy-I)Cl}]\text{PF}_6$ **42** (ca. 100 μM, 2% dmso/98% LB media).

Peak	m/z	Assigned species	Calculated m/z
1	887.00	$[(\eta^5\text{-Cp}^{\text{xBiPh}})\text{Ir(ImPy-I)dmso}]\text{Cl}^+$	887.09
		$[(\eta^5\text{-Cp}^{\text{xBiPh}})\text{Ir(ImPy-I) O-(C=O)CF}_3]^+$	887.09
2	809.04	$[(\eta^5\text{-Cp}^{\text{xBiPh}})\text{Ir(ImPy-I)Cl}]^+$	809.08

6.3.4 Relative Hydrophobicity

Comparison of the retention times (t_R) of complexes **29**, **32-34** and **40-43** (100 μM, 1:9 MeOH:H_2O) by RP-HPLC, where a longer retention time is indicative of a more hydrophobic complex, allows for evaluation of the relative hydrophobicity. Suppression of hydrolysis was achieved by dissolving the complexes in 50 mM NaCl where the complexes should exist as just the chlorido adduct. The resulting HPLC traces are shown in Figure 6.15 with the average t_R indicated for each complex in Table 6.8. No t_R was found for complex **42** as the conditions used for dissolution of the complexes resulted in precipitation. Complex $[(\eta^5\text{-Cp*})\text{Ir(ImPy-}$

OH)Cl]PF_6 **32** is the most hydrophilic with an average t_R of 10.73 min, while the most hydrophobic complex is [(η^5-Cp^{xPh})Ir(ImPy-I)Cl]PF_6 **41** with an average t_R of 21.90 min. As expected, the addition of phenyl substituents to the cyclopentadienyl ligand results in more hydrophobic complexes.

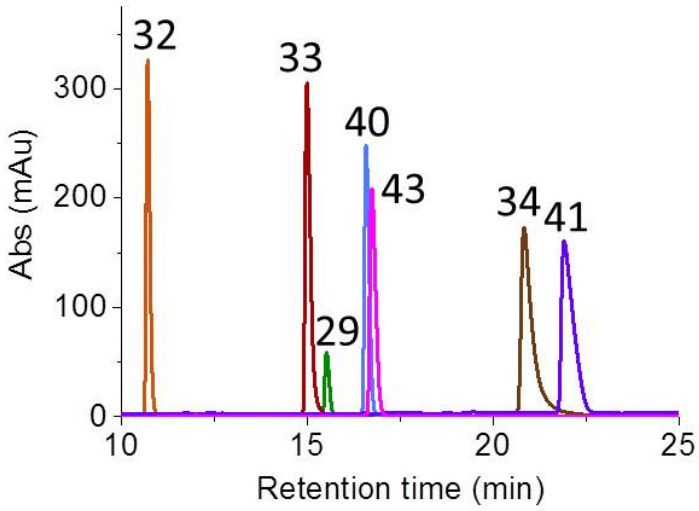

Figure 6.15. RP-HPLC traces (signal = 254 nm, ref = 360 nm) of complexes **29**, **32-34** and **40-43** (100 μM, 1:9 MeOH:H_2O) in the presence of 50 mM NaCl to supress hydrolysis.

Table 6.8. Retention times (t_R) obtained by RP-HPLC for complexes **29**, **32-34** and **40-43** as a measurement of relative hydrophobicity. t_R and standard deviations are based upon triplicate measurements. Complex **43** precipitated out of solution and so no t_R could be found.

Complex	**t_R (min)**
[(η^5-Cp*)Ir(ImPy-NMe_3)Cl]PF_6 **29**	15.4 ± 0.3
[(η^5-Cp*)Ir(ImPy-OH)Cl]PF_6 **32**	10.73 ± 0.03
[(η^5-Cp^{xPh})Ir(ImPy-OH)Cl]PF_6 **33**	15.02 ± 0.03
[(η^5-Cp^{xBiPh})Ir(ImPy-OH)Cl]PF_6 **34**	20.86 ± 0.03
[(η^5-Cp*)Ir(ImPy-I)Cl]PF_6 **40**	16.52 ± 0.05
[(η^5-Cp^{xPh})Ir(ImPy-I)Cl]PF_6 **41**	21.90 ± 0.02
[(η^5-Cp^{xBiPh})Ir(ImPy-I)Cl]PF_6 **42**	n.d.
[(η^5-Cp*)Ir(ImPy-Naphth)Cl]PF_6 **43**	16.73 ± 0.00

6.3.5 Antibacterial Activity

The antibacterial activity of complexes **29-45** was evaluated against the Gram-positive bacterium *Staphylococcus aureus* (*S. aureus*) and the Gram-negative bacterium *Escherichia coli* (*E. coli*). Antibacterial activity was assessed by determining the minimum inhibitory concentration (MIC) which is the lowest concentration that inhibits visible growth of a microorganism over a given incubation period (22 h), and was compared with the known antibacterial agents vancomycin, kanamycin and nisin, Table 6.9. There was minimal antibacterial activity against the Gram-negative *E. coli*, with the most potent complexes (all Cp^{xBiPh} complexes) exhibiting MICs of 100 μM. Antibacterial activity was observed against the Gram-positive *S. aureus* with MIC values generally ranging from 8 – 100 μM. The antibacterial activity appears to increase upon introduction of the extended Cp^{xBiPh} ligand with complexes **31**, **34**, **42** and **45** exhibiting MIC values of between 8-15 μM. The potency of antibacterial action follows the trend Cp^{xBiPh} > Cp^{xPh} ~ Cp*.

The minimum bactericidal concentration (MBC - minimum concentration that will kill a particular bacterium) of some complexes against *S. aureus* was also determined and is shown on Table 6.6. It is evident that the MBC value is dependent on the cyclopentadienyl ligand, with the extended Cp^{xBiPh} giving the lowest MBC values, showing the complexes are bactericidal rather than bacteriostatic.

To assess whether the extended Cp^{xBiPh} ligand is responsible for the antibacterial activity of the complexes, the free ligand ($Cp^{xBiPh}H$) was assessed for activity against *S. aureus*, alongside the iridium dimer $[(Cp^{xBiPh})IrCl_2]_2$ used as the common starting material to synthesise the half-sandwich complexes. The $Cp^{xBiPh}H$ ligand exhibited

no antibacterial activity while the dimer $[(Cp^{xBiPh})IrCl_2]_2$ exhibited a MIC of 30 μM, Table 6.9.

Table 6.9. MIC and MBC values for complexes **29-45** against *E. coli* and *S. aureus*.

			MIC (μM)		MBC (μM)
Complex/ Compound	Cp^x	ImPy	*E. coli*	*S. aureus*	*S. aureus*
29	Cp*	ImPy-NMe_2	>100	>100	n.d.
30	Cp^{xPh}	ImPy-NMe_2	>100	>100	n.d.
31	Cp^{xBiPh}	ImPy-NMe_2	n.d.	10	30
32	Cp*	ImPy-OH	>100	>100	n.d.
33	Cp^{xPh}	ImPy-OH	>100	>100	n.d.
34	Cp^{xBiPh}	ImPy-OH	>100	10-15	30
35	Cp*	ImPy-OMe	>100	100	n.d.
36	Cp*	ImPy-COOH	>100	100	n.d.
37	Cp*	ImPy-F	>100	100	n.d.
38	Cp*	ImPy-Cl	>100	100	n.d.
39	Cp*	ImPy-Br	>100	100	n.d.
40	Cp*	ImPy-I	>100	100	>100
41	Cp^{xPh}	ImPy-I	>100	50-60	100
42	Cp^{xBiPh}	ImPy-I	100	8-10	10
43	Cp*	ImPy-Naphth	>100	50	n.d.
44	Cp^{xPh}	ImPy-Naphth	>100	50	n.d.
45	Cp^{xBiPh}	ImPy-Naphth	100	8	10
$Cp^{xBiPh}H$	Cp^{xBiPh}	n.a.	>100	>100	n.d.
$[(\eta^5\text{-}Cp^{xBiPh})IrCl_2]_2$	Cp^{xBiPh}	n.a.	>100	30	n.d.
Vancomycin	n.a.	n.a.	n.d.	1	n.d.
Kanamycin	n.a.	n.a.	0.05	n.d.	n.d.
Nisin	n.a.	n.a.	n.d.	8	n.d.

MIC = the lowest concentration that inhibits visible growth of a microorganism over a given incubation period (22 h)

MBC = minimum concentration that will kill a particular bacterium

6.3.6 Membrane Integrity of *S. aureus*

To investigate the effect on the cytoplasmic membrane structure of *S. aureus* upon incubation with highly active antibacterial complexes $[(\eta^5\text{-}Cp^{xBiPh})Ir(ImPy\text{-}NMe_2)Cl]PF_6$ **31**, $[(\eta^5\text{-}Cp^{xBiPh})Ir(ImPy\text{-}OH)Cl]PF_6$ **34**, $[(\eta^5\text{-}Cp^{xBiPh})Ir(ImPy\text{-}I)Cl]PF_6$ **42** and $[(\eta^5\text{-}Cp^{xBiPh})Ir(ImPy\text{-}Naphth)Cl]PF_6$ **45**, the BacLight™ DEAD/ALIVE assay

was used.[28] After a short incubation time (25 min, 310 K) of the complexes at 4 × MIC with *S. aureus*, fluorescent dyes SYTO 9 and PI were added. SYTO 9 can penetrate through non-damaged cell membranes and fluoresces green (alive), while PI only enters membrane-damaged cells and fluoresces red (dead) upon binding to DNA. The ratio of green/red fluorescence gives a measure of the pore-forming ability of the antibacterial agents. The ratio is compared with a set of standards that have been prepared to include a given population dead (membrane damaged, red fluorescing) cells and alive (membrane intact, green fluorescing) cells. The green/red fluorescence ratios for complexes **31**, **34**, **42** and **45** are shown in Figure 6.16 and compared with the known pore-forming antimicrobial peptide nisin[29] and the non-pore-forming vancomycin.[30] The results indicate that complexes **31**, **42** and **45** are membrane damaging agents after a short incubation time, while complex **34** showed a mild ability to disrupt the membrane; therefore it is likely that their mechanism of action involves interaction with the cytoplasmic membrane.

Fluorescence confocal microscopy was performed on *S. aureus* upon incubation with complex [(η^5-Cp^{xBiPh})Ir(ImPy-I)Cl]PF_6 **42,** and compared with cells incubated with nisin. The overlaid images of green and red fluorescence for **42** and nisin show either red or orange/yellow images, which is indicative of membrane permeabilisation (Figure 6.17).

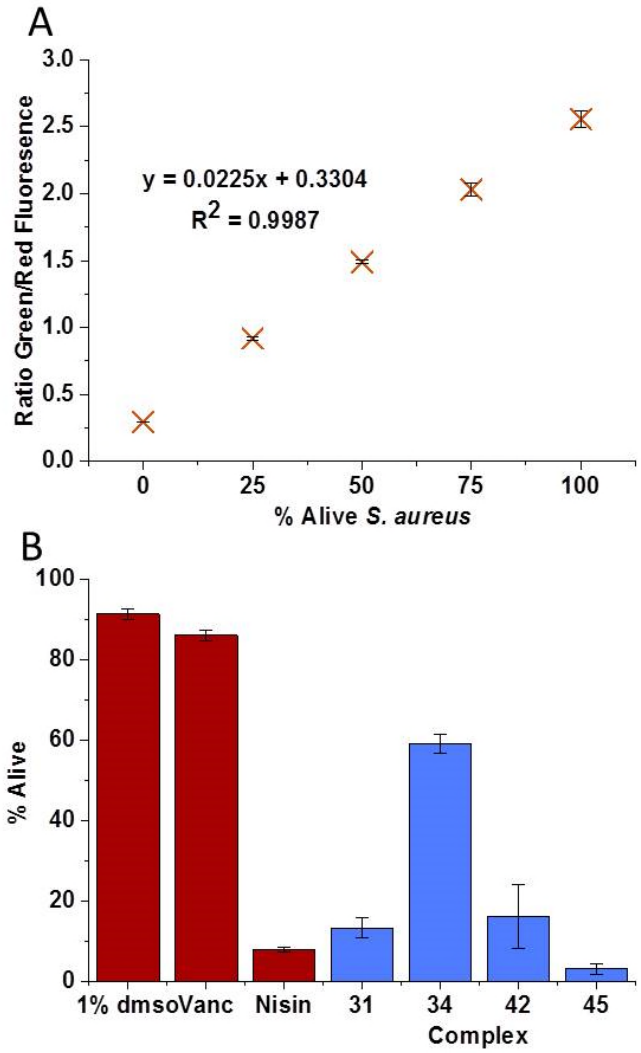

Figure 6.16 Extent of membrane damage in *S. aureus* as determined by the BacLight™ DEAD/ALIVE assay. (A) – Calibration curve for determination of percentage viable cells (non-membrane damaged) as the ratio of green (λem = 530 nm, alive) and red (λem = 630 nm, dead) fluorescence after excitation at 470 nm. R^2 = 0.9987. (B) – Percentage of viable cells (alive) after incubation (25 min, 310 K) with complexes [(η^5-Cp^{xBiPh})Ir(ImPy-NMe$_2$)Cl]PF$_6$ **31**, [(η^5-Cp^{xBiPh})Ir(ImPy-OH)Cl]PF$_6$ **34**, [(η^5-Cp^{xBiPh})Ir(ImPy-I)Cl]PF$_6$ **42** and [(η^5-Cp^{xBiPh})Ir(ImPy-Naphth)Cl]PF$_6$ **45** at 4 × MIC and compared with positive control nisin (pore-former) and negative controls 1% dmso and vancomycin at 4 × MIC (non-pore-forming).

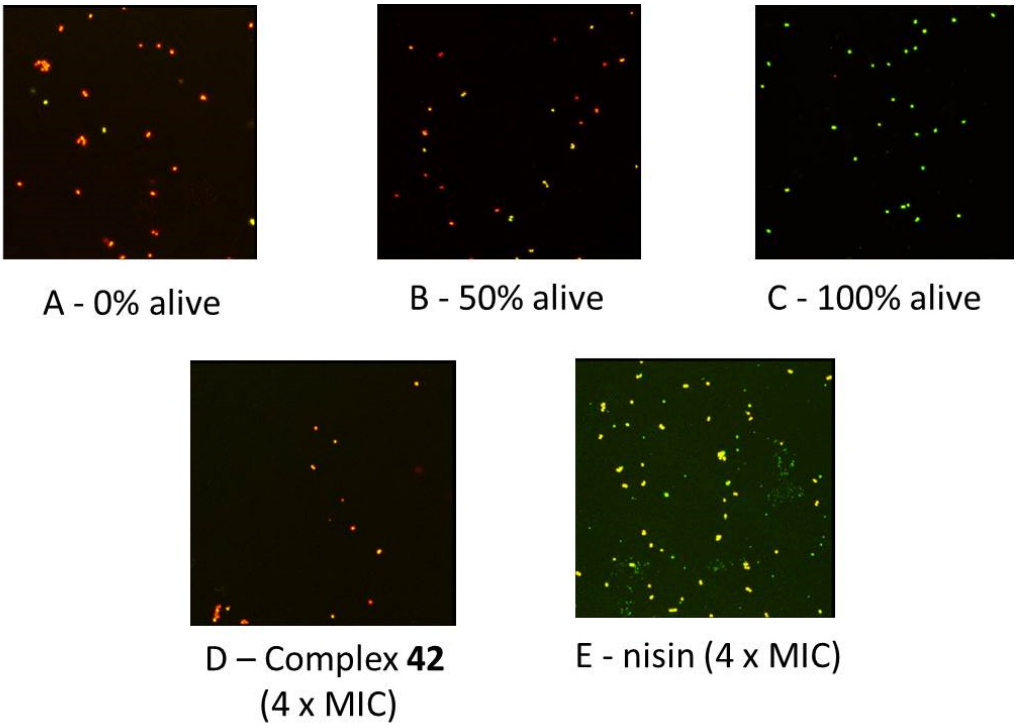

Figure 6.17. Confocal fluorescence microscopy images of *S. aureus*. (A-C) images of standards used for determining the extent of membrane-damage upon exposure to antibacterial agents. A – 0% alive cells (all membrane damaged so fluoresce red), B – 50% alive cells (1:1 ratio of membrane damaged and membrane intact cells) and C – 100% live cells (all membrane intact so fluoresce green). D – *S. aureus* after exposure to complex [(η^5-Cp^{xBiPh})Ir(ImPy-I)Cl]PF$_6$ **42** at 4 × MIC showing red/orange fluorescence indicative of membrane damage. E - – *S. aureus* after exposure to control nisin at 4 × MIC showing orange fluorescence indicative of membrane damage. Some cells present are still membrane intact and so fluoresce green.

6.3.7 Antiproliferative Activity in Human Cell Lines

The antiproliferative action of complexes **29-44** was determined against the A2780 human ovarian cancer cell line (Table 6.10). In general, complexes bearing the Cp* ligand were inactive, with IC_{50} values of >100 μM. Only Cp* complexes **29** and **43** showed any activity with IC_{50} values of 39.6 and 13.3 μM, respectively. Upon introduction of extended Cp^{xPh} and Cp^{xBiPh} ligands, the antiproliferative activity

increased. Within any given set of complexes bearing the same ImPy ligand, the order of potency was $Cp^{xBiPh} > Cp^{xPh} > Cp^*$. It is apparent that the presence of the -NMe_2 and naphthyl group in complexes **29-31** and **43-45**, respectively, result in more potent complexes.

The antiproliferative action against the MRC5 human fibroblast cell line (healthy cell model) for complexes **31**, **34**, **42** and **45** which exhibited the best antibacterial action was determined. All complexes were active, with IC_{50} values ranging from 0.35 – 6.7 μM, Table 6.10.

Table 6.10. IC_{50} values for complexes **29-45** in the A2780 human ovarian cancer cell line and complexes **31**, **34**, **42** and **45** in the MRCF human fibroblast cell line. Drug exposure time was 24 h followed by a 72 h recovery time.

			IC_{50} (μM)	
Complex	Cp^x	ImPy	A2780	MRC5
29	Cp*	ImPy-NMe_2	38.64 ± 0.85	n.d.
30	Cp^{xPh}	ImPy-NMe_2	1.07 ± 0.04	n.d.
31	Cp^{xBiPh}	ImPy-NMe_2	0.64 ± 0.01	0.35 ± 0.04
32	Cp*	ImPy-OH	>100	n.d.
33	Cp^{xPh}	ImPy-OH	34 ± 1	n.d.
34	Cp^{xBiPh}	ImPy-OH	5.59 ± 0.09	6.7 ± 0.6
35	Cp*	ImPy-OMe	>100	n.d.
36	Cp*	ImPy-COOH	>100	n.d.
37	Cp*	ImPy-F	>100	n.d.
38	Cp*	ImPy-Cl	>100	n.d.
39	Cp*	ImPy-Br	>100	n.d.
40	Cp*	ImPy-I	>100	n.d.
41	Cp^{xPh}	ImPy-I	8.9 ± 0.06	n.d.
42	Cp^{xBiPh}	ImPy-I	6.2 ± 0.2	3.57 ± 0.04
43	Cp*	ImPy-Naphth	13.3 ± 0.3	n.d.
44	Cp^{xPh}	ImPy-Naphth	4.44 ± 0.2	n.d.
45	Cp^{xBiPh}	ImPy-Naphth	1.11 ± 0.07	3.9 ± 0.3
Cisplatin	n.a.	n.a.	1.2 ± 0.2	13.2 ± 0.4

6.4 Discussion

6.4.1 Characterisation

A search of the Cambridge Crystallographic Database showed only two previous reports of a Cp* iridium(III) half-sandwich complexes bearing a *N*-(pyrid-2-ylmethylene)amine chelating ligand.[17,27] Complexes [(η^5-Cp^{xPh})Ir(ImPy-I)Cl]PF_6 **41**, [(η^5-Cp^{xBiPh})Ir(ImPy-I)Cl]PF_6 **42**, and [(η^5-Cp^{xPh})Ir(ImPy-Naphth)Cl]PF_6 **44** are the first reported X-ray crystal structures of iminopyridine complexes bearing an extended cyclopentadienyl capping ligand.

In general, the Ir – C ring centroid distances do not vary, with the Cp* complexes **29**, **32** and **43** exhibiting distances of between 1.785 – 1.793 Å while the extended Cp^{xPh} and Cp^{xBiPh} complexes **41**, **42** and **44a-b** exhibit distances of 1.790 – 1.796 Å. The Ir-Cl bond lengths range from 2.3704 - 2.4002 Å with no relation to the type of Cp^x capping ligand or chelating ligand evident. There appears to be no major effect on the structure of the complexes by extension of the Cp^x capping ligand. The angle between the mean plane of the pyridyl ring and the mean plane of the aniline ring was made significantly more obtuse by the presence of the naphthyl group in the chelating ligand of complexes **43** and **44a-b** (65.71 – 73.44°) compared to the para-substituted complexes **29**, **32**, **41** and **42** (50.34 – 58.57°).

Comparison with the previously reported structurally-similar Ir(III) complexes [(η^5-Cp*)Ir(4-propyl-N-(2-pyridylmethylene)-benzenamine)Cl]PF_6[18] and [(η^5-Cp*)Ir(N-(2-pyridylmethylene)-(R)-1-phenylethylamine)-benzenamine)Cl]SbF_6[31] showed that the complexes reported here exhibit bond lengths and angles within same ranges.

DFT analysis of the electrostatic potential surfaces of the complexes showed they are relatively non-polar; the aniline ring has slightly higher electronic density than the

pyridyl ring. The electrostatic potential surface is more positive than for the neutral [(η^5-Cp*)Ir(2-PhPy)Cl] complexes studied in Chapter 3, which is inherently due to the cationic nature of these phenyliminopyridyl complexes.

6.4.2 Hindered Rotation of Complexes 43-45

The naphthyl group of the *N*-(2-pyridnylmethylene)-1-naphthalenamine (ImPy-Naphth) free ligand is able to rotate in solution. When coordinated to iridium(III), the presence of the Cp^x rings produces steric hindrance which restricts rotation of the naphthyl group. This leads to conformational isomerism and two isomers in which the naphthyl group either points away (C1) or towards (C2) the chlorido ligand (Figure 6.6).

Interestingly, analysis of the Gibbs free energy of activation ($\Delta G^{\ddagger}$) showed that the energy barrier to overcome the transition state for the rotation is relatively independent of the Cp^x ligand present in the complex, with $\Delta G^{\ddagger}$ for **43** (Cp*) of 65.4 ± 0.5 kJ mol^{-1} being similar to **44** (Cp^{xPh}) and **45** (Cp^{xBiPh}) ($\Delta G^{\ddagger}$ of 64.2 ± 0.5 and 64.1± 0.5 kJ mol^{-1}, respectively). Therefore, the addition of a large phenyl/biphenyl substituent in place of a methyl group on Cp* does not affect the rotation of the naphthyl ring. This is likely due to the fast rotation exhibited by the Cp^x capping ligand itself.

The ImPy-Naphth chelating has been studied before in the half-sandwich Ru(II) complex [(η^6-1,3,5-triisopropybenzene)Ru(ImPy-Naphth)Cl]Cl where hindered rotation was also observed. Although, the related complex [(η^6-hexamethylbenzene)Ru(N-(2-quinolinyl-methylene)-8-hydroxy-1-napthalenamine)-Cl]Cl (which bears a hydroxyl substituent on the naphthyl group) exhibits no hindered rotation.[20]

Hindered rotation of ligands due to the presence of the Cp^x ligand in metal complexes has not been widely observed.[32,33] The Rh(III) and Ir(III) Cp* complexes [(η^5-Cp*)M(dfppe)Cl]BF_4 (M = Rh or Ir, dfppe = 1,2-bis(dipentafluorophenyl phosphino)ethane showed two fluxional processes due to steric hindrance with different $\Delta G^{\ddagger}$ values.[34] The two processes are likely to be due to the interaction of the pentafluorphenyl rings against the Cp* ligand and the interaction of the pentafluorphenyl ring against the other fluorinated ring bound to the phosphine. The value of $\Delta G^{\ddagger}$ (as calculated from ^{19}F NMR data) showed lower barriers to rotation for the Ir(III) complex than for those studied here (41.5 and 50.0 kJ mol^{-1} compared with 65.4 kJ mol^{-1} for complex **43**). This may be attributed to the longer bond distance of the Ir – P bonds (2.3278(14) and 2.311(2) Å) than the Ir – imino nitrogen bond of **43** (2.052(5) Å), reducing the steric hindrance.

^1H NMR NOESY experiments (Figure 6.7) were performed on complex **43** to investigate which protons on the naphthyl group are close in space to the imine protons, followed by assignment of the protons based on COSY experiments (Figure 6.8). No NOE cross peaks were observed for the minor isomer, but two cross peaks were observed for the major isomer. Analysis indicated that in the major isomer in solution the naphthyl ring points away from the chlorido ligand (C1). The X-ray crystal structures of complexes **43** and **44** also exhibit this conformation. The Hf proton on the naphthyl group (Figure 6.8) appears to be low-field-shifted by ca. 0.7 ppm in the C2 conformation compared to C1, due to being in close proximity to the chlorido ligand. The 2:1 ratio of C1:C2 observed in solution suggests that the isomer C2 is led favoured due to clash of the naphthyl group with the chlorido ligand.

6.4.3 Aqueous Chemistry and Stability

In many chelated piano-stool metal complexes, hydrolysis of the monodentate ligand can be an activation process for the observed biological activity.[5,35] The M-OH_2 bond is believed to be present in the "active species" for many metal-based anticancer complexes, including the clinical drug cisplatin.[36] The aqueous behaviour of representative Ir(III) complexes (**29-34**, **37** and **40-42**) was studied by ^{1}H NMR spectroscopy at 310 K. Either two or three sets of peaks were observed in the aromatic region after 15 min, which may be assigned as the chlorido and aqua/hydroxido adducts (Figure 6.9 and 6.10). The origin of the third species is unknown, but could be a methoxy adduct from the methanol present in the sample.

The extent of hydrolysis after 15 min appears to correlate with the Cp^x capping ligand, following the trend Cp* > Cp^{xPh} > Cp^{xBiPh}. The hydrolysis after 15 min was markedly less than the complexes studied in Chapter 3 which contain the negatively charged 2-PhPy chelating ligand. This is presumably due to extra negative charge on the 2-PhPy complexes which can aid the loss of the chloride ligand. The ImPy chelating ligand is also a π-acceptor, withdrawing electron-density from the metal centre through backbonding. The increase in the positive nature of the metal centre decreases the extent of aquation.

Within 24 h, only two of the initial three peaks for the Cp* complexes remained present in the aromatic region, accompanied by the appearance of a new set of peaks in the high- and low-field regions, implying conversion over time to a new species. A previous study on the formation of aqua adducts in the series of structurally similar Ir(III) complexes of the type [(η^5-Cp*)Ir(N-(2-pyridylmethylene)-(R)-1-phenylethylamine)Cl]SbF_6, used as Diels-Alder catalysts, reported that the complexes could not be isolated due to instability of the aqua species.[31] However, no

investigations into the reasons behind this were carried out. Recently, the related Ir(III) complex [(η^5-Cp*)Ir(4-hydroxymethyl-N-(2-pyridylmethylene)-benzenamine)Cl]PF_6 was reported to exhibit complete stability in aqueous solution.[17] The aqueous stability was measured in the presence of a high concentration of dmso (50% v/v), which may result in suppression of hydrolysis through formation of a dmso adduct, which as has been demonstrated for other half-sandwich metal complexes.[37]

Examination on the effect of the pH* of the solutions by ^{1}H NMR after 24 h incubation (Figure 6.11) showed that at low pH* (2.2-4.2) the unidentified species was not present. Upon an increase in pH* (>6.2) the peaks formed, indicating that the stability of the complexes in aqueous solution is pH dependent. Determination of the pK_a* values of the aqua adducts of complexes [(η^5-Cp*)Ir(ImPy-OH)Cl]PF_6 **32** and [(η^5-Cp*)Ir(ImPy-I)Cl]PF_6 **40** (where the chlorido monodentate ligand is replaced with OD_2, Figure 6.12) showed that the pK_a* is likely to be less than physiological pH (complex **40** ~ 4.6, **32** – not determined due to interference of the pH* titration by the phenolic proton on the chelating ligand, but appears to be between 5.5-7), therefore, likely existing as Ir-OD species rather than Ir-OD_2 at neutral pH. Interestingly, complex **40** shows the largest extent of formation of the new unidentified species, as well as exhibiting a more acidic aqua adduct compared with **32**. This implies that the formation of the new species may be dependent on the formation of a hydroxido adduct. The π-accepting ImPy chelating ligand which can increase the positive nature of the metal centre, can lower the pK_a of an aqua adduct by pulling electron density away from the bound oxygen atom, making the protons on the bound aqua ligand more acidic.

The formation of hydroxido adducts can result in hydroxido bridged dimers. Previously reported Ru(II) and Os(II) half-sandwich complexes with *N,N*-, *N,O*- and *O,O*-chelated ligands have been shown to form hydroxido bridged dimers alongside loss of the chelating ligand in aqueous solution, which all exhibit pK_a values below physiological pH.[38,39] This instability has also been observed in titanocene dichloride where the oxido-bridged oligomers results in the formation of insoluble TiO_2.[40,41] The formation of hydroxido-bridged dimers has been reported for half-sandwich Ir(III) complexes bearing *C,N*-chelated ligands which was accompanied by the release of free chelating ligand, although this only occurred at high pH (>8.7).[42] However, no free chelating ligand was observed in the ^{1}H NMR spectra for the complexes studied here. In contrast, the LC-MS of complexes [(η^5-Cp*)Ir(ImPy-OH)Cl]PF_6 **32** and [(η^5-Cp^{xBiPh})Ir(ImPy-I)Cl]PF_6 **40** in aqueous solution exhibited peaks that contained the m/z fragment ([(η^5-Cp^x)Ir(MeCN)$_3$]-H)$^+$ which implies loss of the chelating ligand (Tables 6.5 and 6.6) The incubation of complex **42** also resulted in a peak which corresponds to free ImPy-I chelating ligand. Further analysis of the solution by LC-MS showed that the peak with the longest retention time for both complexes could be assigned as the chlorido adduct. TFA adducts were also detected at shorter retention times which may correspond to the aqua complexes.

Conflicting data from ^{1}H NMR and LC-MS make identification of the new species formed difficult, but it can be speculated that formation of a bridged hydroxy-dimer is feasible, which would result in loss of the chelating ligand (Figure 6.18 a). Alternatively, an hydroxy-bridged species which retains the chelating ligand could also be the new species formed, which may explain the two Cp* peaks observed for

40 along with the new low-field aromatic resonances which were not due to free-chelating ligand (Figure 6.18 b).

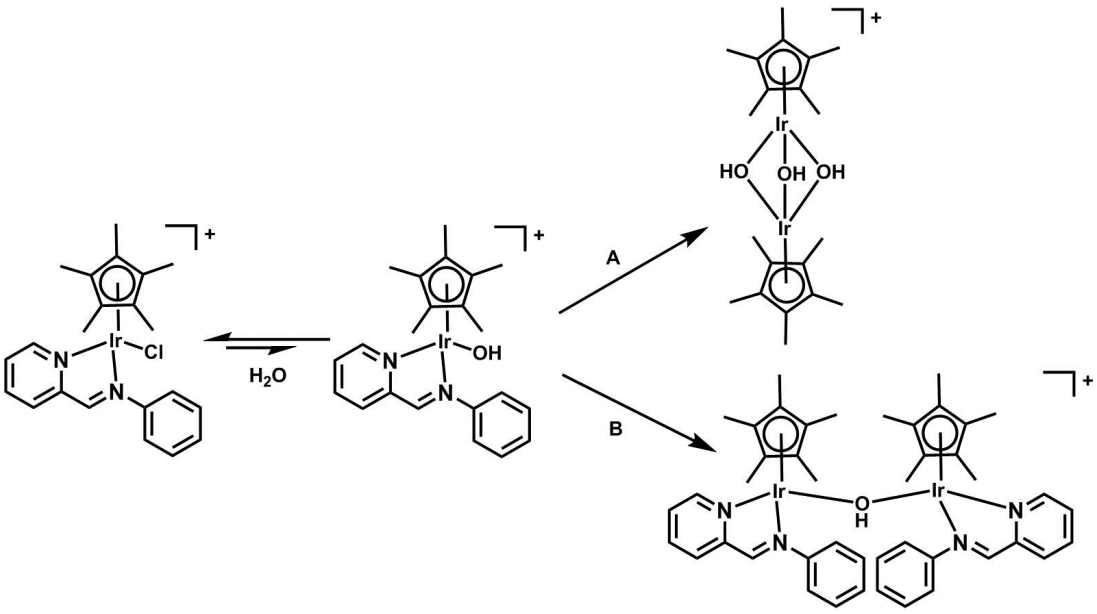

Figure 6.18. Possible species formed in water (in the absence of added chloride) for $[(\eta^5\text{-}Cp^x)Ir(ImPy)Cl]^+$ complexes based on ^1H NMR and LC-MS data. (A) Hydroxy-bridged dimer resulting in release of the chelating ligand and (B) hydroxy-bridged dimer with chelating ligand bound.

However, in the presence of 4 mM NaCl, the complexes appear to exist primarily as the chlorido adduct even after 24 h, as observed by ^1H NMR spectroscopy (Figures 6.9 and 6.10). This suggests that minimal hydrolysis will take place under biological relevant conditions (intracellular $[Cl^-]$) and the complexes remain intact. Therefore, the observed behaviour in the absence of Cl^- in aqueous solution may not be representative of the behaviour of the complexes in a biological medium. The stability of complex **42** in LB (media used for antibacterial testing which contains 171 mM of NaCl, Figure 6.14) was also evaluated and showed that the complex exists as dmso and chlorido adducts after 24 h incubation, further supporting that the presence of chloride appears to prevent the hydrolysis products from forming.

6.4.4 Biological Activity

6.4.4.1 Antibacterial Activity

Due to the rise of antibacterial resistance, new compounds are urgently required that can overcome this resistance. The antibacterial action of complexes **29-45** were evaluated in *E. coli* and *S. aureus* as representatives of Gram-negative and Gram-positive bacteria, respectively. It was found that the complexes exhibit little antibacterial action against the Gram-negative *E. coli* (MIC values of 100 μM), while MICs reached as low as 8-15 μM for complexes [(η^5-Cp^{xBiPh})Ir(ImPy-NMe$_2$)Cl]PF$_6$ **31**, [(η^5-Cp^{xBiPh})Ir(ImPy-OH)Cl]PF$_6$ **34**, [(η^5-Cp^{xBiPh})Ir(ImPy-I)Cl]PF$_6$ **42** and [(η^5-Cp^{xBiPh})Ir(ImPy-Naphth)Cl]PF$_6$ **45** against the Gram-positive *S. aureus*, Table 6.9.

The difference in antibacterial action may be attributed to the differences in the cell wall. The composition of the outer membrane of Gram-negative bacteria includes lipopolysaccharides (LPS)[43] which are highly negatively-charged molecules stabilised by the presence of small metal ions such as Mg^{2+} and Ca^{2+}.[44] This extra outer membrane layer is not present in Gram-positive bacteria and makes Gram-negative bacteria less permeable to antibacterial agents, which increases their antibacterial resistance.[45]

The antibacterial activity against *S. aureus* of the Cp* was only moderate with MICs of 100 μM (with the exception of complexes **29** and **32** which showed no growth inhibition). Upon introduction of the extended Cp^{xPh} capping ligand, the MIC dropped to between 40 – 50 μM for the complexes bearing the ImPy-I and ImPy-Naphth chelating ligands, while the MIC remained >100 μM for complexes bearing the ImPy-NMe$_2$ and ImPy-OH chelating ligands. Therefore, there is a dependence on the antibacterial activity on the nature of the chelating. Upon introduction of the extended Cp^{xBiPh} capping ligand, the MIC values dropped to between 8 – 15 μM.

This effect is demonstrated by the growth curves of *S. aureus* upon incubation with complexes **32-34** and **40-42**, Figure 6.19. The increase in hydrophobicity as a consequence of the extension of the Cp^x capping ligand (as observed within this series of complex, Table 6.8) may play a role in the enhanced antibacterial activity.[46,47] There is also an increase in the lag phase (period in which bacteria adapt to their environment and do not multiply) upon an increase in hydrophobicity. The free capping ligand $Cp^{xBiPh}H$ exhibits no biological activity implying that the presence of the metal as well as the capping ligand are required for activity. Previous reports of Ir(III) complexes studied for antibacterial action against *S. aureus* showed little to no activity for cationic complexes bearing the Cp* capping ligand,[8] whilst the neutral [(η^5-Cp*)Ir(aminoacidato)Cl] complexes showed good activity,[16] suggesting that hydrophobicity is an important design feature.

The addition of a biphenyl substituent leading to enhanced activity has been observed in the lipoglycopeptide oritavancin (similar in structure to vancomycin), where the 4'-chlorobiphenylmethyl group is proposed to disrupt the membrane integrity of *S. aureus*,[48] as well as inhibiting cell wall biosynthesis (independently from the presence of the biphenyl system).[49] Investigations into the effect that complexes **31**, **34**, **42** and **45** on the membrane integrity against *S. aureus* was assessed using the BacLight™ DEAD/ALIVE assay. Complexes **31**, **42** and **45** all caused disruption of the cytoplasmic membrane, while complex **34** caused loss of membrane integrity but to a lesser extent (Figure 6.14). Therefore, the mechanism of antibacterial action is likely to involve disruption of the membrane integrity which is enhanced by the presence of the biphenyl substituent in Cp^{xBiPh} complexes. This may be a consequence of the highly lipophilic nature of the complexes that could result in accumulation in the cytoplasmic membrane. However, further investigations are

required to elucidate whether interaction with other biological targets such as DNA[10] are also responsible for the mechanism of action.

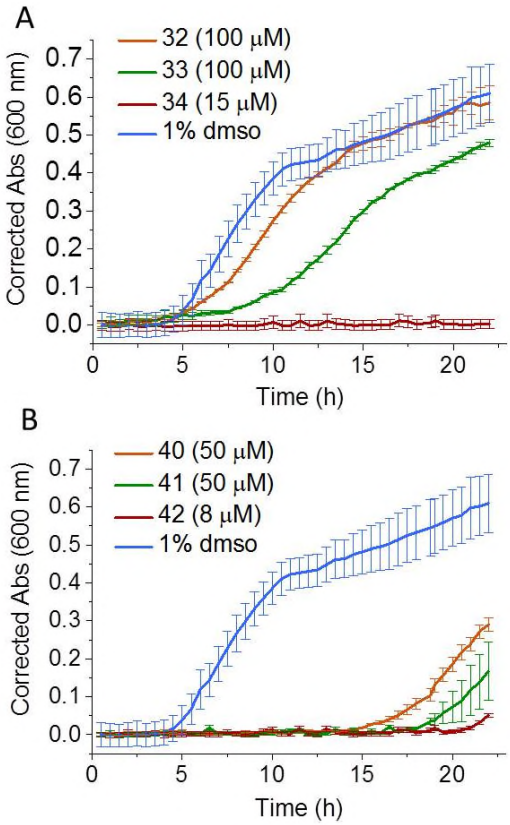

Figure 6.19. Growth curves for *S. aureus* with incubation of (A) – ImPy-OH complexes **32** (100 µM, Cp*), **33** (100 µM, Cp^{xPh}) and **34** (15 µM, Cp^{xBiPh}) and (B) – ImPy-I complexes **40** (50 µM), **41** (50 µM, Cp^{xPh}) and **42** (8 µM, Cp^{xBiPh}) showing the effect of functionalising the cyclopentadienyl ring and different ImPy ligands on the MIC values. Controls with 1% dmso are shown for comparison.

Comparison to currently used antibacterial agents shows that they can exhibit comparable potency to the membrane-damaging agent nisin. However, they are around eight times less active than vancomycin. Although not as active, they may still show use for development as it is unlikely that bacteria will already exhibit an intrinsic resistance towards them.

6.4.4.2 Antiproliferative Activity towards Eukaryotic Cells

Half-sandwich Ir(III) complexes show promise as anticancer agents.[50-52] In general, the Cp* complexes exhibit no activity against A2780 human ovarian cancer cells, with the exception of complexes [(η^5-Cp*)Ir(ImPy-NMe_2)Cl]PF_6 **29** and [(η^5-Cp*)Ir(ImPy-Naphth)Cl]PF_6 **43** which exhibit modest IC_{50} values of 38.64 and 13.3 μM, respectively (Table 6.10). The presence of the naphthyl group in **43** may enhance the antiproliferative activity due to the extended phenyl ring, by either increasing the intercalative ability between DNA base pairs[53] or by enhancing hydrophobicity, both of which have been demonstrated to be of importance towards the design of Ir(III) anticancer agents.[42,54] The $–NMe_2$ group significantly increases the antiproliferative activity of these complexes. Although not fully understood, this effect has been previously observed in half-sandwich Os(II) phenyliminopyridine[55] and phenylazopyridine[2] complexes, suggesting that this functional group may provide promise for further organometallic anticancer drug development.

The introduction of extended Cp^x ligands enhances the antiproliferative activity in all cases, with the Cp^{xBiPh} complexes [(η^5-Cp^{xBiPh})Ir(ImPy-NMe_2)Cl]PF_6 **31**, [(η^5-Cp^{xBiPh})Ir(ImPy-OH)Cl]PF_6 **34**, [(η^5-Cp^{xBiPh})Ir(ImPy-I)Cl]PF_6 **42** and [(η^5-Cp^{xBiPh})Ir(ImPy-Naphth)Cl]PF_6 **45** showing the greatest potency with IC_{50} values ranging from 0.64 – 6.2 μM. The activity of these complexes in the MRC5 healthy human fibroblast model showed IC_{50} values ranging from 0.35 – 6.7 μM, therefore showing minimal selectivity between cancerous and healthy cells. The enhanced antiproliferative action *via* extension of the Cp^x capping ligand has been previously demonstrated for Ir(III) complexes.[42,54] This is again likely due to enhanced hydrophobicity, which was also demonstrated to be of importance in the 2-PhPy complexes studied in Chapter 3.

Although not investigated in this study, previous work on the possible biological targets/mechanism of actions of half-sandwich Ir(III) anticancer complexes have shown that a multi-targeting mechanism is likely to exist.[56] They are capable of binding to DNA via the monodentate site,[54] as well as through intercalative mechanisms through extended planar systems.[57] Inhibition of thioredoxin reductase 1 (Trx-R)[50], as well as the modulation of $NADH/NAD^+$ may also play role in the antiproliferative activity.[58] However, this study has further supported the hypothesis that hydrophobicity is a key property for the biological activity of piano-stool Ir(III) complexes, which can be enhanced by the type of Cp^x capping ligand and chelating ligand used.

6.4.4.3 Structure Activity Relationships (SARs)

Based on the findings from this study, initial structure activity relationships can be formulated for antibacterial and anticancer activity for complexes of the type $[(\eta^5\text{-}Cp^x)Ir(ImPy)Cl]PF_6$. Figure 6.20 shows the differences between hydrophilic (ImPy-OH) and hydrophobic (ImPy-I) chelating ligands. An increase in hydrophobicity as a consequence of functionalisation of the Cp^x or chelating ligand results in enhanced antibacterial activity against Gram-positive *S. aureus* but has little effect on Gram-negative *E. coli*. The antiproliferative activity against A2780 cells is also dependent on the hydrophobicity of the complex. The complexes that exhibit the most promising antibacterial activity are also potent mammalian antiproliferative agents, perhaps making them unsuitable for further development as antibacterial agents. However, the antibacterial activity observed is promising and may provide insight for future design features for half-sandwich Ir(III) antibacterial

agents, with further investigation into mono-, bi-, and tri-dentate ligands being potentially interesting avenues of research to explore.

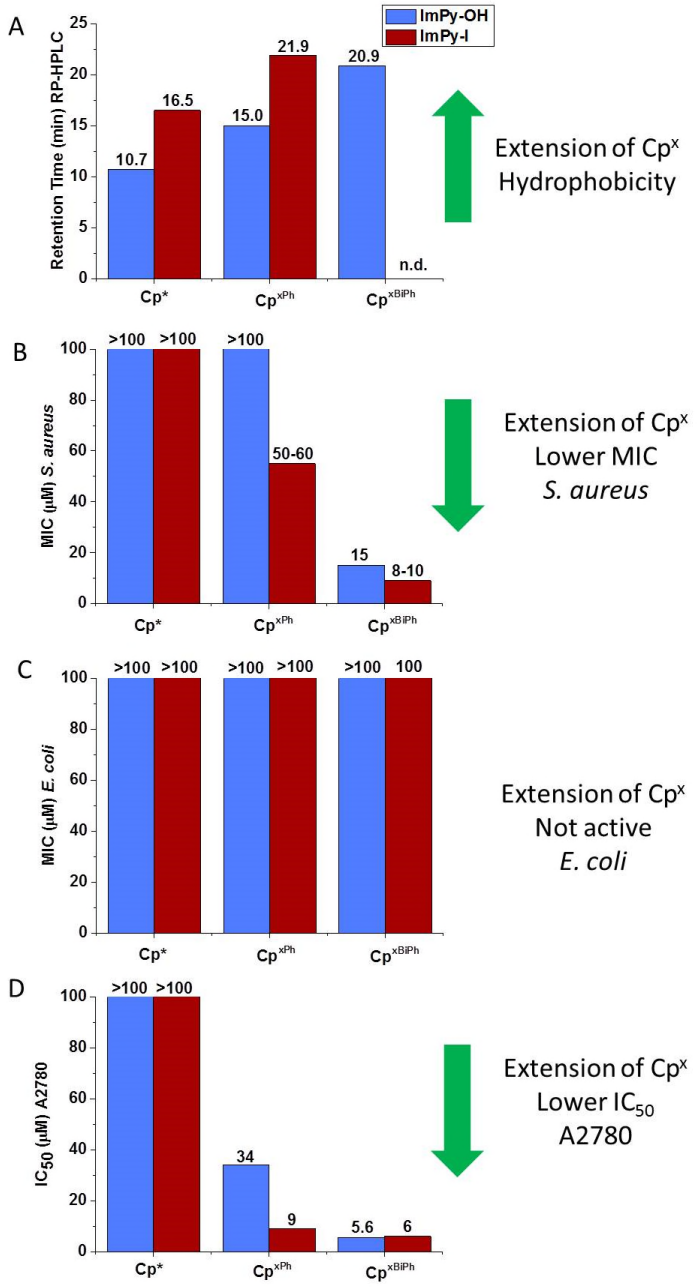

Figure 6.20. Structure activity relationships for [(η^5-Cp^x)Ir(ImPy)Cl]PF$_6$ complexes towards antibacterial and anticancer activity based on extension of the Cp^x capping ligand and differences between hydrophilic (ImPy-OH, blue bars) and hydrophobic (ImPy-I, red bars) chelating ligands. (A) Hydrophobicity, (B) antibacterial activity against *S. aureus*, (C) antibacterial activity against *E. coli* and (D) antiproliferative activity against A2780 human ovarian cancer cells. n.d. = not determined

6.5 Conclusion

This chapter has dealt with the synthesis and characterisation of *N*-(pyrid-2-ylmethylene)amine half-sandwich Ir(III) complexes, with studies of their solution chemistry, as well as investigations into their biological activity as antibacterial and anticancer agents.

Studies of the solution chemistry of complexes **43-45** which bear the naphthyl group on the chelating ligand *N*-(2-pyridnylmethylene)-1-naphthalenamine indicated that two isomers are present in solution. These are due to conformational isomerism arising from hindered rotation of the naphthyl group against the Cp^x capping ligand. VT-NMR studies have shown that the energy barrier to overcome the transition state for rotation is relatively independent on the type of Cp^x capping ligand.

Investigations into their aqueous chemistry showed that they exhibit more complicated speciation compared with previously studied chelated half-sandwich Ir(III) complexes,[42,54] which appears to be initiated *via* hydrolysis at the monodentate site and formation of hydroxido adducts. LC-MS studies show that the chelating ligand may dissociate from the metal centre, which often occurs in half-sandwich metal complexes upon the formation of the hyroxido-bridged dimers.[38,42] This implies that the hydroxido adducts are formed which is due to a low pK_a value of the coordinated water molecule (as observed for complexes **32** and **40**). However, studies in the presence of biologically relevant concentrations of chloride have shown that the complexes are stable and do not hydrolyse, existing primarily as the chlorido adduct. They also exhibit good stability in the biological media used in antibacterial assays (LB).

No significant biological activity was observed against the Gram-negative bacterium *E. coli*, but activity against the Gram-positive *S. aureus* was observed, with MICs as low as 8-15 μM. The activity is largely governed by the presence of the extended Cp^{xBiPh} capping ligand, suggesting that hydrophobicity is important for their activity. There appears to be a dependence on the nature of the chelating ligand, which may also be linked to the overall hydrophobicity of the complexes. The mechanism of action appears, at least in part, to involve reducing the integrity of the lipophilic cytoplasmic cell membrane, which is enhanced in Cp^{xBiPh} complexes that are inherently more hydrophobic than the other complexes studied.

Some of the complexes exhibit high antiproliferative activity against A2780 human ovarian cancer cells, in particular, complex $[(\eta^5\text{-}Cp^{xBiPh})Ir(ImPy\text{-}NMe_2)Cl]PF_6$ **31** has an IC_{50} value of 0.64 μM. Potency increases in the order of the substitution of the capping ligand $Cp^* < Cp^{xPh} < Cp^{xBiPh}$ indicating that hydrophobicity is likely to be an important design feature which has been established in previous Ir(III) anticancer agents.[22,54] Functionality of the ImPy chelating ligand also affects the antiproliferative activity, which again is likely as a consequence of hydrophobic properties. There is little selectivity over healthy MRC5 human fibroblast cells, therefore, further modifications to the complex are required (i.e. replacement of the chloride monodentate ligand with pyridine), which may result in more selective compounds.[3] The importance of the biphenyl substituent on the Cp^x capping ligand in ImPy complexes for good biological activity is apparent, which will be useful for future research into Ir(III) complexes as antibacterial and anticancer agents.

6.6 References

(1) Medici, S.; Peana, M.; Nurchi, V. M.; Lachowicz, J. I.; Crisponi, G.; Zoroddu, M. A. *Coord. Chem. Rev.* **2015**, *284*, 329.

(2) Fu, Y.; Habtemariam, A.; Pizarro, A. M.; van Rijt, S. H.; Healey, D. J.; Cooper, P. A.; Shnyder, S. D.; Clarkson, G. J.; Sadler, P. J. *J. Med. Chem.* **2010**, *53*, 8192.

(3) Liu, Z.; Romero-Canelón, I.; Qamar, B.; Hearn, J. M.; Habtemariam, A.; Barry, N. P. E.; Pizarro, A. M.; Clarkson, G. J.; Sadler, P. J. *Angew. Chem. Int. Ed.* **2014**, *53*, 3941.

(4) Habtemariam, A.; Melchart, M.; Fernández, R.; Parsons, S.; Oswald, I. D. H.; Parkin, A.; Fabbiani, F. P. A.; Davidson, J. E.; Dawson, A.; Aird, R. E.; Jodrell, D. I.; Sadler, P. J. *J. Med. Chem.* **2006**, *49*, 6858.

(5) Fernández, R.; Melchart, M.; Habtemariam, A.; Parsons, S.; Sadler, P. J. *Chem. Eur. J.* **2004**, *10*, 5173.

(6) Barragán, F.; López-Senín, P.; Salassa, L.; Betanzos-Lara, S.; Habtemariam, A.; Moreno, V.; Sadler, P. J.; Marchán, V. *J. Am. Chem. Soc.* **2011**, *133*, 14098.

(7) Liu, Z.; Romero-Canelón, I.; Habtemariam, A.; Clarkson, G. J.; Sadler, P. J. *Organometallics* **2014**, *33*, 5324.

(8) Palepu, N.; Nongbri, S. L.; Premkumar, J. R.; Verma, A.; Bhattacharjee, K.; Joshi, S. R.; Forbes, S.; Mozharivskyj, Y.; Thounaojam, R.; Aguan, K.; Kollipara, M. *J. Biol. Inorg. Chem.* **2015**, 1.

(9) Śliwińska, U.; Pruchnik, F. P.; Ułaszewski, S.; Latocha, M.; Nawrocka-Musiał, D. *Polyhedron* **2010**, *29*, 1653.

(10) Tripathy, S. K.; Taviti, A. C.; Dehury, N.; Sahoo, A.; Pal, S.; Beuria, T. K.; Patra, S. *Dalton Trans.* **2015**, *44*, 5114.

(11) Li, Y.; de Kock, C.; Smith, P. J.; Guzgay, H.; Hendricks, D. T.; Naran, K.; Mizrahi, V.; Warner, D. F.; Chibale, K.; Smith, G. S. *Organometallics* **2013**, *32*, 141.

(12) Beckford, F. A.; Stott, A.; Gonzalez-Sarrías, A.; Seeram, N. P. *Appl. Organomet. Chem.* **2013**, *27*, 425.

(13) Allardyce, C. S.; Dyson, P. J.; Ellis, D. J.; Salter, P. A.; Scopelliti, R. *J. Organomet. Chem.* **2003**, *668*, 35.

(14) Betanzos-Lara, S.; Salassa, L.; Habtemariam, A.; Novakova, O.; Pizarro, A. M.; Clarkson, G. J.; Liskova, B.; Brabec, V.; Sadler, P. J. *Organometallics* **2012**, *31*, 3466.

(15) Dougan, S. J.; Sadler, P. J. *CHIMIA* **2007**, *61*, 704.

(16) Karpin, G. W.; Merola, J. S.; Falkinham, J. O. *Antimicrob. Agents Chemother.* **2013**, *57*, 3434.

(17) Burgoyne, A. R.; Makhubela, B. C. E.; Meyer, M.; Smith, G. S. *Eur. J. Inorg. Chem.* **2015**, *2015*, 1433.

(18) Payne, R.; Govender, P.; Therrien, B.; Clavel, C. M.; Dyson, P. J.; Smith, G. S. *J. Organomet. Chem.* **2013**, *729*, 20.

(19) Govender, P.; Renfrew, A. K.; Clavel, C. M.; Dyson, P. J.; Therrien, B.; Smith, G. S. *Dalton Trans.* **2011**, *40*, 1158.

(20) Chow, M. J.; Licona, C.; Yuan Qiang Wong, D.; Pastorin, G.; Gaiddon, C.; Ang, W. H. *J. Med. Chem.* **2014**, *57*, 6043.

(21) Lalrempuia, R.; Kollipara, M. R.; Carroll, P. J. *Polyhedron* **2003**, *22*, 605.

(22) Liu, Z.; Salassa, L.; Habtemariam, A.; Pizarro, A. M.; Clarkson, G. J.; Sadler, P. J. *Inorg. Chem.* **2011**, *50*, 5777.

(23) Lucas, S. J.; Lord, R. M.; Wilson, R. L.; Phillips, R. M.; Sridharan, V.; McGowan, P. C. *Dalton Trans.* **2012**, *41*, 13800.

(24) Gielen, M.; Willem, R.; Wrackmeyer, B. *Fluxional Organometallic and Coordination Compounds*; Wiley: Chichester, 2005.

(25) Sandström, J. *Dynamic NMR Spectroscopy*; Academic Press: London, 1982.

(26) Hwang, T. L.; Shaka, A. J. *J. Magn. Reson.* **1995**, *112*, 275.

(27) Govindaswamy, P.; Mozharivskyj, Y. A.; Kollipara, M. R. *Polyhedron* **2005**, *24*, 1710.

(28) Boulos, L.; Prévost, M.; Barbeau, B.; Coallier, J.; Desjardins, R. *J. Microbiol. Methods* **1999**, *37*, 77.

(29) van Kraaij, C.; Breukink, E.; Noordermeer, M. A.; Demel, R. A.; Siezen, R. J.; Kuipers, O. P.; de Kruijff, B. *Biochemistry* **1998**, *37*, 16033.

(30) Hammes, W. P.; Neuhaus, F. C. *Antimicrob. Agents Chemother.* **1974**, *6*, 722.

(31) Carmona, D.; Lahoz, F. J.; Elipe, S.; Oro, L. A.; Lamata, M. P.; Viguri, F.; Mir, C.; Cativiela, C.; López-Ram de Víu, M. P. *Organometallics* **1998**, *17*, 2986.

(32) Jones, W. D.; Feher, F. J. *Inorg. Chem.* **1984**, *23*, 2376.

(33) Chianese, A. R.; Li, X.; Janzen, M. C.; Faller, J. W.; Crabtree, R. H. *Organometallics* **2003**, *22*, 1663.

(34) Atherton, M. J.; Fawcett, J.; Holloway, J. H.; Hope, E. G.; Karacar, A.; Russell, D. R.; Saunders, G. C. *J. Chem. Soc., Dalton Trans.* **1996**, 3215.

(35) Wang, F.; Habtemariam, A.; van der Geer, E. P. L.; Fernández, R.; Melchart, M.; Deeth, R. J.; Aird, R.; Guichard, S.; Fabbiani, F. P. A.; Lozano-Casal, P.; Oswald, I. D. H.; Jodrell, D. I.; Parsons, S.; Sadler, P. J. *Proc. Nat. Acad. Sci. USA* **2005**, *102*, 18269.

(36) Lippert, B. *Cisplatin: chemistry and biochemistry of a leading anticancer drug*; Helvetica Chimica Acta: Würzburg, 1999.

(37) Kurzwernhart, A.; Kandioller, W.; Enyedy, E. A.; Novak, M.; Jakupec, M. A.; Keppler, B. K.; Hartinger, C. G. *Dalton Trans.* **2013**, *42*, 6193.

(38) Peacock, A. F. A.; Habtemariam, A.; Fernández, R.; Walland, V.; Fabbiani, F. P. A.; Parsons, S.; Aird, R. E.; Jodrell, D. I.; Sadler, P. J. *J. Am. Chem. Soc.* **2006**, *128*, 1739.

(39) Peacock, A. F. A.; Parsons, S.; Sadler, P. J. *J. Am. Chem. Soc.* **2007**, *129*, 3348.

(40) Erxleben, A.; Claffey, J.; Tacke, M. *J. Inorg. Biochem.* **2010**, *104*, 390.

(41) Toney, J. H.; Marks, T. J. *J. Am. Chem. Soc.* **1985**, *107*, 947.

(42) Liu, Z.; Habtemariam, A.; Pizarro, A. M.; Clarkson, G. J.; Sadler, P. J. *Organometallics* **2011**, *30*, 4702.

(43) Goldman, E.; Green, L. H. *Practical handbook of microbiology*; CRC Press: Boca Raton, 2008.

(44) Erridge, C.; Bennett-Guerrero, E.; Poxton, I. R. *Microb. Infect.* **2002**, *4*, 837.

(45) de Tejada, G. M.; Sánchez-Gómez, S.; Kowalski, I.; Kaconis, Y.; Andrä, J.; Schürholz, T.; Hornef, M.; Dupont, A.; Garidel, P.; Gutsmann, T.; David, S. A.; Brandenburg, K. *Curr. Drug Targets* **2012**, *13*, 1121.

(46) Dathe, M.; Wieprecht, T.; Nikolenko, H.; Handel, L.; Maloy, W. L.; MacDonald, D. L.; Beyermann, M.; Bienert, M. *FEBS Lett.* **1997**, *403*, 208.

(47) Chang, E. L.; Simmers, C.; Knight, D. A. *Pharmaceuticals* **2010**, *3*, 1711.

(48) Belley, A.; McKay, G. A.; Arhin, F. F.; Sarmiento, I.; Beaulieu, S.; Fadhil, I.; Parr, T. R.; Moeck, G. *Antimicrob. Agents Chemother.* **2010**, *54*, 5369.

(49) Allen, N. E.; Nicas, T. I. *FEMS Microbiol. Rev.* **2003**, *26*, 511.

(50) Almodares, Z.; Lucas, S. J.; Crossley, B. D.; Basri, A. M.; Pask, C. M.; Hebden, A. J.; Phillips, R. M.; McGowan, P. C. *Inorg. Chem.* **2014**, *53*, 727.

(51) Tripathy, S. K.; De, U.; Dehury, N.; Pal, S.; Kim, H. S.; Patra, S. *Dalton Trans.* **2014**, *43*, 14546.

(52) Hearn, J. M.; Romero-Canelón, I.; Qamar, B.; Liu, Z.; Hands-Portman, I.; Sadler, P. J. *ACS Chem. Biol.* **2013**, *8*, 1335.

(53) Schäfer, S.; Sheldrick, W. S. *J. Organomet. Chem.* **2007**, *692*, 1300.

(54) Liu, Z.; Habtemariam, A.; Pizarro, A. M.; Fletcher, S. A.; Kisova, A.; Vrana, O.; Salassa, L.; Bruijnincx, P. C. A.; Clarkson, G. J.; Brabec, V.; Sadler, P. J. *J. Med. Chem.* **2011**, *54*, 3011.

(55) Fu, Y.; Romero, M. J.; Habtemariam, A.; Snowden, M. E.; Song, L.; Clarkson, G. J.; Qamar, B.; Pizarro, A. M.; Unwin, P. R.; Sadler, P. J. *Chem. Sci.* **2012**, *3*, 2485.

(56) Romero-Canelón, I.; Sadler, P. J. *Inorg. Chem.* **2013**, *52*, 12276.

(57) Herebian, D.; Sheldrick, W. S. *J. Chem. Soc., Dalton Trans.* **2002**, 966.

(58) Betanzos-Lara, S.; Liu, Z.; Habtemariam, A.; Pizarro, A. M.; Qamar, B.; Sadler, P. J. *Angew. Chem. Int. Ed.* **2012**, *51*, 3897.

Chapter 7

Conclusions and Future Work

7.1 Conclusions

The main focus of this thesis has been investigations into the effects that functionality of the chelating ligand and monodentate ligand have on the chemical and anticancer properties of complexes of the type $[(\eta^5\text{-Cp*})\text{Ir(2-PhPy)X}]^{0/+}$. This work covers three of the four results chapters.

In **Chapter 3**, it was found that the introduction of an electron-donating (-CH_3, -OH, -CH_2OH and –OCH_3) or electron-withdrawing (-F, -CF_3 -CHO and –NO_2) group into the 2-PhPy ligand in $[(\eta^5\text{-Cp*})\text{Ir(2-PhPy)Cl}]$ complexes can dramatically change the anticancer activity. Studies into their aqueous chemistry showed that hydrolysis to the corresponding aqua complex was always rapid but easily supressed by addition of NaCl; hydrolysis was almost completely supressed at 4 mM NaCl which is representative of the chloride concentration in the cell nucleus. Interactions *via* the monodentate site with model DNA nucleobases 9-EtG and 9-MeA showed a definitive preference for binding to 9-EtG, with very little difference observed amongst the functionally diverse complexes. The ability to oxidise the coenzyme NADH to NAD^+ catalytically was demonstrated for both “active” and “inactive” complexes, demonstrating that another factor may be responsible for determining potency, rather than chemical reactivity.

Analysis of the relative hydrophobicity of the complexes showed that both the type and position of the substituent affects the hydrophobicity, which appears to correlate with the extent of metal accumulation in A2780 cells, perhaps demonstrating that passive diffusion into the cell is an important mechanism for cellular accumulation. Correlation analysis between iridium accumulation and potency against A2780 cells showed an apparent trend in which high accumulation results in higher potency. The

position of the substituent can also influence the localisation in cellular compartments, which could have implications on the resulting cytotoxic activities of structural isomers Therefore, it appears that the physicochemical properties arising from the use of different substituents plays a greater role than chemical reactivity in determining the potency in this system.

Chapter 4 investigated the potential to enhance the antiproliferative activity of the most potent complex found in the previous chapter, [(η^5-Cp*)Ir(2-(2'-methylphenyl)pyridine)Cl] **13** (IC_{50} against A2780 cells = 1.18 μM), with pyridine monodentate ligands through modulation of chemical reactivity. It was demonstrated that the extent of monodentate ligand release and the reactivity towards 9-EtG was decreased for pyridyl containing complexes compared with the parent chlorido complex. Interestingly, release of the pyridyl ligands did not result in the detection of the expected aqua adduct, as previously observed in similar systems. The reactivity towards GSH decreased only in the complex bearing the pyridyl monodentate ligand 4-(dimethylamino)pyridine, presumably due to enhanced stability from electron donation from the *N*-dimethyl group para to bonding nitrogen atom. The reactions of all the complexes with GSH do not appear to form the expected Ir-SG adduct, but the oxidised sulfenate (Ir-(S-O)G) and sulfinate (Ir-(S-O_2)G) adducts from O_2 present in the reaction. Intriguingly, the catalysis of NADH was independent on the monodentate ligand.

The antiproliferative activity against A2780 cells indicates no enhancement in potency for the pyridyl complexes over the parent chlorido complex when cells are allowed to recover for 72 h in drug-free media. However, when allowing no cell recovery time after the initial 24 h drug exposure time, the IC_{50} values show greater

variance, with the more chemically-stable pyridyl complexes being more active than the reactive parent chlorido complex. This may indicate that the initial antiproliferative activity is dependent on greater chemical stability. Further biological study shows that the induction of total ROS is high in A2780 cells upon exposure to all complexes, and is likely to contribute to the antiproliferative mechanism. More interestingly, the ability to induce apoptosis after 0 h and 24 h cell recovery time showed that the parent chlorido complex does not induce apoptosis, whereas the pyridyl complexes do induce apoptotic cell death after 24 h recovery time, implying faster action towards cell death for the pyridyl complexes. The initial antiproliferative activity may be showing cytostatic activity rather than cytotoxic activity. Therefore, the change from a chlorido to a pyridyl monodentate ligand not only affects the chemical reactivity, but also the biological activity.

The reactivity of the aldehyde-bearing complex [(η^5-Cp*)Ir(2-phenyl-5-carboxaldehydepyridine)Cl] **6** towards amines was investigated in **Chapter 5** to explore the possibility of functionalising the complex *via* Schiff base formation. Both aliphatic and aromatic organic primary amines were conjugated to complex **6** using microwave-assisted chemistry to form new conjugates using short reaction times (5 min). The reaction of **6** with the lysine-containing peptides Substance P and [Lys-3]-bombesin was analysed by ultra-high resolution FT-ICR-MS techniques, which confirmed that binding of the peptides to **6** could occur *via* Schiff base formation with the lysine residue.

The stability of the new Schiff base conjugates towards imine hydrolysis in water was low over a 24 h period. Reduction of the imine bond in the dansyl-conjuated complex **26** to the secondary amine **27** was performed using Et_3SiH as a hydride

source. Initially, it was believed that the presence of the Pd catalyst $Pd(OAc)_2$ was required to reduce the imine bond, as in the case for organic compounds. However, further analysis of the reaction showed that the Ir centre is involved in the reduction of the imine bond *via* formation of an Ir-H species that can then transfer the hydride to the imine, forming the desired product. The ability to track the secondary amine complex **27** bearing the fluorescent dansyl group was investigated using fluorescence confocal microscopy. A reduction in fluorescence intensity was observed in aqueous solution compared to organic solvents, and no fluorescence was observed in A2780 cells incubated with **27**. This suggests that the **27** does not reside in a sufficiently hydrophobic environment to promote fluorescence, or the cellular accumulation was too low to detect a fluorescence signal.

Finally, the synthesis of a new set of ImPy complexes of the type $[(\eta^5\text{-}Cp^x)Ir(ImPy)Cl]PF_6$ and the evaluation of their chemical and biological properties was described in **Chapter 6**. The addition of a sterically bulky naphthyl group to the aniline ring can incur hindered rotation in solution against the Cp^x capping ligands as observed by ^1H NMR spectroscopy, although the presence of extended arenes on the Cp^x ring had little effect on the energy barrier to rotation. These complexes exhibit complicated aqueous behaviour as studied by NMR and LC-MS methods, which may be due to the low pK_a of the coordinated aqua ligand upon hydrolysis of the chlorido ligand. However, hydrolysis was supressed by the presence of 4 mM NaCl, similarly to the 2-PhPy complexes. The complexes are also stable in the presence of the LB medium used in antibacterial assays. The hydrophobicity of the complexes is dependent on the type of functional group

present on the chelating ligand and increases as a function of the Cp^{x} capping ligand: $Cp^{xBiPh} > Cp^{xPh} > Cp^{*}$.

The antibacterial activity of the complexes was investigated and showed minimal activity against the Gram-negative *E. coli*. The complexes were more active against Gram-positive *S. aureus* with MIC values reaching as low as 8-15 μM, and are some of the most active iridium complexes reported to date. The activity was strongly dependent on the presence of the Cp^{xBiPh} capping ligand. Initial studies into the MoA showed that the active complexes disrupt the membrane integrity of *S. aureus* after short incubation times (25 min). The most active antibacterial complexes were also active against A2780 human ovarian cancer cells and MRC5 healthy human fibroblasts, therefore, further development is required to gain more selective antibacterial agents. However, the antiproliferative activity against mammalian cells of these ImPy complexes bearing the Cp^{xBiPh} capping ligand was an order of magnitude lower than analogous *N,N*-chelated complexes bearing the same capping ligand.

7.2 Future Work

The following describes work that could stem from the results and observations of the research described in this thesis and some initial studies that have been undertaken.

7.2.1 Reactivity of Functional Groups in Cells

It was demonstrated in **Chapter 3** that the presence of functional groups could strongly dictate the observed anticancer activities, despite exhibiting similar reactivity at the iridium centre. Studies showed that this may be as a consequence of

hydrophobicity and the extent of iridium-accumulation. However, some of these functional groups could exhibit interesting chemistry within the cell.

For example, as described in **Chapter 5**, the aldehyde functionality in complex [(η^5-Cp*)Ir(2-phenyl-5-carboxaldehydepyridine)Cl] **6** can react with lysine-containing peptides to form new iridium-peptide conjugates bound *via* the lysine residue. Indeed, the reactivity of aldehydes towards peptides and proteins has been exploited with cross-linking reagents such as glutaraldehyde.[1] This kind of interaction of metallodrugs with peptides and proteins has not been widely reported, and could offer new mechanisms of action, perhaps by disrupting protein function. Alternatively, labelling peptides with iridium may offer scope for high-throughput analysis by HR-MS due to the distinct iridium isotopic pattern.

The incorporation of the nitro functional group into the 2-PhPy chelating ligands resulted in two complexes with contrasting anticancer activities [(η^5-Cp*)Ir(2-phenyl)pyridine)Cl] **7** and [(η^5-Cp*)Ir(2-phenyl -4-nitropyridine)Cl] **8** (IC_{50} A2780 = 24.73 and 2.7 μM, respectively), despite exhibiting similar physicochemical properties. The cytoplasm of cells is known to be a reducing environment due to the presence of reductants such as GSH, ascorbic acid and NADH. It has been demonstrated that the nitro functionality in imidazole compounds can be reduced in mammalian cells using NADH and flavo-proteins like NADPH cytochrome P450 reductase,[2] which can then lead to DNA damage by strand breakage.[3] It would be of interest to study the fate of the nitro group in complexes **7** and **8** in a reducing environment (i.e. using electrochemistry) to determine if reduction potentials could be of importance to their mechanism. The reactivity in the presence of NADH, which is already known to be a hydride donor to this series of complex, may also be

of interest, as it may be possible to reduce the nitro group to the hydroxylamine or possibly primary amine.

7.2.2 Functionalising Complexes with Cell/Organelle-Targeting Moieties

The use of complex [(η^5-Cp*)Ir(2-phenyl-5-carboxaldehydepyridine)Cl] **6** as a "chemical platform" for modification with amines was described in **Chapter 5** which showed that new Schiff base conjugates could be synthesised readily. The further reduction of the water-sensitive imine bond to the stable secondary amine was also achieved. Therefore, further investigations into the types of conjugates that could be made are worth exploring. An interesting avenue may be to attach organelle-targeting molecules such as triphenylphosphonium salts (Figure 7.1 a) which localise in the mitochondria due to their liphophilic and cationic nature.[4] It is believed that half-sandwich iridium(III) complexes cause mitochondrial dysfunction,[5,6] which may be enhanced if the compounds target that organelle. Recently, it was reported that conjugation of triphenylphosphonium to phosphorescent octahedral Ir(III) complexes leads to high localisation in the mitochondria.[7]

Also worth exploring is the attachment of molecules that could exploit receptor-mediated delivery, with the aim of achieving selective uptake into cancerous cells over healthy cells. Folic acid has been widely studied as a vector for platinum anticancer agents.[8] Modification of folic acid to provide a reactive primary amine group may make it suitable for conjugation to complex **6** (Figure 7.1 b).

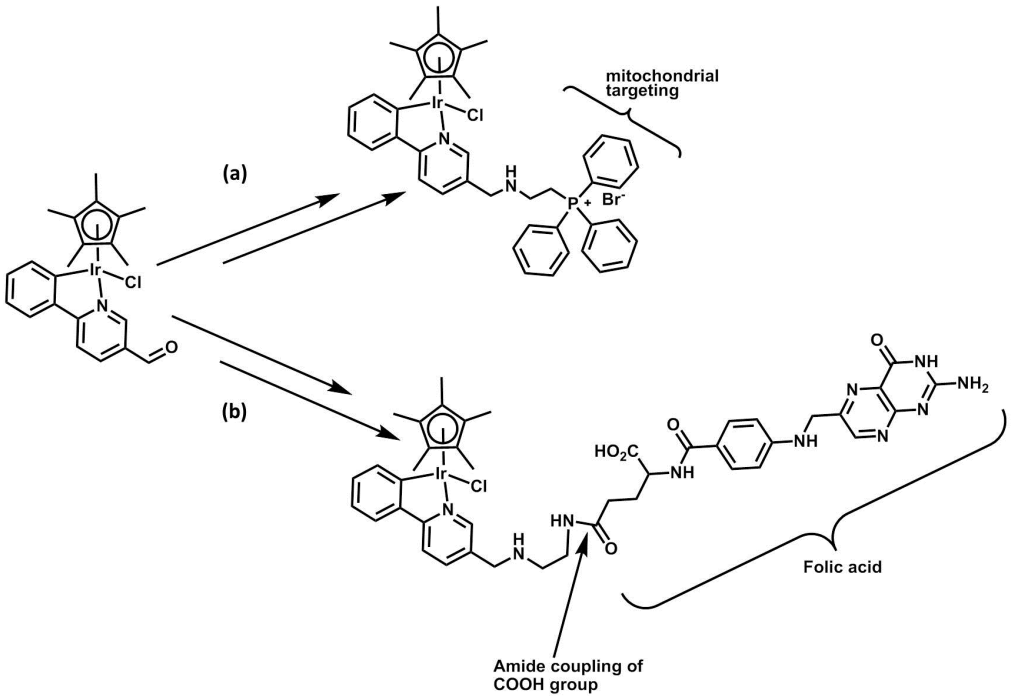

Figure 7.1. (a) Triphenylphosphonium and (b) folic acid conjugated to [(η^5-Cp*)Ir(2-phenyl-5-carboxaldehydepyridine)Cl] **6** to form complexes with cell/organelle –targeting functions using the method developed in Chapter 5.

7.2.3 *N,N,N*-Tridentate Complexes as Antibacterial Agents

The antibacterial activity of the chelated half-sandwich ImPy complexes studied in **Chapter 6** is dependent on the presence of the Cp^{xBiPh} capping ligand. This has been proposed to be due to enhanced hydrophobicity, which may lead to greater accumulation in the bacterial cell membrane of *S. aureus*, resulting in disruption of membrane integrity. The presence of biphenyl substituents aids antibacterial activity of organic compounds *via* disruption of the cell membrane.[9] Therefore, it may be postulated that the complexes act as a structural scaffold for membrane disruption, although the mechanism by which this would occur is currently unknown. Further investigation into the effect on the structures of micelles made of various lipids may give some insight into their mechanism of action.

However, the degree of toxicity towards mammalian cells also increases as the Cp^x capping ligand is extended, presumably as a consequence of increased accumulation and potential DNA intercalation, perhaps making the complexes unsuitable as antibacterial agents. It is believed that the monodentate site in chelated "piano-stool" complexes of iridium is likely to be involved in the antiproliferative mechanism, either through direct binding to guanine or enabling the oxidation of NADH.[10]

No previously reported work has evaluated the biological activity of iridium(III) half-sandwich complexes with *N,N,N*-tridentate ligands. It may be fruitful to explore tridentate ligands such as diethylenetriamine and tris(pyrazolyl)methane (Figure 7.2) for their antibacterial and anticancer activities, in order to evaluate the dependency on a reactive site at the metal centre on biological activity. This could provide complexes that exhibit more selective antibacterial activity and hence reduce the toxicity towards mammalian cells. Such a study would also provide information as to whether a reactive site is required for antibacterial activity or if the presence of the Cp^{xBiPh} capping ligand is enough.

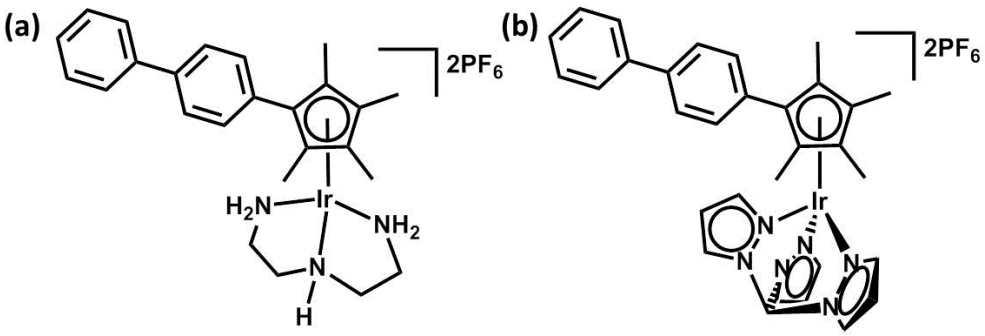

Figure 7.2. Proposed half-sandwich Ir(III) complexes containing the tridentate ligands diethylenetriamine (a) and tris(pyrazolyl)methane (b) for further antibacterial work.

7.2.4 Bi-metallic Complexes

The presence of two metals in one compound could be a useful strategy for increasing the antiproliferative activity of metallodrugs, through providing enhanced reactivity to the compounds, or even combining properties such as luminescence to enable tracking in cells. Bi-metallic and polynuclear complexes have shown excellent anticancer activity *in vitro*.[11,12]

A novel ligand has been developed that provides both *N,N*- and *C,N*- coordination modes (Figure 7.3 a), using the synthesis of substituted imidazoles as reported by Steck and Day.[13] The reactivity towards metallation is controlled by two things; the presence/absence of a base, and the order of the reaction. The coordination of a metal to the *N,N*- site occurs selectively in the first step of the reaction. The isolated metal complex can then be used to react another metal at the *C,N*- coordination site in the presence of a mild base (NaOAc), resulting in a bi-metallic complex (Figure 7.3 b). As the *N,N*- site is already blocked, the new metal can bind only at the *C,N*- site.

Initial studies on forming an *N,N*- and *C,N*-chelated iridium system were made, where the yields of product were 78% and 62% for the mono and bi-metallic complexes, respectively (^{1}H NMR assignments shown in Appendix Figures A1 and A2). Both heterometallic systems incorporating p-cymene Ru(II) and Os(II) compounds, as well as Cp* Rh(III) (Figure 7.3 b) were also formed. Evaluation of the biological activity of these complexes is yet to be performed. Within this general structure, a vast collection of compounds could be synthesised. For example, octahedral Ru(II) and Ir(III) complexes (*via N,N*-chelation) to give photoactive/luminescent complexes attached to an organometallic anticancer agent (*via C,N*-chelation).

Synthesis of a Pt(II)-Ir(III) analogue was unsuccessful due to the poor solubility of the Pt(II)-*N,N*-chelated complex in most organic solvents. It may be interesting to form the more inert Pt(IV) species via oxidation using H_2O_2, perhaps allowing formation of a drug that also contains a "pro-drug" unit that can be activated by irradiation with light or intracellular reduction.[14,15]

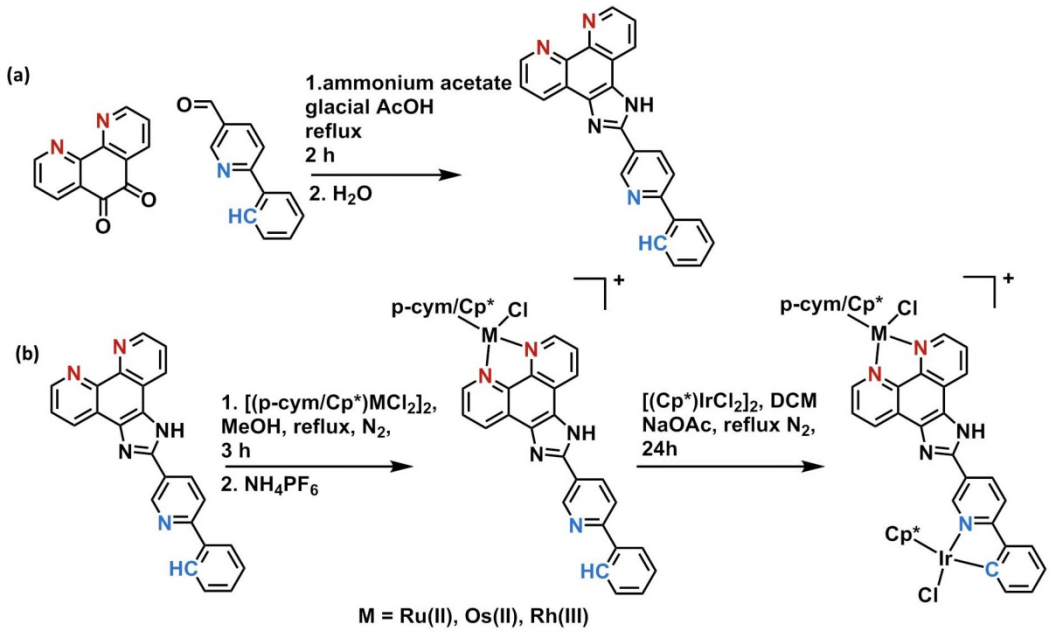

Figure 7.3. Bi-metallic complexes synthesised *via N,N*-chelation, followed by a second reaction with a base to form a *C,N*- coordinated site.

7.3 References

(1) Avrameas, S.; Ternynck, T. *Immunochemistry* **1969**, *6*, 53.

(2) Brown, J. M. *Int. J. Radiat. Oncol. Biol. Phys.* **1982**, *8*, 675.

(3) Edwards, D. I. *Biochem. Pharmacol.* **1986**, *35*, 53.

(4) Jiang, J.; Stoyanovsky, D. A.; Belikova, N. A.; Tyurina, Y. Y.; Zhao, Q.; Tungekar, M. A.; Kapralova, V.; Huang, Z.; Mintz, A. H.; Greenberger, J. S.; Kagan, V. E. *Radiat. Res.* **2009**, *172*, 706.

(5) Liu, Z.; Romero-Canelón, I.; Habtemariam, A.; Clarkson, G. J.; Sadler, P. J. *Organometallics* **2014**, *33*, 5324.

(6) Novohradsky, V.; Zerzankova, L.; Stepankova, J.; Kisova, A.; Kostrhunova, H.; Liu, Z.; Sadler, P. J.; Kasparkova, J.; Brabec, V. *Metallomics* **2014**, *6*, 1491.

(7) Zhang, Q.; Cao, R.; Fei, H.; Zhou, M. *Dalton Trans.* **2014**, *43*, 16872.

(8) Gabano, E.; Ravera, M.; Cassino, C.; Bonetti, S.; Palmisano, G.; Osella, D. *Inorg. Chim. Acta* **2008**, *361*, 1447.

(9) Belley, A.; McKay, G. A.; Arhin, F. F.; Sarmiento, I.; Beaulieu, S.; Fadhil, I.; Parr, T. R.; Moeck, G. *Antimicrob. Agents Chemother.* **2010**, *54*, 5369.

(10) Liu, Z.; Sadler, P. J. *Acc. Chem. Res.* **2014**, *47*, 1174.

(11) Chellan, P.; Land, K. M.; Shokar, A.; Au, A.; An, S. H.; Taylor, D.; Smith, P. J.; Riedel, T.; Dyson, P. J.; Chibale, K.; Smith, G. S. *Dalton Trans.* **2014**, *43*, 513.

(12) Pelletier, F.; Comte, V.; Massard, A.; Wenzel, M.; Toulot, S. p.; Richard, P.; Picquet, M.; Le Gendre, P.; Zava, O.; Edafe, F.; Casini, A.; Dyson, P. J. *J. Med. Chem.* **2010**, *53*, 6923.

(13) Steck, E. A.; Day, A. R. *J. Am. Chem. Soc.* **1943**, *65*, 452.

(14) Shi, Y.; Liu, S.-A.; Kerwood, D. J.; Goodisman, J.; Dabrowiak, J. C. *J. Inorg. Biochem.* **2012**, *107*, 6.

(15) Farrer, N. J.; Woods, J. A.; Munk, V. P.; Mackay, F. S.; Sadler, P. J. *Chem. Res. Toxicol.* **2009**, *23*, 413.

Compound Structures

Complexes studied in Chapter 3

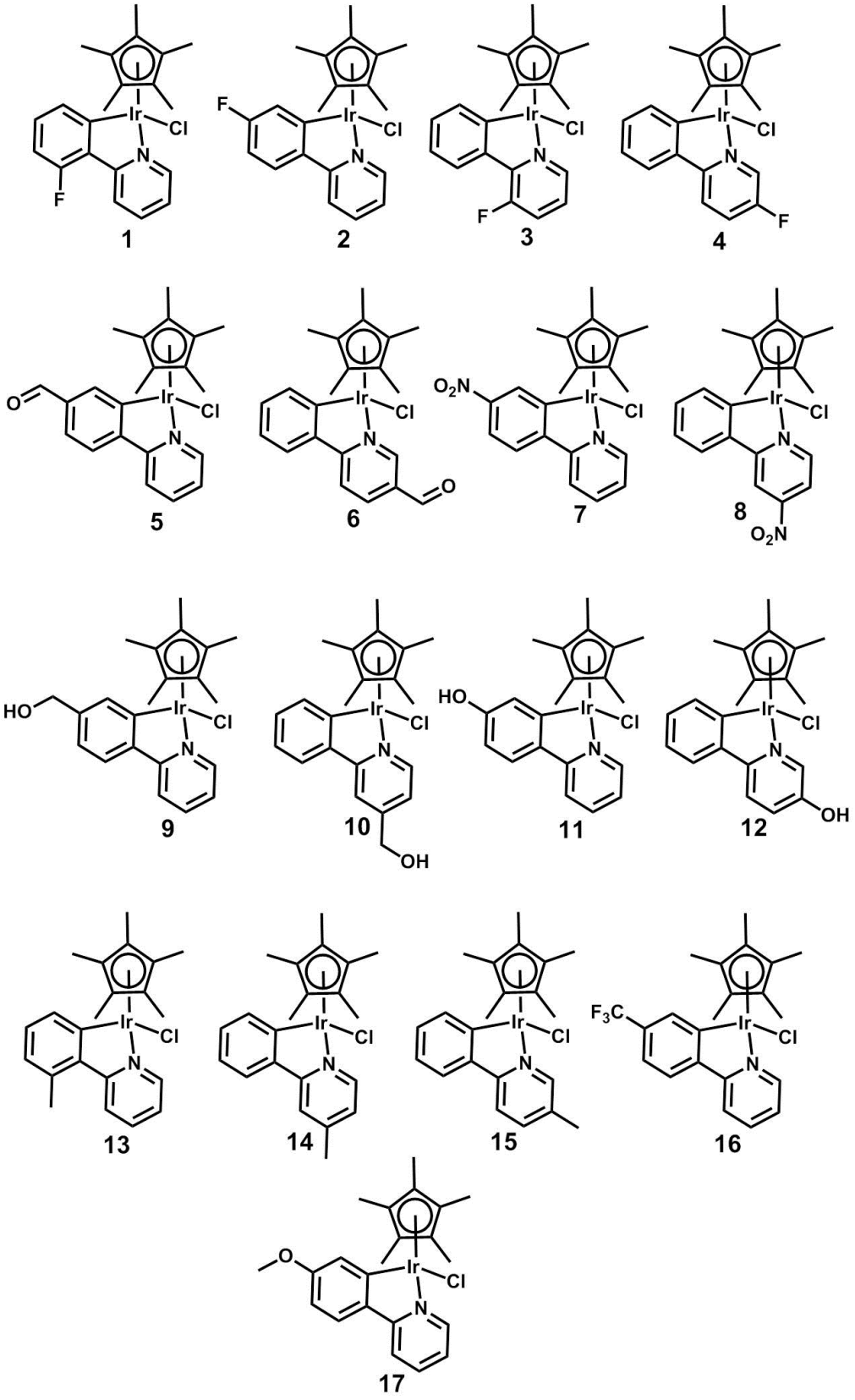

Complexes studied in Chapter 4

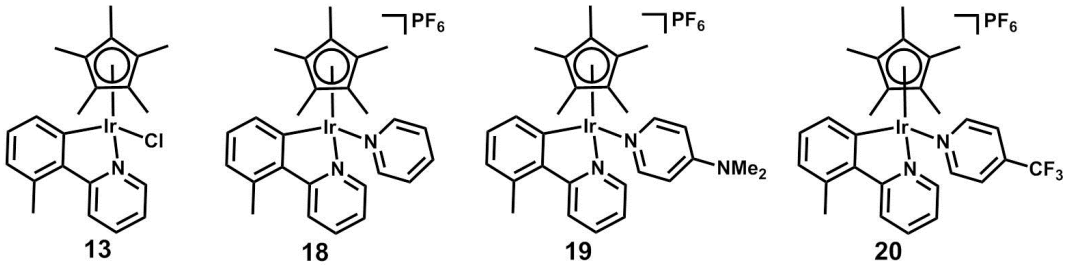

13 18 19 20

Complexes studied in Chapter 5

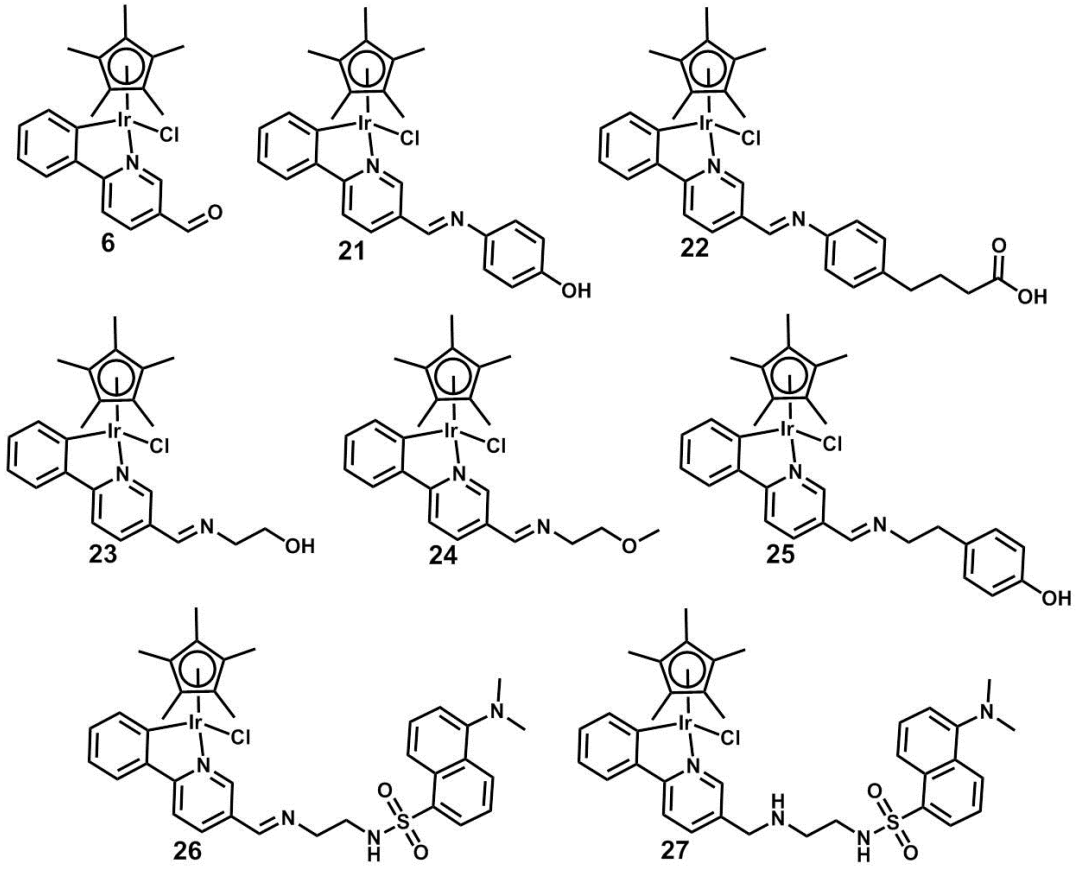

6 21 22 23 24 25 26 27

Complexes studied in Chapter 6

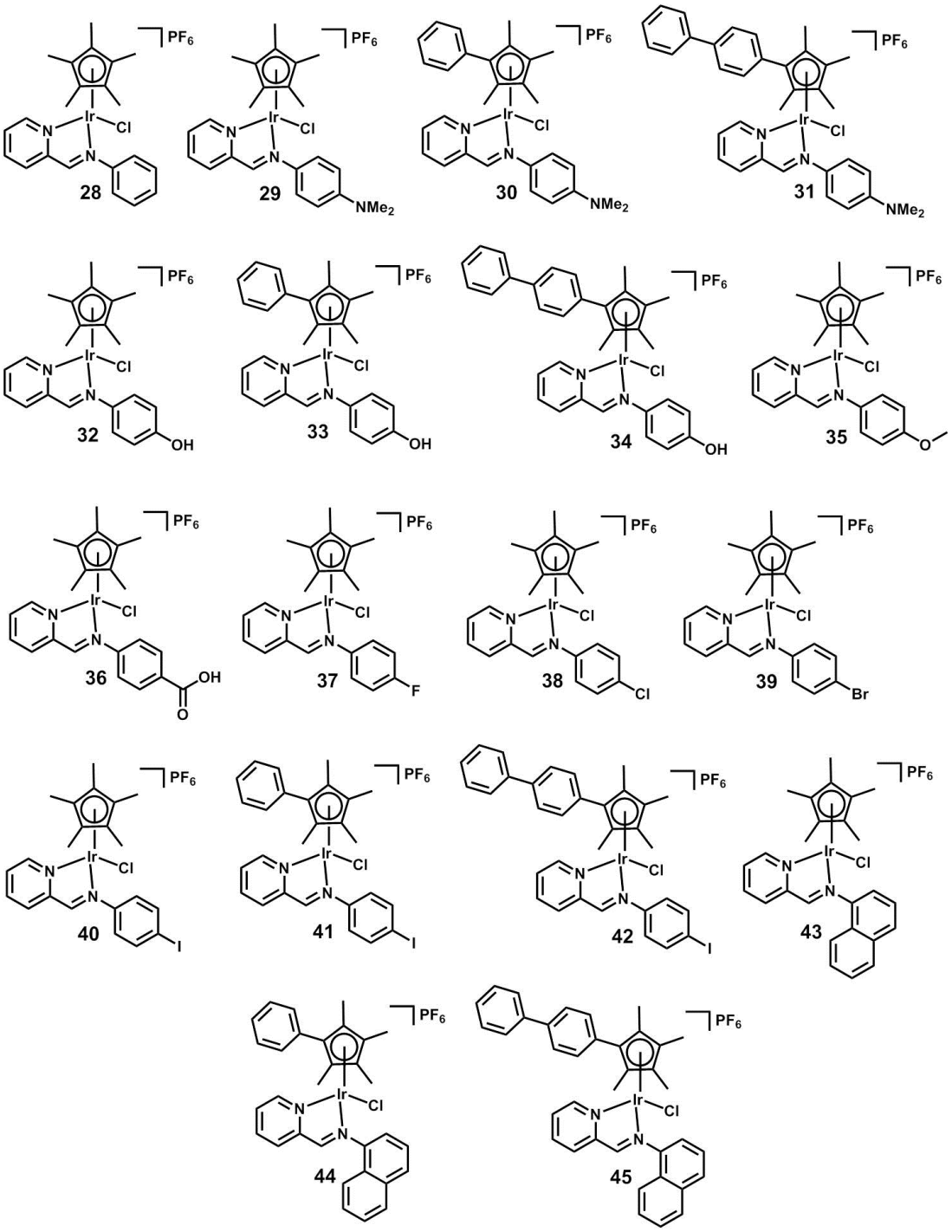

Appendix

Table A1. FT-ICR-MS CAD fragmentation data of the species **6+SubP-H_2O** from Chapter 5.

Fragment	Observed m/z	Exact m/z	Error/ppm
$[b3+6^*-H_2O]^+$	871.37390	871.376815	-3.35
$[b4+6^*-H_2O]^+$	968.42327	968.429575	-6.51
$[b5+6^*-H_2O]^+$	1096.48806	1096.488155	-0.09
$[b6+6^*-H_2O]^+$	1224.54686	1224.546735	0.10
$[b7+6^*-H_2O]^+$	1371.61247	1371.615145	-1.95
$[b8+6^*-H_2O]^+$	1518.66610	1518.683555	-11.49
$[b9+6^*-H_2O]^+$	1575.70497	1575.705015	-0.03
$[b10+6^*-H_2O]^+$	1688.78945	1688.789075	0.22
$[b8+6^*-H_2O]^{2+}$	759.33597	759.3417775	-7.65
$[b9+6^*-H_2O]^{2+}$	787.85204	787.8525075	-0.59
$[y5]^+$	597.30610	597.29793	13.68
$[y8-H]^+$	949.46042	949.460025	0.42
$[y9+6^*-H_2O]^+$	1596.69507	1596.685715	5.86
$[y10+6^*-H_2O]^+$	1693.73084	1693.738475	-4.51

Table A2. FT-ICR-MS CAD fragmentation of the species **6+L3BBS-H_2O** from Chapter 5.

Fragment	Observed m/z	Exact m/z	Error/ppm
b3+(6*-H_2O)-H+	857.313	857.313005	-0.01
b4+(6*-H_2O)-H+	970.39702	970.397065	-0.05
b5+(6*-H_2O)-H+	1027.41868	1027.418525	0.15
b6+(6*-H_2O)-H+	1141.46129	1141.461455	-0.14
b7+(6*-H_2O)-H+	1269.52003	1269.520035	0.00
b8+(6*-H_2O)-H+	1455.59958	1455.599345	0.16
b9+(6*-H_2O)-H+	1526.63602	1526.636455	-0.28
b10+(6*-H_2O)-H+	1625.70466	1625.704865	-0.13
b11+(6*-H_2O)-H+	1682.72557	1682.726325	-0.45
b12+(6*-H_2O)-H+	1819.78479	1819.785235	-0.24
b13+(6*-H_2O)-H+	1932.86903	1932.869295	-0.14
b8+(6*-H_2O)-H+-NH_3	1438.57279	1438.5728	-0.01
b9+(6*-H_2O)-H+-NH_3	1509.60922	1509.60991	-0.46
b10+(6*-H_2O)-H+-	1608.67813	1608.67832	-0.12

b8+(6*-H_2O)-H+-CO	1427.60488	1427.60443	0.32
b9+(6*-H_2O)-H+-CO	1498.64119	1498.64154	-0.23
b10+(6*-H_2O)-H+-CO	1597.71107	1597.70995	0.70
b8+(6*-H_2O)-H+-CO_2	1411.60967	1411.609516	0.11
y5 (+1)	555.30719	555.30715	0.07
y6 (+1)	626.3443	626.34426	0.06
y7 (+1)	812.42356	812.42357	-0.01
y8 (+1)	940.48218	940.48215	0.03
y9 (+1)	1054.52498	1054.52508	-0.09
y10 (+1)	1111.54644	1111.54654	-0.09
y11 (+1)	1224.63048	1224.6306	-0.10
y5-NH_3	538.2806	538.280605	-0.01
y6-NH_3	609.31776	609.317715	0.07
y7-NH_3	795.39692	795.397025	-0.13
y8-NH_3	923.45555	923.455605	-0.06
y10-NH_3	1094.51992	1094.519995	-0.07
y11-NH_3	1207.60419	1207.604055	0.11
b10 -H+ (+2)	813.35599	813.3560725	-0.10
b12 -H+ (+2)	910.39616	910.3962575	-0.11
b13 -H+ (+2)	966.93832	966.9382875	0.03
b13 -H NH_3-(+2)	958.42511	958.425013	0.10
b13 -H+-CO (+2)	952.94074	952.94083	-0.09
b13 -H+-CO-NH_3 (+2)	944.42731	944.4275555	-0.26
[(6*-H_2O)+L3BBS] +	1040.97159	1040.971808	-0.21
[(6*-H_2O)+L3BBS] +	1032.45839	1032.458533	-0.14
[(6*-H_2O)+L3BBS] +	1023.94508	1023.945259	-0.17
y ion+(6*-H_2O)-H+	921.4265	921.426775	-0.30

Table A3. FT-ICR-MS ECD fragmentation of the species **6+L3BBS(His)** from Chapter 5

Fragment	Observed m/z	Exact m/z	Error/ppm
z3dot+6*	891.33643	891.33657	-0.16
z6dot+6*	1118.46426	1118.464091	0.15
z7+6*	1303.53558	1303.53558	0.00
z7dot+6*	1304.54389	1304.543401	0.37
z8+6*	1431.59435	1431.59416	0.13
z8dot+6*	1432.60186	1432.601981	-0.08
z9+6*	1545.63665	1545.63709	-0.28
z9dot+6*	1546.64474	1546.644911	-0.11
z10+6*	1602.65836	1602.65855	-0.12
z10dot+6*	1603.66588	1603.666371	-0.31
z11+6*	1715.7425	1715.74261	-0.06
z12+6*	1843.83686	1843.83757	-0.39
c12+6*	1854.82214	1854.821796	0.19
c13+6*	1967.90497	1967.905856	-0.45

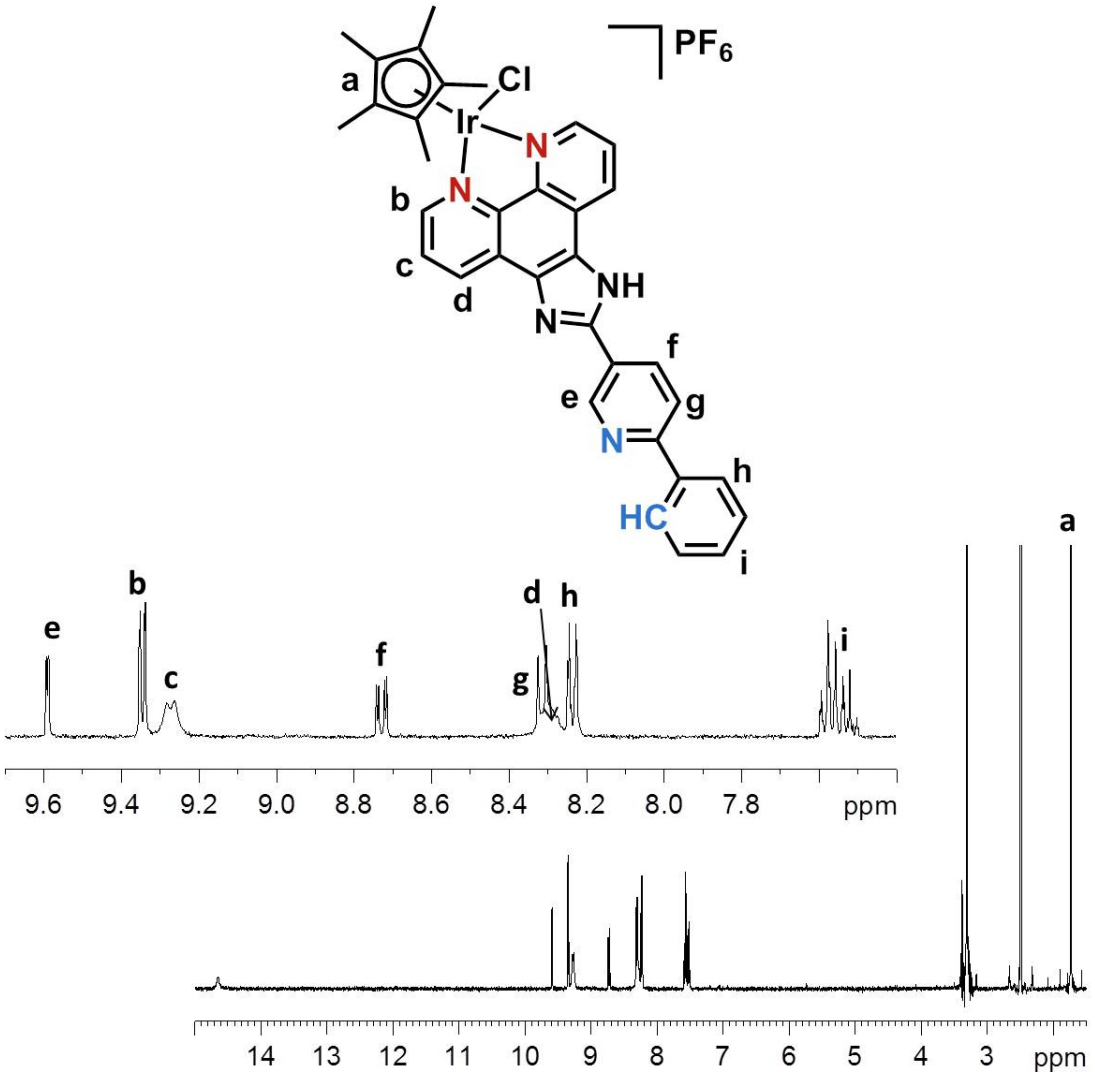

Figure A1. ^{1}H NMR (400 MHZ, dmso-d_6) spectra of the mono-iridium complex discussed in section 7.2.4.

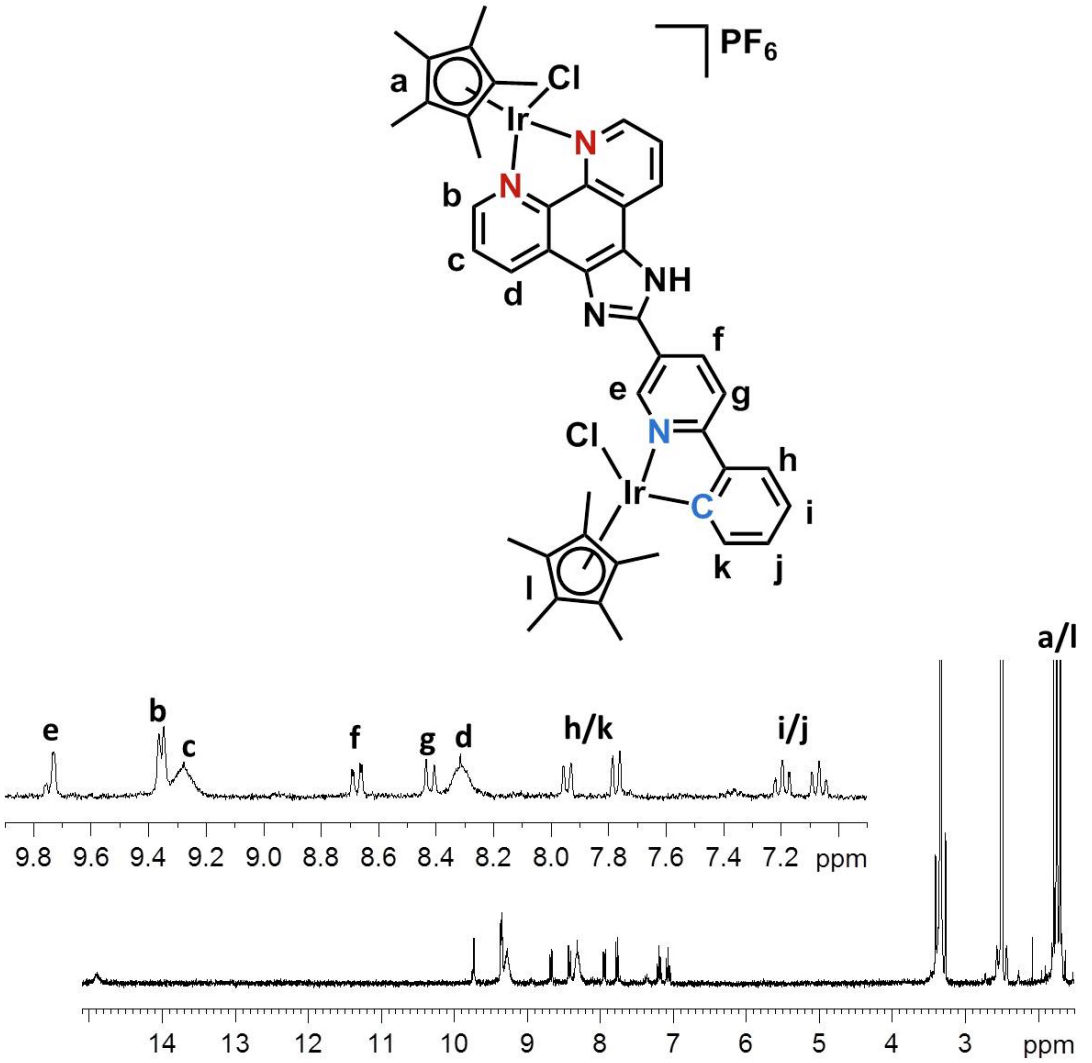

Figure A2. ^{1}H NMR (300 MHZ, dmso-d_6) spectra of the bi-iridium complex discussed in section 7.2.4.